CADMIUM

AND

NEODYMIUM

GEOCHEMICAL CYCLES

IN THE

MARINE ENVIRONEMENT

Myriam Liliane Lambelet

Imperial College London

The Department of Earth Science and Engineering

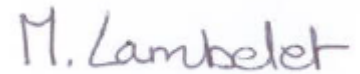Mass Spectrometry and Isotope Geochemistry at Imperial College London

Thesis submitted for the degree of Doctor of Philosophy (Ph.D.), 2014

Declaration of Originality

I declare that the contents of this thesis are completely my own, and that any work of others, published or otherwise, is fully and correctly acknowledged.

Myriam L. Lambelet

M. Lambelet

Acknowledgements

My first thank is for my supervisors Tina van de Flierdt and Mark Rehkamper, for letting me do this project in their MAGIC group, and for supporting me throughout this PhD. Indeed, both of them have always been available for me and the many discussions we have had together were of invaluable help.

A warm thank to Katharina Kreissig for her numerous advice and her great patience and help in the lab. Thanks as well to Barry Coles for his precious help on both the Nu and the Triton.

I would like also to thank a lot Kirsty Crocket for her help with the Nd chemistry, and her many advice. Many thanks to Maxence Paul for helping me with the Triton, and this at any time of the day (and of the night!).

Many thank to all my colleagues from the MAGIC group, and to my "office" mates. A particular thank to Claire Huck, for lifting me up when I was down.

The (technical) staffs of the RSM are warmly thanked for their so appreciated help and support, and this most of the time with a smile!

Thanks as well to Per Andersson and Don Porcelli for providing the Cd samples from the ISSS-08 cruise (Chapter 2). Thank you to Katharina Pahnke and Basak Chandranath for providing seawater samples to test our Nd method (Chapter 3). Many thanks to Micha Rijkenberg, Loes Gerringa and Hein de Baar for providing the seawater samples from the western North Atlantic Ocean (Chapter 4 and 5).

Many thanks to my thesis examiners, Catherine Jeandel and Mark Septhon, who helped me improve this manuscript with their constructive comments.

Gideon Henderson, Malcom Woodward, the scientific party and the crew of the 40˚S GEOTRACES cruise in 2010 are heartily thanked for the unforgettable experience I had the chance to live on board the RRS Discovery.

I am *immensely* grateful to my house mates, and to my friends here and there, that were present to lift me up when I was down, and to celebrate when I was up.

A profound thank to Roger, David, John, George, Fred, Dechen and many others, because their music kept me going and was always a source of inspiration.

Last but not least, a heartily thank to my family, especially to my dad and mum, who always believed in me, and to my brother, Cédric, for his wisdom and support, and to whom this thesis is dedicated.

Abstract

The roles of trace elements and their isotopes in the marine environment are essential and diverse (e.g., nutrients, tracers of oceanic processes, anthropogenic pollutants), but are not well understood yet.

In this thesis, two elements and their isotopes were investigated in two distinct marine environments: cadmium (Cd) in the Siberian shelf seas and neodymium (Nd) in the western North Atlantic Ocean. Whereas the role of Cd as nutrient in the open ocean is reflected by Cd isotope data, its behaviour in estuaries is poorly constrained. Chapter 2 of this thesis presents new Cd isotopes and concentrations of 19 water samples from the mixing zone of Siberian rivers with the Arctic Ocean. The results provide the first constraints on the isotope composition of natural riverine Cd fluxes to the ocean and the cycling of Cd in a shelf environment. Chapter 3 describes the method developed to isolate and analyse seawater Nd isotopes and concentrations in the MAGIC laboratories. The Nd isotopic composition of seawater is a promising tracer for ocean circulation and exchange between the continental margins and the oceans. By analysing 12 seawater depth profiles from the Dutch GEOTRACES transect GA02 (Chapters 4 and 5), we demonstrate that Nd features different behaviour in regions close to the formation area of deep water masses compared to export areas, where it behaves conservatively away from continental margins. Besides, we show that upper- North Atlantic Deep Water (NADW) and lower-NADW have distinct Nd isotopic compositions, and that the signature of lower-NADW is significantly more radiogenic than the commonly accepted value, which should be taken into account for future applications.

Overall, the present thesis underlines the important role that isotope analyses can play in deciphering marine biogeochemical cycles of trace elements.

Table of Contents

List of Figures

List of Tables

Chapter 1

INTRODUCTION

The present thesis focuses on the geochemical cycles of cadmium (Cd) and neodymium (Nd) in the marine environment, and is part of the international GEOTRACES programme. In this introduction, we will first ask ourselves 'why shall we study the oceans'. This will be followed by an overview of the GEOTRACES programme and a summary of the behaviour of Cd and Nd in the ocean.

1.1. Why shall we study the oceans?

The world's ocean covers more than two thirds of the earth. Nowadays, it is well accepted that the ocean plays a central role for the climate system, since it stores and transports heat, freshwater and carbon (Alley et al. 2003). More precisely, the global thermohaline circulation is of central importance for modulating (and potentially regulating) global climate. First described by Wüst in the 1930s, and further developed by Broecker in the 1980s ("The Great Ocean Conveyor", Fig. 1.1 (Broecker 1991)), the thermohaline circulation results from the density differences between water masses involving horizontal and vertical motion. Briefly, dense water sinks at high latitudes, until it reaches a layer having the same density in the water column, to then spread along density surfaces in the global ocean. Continuous dense
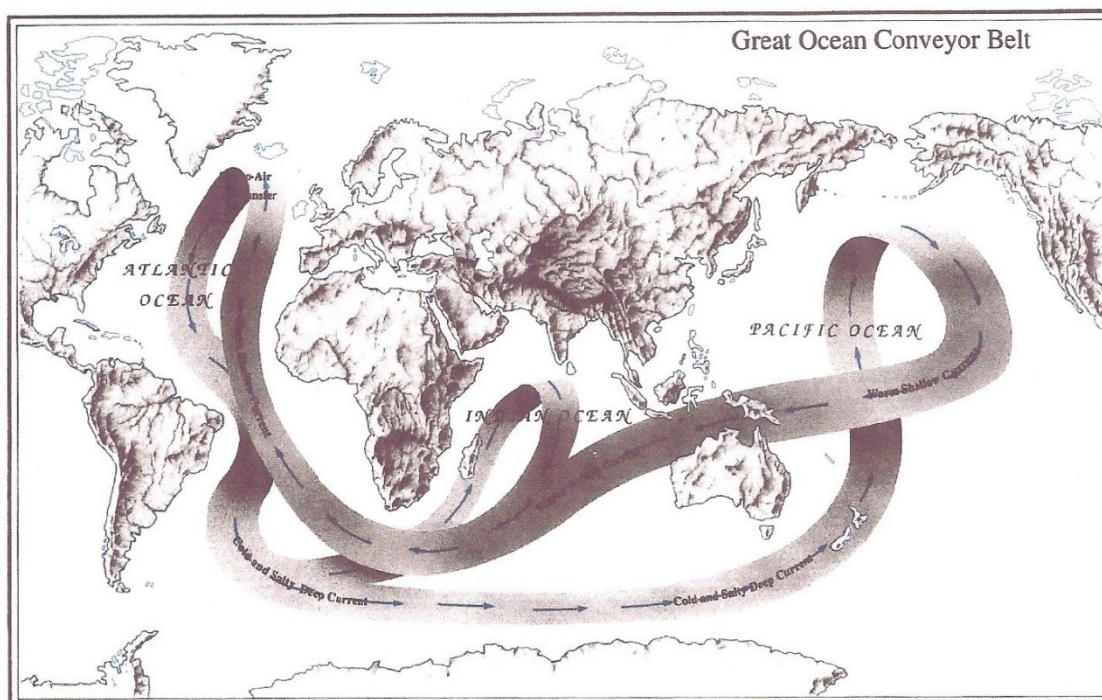
Figure 1.1: Broecker's Great Ocean Conveyor Belt (e.g., the thermohaline circulation) (Broecker 1991).

water production at the surface, which sinks down the water column to form deep water, keeps the ocean in motion (Chester 2000). Because the water that sinks in the northern North Atlantic is warm and salty surface water brought from the tropics via the Gulf Stream and the North Atlantic Current, a very important "benefit" of the thermohaline circulation is that it releases heat to the atmosphere over the northern Atlantic, thus leading to mild climate in Europe (Broecker 1991). If the Great Converyor Belt as pictured by Broecker (Fig. 1.1) is a simplification of the thermohaline circulation (Fig. 1.2), it nevertheless "symbolizes the importance of linkages between realms of the Earth's climate system" (Broecker 1991).

The climate as we know it today has not always been in place, and the earth system has witnessed abrupt climate changes in the past (Alley et al. 2003). It has been shown that the thermohaline circulation was a core variable in these abrupt climate changes (Broecker 1991; Rahmstorf 2002; Alley et al. 2003; McManus et al. 2004; Piotrowski et al. 2004). Indeed, a freshening of the surface North Atlantic, due to enhanced precipitation or fresh water runoff, would result in the surface water not getting dense enough to sink. This failure in sinking would further enhance the freshening of the surface ocean, decreasing even more the surface density, consequently preventing further sinking and the associated inflow of warm water (Alley et al. 2003). Therefore, less heat would be release in the northern Atlantic, thus leading to cooler climate.

Understanding the oceans and the global thermohaline circulation, at present but as well in the past, is consequently of great importance in order to comprehend the future evolution of climate.
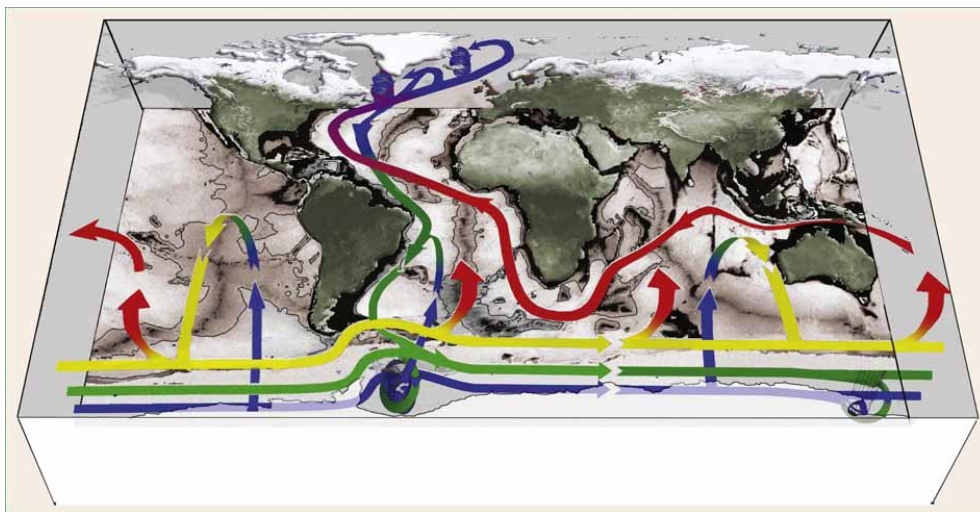
Figure 1.2: The thermohaline circulation revisited. A still schematic, but updated version on the global conveyor belt by Marshall and Speer (2012).

1.2. GEOTRACES overview

The roles of trace elements and their isotopes in the marine environment are diverse and important. Some elements are vital nutrients in the ocean (e.g., Zn, Fe, Cd), while others can be utilised as tracers of past and present oceanic processes (e.g., Nd) or anthropogenic pollution (e.g., Hg, Cd). A better understanding of the biogeochemical cycles and global distributions of the trace elements and their isotopes in the oceans is of central importance for environmental research, as it will improve our knowledge about the climate (e.g., by reconstructing oceanic conditions in the past, or by understanding the fate of contaminants, as well as nutrients, in the marine environment) thus allowing us to be better prepared for future global change.

In the 1970s, the GEOSECS programme (Geochemical Ocean Section Study, Broecker et al. 1974) provided a first overview of the oceanic distribution of several dissolved chemical species, leading to fundamental knowledge about ocean circulation and biogeochemical cycles (see summaries in (GEOTRACES Science Plan 2006; Measures et al. 2007)). Besides, GEOSECS showed the benefits of a global and international study of the ocean geochemistry - many of the data produced are still in use nowadays. Following this programme, improvement in analytical techniques allowed oceanographers to determine the concentration profiles for most elements in the periodic table (Fig. 1.3).
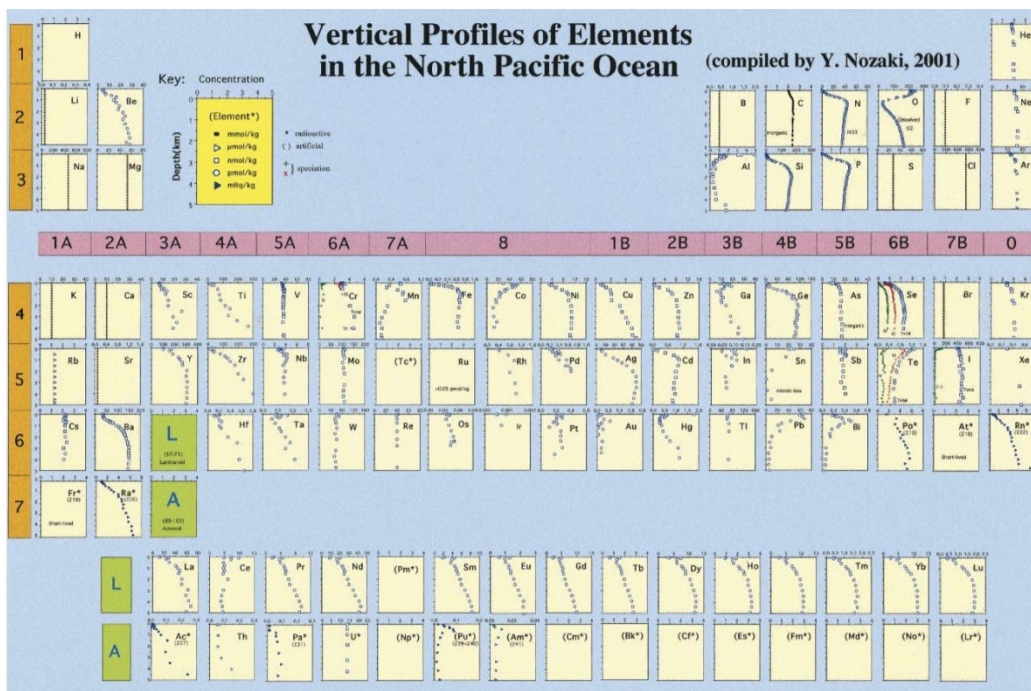
Figure 1.3: Concentration profiles in the North Pacific Ocean, presented in the form of a periodic table by Yoshiyuki Nozaki (Nozaki 1997).

However, even with the technical advances following GEOSECS, the understanding of the global geochemical cycle of many trace elements and their isotopes in the marine environment remained quite poor. For example, elements known to be toxic contaminants (Pb, Cd, As) or to play a crucial role in marine ecosystems (Fe) had been measured only in few regions. Furthermore, little was known about the sources, internal cycling and sinks of many trace elements and isotopes in the oceans. Besides, the recognition that trace metals and their isotopes could be used as proxies for oceanographic parameters in the past was growing (Henderson 2002). In addition, most of the studies on trace elements and their isotopes in the oceans in the decades following GEOSECS were performed in an isolated way and on single cruise, thus making the global distribution of several tracers - as well as the assessment of the interactions between each other - very difficult, if not impossible (Measures et al. 2007). Therefore, the need for a more thorough understanding of global geochemical cycles of the trace elements and their isotopes in the oceans was increasingly recognised, leading the community of marine geochemists to launch the international research programme GEOTRACES about ten years ago. The guiding mission was defined "to identify processes and quantify fluxes that control the distributions of key trace elements and isotopes in the ocean, and to establish the sensitivity of these distributions to changing environmental conditions" (GEOTRACES Science Plan 2006). In more details, three fundamental objectives were defined:

- To determine global ocean distribution of selected trace elements and their isotopes, including their concentration, chemical speciation and physical form, and to evaluate the sources, sinks and internal cycling of these species to characterise more completely the physical, chemical and biological processes regulating their distributions.
- To understand the processes involved in oceanic trace-element cycles sufficiently well that the response of these cycles to global change can be predicted, and their impact on the carbon cycle and climate understood.
- To understand the processes that control the concentrations of geochemical species used for proxies of the past environment, both in the water column and in the substrates that reflect the water column.

In order to achieve these objectives, the research strategies include observations, experiments and modelling, and they are organised under three main themes: (1) fluxes and processes at ocean interfaces (Fig. 1.4) (2) internal cycling (Fig. 1.4), and (3) development of proxies for past changes.
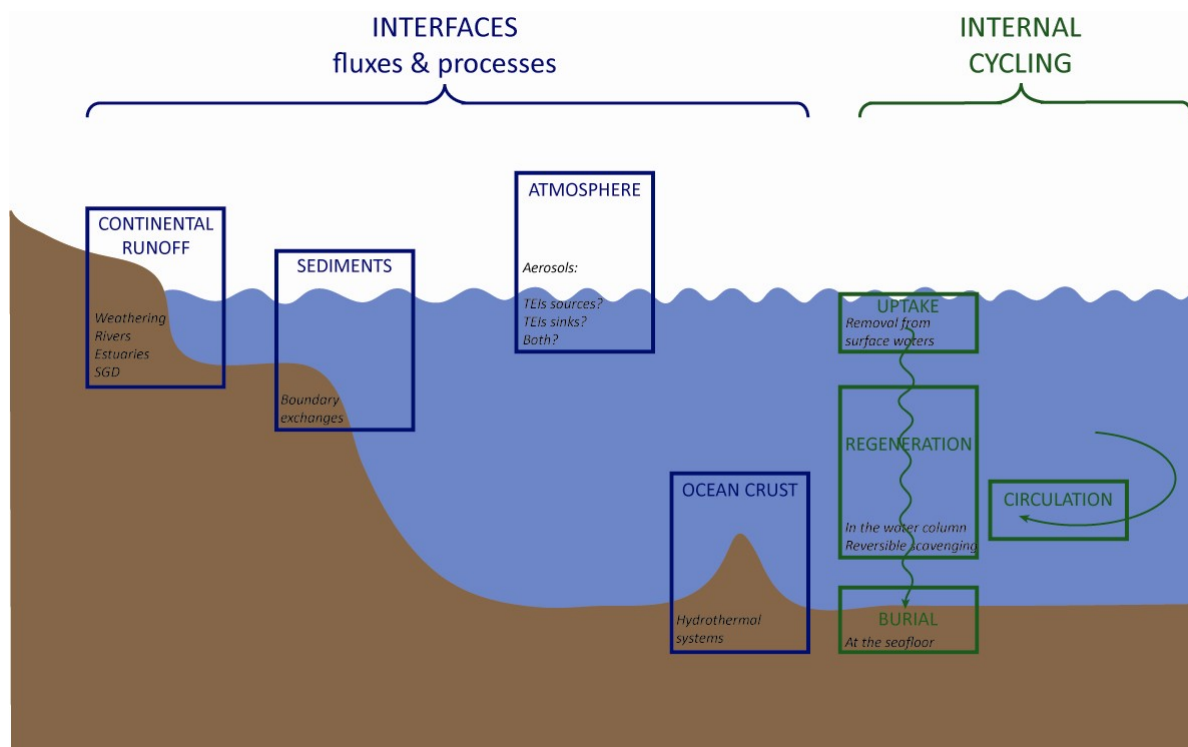
Figure 1.4: Schematic of the major impactors on the distribution of trace elements and their isotopes in the ocean. In blue are the four major ocean interfaces and in green the four major internal processes that account for ocean trace elements and isotopes processes. Adapted from Figure 12 (p. 16) of the GEOTRACES science plan (GEOTRACES Science Plan 2006).

Furthermore, several "key parameters" were defined, and these have to be measured on every GEOTRACES section cruises. These key parameters include cadmium (Cd, essential micronutrient, and proxy for nutrient content of waters) and neodymium isotopes (Nd, tracer of natural sources of trace elements and their isotopes to the ocean, and potential proxy for water mass circulation) (GEOTRACES Science Plan 2006). These two key parameters, as well as Cd isotopes and Nd concentrations, are the focus of the present thesis, and they will be further introduced below.

Since the launch of the GEOTRACES programme, 20 section cruises have been successfully completed, as well as 13 cruises in the context of the International Polar Year, and 12 process studies, which focus on particular regions or processes in the ocean (Fig. 1.5).

Figure 1.5: Map of the GEOTRACES section cruises and their completion status as of January 2014. Red: planned sections; yellow: completed sections; black: sections completed as GEOTRACES contributions to the International Polar Year. Figure taken from the GEOTRACES website: http://www.geotraces.org/.
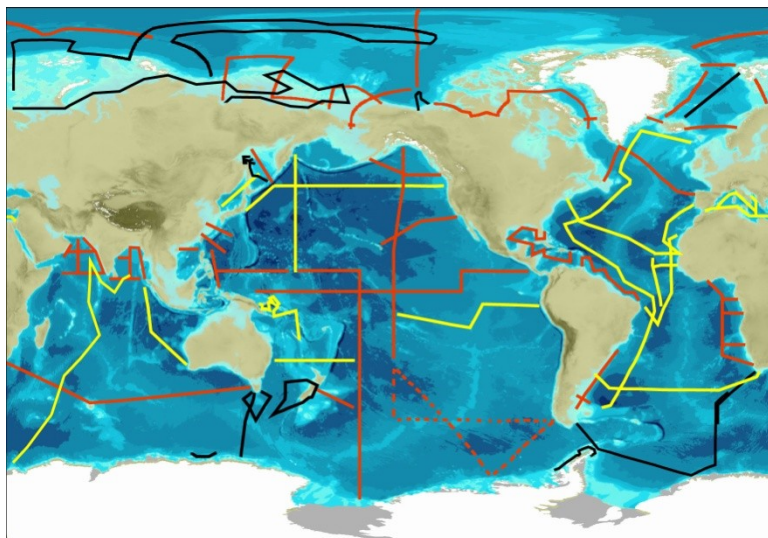
1.3. Cadmium isotopes in the oceans

Cadmium is harmful at elevated concentration (Boyle 1988), but displays an interesting geochemical behaviour in the marine environment that has been studied by numerous scientists for more than 30 years. The reason for this enthusiasm is that Cd exhibits a nutrient-like behaviour in the oceans, comparable to the macro-nutrient phosphate (Boyle et al. 1976; Bruland 1980). Indeed, Cd, and thus phosphate, concentrations show depletion in the surface of the ocean compared to deep water, which indicates an uptake by organisms at the surface and regeneration from sinking biological debris deeper in the water column (Figs. 1.6 a and b) (Boyle et al. 1976; Bruland 1980). The Cd concentration in the ocean increases rapidly from the surface up to about 1 km depth, which corresponds to the phosphate maximum concentration zone, and then decreases slowly at deeper levels (Boyle et al. 1976). While Cd and phosphate concentration in the world ocean are well correlated, this correlation presents a "kink" at intermediate Cd and phosphate contents, which is still not fully understood (de Baar et al. 1994). The excellent correlation between Cd and phosphate distributions in the ocean, as well as the fact that Cd/Ca ratios in foraminiferal shells seem to reflect the ambient seawater the foraminifera calcified from, has lead to the idea of using Cd as a proxy for past marine nutrient (PO_4^{3-}) concentrations (Boyle et al. 1976; Boyle 1988).

At present only a limited amount of direct measurements of the Cd isotope composition of seawater are available (Lacan et al. 2006; Ripperger et al. 2007b; Abouchami et al. 2011; Yang et al. 2012; Gault-Ringold et al. 2012b; Xue et al. 2013; Abouchami et al. 2014).

The Cd isotopic composition in the following is reported using the $^{114}Cd/^{110}Cd$ ratio, relative to NIST SRM 3108 Cd with an ε notation:

$$\varepsilon^{114\ 110}Cd = \left(\frac{\left(\dfrac{^{114}Cd}{^{110}Cd}\right)_{Sample}}{\left(\dfrac{^{114}Cd}{^{110}Cd}\right)_{Standard}} - 1 \right) \times 10^4$$

The pioneer studies of Lacan et al. (2006) and Ripperger et al. (2007b) have shown that Cd isotopes are fractionated upon uptake by phytoplankton at the surface of the ocean. Indeed, depth profiles analysed by Ripperger et al. (2007b) showed that the Cd isotopic composition of seawater was inversely proportional to Cd concentrations (Figs. 1.6 b and c), with the Cd depleted surface water samples displaying large isotopic fractionations (characterized by larger positive $\varepsilon^{114/110}Cd$ values) for most of the samples. The authors suggested that this Cd isotopic fractionation reflects kinetic isotope effects from the uptake of the lighter isotopes by phytoplankton. The data furthermore showed that the fractionation follows closed system Rayleigh distillation curves. Some shallow water samples, however, did not follow this trend and showed very little isotopic fractionation ($\varepsilon^{114/110}Cd$ = -6 ± 6 to + 6 ± 2.7) even for very low Cd concentrations (< 0.008 nM). This was argued to be due to either other Cd uptake mechanisms (e.g., adsorption instead of biological uptake) that do not produce isotopic fractionation, atmospheric input of lighter Cd isotopes, or even mixing of fractionated surface water with Cd-rich deep water characterized by $\varepsilon^{114/110}Cd \le 3$. Importantly, Ripperger et al. (2007b) also found that water samples from below 900 m depth were characterized by quite uniform Cd isotopic compositions. For these deep water samples (n = 7), Ripperger et al. (2007b) determined an average value of $\varepsilon^{114/110}Cd$ = +3.3 ± 0.5. This value was reassessed recently to $\varepsilon^{114/110}Cd$ = +3.0 ± 0.3 for the world ocean (n = 27, Xue et al. 2013). This constancy is particularly notable as the different sampling sites displayed quite variable Cd concentrations, which varied between about 0.3 nM for the Atlantic Ocean to about 0.9 nM for the Pacific Ocean, thus featuring an increase along the thermohaline circulation. More recently, the link between Cd isotope fractionation and primary productivity has been demonstrated for seawater samples from the Southern Ocean (Abouchami et al. 2011; Xue et al. 2013; Abouchami et al. 2014) and from the South China Sea (Murphy et al. ; Yang et al. 2012). However, a study about subantarctic surface waters

demonstrated a 50-fold seasonal decrease in Cd concentration that was decoupled from Cd isotopes fractionation and phosphate concentration (Gault-Ringold et al. 2012b). The authors suggested that this lack of fractionation was due to the phytoplankton taking up every isotope of this element, without preference for the lighter ones, due to Cd limitation, thus leading to an unfractionated Cd isotope signature.
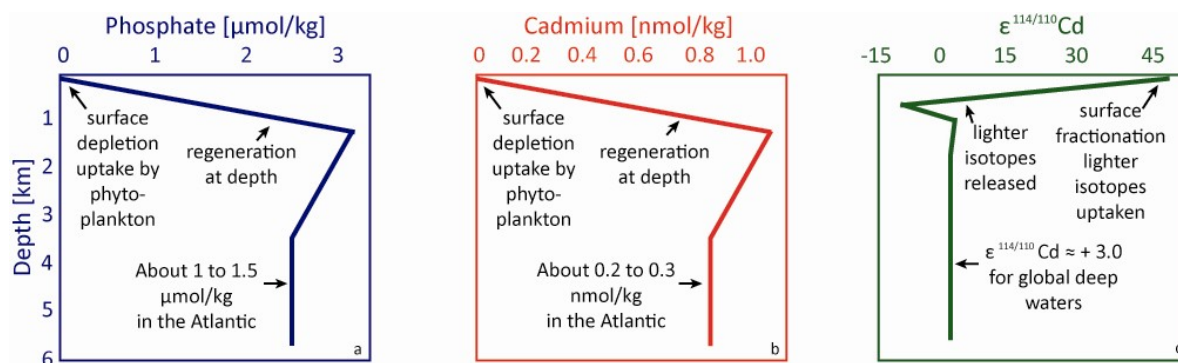
Figure 1.6: Schematic of typical depth profile for seawater (a) phosphate concentrations [µmol/kg], (b) Cd concentrations [nmol/kg], and (c) Cd isotopic compositions in the North Pacific. Note that the phosphate and Cd deep water concentrations are lower in the Atlantic, whereas the Cd isotopic composition stays the same in the global deep ocean ($\varepsilon^{114/110}$Cd ≈ + 3.0, see text).

If the Cd isotopic composition of open ocean seawater has been lately of growing interest, information about its behaviour in rivers and mixing areas (e.g., estuaries) are still poor. Chapter 2 of the present thesis addresses this shortcoming by providing Cd isotope and concentration data for the mixing zone of four major Siberian rivers with the coastal seas occupying the Siberian continental shelf of the Arctic.

1.4. Neodymium isotopes in the oceans

Even if the history of analysing the Nd isotopic composition of seawater is much longer than that for Cd isotopes (e.g., since the 1980s), our understanding of the Nd cycle in the ocean is still relatively poor. The Nd isotopic composition is expressed as

$$\varepsilon_{Nd} = \left(\frac{\left(\dfrac{^{143}Nd}{^{144}Nd} \right)_{Sample}}{\left(\dfrac{^{143}Nd}{^{144}Nd} \right)_{CHUR}} - 1 \right) \times 10^4$$

where CHUR (Chondritic Uniform Reservoir) represents a present day average earth value $((^{143}Nd/^{144}Nd)_{CHUR} = 0.512638$ (Jacobsen and Wasserburg 1980)).

The systematic geographic variability of Nd isotope ratios in the ocean has lead to the idea that it could be used as a proxy for oceanic circulation in the past (e.g., summaries by von Blanckenburg 1999; Frank 2002; van de Flierdt and Frank 2010). Indeed, the reconstruction of past water mass configurations and circulation patterns are vital to understand the role of the ocean in past climate change and hence comprehend the future evolution of climate. The Nd isotopic composition of seawater features large variations between the ocean basins, ranging from low values in the North Atlantic due to the imprint from the surrounding old continents (ε_{Nd} = -25 to -10) to higher values in the Pacific, which is surrounded by younger basaltic arc (ε_{Nd} = -5 to 0), and intermediate values in the Indian and Southern Ocean (ε_{Nd} = -10 to -7) (Goldstein and Hemming 2003). These observations, as well as the co-variation of Nd isotopes with salinity (e.g., Fig. 1.7, von Blanckenburg 1999) have made Nd isotope a prime water mass proxy. Indeed, salinity, together with temperature, are two key properties to determine the circulation in the modern ocean, but are hard to reconstruct in the past; hence the need for a reliable proxy.
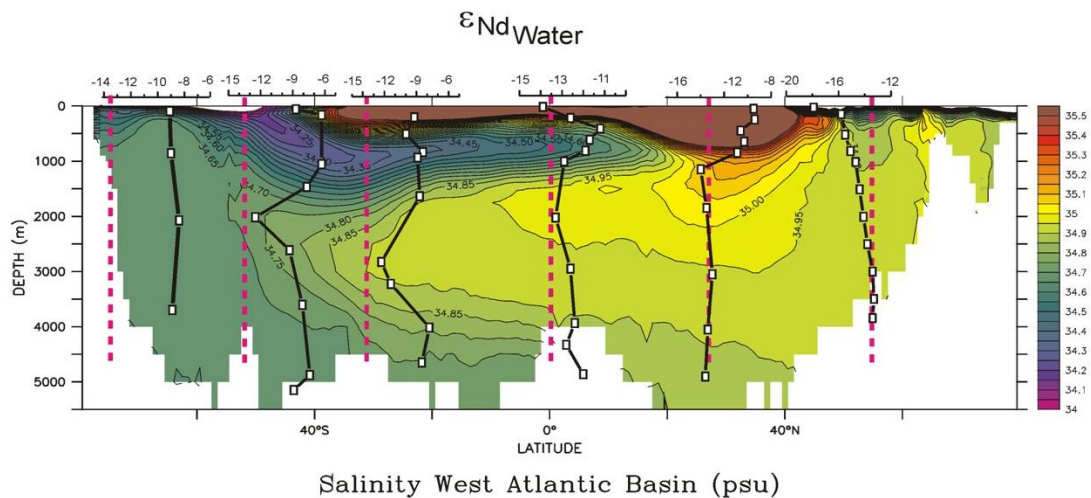
Figure 1.7: Salinity distribution integrated over the western North Atlantic Ocean, with Nd isotopic compositions of seawater superimposed. Red dotted lines represents the 'accepted' Nd isotopic

composition of North Atlantic Deep Water (NADW; ε_{Nd} = -13.5). Figure taken from von Blanckenburg (1999). For a revised estimate of the Nd isotopic composition of NADW see Chapter 4.

A number of studies have been published to exploit this prospectus (see van de Flierdt and Frank (2010) for a recent summary), but comparison with another promising tracer for the flux of water masses, ^{231}Pa/^{230}Th, reveals fundamental disagreements when it comes for example to statements about the strength of the meridional overturning circulation during the last glacial maximum (LGM) (Fig. 1.8).

Figure 1.8: Comparison of ^{231}Pa/^{230}Th (middle panel) and Nd isotopes (lower panel), two tracers thought to give information about the rate of past flow of NADW (McManus et al. 2004; Piotrowski et al. 2004). ^{231}Pa/^{230}Th ratios suggests a high rate of flow at about 19 kyr, whereas Nd isotopes suggest a lower flow rate (see black arrow). This shows that two of the commonly applied proxies for reconstructing past ocean circulation need to be better understood. The upper panel shows a record for air temperature over Greenland, based on oxygen isotopic composition of the ice. Figure taken from the GEOTRACES science plan (p. 15) (GEOTRACES Science Plan 2006).
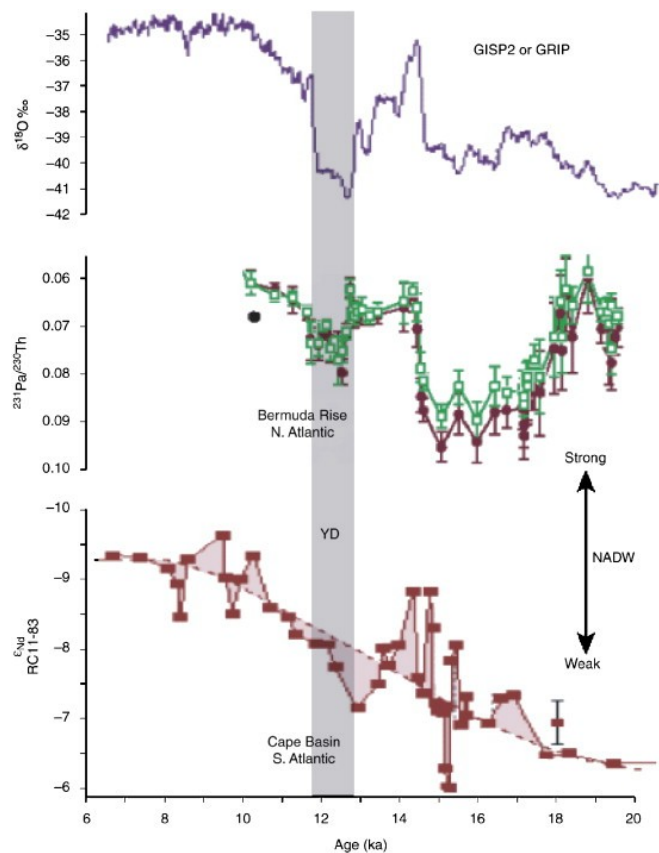
Other authors have rather focussed on the exciting prospect of Nd isotopes as a tracer for exchange between the continental margins and the oceans (e.g., Lacan and Jeandel, 2005). Indeed, it is of fundamental importance to know the fluxes and processes of continental inputs to the ocean, and it is one of the central aims of the GEOTRACES programme (Fig. 1.4, (GEOTRACES Science Plan 2006)). The global riverine particulate flux to the ocean (~30 Gt/yr, suspended sediment and bedload transport) exceeds by far the dissolved riverine

load (~1 Gt/yr) and the dissolution of atmospheric dust (~0.45 Gt/yr), suggesting that dissolution of only a small amount of this riverine particulate material can have a large impact on the chemical composition of seawater (Pearce et al. 2013). However, little is known about the processes governing margin-seawater interaction. Studies in different regions of the global ocean have shown that Nd concentrations and/or isotopic compositions can trace such interaction, and modelling studies have shown that boundary exchange is probably the major contributor to the Nd budget in the ocean (Arsouze et al. 2009; Rempfer et al. 2011). Neodymium isotopes are a promising tool to understand these margin-seawater interactions, as they are tagged by lithogenic fingerprints, thus allowing to trace back the origin of the inputs. Furthermore, when coupled with Nd concentration measurements, it is possible to differentiate between boundary input and exchanges, thus shedding a light on the actual mechanism involved.

Regardless of whether research efforts are motivated by palaeo-applications or modern tracer understanding, a hampering fact for both is the poor coverage of the global ocean with seawater Nd analyses (see Lacan and Jeandel (2012) for a recent summary) and the associated lack of understanding in Nd cycling. Indeed, whereas Nd isotopes seem to trace water masses away from any continental inputs, Nd concentrations in the open ocean shows an increase with depth and along the conveyor belt, akin to nutrients, thus suggesting the importance of vertical cycling (Elderfield and Greaves 1982; de Baar et al. 1985; Elderfield 1988; Bertram and Elderfield 1993). This decoupling between Nd isotope and concentration has been termed the "Nd paradox" (Jeandel et al. 1995; Tachikawa et al. 2003; Siddall et al. 2008; Arsouze et al. 2009), and will be investigated in Chapter 5 in more detail.

1.5. Thesis aims and objectives

The overall aim of the present thesis is to better constrain the geochemical cycles of the trace elements cadmium and neodymium and their isotopes in the marine environment. In order to achieve this objective, we will use concentration and isotopic composition measurements on several selected samples, and each chapter will focus on specific objectives (see thesis outline).

1.6. Thesis outline

Chapter 2:

In order to study the Cd behaviour in estuaries, nineteen water samples were analysed for their Cd concentrations and isotopic composition. These samples were collected in the mixing zones of four major rivers (Ob, Yenisei, Lena and Indigirka) during the ISSS-08 expedition, and span a broad range of salinities (e.g., between 1 and 32). Additional results are presented for the Cd concentration and isotopic composition of a sample from the pristine Kalix River (northern Sweden). The specific aims of the present chapter are:

- to constrain the isotopic composition of natural riverine Cd flux to the ocean
- to determine the Cd isotopic fractionation incurred during weathering
- to better understand the cycling of Cd in a shelf environment.

Chapter 3:

Here, we describe the method used in this thesis to isolate and measure Nd isotopes and concentration from seawater samples with high precision and accuracy. The specific aims of the chapter are:

- to establish a suitable method to pre-concentrate Nd from seawater in the MAGIC laboratories
- to develop a column chemistry that is suitable to run Nd isotopes and concentrations simultaneously as NdO^+ on the Triton TIMS in the MAGIC laboratories
- to refine a methodology to run low abundance Nd samples as NdO^+ on the Triton TIMS in the MAGIC laboratories
- to verify our methodology by repeat analyses of seawater samples and GEOTRACES intercalibration samples

Chapter 4:

In order to further the application of Nd isotopes in seawater we analysed the Nd isotopic composition of 137 samples from twelve seawater depth profiles, containing each 10 to 13 depths, that were collected in the north to equatorial western Atlantic Ocean during the Dutch GEOTRACES GA 02 transect. The specific aims of this chapter are the following:

- to evaluate if Nd isotopes behave conservatively in deep waters away from ocean margins,

25

- to determine whether Nd isotopes feature the same behaviour in the northern north Atlantic (subpolar formation region of NADW constituents) compared to the export area (subtropical western Atlantic),
- to assess the ability of the Nd isotopic composition of seawater to trace water masses.

Chapter 5:

One long-lasting dilemma in understanding the marine biogeochemical cycle of Nd isotopes and concentrations is their decoupled behaviour ('Nd paradox'). In this last data chapter we present Nd concentrations for the same 137 seawater samples collected from twelve depth profiles studied in Chapter 4. The specific objectives of this chapter are:

- to investigate the vertical profiles of Nd concentrations in the North Atlantic Ocean with specific regards to the process of reversible scavenging,
- to determine whether Nd concentrations feature the same behaviour in the northern north Atlantic (subpolar formation region of NADW constituents) compared to the export area (subtropical western Atlantic),
- to constrain the major sources of Nd to surface and deep waters of the western North Atlantic Ocean by using combined Nd isotope and concentration constraints.

Chapter 6:

This chapter summaries the major finding and conclusions that can be drawn from our studies.

Chapter 2

ISOTOPIC ANALYSIS

OF

CADMIUM

IN THE MIXING ZONE

OF

SIBERIAN RIVERS

WITH THE

ARCTIC OCEAN

Abstract

The cadmium (Cd) concentrations and isotopic compositions were determined for 19 water samples which cover the mixing zones of four major rivers with the coastal seas of the Siberian Shelf. The waters span salinities from about 1 to 32, with Cd concentrations of about 0.02 to 0.46 nmol/kg and small but resolvable Cd isotope fractionations, with $\varepsilon^{114/110}$Cd values of between +1.4 and +5.7. The data for the majority of the samples are in accord with the systematics expected for quasi-binary mixing of Arctic seawater ($\varepsilon^{114/110}$Cd $\approx$ +5.5 ± 0.5 and Cd concentration between 0.1 and 0.25 nmol/kg) with river waters characterized by $\varepsilon^{114/110}$Cd $\approx$ +2 ± 1 and low pristine Cd contents of about 0.02 to 0.06 nmol/kg. The river values are similar to the inferred composition of the continental crust, which implies that weathering produces no or only limited Cd isotope fractionation. The results for five samples provide clear evidence for non-conservative behaviour of Cd, as the element is released from suspended riverine particles during mixing with seawater. The isotopic data furthermore show that the desorbed Cd is characterized by $\varepsilon^{114/110}$Cd $\approx$ +3, in accord with a natural origin. This implies that the (natural) net riverine Cd fluxes of the Siberian rivers to seawater are also likely be to characterized by $\varepsilon^{114/110}$Cd $\approx$ +2 ± 1, a value that is either identical to or intermediate between the composition of the continental crust and marine deep waters. Additional data for the boreal Kalix River in Sweden contrasts with the results obtained for the Siberian rivers, as the former exhibits a much lighter Cd isotope composition of $\varepsilon^{114/110}$Cd = –3.8 coupled with a much higher Cd content of ~0.24 nmol/kg. These characteristics appear to be a consequence of the distinct hydro-geological setting of the Kalix drainage basin, which suggests that the riverine input of Cd isotopes to the oceans might display significant regional variability. In summary, our study underlines the important role that stable isotope analyses can play in biogeochemical investigations of trace metals. Here, the Cd isotope results provide important constraints, which are not available from concentration data alone, on the cycling of Cd in riverine and shelf environments.

2.1. Introduction

Cadmium is an enigmatic element as it is highly toxic but in the oceans it displays a distribution akin to the macronutrient phosphate (Boyle et al. 1976; Bruland 1980). Both Cd and phosphate abundances are commonly depleted in the surface ocean compared to deep water, presumably due to uptake by organisms. This conclusion is supported by work that has shown that Cd can substitute for Zn in the enzyme carbonic anhydrase, which plays an important role in the process of inorganic carbon acquisition. Cadmium is hence generally considered to be a micronutrient element (Price and Morel 1990; Cullen et al. 1999; Lane et al. 2005; Xu et al. 2008). The marine Cd concentration rises rapidly in deeper waters due to regeneration from sinking biological debris, and reaches a maximum at about 1 km depth. The same open-ocean seawater concentration profile can be observed for phosphate (Boyle et al. 1976; Bruland 1980). As a result, there exists a well-defined global correlation between Cd and phosphate concentrations in open-ocean seawater (Boyle et al. 1976), but this exhibits a "kink" at intermediate Cd and phosphate levels, the origin of which remains to be fully understood (de Baar et al. 1994). These findings, as well as the application of Cd/Ca ratios in foraminiferal shells to reconstruct the nutrient status of past seawater (Boyle 1988), have spurred continued interest in the marine biogeochemistry of Cd.

Recently, a number of studies have shown that the Cd isotope composition of seawater exhibits significant variability. Whilst samples from depths greater than about 1 km were observed to have nearly uniform Cd isotope compositions of $\varepsilon^{114/110} \approx +2.5$, Cd-depleted surface waters are generally isotopically heavier, with some samples featuring $\varepsilon^{114/110}Cd$ values as high as $+ 20$ to $+40$ (all $\varepsilon^{114/110}Cd$ data are relative to NIST SRM 3108 Cd) (Ripperger et al. 2007b; Abouchami et al. 2011; Abouchami et al. 2012; Xue et al. 2012). The observed fractionations in the surface waters have been attributed to kinetic isotopic effects that result from preferential uptake of the lighter Cd isotopes by phytoplankton. This interpretation is supported by data for cultured freshwater (Lacan et al. 2006) and Southern Ocean phytoplankton (Gault-Ringold 2011), which were found to have isotopically light Cd with $\varepsilon^{114/110}Cd$ values as low as -24.

Numerous surface water samples furthermore show a systematic increase of $\varepsilon^{114/110}Cd$ with decreasing Cd content, suggesting a fractionation factor for biological uptake of Cd between $\alpha \approx 1.0002$ and $\alpha \approx 1.0006$ (Ripperger et al. 2007b; Abouchami et al. 2011; Abouchami et al. 2012; Xue et al. 2012). However, both Ripperger et al. 2007b and Gault-Ringold et al. 2012 observed that some surface water samples with highly depleted Cd

concentrations of < 0.05 nmol/kg display no or only limited fractionation relative to deep water (e.g., $\varepsilon^{114/110}$Cd values of less than +5). Potential interpretations that have been invoked for the lack of coupling of Cd concentrations and isotopic composition in such samples are effect of water mass mixing, 'supply-limited' uptake conditions for Cd, or other unusual marine conditions (Ripperger et al. 2007b; Gault-Ringold et al. 2012b), demonstrating that isotopic data can provide insights into the marine cycling of the micronutrient element Cd beyond what can be learned from concentration data only. However, the current database for marine Cd isotope data is still sparse (Lacan et al. 2006; Ripperger et al. 2007b; Abouchami et al. 2011; Yang et al. 2012; Gault-Ringold et al. 2012b; Xue et al. 2013; Abouchami et al. 2014), and considerable uncertainty is associated with the inputs of Cd to the ocean.

Next to atmospheric fluxes, rivers are thought to be the most important source of marine Cd (Duce et al. 1991). Previous work has revealed that dissolved riverine Cd fluxes to the oceans may be affected by both non-conservative behaviour during estuarine mixing (Elbaz-Poulichet et al. 1987; Comans and Vandijk 1988; Elbaz-Poulichet et al. 1996; Waeles et al. 2004; Waeles et al. 2005), and industrial discharges (Huynhngoc et al. 1988; Weigold and Baborowski 2009). The anthropogenic impact on riverine Cd budgets can be overwhelming, as Cd contents of more than 0.6 nmol/L have been reported for rivers (Rhine, Rhone and others) from industrialized regions (Duinker and Nolting 1977; Huynhngoc et al. 1988), whilst pristine river water generally appears to exhibit dissolved Cd concentrations of less than 0.1 nmol/L (Guieu et al. 1996; Mackey et al. 1996; Moran and Woods 1997).

The impact of rivers and estuarine processes on the isotopic mass balance of marine Cd has not been studied to date, however, and the current investigation addresses this shortcoming. To this end, we have carried out coupled Cd isotope and concentration measurements for 19 water samples that span nearly the complete salinity gradient that is generated by the discharge of four major Siberian rivers (Ob, Yenisei, Lena and Indigirka) into the coastal seas that occupy the Siberian continental shelf of the Arctic Ocean. In addition, we also analysed a further sample from the pristine Kalix River in northern Sweden. The results of these analyses provide the first constraints on the isotope composition of natural riverine Cd fluxes to the ocean, the Cd isotope fractionation that is incurred during weathering and the cycling of Cd in a shelf environment.

2.2. Samples

Nineteen water samples from the International Siberian Shelf Study 2008 (ISSS-08) were analysed for both Cd isotope compositions and concentrations. This sample suite records mixing of seawater with freshwater delivered by four major Siberian rivers and encompasses two samples obtained from near the mouth of the Ob, two from near the mouth of the Yenisei, 12 from the Lena River area and three from the East Siberian Sea area (Fig. 2.1, Table 2.1). Together the samples nearly span the entire gradient from freshwater to open ocean Arctic seawater (salinity range: 1 to 32) and are hence well suited for studying estuarine processes.

Figure 2.1: Map indicating the samples' location. The labels YS followed by numbers represent the stations of the ISSS-08 cruise.

Brown triangle: Mouth of Ob; green diamond: Mouth of Yenisei; red circles: Lena Area; black squares: East Siberian Sea Area. Samples collected at 2 different depths: YS-2, YS-3, YS-4, YS-6 and YS-8. For all other samples, only one depth was available.
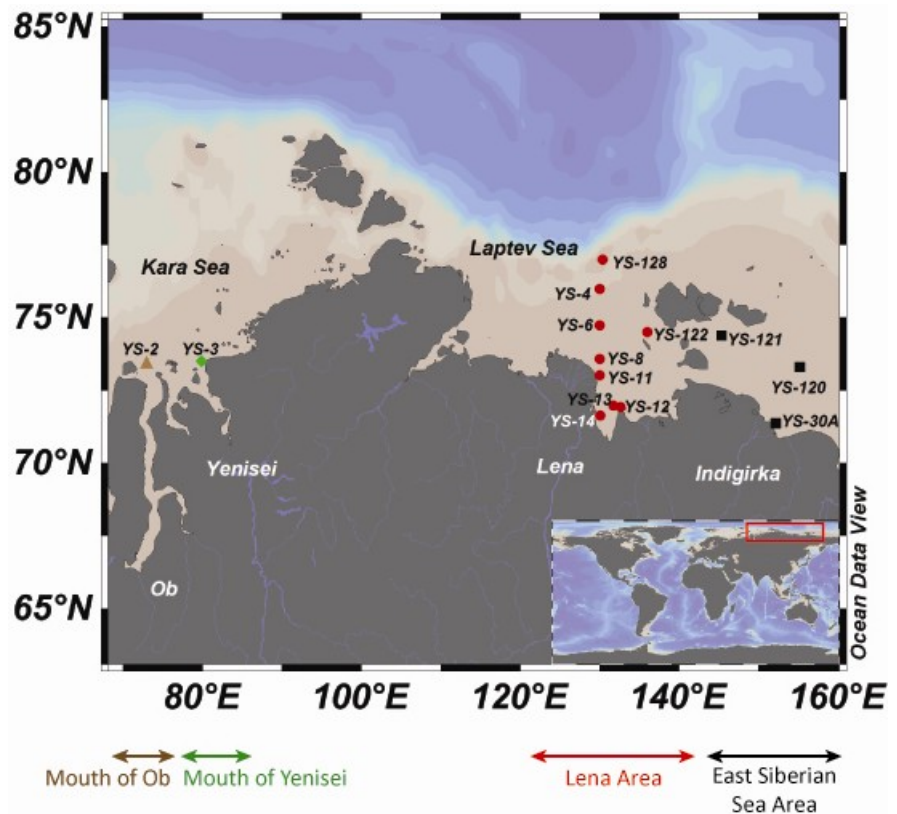
The Siberian Shelf is the largest continental shelf in the world and it encompasses several coastal seas. The Ob and Yenisei drain into the Kara Sea (Fig. 2.1, Table 2.1), where more than one third of the total freshwater discharge into the Arctic Ocean is received (Dai and Martin 1995). In contrast, the Lena and the Indigirka Rivers flow into the Laptev and the East Siberian Seas, respectively (Fig. 2.1). All four rivers have strongly seasonal water discharges,

which are largest in the summer, and the hydrology of the respective mixing zones with the coastal seas appears to be similar. For example, the brackish plume of the Ob River in the Kara Sea features a warmer (about 3ºC), less saline (S < 15) surface layer that reflects riverine inputs, a thin intermediate layer and, at depths of more than ~30 m, a cold (~1ºC), saline (S ≈ 30) bottom layer that is akin to Arctic Ocean seawater (Dai and Martin 1995). The sea surface of the mixing zones is frozen to a thickness of about 2 m for approximately nine months each year, from October/November to June/July (Martin et al. 1993).

The ISSS-08 samples were collected from on-board the research vessel Yacob Smirnitskyi in August and September 2008. Surface waters from depths of less than 4 m were pumped through acid-cleaned Teflon tubing that extended from up-current of the ship at the end of a 14 m long glass fibre flagpole and into cleaned carboy containers. All other samples were collected using either 20 L or 60 L metal-free Go-Flo sampling bottles that featured Teflon-coated internal surfaces. On deck, the water was transferred into 25 L acid-cleaned carboys using silicone tubing. Whilst on the ship, all samples were furthermore pumped through 0.22 µm nitrocellulose membrane filters and acidified to pH 2 using distilled HCl.

One additional sample from the Kalix River in northern Sweden (Table 2.1) was obtained on June 10, 1995 at Kamlunge, which is about 30 km upstream from the mouth of the river in the Baltic Sea (Porcelli et al. 1997). Following collection of a large sample, the water was pumped through 0.45 µm nitrocellulose membrane filters (pre-cleaned in weak acetic acid) into a 10 L container for storage, following acidification to about pH 1 with distilled HCl. Three 1 L aliquots of this sample were taken from the stock bottle several months prior to use. All plasticware that was used for the collection and storage of the Kalix samples were pre-cleaned using dilute mineral acids (Porcelli et al. 1997).

Table 2.1: Reference data for the Ob, Yenisei, Lena and Indigirka Rivers in Siberia and the Kalix River in Sweden.

	Ob[a]	Yenisei[a]	Lena[b]	Indigirka[c]	Kalix[d]
Length (km)	5410	3844	4400	1820	450
Catchment area (km^2)	$2.99{\cdot}10^6$	$2.5{\cdot}10^6$	$2.43{\cdot}10^6$	$3.62{\cdot}10^5$	$2.38{\cdot}10^4$
Water discharge (m^3/s)	$1.35{\cdot}10^4$	$1.98{\cdot}10^4$	$1.66{\cdot}10^4$	$1.93{\cdot}10^3$	$2.96{\cdot}10^2$
Published [Cd] data					
Range [nM]	0.001 – 0.13 [e]	0.009 – 0.15 [f]	0.02 - 0.11 [g]	–	–
Average [nM]*	0.04 ± 0.03 [e]	0.05 ± 0.04 [f]	0.06 ± 0.04 [g]	–	–

a (Dai and Martin 1995); b (Martin et al. 1993); c (Huh et al. 1998); d (Ingri et al. 1997)   e (Moran and Woods 1997) f (Guay et al. 2010) g (Guieu et al. 1996). * The uncertainties are given as 1sd.

2.3. Methods

2.3.1. Analytical procedures

Sample preparation, chemical separation of Cd and the isotopic analyses were performed following published procedures (Ripperger and Rehkämper 2007a; Xue et al. 2012) at the Imperial College MAGIC Laboratories. This laboratory has successfully participated in the intercalibration exercise for the measurements of Cd isotopes and concentration in seawater samples (Boyle et al. 2012).

Between 1 and 3 litres of water were used in order to have a final total natural Cd content of more than 5 ng. A ^{111}Cd-^{113}Cd double spike was added to the samples and Cd was then isolated by means of a three stage column chemistry procedure.

For each step, a fresh resin bed was prepared and cleaned according to the procedure described in Table 2.2. Prior to loading of the resin, the columns were cleaned with acid in several steps in order to get rid of any Cd traces.

The first stage involved 3 mL glass columns with a reservoir of about 100 mL and these were filled with 1.5 mL of strongly basic anion exchange resin (Biorad AG 1-X8, 100-200 mesh). Up to 2 L of sample were loaded on the column; larger volumes were split and loaded on several column. After elution of matrix elements, Cd was eluted from the resin with 2M HNO$_3$ and collected in small Teflon beakers. The residues were then allowed to dry on a hotplate overnight at about 110°C and redissolved with 10M HCl for conversion into the chloride form. They were dried again, dissolved in 0.7M HCl and then ready for loading onto the next column.

The second stage used 100-µL Teflon columns with a reservoir of about 3 mL, and these were filled with about 100 µL of strongly basic anion exchange resin (Biorad AG 1-X8, 200-400 mesh). The procedure was the same as for the first stage, except that (1) all volumes were scaled to the smaller size of the resin column and (2) resin with a smaller particle size (200-400 mesh instead of 100-20 mesh) was employed. As in the first separation stage, the Cd fractions were evaporated and converted to the chloride form by adding 10M HCl and drying again. Following this, the samples were taken up in 200 µL 8M HCl for loading onto the third stage columns of the procedure.

The third separation stage involved the same columns of the same size as the second stage (100-µL Teflon columns with a reservoir of about 3-mL), but the resin is different: 100 µL of

Eichrom TRU Spec resin was used. This resin efficiently holds on to Sn, Mo, Nb and Zr in HCl media, while Cd is not absorbed. Hence the third column chemistry stage provides an efficient separation of Cd from the former elements (Wombacher et al. 2003). The Cd fractions that were eluted from the TRU Spec columns were dried and one drop of concentrated HNO_3 was added to get rid of any chloride. This process was repeated twice and the samples were stored in concentrated HNO_3 until further use. Just prior analysis by MC-ICP-MS, the samples were dried down again and dissolved in an appropriate volume of 0.1M HNO_3.

Table 2.2: Column chemistry procedure for Cd separation, adapted from (Ripperger and Rehkämper 2007a).

First Stage Column		*Second Stage Column*
Biorad AG 1-X8 anion-exchange resin, 100-200 mesh		**Biorad AG 1-X8 anion-exchange resin, 200-400 mesh**
1.5 mL resin in large quartz columns		100 µL resin in small Teflon columns
12 mL HNO_3 2M	Cleaning (important because Cd is eluted with HNO_3 2M)	750 µL HNO_3 2M
0.5 mL MQ-H_2O		100 µL MQ-H_2O
25 mL HCl 6M	Resin conversion to Cl⁻ form	1000 µL HCl 6M
11 mL HCl 0.7M	Resin equilibration	800 µL HCl 0.7M
2 x 800µl seawater + rest of sample	Sample loading	2 x 700 µL sample solution in HCl 0.7M
23 mL HCl 0.7M	Matrix elution	1000 µL HCl 0.7M
10 mL HCl 1M	Matrix elution	650 µL HCl 1M
10 mL HCl 2M	Matrix elution	650 µL HCl 2M
10 mL HCl 8M	Elution of Ag	650 µL HCl 8M
10 mL 0.5M HNO_3 – 0.1M HBr	Elution of Zn	650 µL 0.5M HNO_3 – 0.1M HBr
2 mL HNO_3 2M		130 µL HNO_3 2M
10 mL HNO_3 2M	Collect Cd	700 µL HNO_3 2M

Third Stage Column	
Eichrom TRU Spec Resin	
100 µL resin in Small Teflon column	
10 mL HCl 6M	Column cleaning
100 µL HCl 8M	Column equilibration
200 µL sample solution in HCl 8M	Sample loading
200 µL HCl 8M	Collect Cd
1400 µL HCl 6M	

The Cd isotope measurements were performed with a Nu Plasma HR MC-ICP-MS instrument using a DSN-100 desolvation system (Nu Instruments Ltd, Wrexham, UK) for sample introduction, fitted with glass nebulizers that were operated at flow rates of about 100 to 120 µL min^{-1}. For the analyses, the zoom lens system of the Nu Plasma was adjusted to permit simultaneous collection of the ion beams of ^{114}Cd, ^{113}Cd, ^{112}Cd, ^{111}Cd, ^{117}Sn, and ^{115}In (the last for the correction of isobaric interferences) using Faraday cups connected to 10^{11} Ω amplifiers. Each isotopic analysis consisted of an initial peak centre sequence followed by 3 blocks of 20 integrations (5 s each). A baseline measurement was carried out prior to each block for 15 s, whilst the ion beam was deflected by the electrostatic analyser. The isotopic measurements of samples were carried out using solutions that typically had total Cd concentrations of between 20 and 60 ng/mL, at spike to sample ratios of about 1. On most measurements sessions, the Nu Plasma instrument featured sensitivities for Cd of about 300 to 430 V/µg/mL.

The 'raw' isotopic data acquired by the MC-ICP-MS instrument were processed offline, to determine the 'true', mass-bias-corrected Cd isotope ratios of the unspiked samples, which are reported here using an ε notation, relative to the NIST Standard Reference Material (SRM) 3108 Cd (Abouchami et al. 2013):

$$\varepsilon^{114\ 110}Cd = \left(\frac{\left(\frac{^{114}Cd}{^{110}Cd}\right)_{Sample}}{\left(\frac{^{114}Cd}{^{110}Cd}\right)_{Standard}} - 1 \right) \times 10^4$$

$$(2.1)$$

Unless otherwise stated, the uncertainties of the Cd isotope data reported in Tables 2.3 and 2.4 are based on the 2sd (standard deviation) reproducibilities obtained for multiple bracketing analyses of NIST SRM 3108 Cd – Cd double spike mixtures, which featured Cd concentrations and spike to sample ratios that closely matched the corresponding samples.

The measured ^{111}Cd/^{114}Cd ratios of the spiked samples were used for the determination of the Cd abundances, using the isotope dilution technique. The uncertainties for the concentration data were derived by propagating the 2sm (standard error of the mean) within-run reproducibilities, which were obtained for ^{111}Cd/^{114}Cd through the isotope dilution equations. Based on these calculations, all Cd concentrations have uncertainties of less than ±0.015%, whilst the great majority of samples feature values of better than ±0.007%.

2.3.2. Data quality

Total procedural blanks were determined by processing 1 to 2 litres of >18 MΩ cm acidified water through the column chemistry procedure, and were treated alongside samples in each of the four batches of column chemistry that were performed. These yielded results of 0.2 pg, 1.7 pg, 3.6 pg and 8.1 pg Cd, which is equivalent to less than 0.2% of the total Cd present in the samples. The Cd concentrations were adjusted for these small blank contributions but no corrections were applied to the $\varepsilon^{114/110}$Cd data, as the blank effects were negligible compared to the analytical uncertainty (Tables 2.3, 2.4).

The quality of the Cd isotope and concentration data was monitored by analyses of two well-characterized secondary Cd isotope reference standards (BAM-I012 Cd and Alfa Cd Zurich; Abouchami et al., 2013) and our in-house Solent Seawater reference material (Xue et al. 2012). These standards were analyzed on five different days over a period of two years, and the $\varepsilon^{114/110}$Cd values obtained for both are in excellent agreement with reference values that were recently compiled and based on the results of an inter-laboratory comparison (Table 2.3; Abouchami et al., 2013). The Cd isotope data that were obtained for four separate aliquots of the Solent Seawater were also identical, within uncertainty, to the values published by Xue et al. (2012). However, a small difference in Cd concentration (of about 3 ± 2%) relative to the value found by Xue et al. (2012) could be resolved (Table 2.3). This small discrepancy might be explained by (i) adsorption of Cd onto container walls, as the samples had been stored for more than 2 years prior to the present analyses, or (ii) a minor systematic offset in the calibration of the different Cd double spikes that were used in the present investigation and the study of Xue et al. (2012).

In addition, we also performed triplicate analyses of two water samples, (i) YS-2, 4 m depth from the Mouth of the Ob River and (ii) the Kalix River (Table 2.3). In all cases, the replicate samples were obtained in separate bottles (filled individually from the stock bottle several months prior to use), and they were processed individually through the column chemistry. The results obtained for the Kalix River show excellent reproducibility between the three aliquots, for both $\varepsilon^{114/110}$Cd (total variability of data is ±0.5 ε) and Cd concentration (total variability of ±0.3 pmol/kg; Table 2.3). For the Mouth of Ob, two aliquots show nearly identical Cd concentrations and isotope compositions, whilst the third aliquot is characterized by a much higher Cd content and a highly unusual $\varepsilon^{114/110}$Cd value of about –7 (Table 2.3). Given that the latter sample features both a high Cd abundance and an isotope composition that is more akin to anthropogenic Cd (Rehkämper et al. 2011) than to the other Artic water

36

Table 2.3: Cd concentration and isotope data (as $\varepsilon^{114/110}$Cd) obtained for 2 isotope reference materials, an in-house seawater reference sample and two water samples that were processed in triplicate.

	n[a]	$\varepsilon^{114/110}$Cd	Uncertainty (2sd)	Cd (nmol/kg)[d]
BAM-I012 Cd				
BAM solution 20 ng/g Cd	4	-12.9	±1.0[b]	
BAM solution 30 ng/g Cd	3	-13.7	±0.7[b]	
BAM solution 60 ng/g Cd	2	-13.3	±0.5[b]	
BAM average	9	-13.3	±1.0[c]	
Reference value [e]		-13.3	±0.4	
Alfa Cd Zurich				
Alfa solution 20 ng/g Cd	1	-0.9	±0.7[b]	
Alfa solution 30 ng/g Cd	3	-0.6	±0.8[b]	
Alfa solution 60 ng/g Cd	5	-0.3	±0.5[b]	
Alfa Cd Zurich average	9	-0.5	±0.9[c]	
Reference value [e]		-0.2	±0.5	
Solent Seawater Batch E				
This study	4	+3.0	±0.5[c]	0.1427
Reference value [f]	3	+3.1	±0.3	0.1472
YS-2, 4m depth	1	-7.3	0.9[b]	0.1475
	1	1.4	1.0[b]	0.0192
	1	1.3	1.0[b]	0.0189
Kalix River	1	-4.3	1.0[b]	0.2349
	1	-3.8	1.0[b]	0.2352
	1	-3.3	1.0[b]	0.2351

The concentrations of the BAM and Alfa Cd solutions indicate total Cd concentrations at a spike to sample ratio of ~1.

[a] number of analyses conducted for a sample.

[b] The 2sd uncertainties are based on data obtained for multiple interspersed analyses of the standard, which were carried at similar conditions (Cd concentration, spike/sample ratio) to the sample runs on the same measurement session.

[c] The 2sd uncertainties are calculated based on the n available analyses for this sample.

[d] The Cd concentrations (2sd) have uncertainties of better than 0.015%. (see text).

[e] Abouchami et al. (2013); [f] (Xue et al. 2012)

samples analysed here (Table 2.4), it appears very likely that the unusual result is an artefact of sample contamination. Based on this conclusion, the data obtained for this aliquot are not further considered in this manuscript. The observation furthermore underlines the fact that Cd

is a contamination-sensitive trace element with respect to the sampling of rivers and seawater, and it is hence important to check unusual or spurious results for their integrity by replicate analyses.

2.4. Results and Discussion

2.4.1. Results

The Siberian Shelf samples from the four different localities (Fig. 2.1) have highly variable salinities, which range from near freshwater values (S ≈ 1) to those that approach seawater, with S ≈ 32 (Table 2.4, Fig. 2.2a). The samples from the Ob, Yenisei and Lena areas are in accord with previous hydrological studies in that they reveal a strong stratification of the water column, whereby high-salinity bottom waters are overlain by water with lower salinity (Table 2.4) (Dai and Martin 1995; Guieu et al. 1996). Previous studies have, furthermore, demonstrated that the freshwater imprint on the surface layer is primarily derived from riverine input rather than the melting of sea ice (Dai and Martin 1995; Guieu et al. 1996). Whilst the three samples from the East Siberian Sea area do not provide evidence of water column stratification, this observation presumably reflects only that these samples were all collected at shallow depths of between 3 and 10 m (Table 2.4).

Both phosphate and Cd abundances of the Siberian Shelf water exhibit appreciable variability, with $[PO_4]$ ranging from 0.002 to almost 0.9 µmol/L and [Cd] from 0.02 to 0.46 nmol/kg (Figs. 2.2a and b; Table 2.4). In contrast, these samples only display a narrow range of $\varepsilon^{114/110}Cd$ values, with results of between +1.4 and +5.7 (Fig. 2.2c, Table 2.4). Nonetheless, small differences in Cd isotope compositions can be discerned, as most data have uncertainties of better than ±1 $\varepsilon^{114/110}Cd$ (2sd). Two shelf samples, however, feature higher uncertainties of about ±3 $\varepsilon^{114/110}Cd$ (2sd) due to the low Cd contents (Table 2.4) and the limited sample volume available. The Kalix River is readily distinguished from the Siberian waters, as it has a much lighter Cd isotope composition of $\varepsilon^{114/110}Cd$ = - 3.8 ± 1.0, coupled with a relatively high Cd content of about 0.24 nmol/kg (Table 2.4).

2.4.2. Behaviour of Cd in the mixing zones of the Siberian Shelf

The samples from the Lena area of the Siberian Shelf define a broad positive correlation between a riverine and a seawater endmember in a diagram of [Cd] vs. salinity, and the

endmember compositions are confirmed by three additional samples from the coastal inlets of the Ob and Yenisei Rivers (Fig. 2.2a). In contrast, there are four samples, one from the Ob Mouth and three from the East Siberian Sea area, which deviate from the trend that is delineated by the others (Fig. 2.2a).

The interpretation that quasi-binary mixing plays a key role in governing the distribution of Cd in the shelf waters is supported by the phosphate data. It is notable that the East Siberian Sea samples that are seen to be anomalous in Figure 2.2a also do not fall on the correlation between PO_4 contents and [Cd], which is exhibited by the majority of the waters in Fig. 2.2b (PO_4 contents are not available for the other anomalous samples). These observations are in accord with a scenario where the PO_4 concentrations are primarily determined by mixing of freshwater and seawater with low and high phosphate contents, respectively, whilst the decoupled behaviour of the two elements in some samples (Figs. 2.2a and b) reflects the anomalous distribution of Cd.

The importance of binary mixing is further underlined by the Cd isotope results. In a plot of $\varepsilon^{114/110}Cd$ vs. Cd abundance, the majority of the samples are in accord with a curvilinear trend, which is expected for binary mixing between a low-$\varepsilon^{114/110}Cd$ riverine endmember and seawater with higher $\varepsilon^{114/110}Cd$ (Fig. 2.3c). Whilst it could be argued that biological processes may also be responsible for the variations seen here in Cd isotope compositions, mixing processes are likely to be the primary driver, given the clear correlation that is seen for most samples between Cd contents and salinity (Figs. 2.2a, 2.3a). Based on these findings, the compositions that are expected for binary mixing of river and seawater are investigated in more detail, whereby $\varepsilon^{114/110}Cd$ values are calculated using the following equation (Mariotti et al. 1988):

$$\varepsilon^{114\ 110}Cd_{mix} = \frac{\varepsilon^{114\ 110}Cd_S \cdot Cd_S \cdot f_S + \varepsilon^{114\ 110}Cd_R \cdot Cd_R \cdot f_R}{f_S \cdot Cd_S + f_R \cdot Cd_R}$$

$$= \frac{\varepsilon^{114\ 110}Cd_S \cdot Cd_S \cdot f_S + \varepsilon^{114\ 110}Cd_R \cdot Cd_R \cdot f_R}{Cd_{mix}}$$

(2.2)

where the subscripts *Mix*, *S*, and *R* stand for the mixture, seawater and river water, respectively, and f denotes the respective mass fractions, where $f_R + f_S = 1$. Given that our waters sample three different coastal seas that receive discharges from various rivers (Fig. 2.1), it is too simplistic to expect the distribution of Cd to record perfect binary mixing.

Table 2.4. Name, location, salinity, phosphate concentration, cadmium concentration and isotope composition data for the ISSS-08 and Kalix River samples analyzed in this study.

Area	Station	Water depth [m]	Sample depth [m]	Sampling date	Latitude	Longitude	Salinity	PO_4^{3-} [μmol/L][a]	Cd [nmol/kg][b]	$\varepsilon^{114/110}Cd$	±2sd[c]
Mouth of Ob	YS-2	30	4	19/08/08	73° 24.30' N	72° 59.71' E	7.9	-	0.0191[d]	1.4[d]	1.0
	YS-2	30	20	19/08/08	73° 24.30' N	72° 59.71' E	31.5	0.324	0.2207	5.7	0.7
Mouth of Yenisei	YS-3	38	4	19/08/08	73° 29.52' N	79° 53.09' E	5.5	0.002	0.0327	4.6	3.5
	YS-3	38	25	19/08/08	73° 29.52' N	79° 53.09' E	32.3	0.832	0.1993	5.6	0.6
Lena Area	YS-4	52	3	23/08/08	75° 59.22' N	129° 59.05' E	11.5	-	0.0535	5.4	1.0
	YS-4	52	25	23/08/08	75° 59.22' N	129° 59.05' E	31.9	0.520	0.1206	4.8	0.9
	YS-6	34	3	24/08/08	74° 43.44' N	130° 0.98' E	5.2	-	0.0584	2.6	1.0
	YS-6	34	20	24/08/08	74° 43.44' N	130° 0.98' E	29.8	0.697	0.1853	4.4	0.6
	YS-8	13	3	24/08/08	73° 33.94' N	130° 0.47' E	5.3	0.008	0.0447	4.9	0.9
	YS-8	13	9	24/08/08	73° 33.94' N	130° 0.47' E	14.5	0.064	0.1063	4.4	0.9
	YS-11	12	2	25/08/08	73° 1.11' N	129° 59.35' E	2.7	0.094	0.0269	2.9	1.8
	YS-12	13	4	26/08/08	71° 54.99' N	132° 34.54' E	24.9	0.584	0.1894	3.2	0.8
	YS-13	22	5	26/08/08	71° 58.08' N	131° 42.08' E	3.8	0.014	0.0476	3.8	0.7
	YS-14	8	5	27/08/08	71° 37.82' N	130° 2.97' E	1.3	0.150	0.0230	2.5	2.8
	YS-122	28	28	16/09/08	74° 30.19' N	136° 0.58' E	31.2	0.874	0.2163	3.4	0.6
	YS-128	60	4	17/09/08	76° 59.22' N	130° 21.34' E	20.7	–	0.0701	4.9	1.0
East Siberian Sea Area	YS-30A	10	3	01/09/08	71° 21.46' N	152° 9.16' E	18.3	–	0.4639	3.4	0.5
	YS-120	35	4	15/09/08	73° 17.51' N	155° 10.05' E	20.9	0.759	0.4024	3.2	0.7
	YS-121	18	10	16/09/08	74° 22.31' N	145° 16.85' E	18.0	0.365	0.3232	2.4	0.6
Kalix River	Kamlunge		1	10/06/95	66° 00' N	22° 85' E	~0	–	0.2351	–3.8[d]	1.0

[a] The phosphate concentration were measured on board using a Westco SmartChem spectrophotometer.

[b] The Cd concentrations have uncertainties of ±0.015%, with the great majority better than ±0.007%; these uncertainties are based on the 2sm within-run precision of the $^{111}Cd/^{114}Cd$ data that were used in the isotope dilution calculations (see text for details).

[c] The 2sd uncertainties of the Cd isotope data are based on data obtained for multiple interspersed analyses of the standard, which were carried at similar conditions (Cd concentration, spike/sample ratio) to the sample runs on the same measurement session.

[d] Average of several samples analysed for this station (see Table 2.3).

Hence, the calculations incorporate limited, albeit realistic, variability in the endmember compositions, such that the mixing generates quasi-binary mixing arrays.

Figure 2.2: Cd concentrations versus (a) salinity, (b) phosphate, and (c) Cd isotopic composition for the ISSS-08 samples from the Siberian Shelf. The error bars for the Cd concentration are smaller than the size of the symbol, and the uncertainties for the Cd isotopic compositions are given in Table 2.4. In (b), a linear regression for the samples from the Ob, Yenisei, and Lena areas gives a regression coefficient of $r^2 = 0.71$. Brown triangles: Mouth of Ob; green diamonds: Mouth of Yenisei; red circles: Lena Area; black squares: East Siberian Sea Area; small grey dots: samples collected in the Lena River and in the Laptev Sea in September 1991 (Guieu et al. 1996).
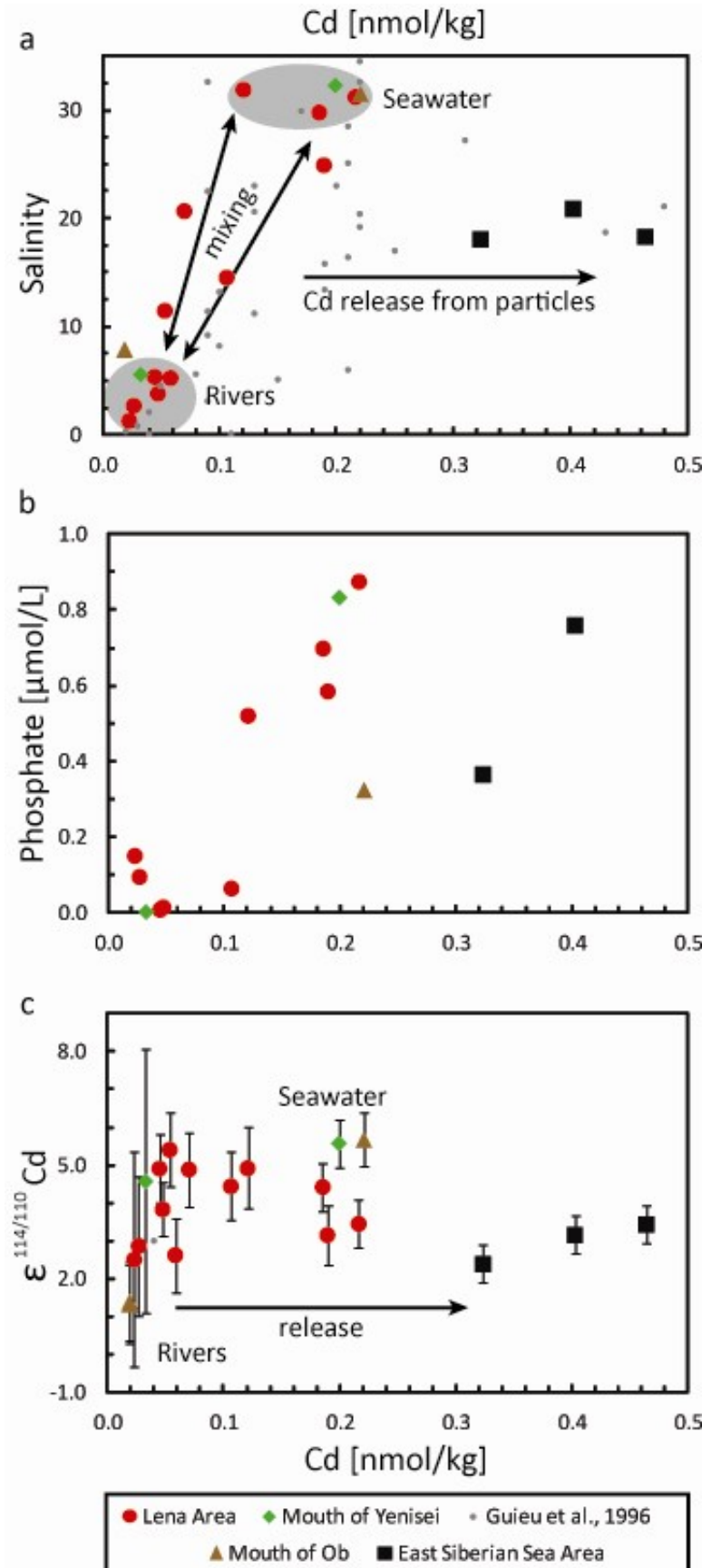
For the seawater endmember, the calculations assume a composition characterized by S = 34.5, [Cd] = 0.10 to 0.25 nmol/kg and $\varepsilon^{114/110}$Cd values of between +5 and +6, in agreement with results of previous work (Fig. 2.3). In particular, published studies (Ripperger et al. 2007b) provide $\varepsilon^{114/110}$Cd values of +4.8 ± 1.0 and +6.0 ± 1.4 for Arctic Ocean surface water, following correction for the offset between the different zero-epsilon reference materials used here and previously (Abouchami et al. 2012). The general conclusions of the modelling are furthermore identical, for seawater $\varepsilon^{114/110}$Cd values as low as +4.5. Typical Cd concentrations of 0.19 to 0.37 nmol/L and 0.09 to 0.30 nmol/L were reported for the Kara and Laptev Seas, respectively, at salinities of up to 34.5 (Martin et al. 1993; Dai and Martin 1995; Guieu et al. 1996).

For the riverine endmember, which should be characterized by S ≈ 0, the calculations assume Cd contents of 0.02 to 0.06 nmol/kg (Fig. 2.3). These concentrations are justified by previous Arctic river studies, which determined typical Cd abundances of 0.01 to 0.06 nmol/L for water samples from the Ob, Yenisei and Lena Rivers (Table 2.1). Higher Cd concentrations of 0.13 to 0.15 nmol/L were found for a few samples from the Ob and Yenisei Rivers, but these were thought to reflect contributions from anthropogenic sources (Moran and Woods 1997; Guay et al. 2010). Cadmium isotope data are currently not available for any of the Arctic rivers, but key constraints are provided by the present data. A robust regression calculated for the $\varepsilon^{114/110}$Cd vs. 1/[Cd] data of samples that are in accord with conservative mixing (Fig. 2.4), clearly reveals a non-zero slope (despite of the uncertainty), which is indicative of a riverine composition with isotopically lighter Cd than the seawater. This conclusion is supported by the observation that the Siberian Shelf samples with the lowest salinities (S = 1.3 to 5.5) feature $\varepsilon^{114/110}$Cd ≈ +2.5 to +4.9 at Cd contents (of 0.023 to 0.058 nmol/kg) that closely resemble Arctic rivers (Table 2.1). This suggests that the rivers are unlikely to be characterized by $\varepsilon^{114/110}$Cd values of less than +0 and greater than +5. A more detailed investigation shows, however, that the mixing lines of Figures 2.3 b and c for river endmembers with $\varepsilon^{114/110}$Cd values of 0 and +5 (black dashed lines) clearly provide only a very poor fit to the observed data trends. In contrast, a satisfactory fit can be achieved if the river waters are assigned an endmember composition of $\varepsilon^{114/110}$Cd = +2 ± 1 (grey fields shown in Figs. 2.3 b and c) and it is therefore reasonable to assume that this represents a reasonable estimate for the Cd isotope composition of the Arctic rivers.

Figure 2.3: Comparison of the analytical data (see Fig. 2.2 for legend) with compositions predicted for binary mixing between inferred Arctic river water and a seawater endmember (grey fields). Note the reduced scales in comparison to Fig. 2.2, which leads to East Siberian Sea samples not being shown in panels a and b. (a) Salinity and (b) $\varepsilon^{114/110}$Cd vs. Cd concentrations; panel (c) shows $\varepsilon^{114/110}$Cd vs. salinity. The salinity ranges from 0.1 to 34.5. Seawater endmember: [Cd] = 0.1 to 0.25 nmol/kg and $\varepsilon^{114/110}$Cd = +5.5 ± 0.5, both for the grey lines and for the black dashed lines. River water endmember: [Cd] = 0.02 to 0.06 nmol/kg; $\varepsilon^{114/110}$Cd = +2 ± 1 for the grey areas, and $\varepsilon^{114/110}$Cd = 0 to +5 for the black dashed lines.
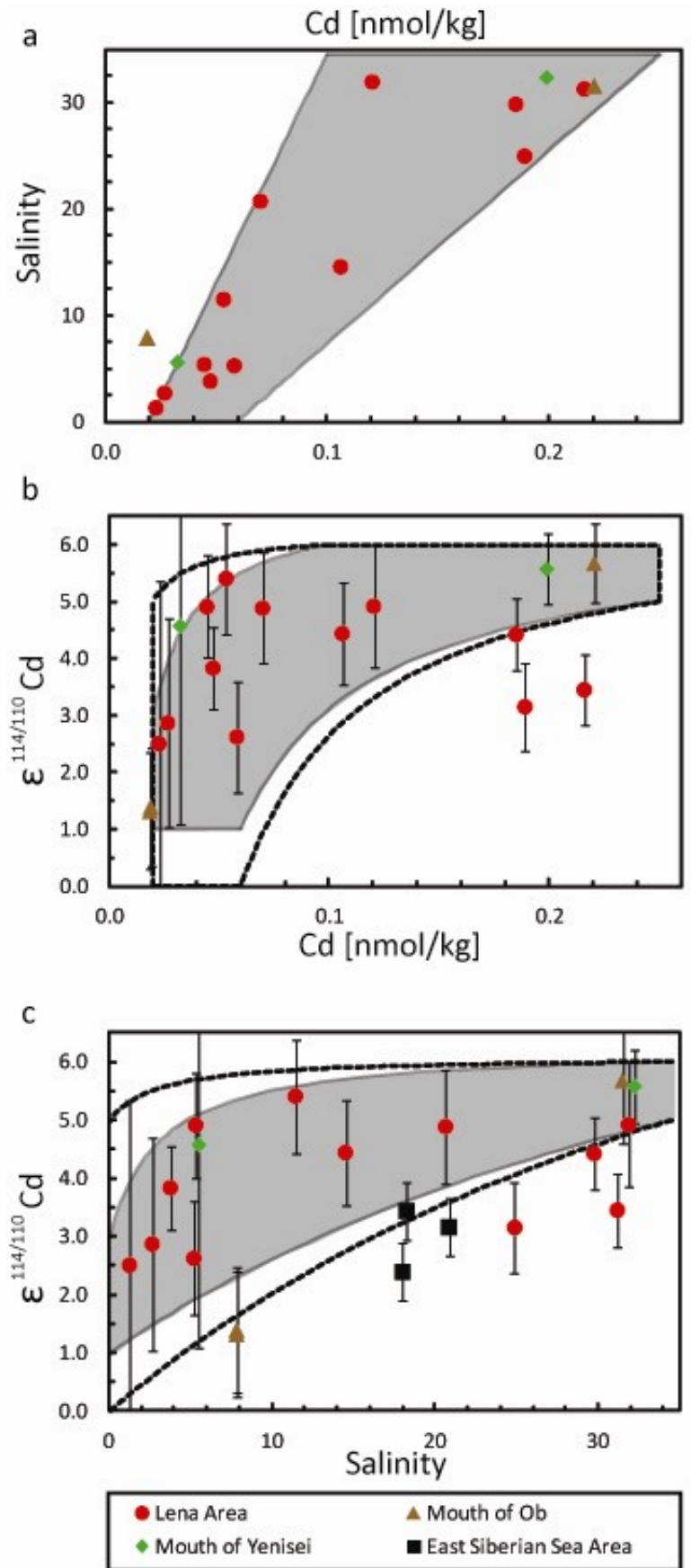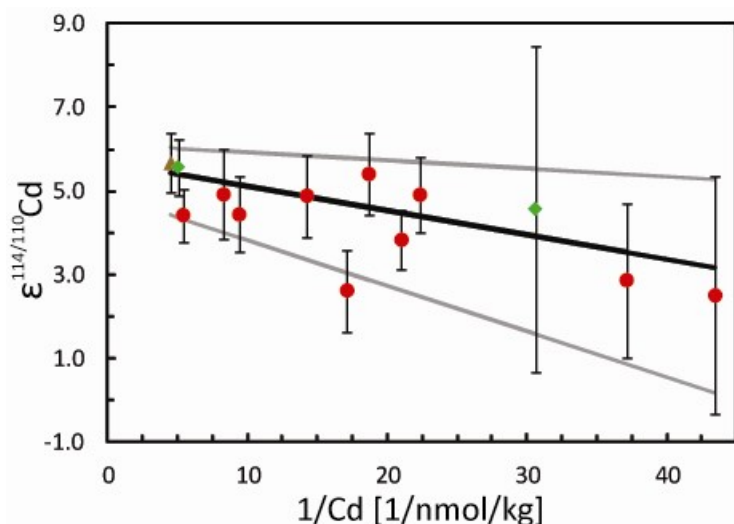
Figure 2.4: Robust regression (black line) made on a diagram of $\varepsilon^{114/110}$Cd vs. the inverse of the Cd concentrations with the samples behaving conservatively only. The grey lines represent the regression taking into account the errors on the slope and on the intercept (95% confidence level).

2.4.3. Non-conservative behaviour of Cd in the mixing zone of the Siberian Shelf

Whilst the previous discussion demonstrated that mixing between riverine and seawater plays a key role in determining the distribution of dissolved Cd on the Siberian Shelf, there are a few samples which are not in accord with this simple scenario (Fig. 2.2). Of these, only the shallow-water from the mouth of the Ob shows a small, yet clear, deviation toward lower Cd contents (Fig. 2.2a), indicating that this sample may record minor loss of Cd, presumably due to adsorption onto particles at low salinities. Such behavior of Cd has not been previously reported for Siberian rivers but was observed to play an important role in the Rhine estuary (Duinker and Nolting 1977) and may possibly have been missed in earlier investigations because it requires the detection of small differences in Cd concentrations at low Cd contents (Fig. 2.2a). This is consistent with the high concentration of suspended material, and so high effective surface area per volume for adsorption in the Ob River (Dai and Martin 1995; Hatje et al. 2003).

In contrast, the remaining deviations from conservative mixing are for samples that exhibit an excess of dissolved Cd contents. This is most clearly seen for three samples from the East Siberian Sea area, as they show deviations from the binary mixing trends that are evident from the (anomalously high) Cd concentrations alone (Fig. 2.2a). Similar deviations from conservative mixing have also been found for Cd in previous studies (Martin et al. 1993; Dai and Martin 1995; Guieu et al. 1996) of Siberian rivers (small symbols in Fig. 2.2a). Of interest is the observation that the Cd isotope data reveal small but significant deviations for two further samples from the mixing zone of the Lena River (Figs. 2.3 b and c). The finding

that some anomalous Cd samples are only detectable with the aid of the $\varepsilon^{114/110}$Cd data is significant in itself, because it confirms that isotopic analyses can be a valuable tool for tracing the cycling of Cd in the marine environment. In the following, we discuss the anomalous East Siberian Sea and Lena samples, which all feature $\varepsilon^{114/110}$Cd values of about +2.5 to +3.5.

The anomalous samples from the Lena and East Siberian Sea areas are characterized by $\varepsilon^{114/110}$Cd values that are intermediate between the riverine and seawater endmembers (Figs. 2.3 b and c) and which are not too dissimilar from average crustal materials ($\varepsilon^{114/110}$Cd = +0.5 ± 1.0; (Schmitt et al. 2009; Rehkämper et al. 2011). This indicates that the high Cd contents are probably of natural origin. If one accepts this conclusion there are, in principle, two possible sources for the excess Cd. It is conceivable that this is derived from further endmember sources of dissolved Cd and these are most likely to be either additional rivers and/or benthic fluxes from reduced C-rich, and hence Cd-rich sediments. Alternatively, the high Cd contents may be due to desorption of Cd from suspended riverine particles, as a result of reactive behaviour of Cd in the mixing zone.

An evaluation of results from this and previous investigations strongly argues against additional riverine or benthic fluxes. First, the data of this study essentially rule out that the anomalous samples reflect dissolved Cd fluxes from additional riverine discharges to the Siberian Shelf. This follows from the extrapolations of the results, which suggests that such riverine sources would typically need to feature Cd contents of >0.2 nmol/L (Figs. 2.2, 2.3) but this significantly exceeds the dissolved Cd concentrations that were observed in this (Table 2.4) and other investigations (Table 2.1) for Siberian rivers. Second, Cd contributions from benthic fluxes are unlikely, because previous work has shown that anoxic and suboxic shelf sediments typically accumulate Cd and are not a significant source of dissolved Cd fluxes to seawater (van Geen et al. 1995; Böning et al. 2004). This conclusion is further supported by the anomalously high dissolved Cd/PO$_4$ ratios of the East Siberian Sea samples (Fig. 2.2b), which require preferential release of Cd relative to PO$_4$, but benthic fluxes are known to be an important source of dissolved marine phosphorous (Ruttenberg 2003). In addition, all but one of the East Siberian Sea and Lena samples with anomalous Cd contents were collected more than 7 m above the seafloor (Table 2.4), such that the stratification of the water column will essentially prevent the incorporation of benthic fluxes.

Together, these results provide firm evidence against the interpretation that either further rivers or benthic fluxes from sediments can account for the anomalous Lena and East

Siberian Sea samples. Hence, it is more likely that the excess Cd contents of these waters are due to non-conservative behaviour of Cd in the mixing zone. This inference is in accord with the results of previous studies of Arctic (Fig. 2.2a) and numerous other rivers, which have found evidence for the release of Cd from suspended riverine particles during mixing with seawater (Boyle et al. 1982; Elbaz-Poulichet et al. 1987; Shiller and Boyle 1991; Martin et al. 1993; Dai and Martin 1995; Guieu et al. 1996). A number of explanations have been put forward to account for this behaviour, including (i) the formation of stable Cd chloro- and sulfato-complexes in seawater (Elbaz-Poulichet et al. 1987; Comans and Vandijk 1988; Waeles et al. 2005), (ii) the competition between Cd^{2+} and major seawater cations, such as Ca^{2+} and Mg^{2+}, as a driver for the desorption of Cd from particles (Paalman et al. 1994), and (iii) the presence of organic matter supplied by rivers (Elbaz-Poulichet et al. 1996; Waeles et al. 2004; Waeles et al. 2005; Waeles et al. 2009).

Regardless of the mechanism, non-conservative behaviour of riverine Cd during mixing with seawater is important, because this can significantly increase the riverine Cd fluxes that are delivered to the oceans beyond the levels which are expected from the generally low dissolved Cd contents of the rivers (Figs. 2.2, 2.3; Table 2.1). Processes such as complexation and ion exchange may furthermore be associated with significant isotope fractionation, and hence it will be useful to evaluate the isotopic impact of the Cd fluxes that are derived by release from particles. Extrapolation of our data to a zero-salinity concentration for the Lena suggests that this river may deliver a net Cd input concentration of >0.2 nmol/kg to the Siberian Shelf and even higher values are implied by the East Siberian Sea results (Figs. 2.2, 2.3). Such inputs exceed the typical dissolved Cd content of ~0.05 nmol/L for Siberian rivers (Tables 2.1 and 2.4) by more than a factor of four. In comparison, previous studies have found that the effect of estuarine processes on dissolved Cd fluxes differs widely between rivers but increases in the net Cd fluxes by factors of between 2 and 20 (in comparison to the riverine fluxes) were inferred for many localities (Elbaz-Poulichet et al. 1987; Guieu et al. 1996).

2.4.4. The $\varepsilon^{114/110}$Cd of the riverine input to the ocean

The conservative behaviour of Cd which is observed for the mixing zone of the Siberian Shelf is of particular significance because it provides a well-defined average composition of $\varepsilon^{114/110}$Cd = +2 ± 1 for the dissolved riverine Cd flux, which characterises several large Siberian rivers. This estimate is valuable because it can be compared with the isotope

composition of $\varepsilon^{114/110}Cd$ = +0.5 ± 1.0 that was previously inferred for average continental crust (Schmitt et al. 2009; Rehkämper et al. 2011), even though such a comparison must be undertaken with care, as both values are derived from limited and geographically unrelated datasets. Taken at face value, the dissolved Cd of the Siberian rivers is either identical to or slightly heavier than the crustal composition and this implies that Cd isotope fractionation during weathering is either minor or insignificant. The Lena and East Siberian Sea data of Figures 2.2 and 2.3 also suggest that the Cd desorbed from particles features an $\varepsilon^{114/110}Cd$ value of about +2 to +3, to account for the measured isotope data of $\varepsilon^{114/110}Cd$ = +2.4 to +3.4 (Table 2.4). This result indicates that the isotope composition of desorbed Cd is identical to or only slightly heavier compared to the dissolved riverine Cd, which was inferred to feature $\varepsilon^{114/110}Cd \approx$ +2 ± 1. This lack of isotopic contrast is in accord with the observation that adsorption of dissolved Cd from seawater onto ferromanganese sediments is not accompanied by isotope fractionation (Schmitt et al. 2009; Horner et al. 2010) and it thus supports the conclusion that weathering is associated with no or only minor Cd isotope effects.

If these above results are taken as representative, they can be applied to further develop models of the global marine Cd isotope mass balance. In particular, they suggest that release of particle-bound Cd during mixing with seawater will primarily increase the net Cd fluxes to the oceans from rivers, whilst the $\varepsilon^{114/110}Cd$ value will be unchanged or experience only a marginal increase with respect to the dissolved riverine isotope composition. Hence, the total riverine Cd fluxes to the Siberian Shelf will also exhibit an isotope composition that is either identical to or slightly heavier than average continental crust ($\varepsilon^{114/110}Cd \approx$ –0.5 to +1.5). In the latter case, the Cd fluxes of the Siberian rivers would closely resemble the well-characterized and nearly constant Cd isotope composition of marine deep waters, which feature $\varepsilon^{114/110}Cd \approx$ +3.0 (Ripperger et al. 2007b; Xue et al. 2013).

In contrast to the Siberian rivers, the Kalix River features a significantly lower $\varepsilon^{114/110}Cd$ value of –3.8, coupled with a relatively high Cd concentration of 0.235 nmol/kg (Table 2.4). Given this significant difference in composition, it is reasonable to consider whether the three Kalix samples (Table 2.3) were potentially contaminated during collection and/or storage. This possibility is underlined by the observation that the Kalix samples feature Cd systematics which resemble the Mouth of Ob sample aliquot that was thought to be contaminated with isotopically light anthropogenic Cd (Table 2.3). Whilst contamination cannot be ruled out completely it is, however, probably not (primarily) responsible for the distinct composition of the Kalix River samples because sample collection and storage used

techniques and materials that are very similar to those of other sampling campaigns, which yielded water samples that did not feature significant Cd contamination (e.g., Semiletov et al. 2008 and Ripperger et al. 2007b). Hence, it is more likely that the distinct Cd systematics of the Kalix are a true signature of the river, which could either have a natural or anthropogenic origin.

The Kalix River is part of a large unregulated water system, which drains a rural region without larger settlements and industrial plants, and that features only minor agricultural activity. It is nonetheless conceivable that the Aitik open-pit porphyry Cu-Ag-Au mine, which is situated about 100 km upriver from the Kamlunge sampling station on a tributary of the Kalix, has an impact on the riverine budgets of Cd and other metals. Published geochemical data, which has been obtained for various elements (including Zn and Pb but not Cd) provide no evidence, however, that this mine is a significant source of riverine contamination. As a consequence, the Kalix River is generally considered to be in a pristine, natural state (Ingri 1996; Ingri et al. 1997; Andersson et al. 2001; Ingri et al. 2005; Dahlqvist et al. 2007; Pekka et al. 2008).

Importantly, our samples were collected in early June, when the Kalix featured the particularly high water discharge rates that are characteristic of the spring snowmelt. This annual melt phase is accompanied by high riverine TOC (total organic carbon) contents that are thought to reflect a surge of organic material, which is flushed from the peatlands that cover about 20% of the drainage basin (Ingri et al. 1997; Andersson et al. 2001; Ingri et al. 2005; Dahlqvist et al. 2007). The high Cd concentrations of our Kalix River samples are thus thought to represent a seasonal peak, which is caused by or related to this flushing. Support for this conclusion is provided by (i) the observation that mire environments can act to both accumulate and release large quantities of Cd and other metals depending on environmental conditions, such as outflow intensity (Kruk and Podbielska 2005) and (ii) previous work, which has shown that seasonal peaks also occur for Zn, whereby the maximum Zn contents exceed the average baseflow value, which resembles the Zn concentration of the Lena River at 0.74 µg/L, by about a factor of 10 (Guieu et al. 1996; Ingri 1996; Pekka et al. 2008). Whilst these conditions can account for the high Cd content of the Kalix River, it is currently not possible to identify the origin of the distinct negative $\varepsilon^{114/110}$Cd value of -3.8 (Table 2.4). It is conceivable, however, that this result reflects biological isotope fractionations that took place in the mire setting and/or preferential leaching of isotopically light Cd from peatland stores, such as minerals and/or organic matter with high contents of (adsorbed) Cd.

Regardless of the origin of the light isotope signature, the Kalix data suggest that local hydro-geological conditions may have a profound impact on the Cd isotope composition of rivers. It will hence be important to sample rivers that drain regions with distinct geological and environmental features and which may thus be expected to produce different Cd signatures, to obtain a more reliable estimate of the global average Cd isotope composition for the dissolved riverine flux to the ocean. Such studies should furthermore consider the role of anthropogenic inputs, as these may also have an important impact on both riverine Cd concentrations and isotope compositions.

2.5. Conclusion

Nineteen water samples that were collected along the Siberian Shelf reveal highly variable salinities and Cd concentrations, as they sample the mixing zones of four large Siberian rivers with the coastal seas of the Arctic Ocean. The waters also exhibit small, but resolvable, Cd isotope fractionations with $\varepsilon^{114/110}Cd$ values ranging from about +1.4 to +5.7. The data for the majority of the samples are in accord with the systematics expected for quasi-binary mixing between Arctic seawater, characterized by $[Cd] \approx 0.10$ to 0.25 nmol/kg, $\varepsilon^{114/110}Cd \approx +5.5 \pm 0.5$, and river waters with Cd contents of 0.02 to 0.06 nmol/kg and $\varepsilon^{114/110}Cd \approx +2 \pm 1$. The latter result implies that the Siberian rivers have an isotope composition that is similar to or only slightly heavier than average continental crust, which was previously inferred to be characterized by $\varepsilon^{114/110}Cd = +0.5 \pm 1.0$ (Rehkämper et al. 2011). This suggests that weathering processes generate no significant or only relatively minor Cd isotope fractionations.

Five water samples from the Lena and East Siberian Sea areas have excess Cd contents, which reveal non-conservative Cd behaviour in the mixing zone. Our data thus concur with previous studies that provided evidence for the release of Cd from suspended riverine particles during mixing with seawater and which have suggested that the net riverine Cd fluxes to the oceans may be significantly affected by this reactive behaviour. The isotopic data obtained for these samples show that the released particulate Cd is characterized by $\varepsilon^{114/110}Cd \approx +3$. This implies that the net Cd fluxes of the Siberian rivers to seawater are also likely be to characterized by $\varepsilon^{114/110}Cd \approx +2 \pm 1$, a value that is either identical to or intermediate between the composition of the continental crust and marine deep waters that

were previously demonstrated to feature $\varepsilon^{114/110}Cd \approx +3.0$ (Ripperger et al. 2007b; Xue et al. 2013).

Triplicate analyses of a sample from the pristine boreal Kalix River yielded a Cd concentration much higher than that observed in the Siberian rivers and a distinct light isotope composition of $\varepsilon^{114/110}Cd \approx -3.8$. Whilst we currently cannot exclude that these systematics reflect anthropogenic contamination of either the river or the sample (during collection/storage), they are most likely a consequence of the distinct hydrological and geological setting of the Kalix catchment basin. If correct, this conclusion indicates that the Cd isotope composition of rivers may display significant regional variability, such that more river samples from distinct areas will need to be analysed before the global average Cd isotope composition of the riverine flux to the ocean can be determined with certainty.

In summary, these observations emphasize the importance of stable isotope analyses for investigations of the biogeochemical cycles of trace metals. In particular, the Cd isotope results are shown to provide important constraints, which are not available from concentration data alone, for studying the behaviour and distribution of Cd in a shelf environment.

Acknowledgements

Chapter 3

MATERIALS AND METHODS FOR THE ANALYSIS OF NEODYMIUM ISOTOPIC COMPOSITIONS AND CONCENTRATIONS IN SEAWATER

Abstract

Precise and accurate measurements of neodymium (Nd) isotopic compositions and concentrations of small sample masses (≤30 ng Nd) are increasingly necessary in the geosciences. This chapter presents the method established in the MAGIC laboratory for the simultaneous analysis of seawater Nd isotopic compositions and concentrations. Five to ten litres seawater samples are spiked with ^{150}Nd, equilibrated, and pumped through C_{18} cartridges loaded with a complexing agent to isolate the rare earth elements (REE) from the seawater matrix. Neodymium is subsequently isolated using TRU spec and Ln spec chemistries, with an important oxidation step ($HClO_4$) inbetween to ensure good yields. Neodymium isotopes and concentrations are subsequently analysed as NdO$^+$ on a Trition TIMS using a micro-loading technique and TaF_5 activator on single W filaments. Long term external reproducibility obtained for 5 ng pure metal standard (JNdi-1) is 23 ppm (2sd) and repeated measurements of our in-house seawater standard (~10-15 ng Nd) yielded 31 ppm (2 sd), and <0.1 ppt for Nd concentrations over the course of 19 months. Accuracy of results has been verified during the international GEOTRACES intercalibration and is continuously monitored using certified rock standard BCR-2.

3.1. Introduction

The neodymium isotopic composition of seawater has spurred a wide interest in the scientific community for more than 30 years (Piepgras et al. 1979; Piepgras and Wasserburg 1980). However, the amount of data available so far is relatively scarce, and not homogenously distributed in the ocean basins: ~ 880 measurements have been carried out on dissolved Nd isotopes, a quarter of which are surface samples, and about half of the deep water analyses are coming from the North Atlantic and North Pacific Ocean (Lacan et al. 2012). This scarcity of data is related to the low concentration of neodymium in seawater, which is in the order of ~ 1 to ~ 10 ppt (10^{-12} to 10^{-11} g/g). The isotopic analysis of low abundance Nd samples from the ocean is not trivial and typically large volumes of seawater are required (~10 litres).

Neodymium isotopic ratios are typically measured by Thermal Ionisation Mass Spectrometry (TIMS) or by Multiple Collector Inductively Coupled Mass Spectrometry (MC-ICP-MS). Whereas arguments in favour of MC-ICP-MS are a significantly reduced analysis and sample preparation time, the advantage of TIMS measurement, especially when considering improved ionization efficiency during NdO^+ measurements compared with metal runs (Nd^+), is the ability to obtain high precision data on small abundance samples (e.g., Li et al. 2007; Chu et al. 2009; Harvey and Baxter 2009; van de Flierdt et al. 2012). However, these days the most sensitive MC-ICP-MS instruments can compete with the precision achievable by TIMS. Practically, the choice of measurement method is limited by the instruments available in the laboratory. For the present study, a Thermo Finnigan Triton TIMS and a Nu Plasma HR MC-ICP-MS were at disposition. While an internal precision of 0.5 epsilon units can be achieved for ~10ng Nd samples on the Nu Plasma instrument, an internal precision of 0.1 epsilon units for samples as small as 2-5 ng on the Triton TIMS offer the superior data quality. We therefore chose to develop a NdO^+ methodology to analyse small abundance Nd isotope samples on the TIMS in the MAGIC laboratory. The goal of analysing seawater samples with less than 10 ng of Nd using this methodology required (i) to develop an efficient separation of Nd from the other rare earth elements (REE), (ii) to establish well characterised oxygen isotope ratios and, (iii) to perform an efficient separation of the REE from the seawater matrix (i.e. high Nd recovery and time-efficient).

This chapter presents in detail how the separation of REE from seawater has been achieved, and gives details about the chemistries used to further isolate the Nd. The method development for measurements of Nd as NdO^+ by TIMS is only described briefly, as a detail account can be found elsewhere (Crocket et al. 2014). Figure 3.1 presents an overview of the method used in the present study. Other methods to analyse the Nd isotopic composition of seawater used by the international community are described in van de Flierdt et al. (2012).
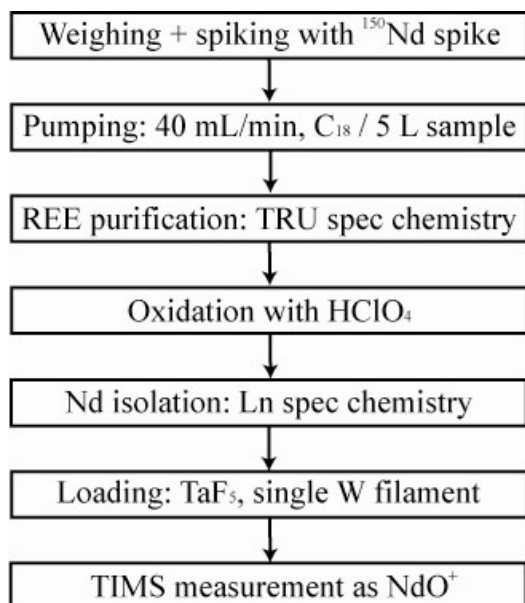
Figure 3.1: Overview of the method used to purify seawater samples and analyze them for their Nd isotopic composition and Nd concentration.

3.2. Reagents

Concentrated HNO_3 (15.4 M) and 6 M HCl were purified by distillation in quartz stills, while concentrated HCl was distilled in a Savillex elbow-style assembly. Diluted acids were prepared using ultrapure water (18.2 MΩ cm, Milli-Q®, Millipore, USA; called MQ-H_2O hereafter). The following additional reagents were purchased from Fisher Scientific (i–iv) and Merck (v-vi): (i) perchloric acid, 65-71% $HClO_4$, Optima grade; (ii) hydrogen fluoride, 47-51% HF, Optima grade; (iii) sulphuric acid, 93-98% H_2SO_4, Optima grade; (iv) ammonia solution, 20-22% NH_3, Optima grade; (v) hydrogen peroxide, 30% H_2O_2, Suprapur; (vi) ortho-phosphoric acid, 85% H_3PO_4. Acid-cleaned Savilex Teflon vials were used throughout the entire study.

3.3. Preconcentration of REE from seawater samples

3.3.1. Materials and preparation

Sep-Pak® C18 Classic cartridges were purchased from Waters. They consist of silica-based bonded phase with strong hydrophobicity, used to adsorb analytes of even weak hydrophobicity from aqueous solutions. Prior to use, cartridges were cleaned by filling them with 0.5 M distilled HCl and allowing equilibration for 24 hours in a Class 100 Laminar Flow hood within a general wet chemistry laboratory with pre-filtered air. Following several rinses

with MQ-H$_2$O, the cartridges were left to equilibrate with ultrapure water for 24 hours. After another rinse with about 10 mL MQ-H$_2$O, the pH of the deionised water dripping from the cartridges was checked to ensure all HCl had been washed off. If the pH was found to be lower than that of MQ-H$_2$O, the cartridges were further rinsed. The cleaned cartridges were then wrapped individually in cling film and stored in a sealed plastic bag until loading with the complexing agent.

The complexing agent consisted of a mixture of 65% bis(2-ethylhexyl) hydrogen phosphate and 35% 2-ethylhexyl dihydrogen phosphate. It was purchased from TCI Europe N.V. and used as received. 300 mg (~300 µL) of this agent was loaded into the long end of each cartridge using a 10-100 µL pipette. The mixture was then pushed using a 100-1000 µL pipette, the tip of which had been cut off, and penetration levels down to two thirds of the cartridge volume were monitored through discolouration (glassy look). This step had to be done under an extraction hood due to the potential toxicity of the reagent. In order to use the loaded cartridges to pre-concentrate REE from up to 10 L of seawater samples, a peristaltic pump was used (Masterflex$^®$ L/S$^®$ Series Precision Pump Drives mounted with four pump heads (Masterflex$^®$ L/S$^®$ Easy-Load$^®$), purchased from Cole-Parmer through Fisher Scientific). The tubing used for pumping was tygon Masterflex$^®$ L/S 16 (inner diameter of 3.2 mm) ordered from Cole-Palmer (UK). Prior to use, it was leached for 2 days in 1M distilled HCl, followed by repeated rinsing with MQ-H$_2$O. Importantly, the tubing was not reused for different samples, since the blank was higher when the tubing was reused (~ 150 pg Nd for a new tubing (0.016 pg(Nd) / g(MQ-H$_2$O)) against ~ 420 pg for a tubing used previously for another sample and cleaned with 1M HCl afterwards (0.047 pg(Nd) / g(MQ-H$_2$O))).

Cartridges and tubing were connected via PVDF straight connectors (barbed fittings, 1/8") purchased from Cole-Parmer, leached for 48 hours in 3M HCl distilled and rinsed with MQ-H$_2$O before use.

3.3.2. Working procedure

The working procedure to use C18 cartridges to pre-concentrate REE from seawater samples was based on the method of Shabani et al. (1992).

All seawater samples were first weighted, and then spiked with ^{150}Nd spike in order to achieve a ratio ^{150}Nd$_{sample}$/^{150}Nd$_{spike}$ = 1. The samples were then let to equilibrate for at least one week.

The pH of the samples, which were typically acidified at sea to pH < 2, was raised to 3.5 a couple of days before pumping using NH$_4$OH, and checked again just before starting the procedure (Shabani et al. 1992). Typically between 1 and 2 mL of ammonium hydroxide had to be added per L of seawater to achieve the right pH. Seawater was pumped through the cartridges (typically two in sequence) at a flow rate of 40 mL/min. Neodymium recovery was about 90% when the sample was pumped at 20 mL/min or at 40 mL/min, and it dropped to about 80% when pumped at 60 mL/min. It is important to note that the set up should pump the seawater into the cartridge through the longer end. The shorter end was connected to tubing which was reused and channelled the waste water (i.e. REE-free seawater) into a waste container. Since only up to 5 L of seawater can be pumped through one cartridge (Jeandel et al. 1998), two cartridges connected via PVDF straight connectors were mounted in sequence for larger seawater samples (up to 10 L). The cartridges were not reused for different samples.

The REE retained on the complexing agent were subsequently eluted with 5 mL 0.01M HCl (with a pipette) in order to remove most of Ba, followed by 35 mL 6M HCl (10 mL/min) to collect the REE. Following elution, the samples were dried at 160˚C, and refluxed with 4 mL aqua regia (3 mL concentrated HCl + 1 mL concentrated HNO$_3$) at 120˚C for about 24 hours. This drying step, as well as all the following steps and the column chemistries, was performed in a class 10 laminar flow hood in the Class 1000 clean room laboratory of the MAGIC facilities at Imperial College London (UK). The samples were subsequently converted to nitric form by dissolving/drying three times in ~15M HNO$_3$.

3.4. Preparation of in-house and certified rock standards

3.4.2. In-house seawater standard

In order to set up the pumping method, and to assess reproducibility of the entire procedure, two in-house seawater standards were used: BATS 15 m depth, and BATS 2000 m depth, both collected on the R/V Knorr in June-July 2008 in the Atlantic Ocean (Bermuda-Norfolk; KN193-6) during the first GEOTRACES intercalibration cruise. Sub-surface waters were collected using the UCSC designed 'GeoFish' towed sampling system, while deep

waters were collected using multiple casts of the trace metal clean GEOTRACES rosette. Samples were filtered using 0.2 µm Osmonics cartridge filters in a portable clean van environment and homogenised in two interconnected 500 L LDPE tanks (UCSC SAFe tanks) (van de Flierdt et al. 2012).

3.4.3. Rock standard

In order to monitor each batch of column chemistry and mass spectrometry we used the certified USGS Columbia River basalt BCR-2 as standard reference material. Either about 18 mg or 36 mg of powdered BCR-2 was weighted into a Savilex vial and dissolved using a mixture of HF : HNO_3 (4 : 1) by refluxing for 3 days at 120˚C. The solution was then dried down at 120˚C. To ensure that all fluorides are converted to nitrates, the samples were redissolved in concentrated nitric and dried down three times (Thirlwall 1991). The samples were finally taken up in 10 mL 6 M HCl, and this served as a stock solution for column chemistry aliquots (50 ng(Nd)/ mL(HCl) and 100 ng(Nd)/ mL(HCl) stock solutions respectively).

3.5. Column chemistry

Neodymium from seawater samples and rock standards was isolated using two stages of ion chromatography. In the first stage REEs were separated from any residual samples matrix, and the second stage was performed to purify Nd from the other REE elements (Table 3.1).

3.5.1. TRU spec chemistry

The first stage used 100-µL Teflon columns, made from shrink Teflon, with a reservoir of ~3 mL, ~ 2.3 cm in length and 3.0 mm inner diameter. Columns were cleaned with 6M HCl, MQ-H_2O and 1M HNO_3, and then filled with about 100 µL of Eichrom TRU spec resin (100-150 µm bead size). The resin was cleaned with 750 µL 4M HCl and 500 µL MQ-H_2O, and was then charged with 500 µL 1M HNO_3 before loading the samples in 300 µL 1M HNO_3. The matrix was eluted in 1 mL 1M HNO_3 and the REE were collected in 600 µL 4M HCl. The REE fraction was then dried at 120˚C. The TRU spec chemistry showed Nd yields of ~ 95%.

Table 3.1: Column chemistries for REE and Nd purification.

REE purification (100-µl Teflon columns: 3 mm id, ~ 2.3 cm capillary length)	
Resin loading	Eichrom TRU-spec, 100-150 µm, stored in MQ-H$_2$O
Resin cleaning	750 µL 4M HCl 500 µL MQ-H$_2$O
Resin conditioning	500 µL 1M HNO$_3$
Sample loading	300 µL 1M HNO$_3$
Matrix elution	1000 µL 1M HNO$_3$
REE collection	600 µL 4M HCl

Nd purification (Savilex Teflon columns: 3.2 mm id, 4 cm capillary length)		
	0.142M HCl	*0.139M HCl*
Resin loading	Eichrom Ln-spec, 20-50 µm, stored in MQ-H$_2$O	
Resin cleaning	1 mL 6M HCl 1 mL MQ-H$_2$O	
Resin conditioning	1 mL 0.142M HCl	1 mL 0.139M HCl
Sample loading	0.2 mL 0.142M HCl	0.2 mL 0.139M HCl
Matrix elution	8.25 mL 0.142M HCl	9.8 mL 0.139M HCl
Nd collection	3.4 mL 0.142M HCl	3.4 mL 0.139M HCl
Resin cleaning	1 mL 6M HCl 1 mL MQ-H$_2$O	

3.5.2. Post TRU spec oxidation

The TRU spec resin is known to leak organics (Gault-Ringold et al. 2012b). Yield tests on the second stage of column chemistry (Ln spec) showed a high variability (between 2 and 80% Nd recovery), presumably due to the presence of organic compounds. Four different oxidants were tested in order to destroy these organics (Table 3.2):

(i) Refluxing in aqua regia (150 µL concentrated HNO$_3$ + 450 µL concentrated HCl) overnight at 80°C followed by 48 hours at 120°C, and drying down at 150°C proved not to be very efficient, as three samples featured a yield > 40%, while one sample had a yield as low as ~ 20%. Therefore, this method was dismissed.

(ii) Sulfuric acid (50 µL concentrated H$_2$SO$_4$ refluxing overnight at 80°C followed by 48 hours at 120°C, and dried down at 250°C) showed improved efficiency. All samples processed (n = 4) showed yields > 40%, and three samples even showed yields of > 60%. However, it was decided to not use this method on a routine basis due to the high boiling point of H$_2$SO$_4$ (330°C), making it difficult to evaporate this acid.

(iii) Reacting samples with hydrogen peroxide (250 µL concentrated H_2O_2 + 250 µL concentrated HNO_3) overnight at 80˚C, and then for about 48 hours at 120˚C, followed by drying down at 150˚C produced yields > 40% for all the samples (n = 5), but yields for three samples were below 60%.

(iv) The final method tested was to use perchloric acid (250 µL concentrated $HClO_4$ + 1 mL concentrated HNO_3), refluxing in an open beaker at 80˚C, 120˚C, 180˚C and 225˚C. All the samples processed showed yields > 60% (n = 18) and it was therefore decided to use the latter method to oxidise the organics leached from the TRU spec resin. Blanks measurements showed that the addition of the perchloric acid step did not add significant contamination (Nd ~ 3 pg, n = 3). After the oxidation of the organics, the samples were converted back to chloride form using concentrated HCl.

Table 3.2: Results obtained for various oxidation tests after TRU spec columns. All tests were performed using 10 ng Nd (BCR-2). Yields from the TRU spec chemistry (~ 95%) have been taken into account to calculate Ln spec yields.

Oxidant	ε_{Nd}	Internal 2se	Nd [ng]	Ln spec yield [%]	Oxidant	ε_{Nd}	Internal 2se	Nd [ng]	Ln spec yield [%]
Aqua Regia	0.10	0.12	5.25	48.4		0.05	0.15	7.33	68.2
	0.05	0.22	4.61	42.6		0.07	0.16	9.21	85.6
	-0.07	0.15	6.09	56.4		0.05	0.18	7.55	70.1
	0.10	0.15	2.39	22.2		0.10	0.10	9.45	87.4
H_2SO_4	0.03	0.12	8.02	74.8		0.04	0.12	7.58	70.6
	-0.05	0.15	7.56	69.6		0.07	0.22	8.21	76.6
	0.11	0.15	4.65	43.3		-0.50	0.36	6.75	63.7
	0.00	0.16	7.14	66.6	**$HClO_4$ (continued)**	-0.02	0.17	7.75	72.2
H_2O_2	0.23	0.11	5.99	55.1		0.01	0.23	8.13	77.1
	0.14	0.14	8.53	78.3		-0.10	0.25	9.40	88.6
	0.00	0.17	5.20	48.0		0.03	0.20	7.08	66.7
	0.09	0.12	8.77	80.6		0.37	0.14	8.49	79.3
	0.14	0.14	4.62	42.8		0.02	0.09	8.28	78.6
$HClO_4$	-0.09	0.12	8.53	81.2		0.01	0.11	8.07	76.7
	-0.12	0.16	8.13	76.3		0.14	0.12	8.99	84.2
	-0.04	0.10	9.40	88.6					

3.5.3. Ln spec chemistry

The second stage used Savillex Teflon columns, with a reservoir of about 6 mL, 4 cm in length and 3.2 mm inner diameter (resin bed volume: ~0.32 mL), filled with Eichrom Ln spec resin (20 – 50 μm bead size). The stopping frits used in the columns were cut from a 1.5 mm thick Ultra-Fine PE sheet, having a maximum pore size of 25 μm and a mean pore size of 21 μm (SPC technologies, UK). It is essential that the pore size of the frits is not too large compared to the resin bead size in order to avoid leaching of resin grains in the samples. Importantly, every new batch of resin should be tested with some pure metal standard, such as JNdi-1, prior to use with samples. During the course of this study we witnessed a batch of resin of poor quality, making TIMS analyses almost unfeasible due to poor Nd yields and unresolved matrix effect from the Ln column.

The columns were cleaned with 6M HCl and MQ-H$_2$O. The resin was cleaned with 1 mL 6M HCl and 1 mL MQ-H$_2$O, and it was subsequently charged with 1 mL ~0.14M HCl. The choice of the acid concentration is very important for the separation of Nd from the lighter REE. Indeed, the less concentrated the acid, the better the separation of Nd from Pr and Ce. However the less concentrated the acid, the longer the time required to perform the chemistry. About one third of the samples were processed with 0.142M HCl (Crocket et al. 2014). After loading the sample in 200 μL 0.142M HCl, the LREE were eluted in a total of 8.35 mL 0.142M HCl, and Nd was collected in 3.4 mL 0.142M HCl (Fig. 3.2a). When using 0.139M HCl, the elution of the LREE required a total of 9.8 mL 0.139M HCl, and Nd
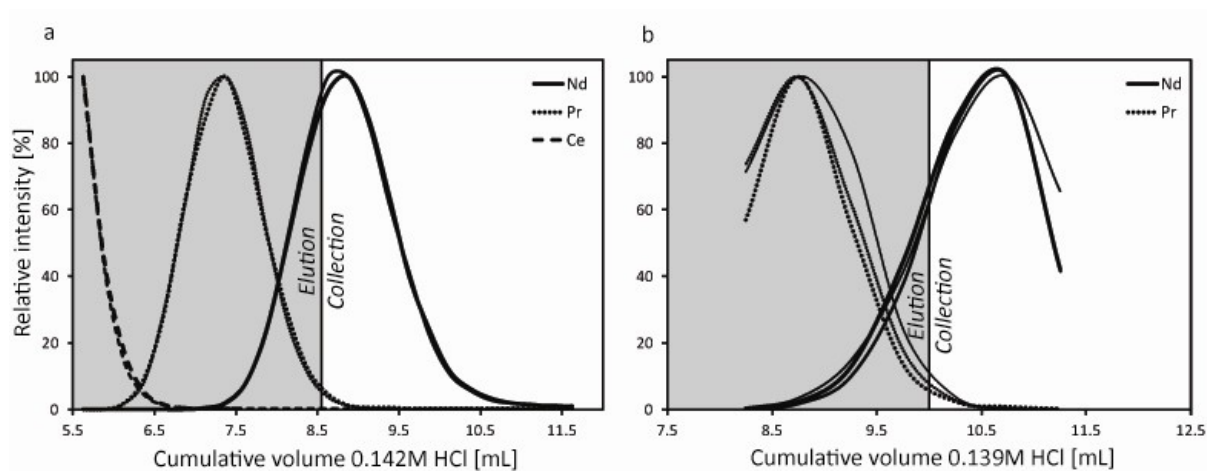
Figure 3.2: Calibration curves for Ln spec separation of Nd from Pr and Ce using (a) 0.142M HCl on two different columns, and (b) 0.139M HCl on 12 different columns (only three shown for simplicity).

was collected in 3.4 mL (Fig. 3.2b). It has to be mentioned that every column might be different, due to small differences in column diameter and/or position of frit material and that the calibration of each column might be recommended (Fig. 3.3). Neodymium recovery will depend on the exact quantity of HCl eluted prior to Nd collection since the Pr peak will always overlap with the Nd peak (see Figs. 3.2 and 3.3). The decision to be made is how much of the Nd cut is sacrificed in order to achieve the smallest amount of Pr acceptable for mass spectrometry (see section 3.6.3). Since the samples are measured as NdO^+ on the TIMS, the separation of Nd from other REE must be more efficient than when measured as Nd^+ due to the greater number of isobaric interferences created with the different oxygen isotopes combinations (see section 3.6.3 and Table 3.3). Therefore, the Ln spec calibration has to be such that the Nd fraction is Sm free, and has minimal amount of Ce and Pr. Getting a Sm free fraction was not a problem, as Sm has never been detected in the column calibration. Spiked samples have shown that the Nd yields were about 60 to 80% when 0.139M HCl was used as described above, and when the $HClO_4$ was used prior the Ln spec.

After collection of the Nd cut, 10 µL 0.001M H_3PO_4 was added to the samples in order to contract the samples in a visible dot while drying. The resin was cleaned in the columns by adding 1 mL 6M HCl followed by 1 mL MQ-H_2O. The columns were cleaned by backwashing them with MQ-H_2O (squeeze bottle), let them sit in 1 M HCl in an ultrasonic bath for about 30 minutes and backwashing them again with MQ-H_2O in order to dislodge all the resin grains that might be stuck in the frits. After that, a full reservoir of 6M HCl was let through the columns, followed by a full reservoir of MQ-H_2O. The columns were stored in 0.5M HCl.
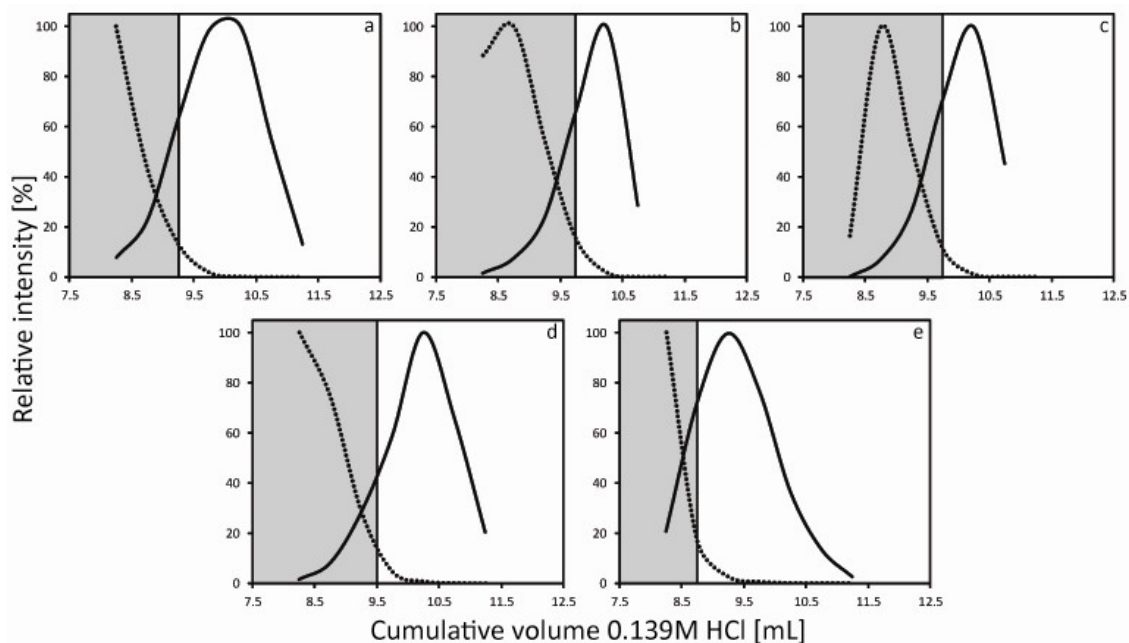
Figure 3.3: Calibration curves for five columns that proved to behave differently from the other 12 columns during elution with 0.139M. Black line: Nd, dotted line: Pr. a = column #8 (elution = 9.25 mL 0.139M HCl); b = column #13 (elution = 9.75 mL 0.139M HCl); c = column #14 (elution = 9.75 mL 0.139M HCl); d = column #16 (elution = 9.5 mL 0.139M HCl) and e = column #17 (elution = 8.75 mL 0.139M HCl). The grey area represents the fraction that was eluted, and the white area the fraction that was collected.

3.6. Measurements by Thermal Ionization Mass Spectrometry (TIMS)

Neodymium isotopic compositions and concentrations were collected over a 19 months period on a Thermo Finnigan Triton thermal ionization mass spectrometer (TIMS) equipped with a pyrometer at the MAGIC facilities at Imperial College London (UK). More details about the different tests made in order to develop the used measurement protocol can be found in Crocket et al., 2014, and are summarised in brief below.

3.6.1. Filament loading

The samples were dissolved in 1 µL of 2.5 M HCl and loaded on single W filaments (0.025 mm thick, 0.51 mm wide, 99.95% pure from H. Cross Company) using TaF_5 as emitter (Chu et al. 2009). Samples measured until early 2012 were loaded with a purified TaF_5 emitter (Charlier et al. 2006). However, since the Nd blank was measured to be ~ 1.7 pg for non-purified TaF_5 and ~1.1 pg for the purified emitter, the purification step was no longer

performed after early 2012. Using a micro syringe, 0.5 µL of the TaF_5 emitter was loaded as the smallest spot possible onto a degassed W filament at a current of 0.9A. The activator was allowed to dry between each loaded drop (typically 0.5 µL were loaded in ~ 10 drops). Subsequently, 2 x 0.5 µL of the sample was loaded followed by a second layer of 0.5 µL TaF_5. This "sandwich" was allowed to dry before increasing the current to about 2.0A. It was noticed that the sample had a tendency to spread when it was not dry before increasing the current.

3.6.2. NdO^+ measurements

The cup configuration used to measure Nd oxides can be found in Table 3.3. Filaments were preheated before opening the analyzer gate. Prior to the acquisition of a pre-heater device in summer 2012 (and for the 1st filament of each measurement session), samples were heated at 60 mA/min up to 980 ˚C (~ 30 minutes), and then left at this temperature for 30 minutes. For the samples run with the help of the pre-heater device, they were heated at 60 mA/min up to 1500 mA, and left there for at least 30 minutes (longer if the previous measurement was taking more than 9 blocks). After opening the analyser gate, the filaments were further heated up to 1100 ˚C, and the SEM was used to find and tune the beam in order to get between 2.5 and 3.5 mV on the central cup ($^{144}Nd^{16}O$). After switching over to Faraday mode, the sample beam in the central cup was tuned at ~3, 20, 100-300 mV and prior to the start of the analysis. All filaments were peak centred at about 20 mV and before starting the measurement. A peak scan was performed on the pure standards (JNdi-1) to make sure that the peaks were properly aligned in the beginning of each day.

Running conditions (e.g., $^{146}Nd^{16}O/^{144}Nd^{16}O \approx 0.719$) were typically achieved at ~ 1500˚C. Data were collected in blocks of 20 integration cycles of 8.389 s. The number of blocks depended on the central cup intensity ($^{144}Nd^{16}O^+$): if the average intensity was < 1 V after 9 blocks and enough sample Nd was still present, the measurement was continued to increase counting statistic (a maximum of 18 blocks was measured on one sample). Baselines were measured between each block, and an amplifier rotation to the left was done in order to eliminate gain biases and associated uncertainties. Monitoring of the HV pressure showed that it did not exceed $2 \cdot 10^{-7}$ mbar throughout the cause of an analysis. Central cup intensities were variable, ranging from 0.1 to 1.4 V on $^{144}Nd^{16}O^+$ per ng for pure metal standards (JNdi-1) (average = 0.6 V/ng, n = 70). The intensities were kept as close as possible to the samples intensities for one measurement session. Column processed samples yielded

lower intensities than pure JNdi-1 standards. Seawater samples measured before adding the post TRU-spec oxidation step were giving ~0.01 to 0.26 V/ng on $^{144}Nd^{16}O^+$ (average = 0.04 V/ng, n = 59), while the ones measured once $HClO_4$ was used lead to 0.02 to 0.49 V/ng (average = 0.12 V/ng, n = 104). This calculation is however based on total sample Nd, which does not take into account sample loss from the Ln columns. Column processed BCR-2 standards, used to determine the yields of the Ln columns after oxidation with $HClO_4$ gave 0.04 to 0.44 V/ng (average = 0.19 V/ng, n = 19). It seems that efficiency of the activator (batch synthesized, age) and the way the aliquot was loaded was often more important for the beam obtained than the actual amount of Nd loaded onto the filament. It was for example noticed that the activator lost efficiency with time, requiring reviving with small amount of concentrated HF and H_3PO_4. For unresolved reasons it however proofed difficult to produce a high-quality activator each time a new batch was synthesised.

Figure 3.4 documents the expected exponential correlation between beam intensity and internal uncertainty on measured $^{143}Nd/^{144}Nd$ ratios, but also highlights that loaded Nd quantity [ng] not always correlated with measured beam intensity. For example, some 5 ng JNdi-1 loads yielded higher beam intensity than 15 ng JNdi-1 loads, therefore providing a smaller internal uncertainty.
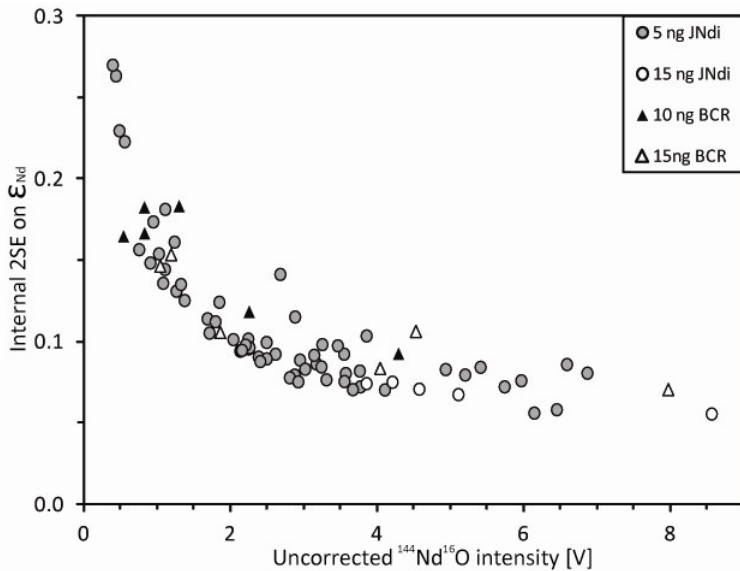
Figure 3.4: Internal precision (2se ε_{Nd}) of the corrected $^{143}Nd/^{144}Nd$ ratio vs. uncorrected $^{144}Nd^{16}O$ intensity of the standard JNdi-1 (5 ng: grey circles; 15 ng Nd: open circles) and of the rock standard BCR-2 provided by the USGS (10 ng: black triangles; 15 ng Nd: open triangles). Epsilon Nd is defined as the deviation of the measured $^{143}Nd/^{144}Nd$ ratio from CHUR (chondritic uniform reservoir) inparts per ten thousands ($^{143}Nd/^{144}Nd$ (CHUR) = 0.512638; (Jacobsen and Wasserburg 1980)).

3.6.3. Interference and mass bias corrections

Interference and mass bias corrections were performed offline cycle by cycle. The oxide masses from 156 ($^{140}Ce^{16}O^+$) to 166 ($^{150}Nd^{16}O^+$) were collected, one in each cup (nine in total, since mass 161 ($^{145}Nd^{16}O^+$) was not collected) (Table 3.3). In order to correct for the mass spectrometer bias, samples were normalized to a JNdi-1 reference value of 0.512115 (Tanaka et al. 2000). To do this, five filaments of 5 ng or 15 ng JNdi-1 were measured with each turret. The long term average $^{143}Nd/^{144}Nd$ ratio is 0.512103 ± 0.000011 (2sd, n = 70).

An important assumption for the isobaric interference corrections is that the intensity measured on cup L1 (mass 156) corresponds only to $^{140}Ce^{16}O^+$. LaO^+, BaO^+ and BaF^+ contributions were considered to be insignificant due to (i) the efficiency of the chemistries to separate these elements from Nd and (ii) the low beam intensity measured on this cup. Mass 156 ($^{140}Ce^{16}O^+$) was monitored to allow corrections for the isobaric interferences on masses 157 ($^{140}Ce^{17}O^+$), 158 ($^{140}Ce^{18}O^+$), 159 ($^{142}Ce^{17}O^+$) and 160 ($^{142}Ce^{18}O^+$) and mass 157 ($^{141}Pr^{16}O^+$) was measured to correct for the masses 158 ($^{141}Pr^{17}O^+$) and 159 ($^{141}Pr^{18}O^+$). JNdi-1 doped with Ce showed that if the raw $^{140}Ce^{16}O/^{144}Nd^{16}O$ ratio was below 0.148, the combined interference and mass bias corrections yielded an accurate $^{143}Nd/^{144}Nd$ ratio. Similarly, column processed BCR-2 proved that raw $^{141}Pr^{16}O/^{144}Nd^{16}O$ ratio as high as 0.54 would lead to accurate $^{143}Nd/^{144}Nd$ ratio (Crocket et al. 2014). Mass 163 was measured to monitor the interference from $^{144}Sm^{16}O^+$ on $^{144}Nd^{16}O^+$. No Sm correction was made due to excellent separation of Nd and Sm achieved during the Ln chemistry. Mass 161 was not measured ($^{145}Nd^{16}O^+$), and interferences from $^{145}Nd^{17}O^+$ and $^{145}Nd^{18}O^+$ on masses 162 and 163 were corrected by calculating a value for $^{145}Nd^{16}O^+$ based on multiplying the interference-corrected value for $^{142}Nd^{16}O^+$ by a $^{145}Nd/^{142}Nd$ ratio of 0.305123 (Andreasen and Sharma 2006).

To determine the Nd concentrations, the samples were spiked with ^{150}Nd spike (97.8% purity) provided by Derek Vance (ETH Zurich), aiming for a spike ^{150}Nd : sample ^{150}Nd ratio of ~ 1 in order to minimise the error magnification on the $^{143}Nd/^{144}Nd$ ratio. The exponential law was used to correct for the mass bias and normalisation to $^{146}Nd/^{144}Nd$ was applied (Wasserburg et al. 1981; Thirlwall 1991; Li et al. 2007).

Table 3.3: Cup configuration for the measurement of NdO^+ with isobaric interferences present on each cup.

Cup:	L4	L3	L2	L1	C	H1	H2	H3	H4
Oxide mass	156	157	158	159	160	162	163	164	166
Metal mass	140	141	142	143	144	146	147	148	150
Isotopes	$^{140}Ce^{16}O$	$^{141}Pr^{16}O$	$^{142}Nd^{16}O$	$^{143}Nd^{16}O$	$^{144}Nd^{16}O$	$^{146}Nd^{16}O$	$^{147}Sm^{16}O$	$^{148}Nd^{16}O$	$^{150}Nd^{16}O$
Interferences	$^{139}La^{17}O$	$^{140}Ce^{17}O$	$^{141}Pr^{17}O$	$^{142}Nd^{17}O$	$^{143}Nd^{17}O$	$^{145}Nd^{17}O$	$^{145}Nd^{18}O$	$^{146}Nd^{18}O$	$^{148}Nd^{18}O$
	$^{138}La^{18}O$	$^{139}La^{18}O$	$^{140}Ce^{18}O$	$^{141}Pr^{18}O$	$^{142}Nd^{18}O$	$^{144}Nd^{18}O$	$^{146}Nd^{17}O$	$^{147}Sm^{17}O$	$^{148}Sm^{18}O$
	$^{138}Ba^{18}O$	$^{138}Ba^{19}F$	$^{142}Ce^{16}O$	$^{142}Ce^{17}O$	$^{144}Sm^{16}O$	$^{144}Sm^{18}O$		$^{148}Sm^{16}O$	$^{149}Sm^{17}O$
					$^{142}Ce^{18}O$				$^{150}Sm^{16}O$

Table 3.4: Cup configuration for the measurement of the oxygen ratios.

Cup	L4	L3	L2	L1[a]	C	H1	H2	H3	H4[b]
Oxide mass	162	163	164	165	166	167	168	169	170
Isotopes	$^{146}Nd^{16}O$	$^{147}Sm^{16}O$	$^{148}Nd^{16}O$	$^{149}Sm^{16}O$	$^{150}Nd^{16}O$	$^{150}Nd^{17}O$	$^{150}Nd^{18}O$		$^{154}Sm^{16}O$
	$^{145}Nd^{17}O$	$^{146}Nd^{17}O$	$^{148}Sm^{16}O$	$^{148}Nd^{17}O$	$^{150}Sm^{16}O$		$^{152}Sm^{16}O$		
Interferences	$^{144}Nd^{18}O$	$^{145}Nd^{18}O$	$^{146}Nd^{18}O$		$^{148}Nd^{18}O$				

[a] In cup L1, $^{148}Nd^{17}O$ was monitored to calculate the interference of $^{148}Nd^{18}O$ on $^{150}Nd^{16}O$.

[b] The oxide $^{154}Sm^{16}O$ was collected in H4 to monitor if any Sm was present.

3.6.4. Oxygen isotope ratio

All isobaric interferences outlined above require precise knowledge of the oxygen isotopic composition of the oxygen in the TIMS source. In order to measure this oxygen isotopic composition, an aliquot of ~ 100 ng ^{150}Nd spike was processed through the Ln-spec chemistry, in order to remove any trace of Sm. This aliquot was then split and loaded on 10 different filaments in sandwich-style as described above. The cup configuration used to measure the oxygen ratio, which can be found in Table 3.4, used ^{150}Nd^{16}O in the central cup. Filaments were run at several different mean temperatures (1450 ˚C to 1640 ˚C), currents (2309 to 2611 mA) and intensities (0.3 to 44 V) in order to mimic the conditions found during sample measurements. The oxygen isotope ratios were calculated from the beam intensities measured in the central cup, H1 and H2. The measured oxygen isotope compositions are 0.000390 ± 0.000003 for ^{17}O/^{16}O and 0.002073 ± 0.000007 for ^{18}O/^{16}O (2sd, n = 12; Fig. 3.5; see also Crocket et al., 2014 for more details). These values were applied for all of the data reduction.

Figure 3.5: Published oxygen isotope ratios, grouped according to method of measurement. Data from (Amelin et al. 1997), (Chavagnac et al. 1999), (Chu et al. 2009), (Griselin et al. 2001), (Harvey and Baxter 2009), (Li et al. 2007), (Nier 1950), (Reisberg and Zindler 1986), (Thirlwall 1991), and (Wasserburg et al. 1981).
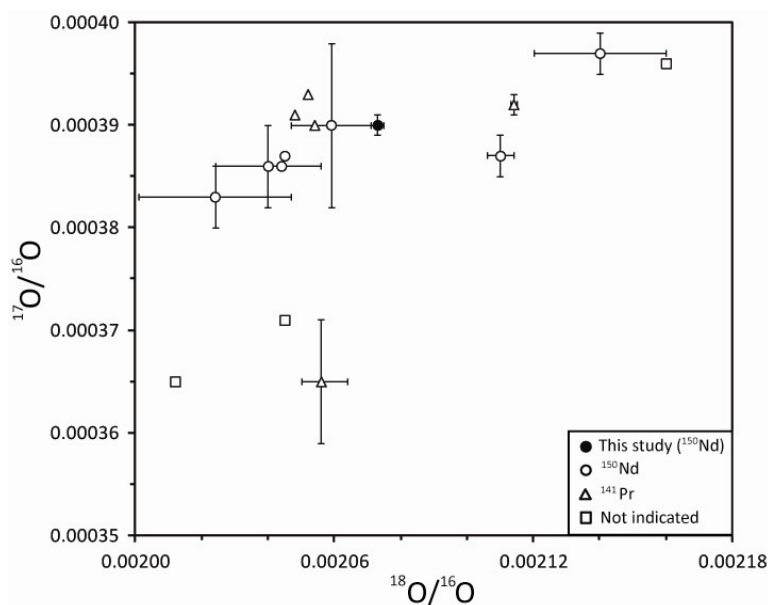
3.6.5. Blanks

Total blanks were obtained by processing about 10 L of MQ-H$_2$O through 2 cartridges followed by the above described two stage ion chromatography. Some of these blanks were processed before including the HClO$_4$ oxidizing step and some afterwards. The average Nd content is 163 pg ($\pm$ 20 pg 2se, n = 16), or 0.020 pg(Nd) / g(MQ-H$_2$O) ($\pm$ 0.02 pg/g 2se). Eleven blanks were $\leq$ 0.020 pg/g, but one blank yielded 0.028 pg/g (205 pg Nd), one 0.029 pg/g (215 pg Nd) and one was as high as 0.043 pg/g (236 pg Nd). These high blanks could

not be linked with a particular batch of complexing agent (4 different batches used in this study). The Nd blank of MQ-H_2O has been measured at two different times during this study. The first measurement was performed in December 2011 and the result was 0.009 pg(Nd) / g(MQ-H_2O). The second attempt was made in November 2012 and the results were 0.001 pg/g and 0.002 pg/g for 2 different samples. Therefore, if the MQ-H_2O blank is subtracted from the total blanks, the average Nd content ranges from 83 (± 24 pg 2se) to 158 pg Nd (± 20 pg 2se).

Chemistry blanks were determined by processing an aliquot of ^{150}Nd spike through TRU spec and Ln spec. Some were processed before including the $HClO_4$ oxidizing step and some afterwards. The average Nd content was 5.1 pg (± 2.4 pg, 2se, n = 11), ranging from 0.8 pg to 11.2 pg Nd.

Loading Nd blanks were ~ 1.7 pg for non-purified TaF_5 and ~1.1 pg for the purified emitter (see paragraph 3.6.1).

3.7. Reproducibility

The long term reproducibility obtained for combined 15 ng and 5 ng JNdi-1 loads is 22 ppm (2 rsd) on ^{144}Nd/^{143}Nd (Fig. 3.6).

Beside the fact that some activator batches were less efficient than others, some standards were run at lower intensities in order to match sample beams. Only one turret was normalized using 15 ng JNdi-1, and the 2rsd was 6.4 ppm. Thirteen turrets included 5 ng JNdi-1 loads, yielding an overall 2rsd of 23 ppm, ranging from 5.6 to 32.7 ppm within individual turrets. This large range is correlated with the intensities at which the standards were run: when they were deliberately run at an average intensity below 1 V on ^{144}Nd^{16}O, the 2rsd was typically above 25 ppm. The average ^{143}Nd/^{144}Nd ratio of 0.512103 ± 0.000011 (2sd, n = 70) deviates by 24 ppm from the reference value of 0.512115 ± 0.000007 (Tanaka et al. 2000). The exact offset between published and measured JNdi-1 (per turret) has been used to correct all sample results reported in the following.

It is however well known that pure standards tend to reproduce better than natural samples. In order to determine the reproducibility of combined ion exchange chromatography
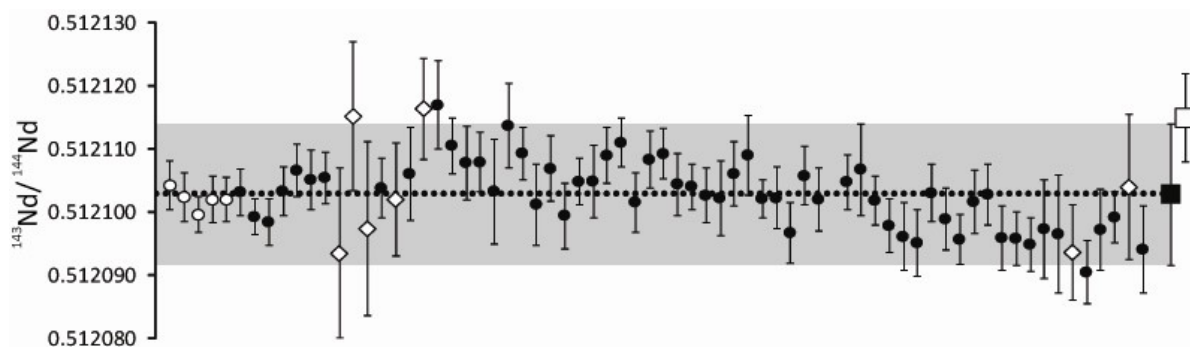
Figure 3.6: Interference and mass bias corrected $^{143}Nd/^{144}Nd$ values for 15 ng (open circles) and 5 ng (closed circles) Nd JNdi-1 runs. Error bars represent the internal 2se. Open diamonds represent 5 ng JNdi-1 runs preformed at an average $^{144}Nd^{16}O$ intensity of less than 1 V. The average $^{143}Nd/^{144}Nd$ ratio of 0.512103 ± 0.000011 for all JNdi-1 results (n = 70) is represented by the filled square, and the corresponding uncertainty (2sd) is marked by the grey area. The recommended literature value for JNdi-1 $^{143}Nd/^{144}Nd$ is 0.512115 ± 0.000007 (2sd) (Tanaka et al. 2000) and is represented by the open square. Averages for JNdi-1 runs at different concentrations: 15 ng Nd: ε_{Nd} = 0.512102 ± 0.000003 (2sd, n = 5); 5 ng Nd: ε_{Nd} = 0.512103 ± 0.000012 (2sd, n = 65). All $^{143}Nd/^{144}Nd$ values reported in this thesis are corrected for the offset of the respective measurement session to the published JNdi-1 value by Tanaka et al. (2000).

and mass spectrometry, rock standard BCR-2 was processed along with every batch of samples (Fig. 3.7). The external reproducibility obtained this way was 20 ppm on $^{143}Nd/^{144}Nd$ (2sd, n = 12). More precisely, the external reproducibility for 10 ng runs was 23 ppm (2sd, n = 6), and for the 15 ng loads was 15 ppm (2sd, n = 6). JNdi-1 corrected values show excellent accuracy and agree within uncertainty with published values by Weis et al. (2006) (0.512639 ± 0.000010 and 0.512637 ± 0.000012 respectively).

As mentioned in paragraph 3.4.3, two batches of BCR-2 solution have been prepared and hence the reproducibility of sample digestion could not be tested with this set up. The BCR-2 samples however provided the additional opportunity to test how accurate Nd concentration measurements by isotope dilution were. Batch 1 yielded concentrations of 29.0 ± 0.2 μg/g (2sd, n = 4), and concentrations of 26.4 ± 0.2 μg/g (2sd, n = 8) were obtained for batch 2. Both of these results are in excellent agreement with the certified BCR-2 Nd concentration of 28 ± 2 μg/g (1sd).
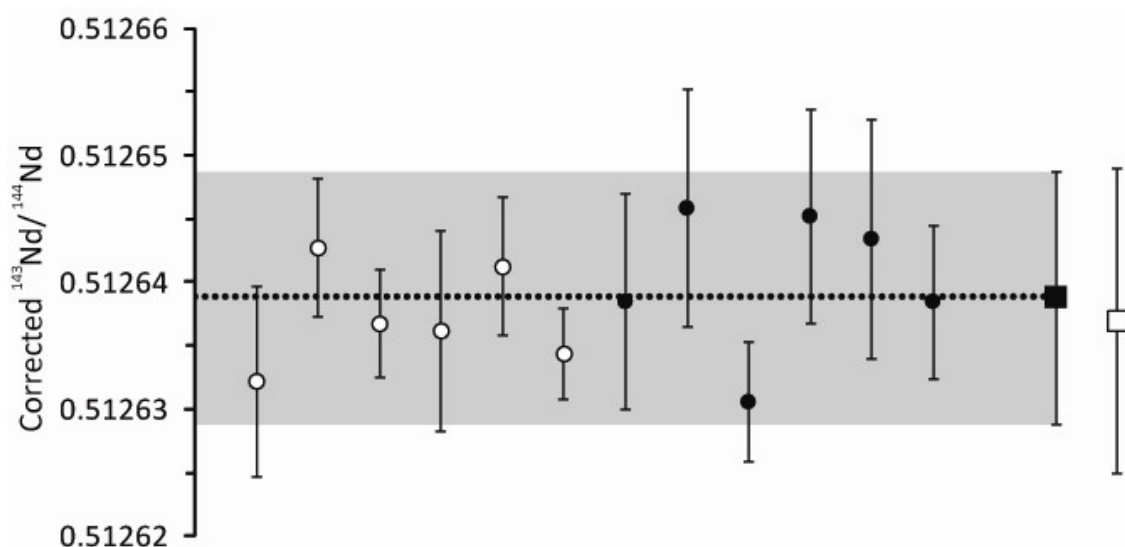
Figure 3.7: $^{144}Nd/^{143}Nd$ ratios derived for the BCR-2 rock standard, corrected for mass bias, interferences, and offset from the recommended JNdi-1 value (see Figure 3.6). Open circles = 15 ng Nd; closed circles = 10 ng Nd. The average of all BCR-2 results (n = 12) and associated uncertainty (2sd) is represented by the filled square and the grey shading respectively. The recommended BCR-2 reference value is shown as open square (Weis et al. 2006).

Finally, an attempt to determine the true external reproducibility of the presented method has been undertaken by repeat analyses of multiple seawater samples. For this purpose two large homogeneous water samples from the Bermuda Atlantic Time Series Station BATS (15 m and 2000 m depth) were used as in-house seawater standard and results are reported in Table 3.5. As these samples were collected on the same cruise as the international GEOTRACES intercalibration samples in 2008, albeit from a different tank, we here combine them with the results reported for our laboratory in the intercalibration exercise (Pahnke et al. 2012; van de Flierdt et al. 2012) (Table 3.5, Figs. 3.8 and 3.9). For BATS 15 m depth waters, the average ε_{Nd} is -9.17 ± 0.05 and the average Nd concentration is 2.06 ± 0.08 ppt (2sd, n = 6 and n = 3 respectively, Table 3.5). Both values are in good agreement with the average Nd isotopic composition of -9.19 ± 0.57 and the average concentration of 2.04 ± 0.18 ppt (2sd for 13 and 11 labs respectively) obtained during the international intercalibration exercise (van de Flierdt et al. 2012). For BATS 2000 m depth, the average values obtained during the course of our study are ε_{Nd} = -13.17 ± 0.31 and Nd concentrations of 2.53 ± 0.09 ppt (2sd, n = 5). Similarly to the first sample, these results are in excellent agreement with the results of the international intercalibration exercise (ε_{Nd} = -13.14 ± 0.57 and [Nd] = 2.50 ± 0.18 ppt, 2sd for 13 and 11 labs respectively). It is worth noting that the samples were purified and analysed

over a duration of 19 months (Table 3.5), and that the TIMS analyses were performed between 3 and 5 years after initial sample collection. Hence the present results show that storage in pre-cleaned container for up to five years does not affect the isotopic composition nor the concentration of Nd (Table 3.5). Finally, one single sample from the Pacific Ocean (SAFe station, 3000 m) was also analysed for its Nd isotopic composition during the intercalibration exercise for which we measured an isotopic composition of -3.12 ± 0.16 (internal 2se, Table 3.5), comparing well with the average value of -3.17 ± 0.47 (2sd) obtained by eight different laboratories (van de Flierdt et al. 2012).

Table 3.5: Nd isotopic composition measured in the present study for the international intercalibration exercise and for in-house monitoring of sample reproducibility.

		Analysis date	Sample volume [L]	ε_{Nd}[a]	Internal 2se[b]	External 2sd[c]	Nd [ppt][d]	Internal 2se[e]
Intercalibration	**SAFe 3000 m**	19/12/2011	5	-3.12	0.16	0.06	6.42	0.003
Intercalibration	**BATS 15 m**	29/09/2011	10.7	-9.17	0.06	0.19	2.05	0.001
		17/10/2011	7.6	-9.13	0.08	0.13	2.10	0.001
In-house monitoring of sample reproducibility	**BATS 15 m**	18/10/2011	9.5	-9.20	0.06	0.13	-	-
		23/11/2011	9	-9.17	0.16	0.16	2.02	0.001
		02/02/2012	5.2	-9.16	0.26	0.08	-	-
		02/02/2012	5	-9.19	0.21	0.08	-	-
Average and 2sd BATS 15 m				*-9.17*	*0.05*		*2.06*	*0.08*
Intercalibration	**BATS 2000 m**	29/09/2011	10.4	-13.07	0.08	0.19	2.60	0.001
		17/10/2011	7.2	-13.27	0.09	0.13	2.56	0.002
In-house monitoring of sample reproducibility	**BATS 2000 m**	28/02/2013	4.9	-13.34	0.10	0.14	2.49	0.0002
		11/04/2013	4.5	-13.23	0.11	0.14	2.50	0.0003
		25/04/2013	4.8	-12.96	0.08	0.06	2.50	0.0003
Average and 2sd BATS 2000 m				*-13.17*	*0.31*		*2.53*	*0.09*

[a] Normalized to 5 analyses of JNdi-1 relative to JNdi-1 value of 0.512115 (Tanaka et al., 2000).

ε_{Nd} values were calculated relative to a CHUR of 0.512638 (Jacobsen and Wasserburg, 1980).

[b] Internal error are derived from the 2 sigma error on the instrument measurement (≤ 360 cycles).

[c] The external errors are derived from the analysis of repeat standards (JNdi-1) during the measurement session.

[d] Some samples from BATS 15 m were used to test the yields obtained with different pumping flow rates during the development of the present method; therefore, their Nd concentration is not available.

[e] The internal errors for the concentration is the absolute uncertainty [ppt] and takes into account the relative uncertainty on the weighing of the sample and of the spike, as well as the relative uncertainty of the measurement on the TIMS.
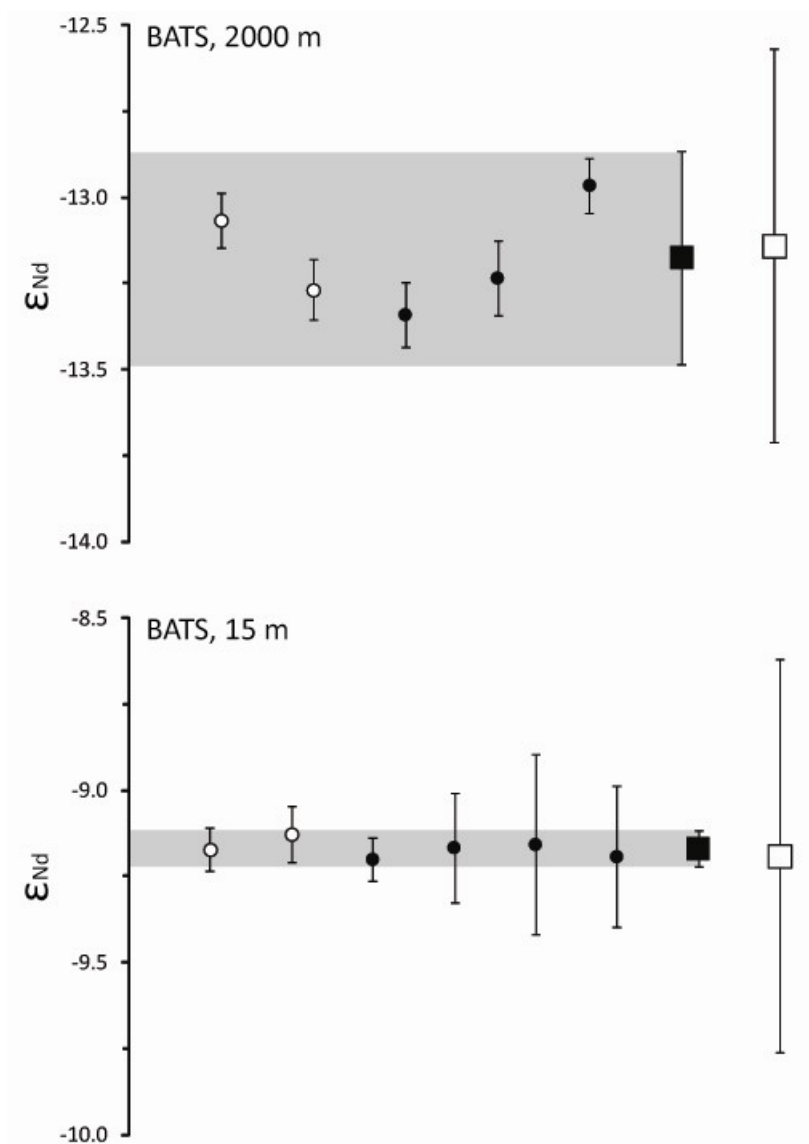
Figure 3.8: Dissolved neodymium isotopic composition derived for seawater samples from 2000 m depth (upper panel) and 15 m depth (lower panel) at the Bermuda Atlantic Time-series Study (BATS). The values are corrected for mass bias, interferences, and offset of the JNdi-1 during the analytical session from the published value (see Figure 3.6). Open circles = intercalibration samples (van de Flierdt et al. 2012); closed circles = in-house seawater standard; error bars represent the internal 2se. The average of all BATS results (n = 5 for 2000 m depth and n = 6 for 15 m depth) and associated uncertainty (2sd) is represented by the filled square and the grey shading respectively: ε_{Nd} (BATS, 2000 m) = -13.17 ± 0.31 (2sd) and ε_{Nd} (BATS, 15 m) = -9.17 ± 0.05 (2sd). The average Nd isotopic composition obtained from 13 laboratories during the intercalibration exercise is represented by the open squares: ε_{Nd} (BATS, 2000 m) = -13.14 ± 0.57 (2sd) and ε_{Nd} (BATS, 15 m) = -9.19 ± 0.57 (2sd) (van de Flierdt et al. 2012).
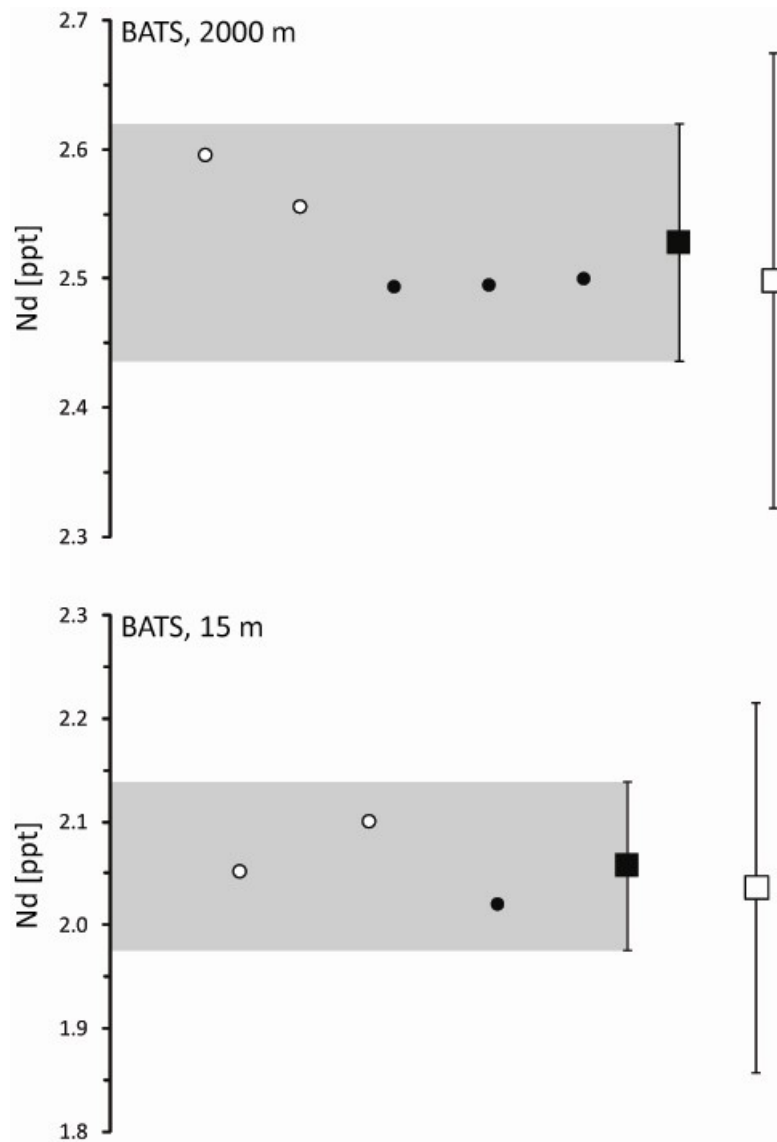
Figure 3.9: Dissolved neodymium concentration derived for seawater samples from 2000 m depth (upper panel) and 15 m depth (lower panel) at the Bermuda Atlantic Time-series Study (BATS). Open circles = intercalibration samples (van de Flierdt et al. 2012); closed circles = in-house seawater standard; error bars, representing the internal 2se, are smaller than the symbols. The average of all BATS results (n = 5 for 2000 m depth and n = 3 for 15 m depth) and associated uncertainty (2sd) is represented by the filled square and the grey shading respectively: [Nd] (BATS, 2000 m) = 2.53 ± 0.09 ppt (2sd) and [Nd] (BATS, 15 m) = 2.06 ± 0.08 ppt (2sd). The average Nd isotopic composition obtained from 11 laboratories during the intercalibration exercise is represented by the open squares: [Nd] (BATS, 2000 m) = 2.5 ± 0.18 ppt (2sd) and [Nd] (BATS, 15 m) = 2.04 ± 0.18 ppt (2sd) (van de Flierdt et al. 2012).

3.8. Conclusions

The method presented here proved efficient to purify Nd and analyse its isotopic compositions and concentrations in low abundance Nd seawater and rock samples. This achievement is demonstrated by (i) the external reproducibility of 20 ppm (2sd) on combined 10 and 15 ng Nd BCR-2 samples (n = 12), (ii) the external reproducibility of 30 ppm and 5 ppm (2sd) on seawater samples (BATS, 2000 m, n= 5 and BATS, 15 m, n = 6 respectively), (iii) the excellent agreement between the Nd concentrations measured in the present study and the certified BCR-2 values or the seawater samples from BATS.

Moreover, the new method shows that an internal error of ~ 10 ppm (2se) can be achieved on samples containing ~ 11 ng Nd before being processed (Table 3.5, BATS 2000 m). This demonstrates that the volume required for the analyses using this method could be decreased to 5 L for future GEOTRACES cruises.

Finally, this method allows the measurement of Nd isotopic composition and concentration at the same time using one single sample, which makes it very time and labour effective.

A further improvement for this method would be to understand why the activators synthesised are not always efficient. Indeed, as mentioned in paragraph 3.6.2, the precision of a measurement is not only dependent on the quantity of Nd loaded on the filament, but also on the efficiency of the activator batch. More tests would be needed to identify a way to synthesise highly efficient activators.

Acknowledgements

Chapter 4

THE NEODYMIUM ISOTOPIC COMPOSITION OF NORTH ATLANTIC DEEP WATER

–

REVISITED

Abstract

The neodymium (Nd) isotopic composition of seawater is commonly used as a proxy to study changes in the thermohaline circulation in the past. The modern data base for such reconstructions, as well as the understanding of the underlying processes, is however still sparse. We here present new observational data for Nd isotopes from twelve seawater depth profiles, which follow the flow path of North Atlantic Deep Water (NADW) from its formation region in the North Atlantic to the northern equatorial Atlantic. Samples were collected during the Dutch GEOTRACES cruise GA02 in 2010. The results show that the different water masses in the subpolar North Atlantic Ocean, which ultimately constitute NADW, have the following Nd isotope characteristics: Upper Labrador Sea Water (ULSW) - ε_{Nd} = -14.24 ± 0.26; Labrador Sea Water (LSW) - ε_{Nd} = -13.67 ± 0.86; Northeast Atlantic Deep Water (NEADW) - ε_{Nd} = -12.48 ± 0.59; Northwest Atlantic Bottom Water (NWABW) - ε_{Nd} = -11.82 ± 1.38. In the subtropics, where the source water masses described above have mixed to the signal of NADW, which is exported to the global ocean, Nd isotopes can distinguish between upper-NADW (ε_{Nd} = -13.20 ± 1.00) and lower-NADW (ε_{Nd} = -12.44 ± 0.39). This is an important observation, as in many previous studies NADW got treated as one homogenous water mass with a Nd isotopic composition of -13.5. We here however show that lower-NADW is significantly more radiogenic due to the dominance of source waters from the Nordic Seas (NWABW and NEADW). While our data set provides additional insights into the contribution of boundary exchange in areas of sediment resuspension, the results for open ocean seawater below 2500 m showcase at an unprecedented level the ability of Nd isotopes to trace water masses in the strongly advecting western Atlantic Ocean.

4.1. Introduction

The ocean plays a central role for the climate system, as it stores and transports heat, freshwater and carbon (Alley et al. 2003). In particular, the global thermohaline circulation is a key concept of water mass transport as it brings warm and salty surface waters to northern high latitudes where they cool down, sink, and return as deep waters to the global ocean. Ultimately, these deep waters upwell in the Indian and Pacific Oceans and return to the North Atlantic as intermediate and surface waters. The formation and spreading of North Atlantic Deep Water (NADW, Table 4.1) has hence often been considered as the 'motor of the

thermohaline circulation' or the 'global conveyor belt'(Broecker 1991). Over the past decade or so, the more detailed picture of a two-cell meridional overturning circulation (MOC) in the Atlantic Ocean has emerged from many tracer fields, with the upper cell being fed by warm and salty waters from the north and the lower cell being fed by carbon and nutrient-rich waters from the south (see Marshall and Speer 2012 for a recent summary). While the role of Southern Ocean upwelling of the MOC has received a lot of recent attention, and is without doubt an important player in understanding past and present climate change, we will here focus on the upper cell of the MOC and the part of the lower cell that is present in the North Atlantic.

The most prominent water mass to discuss is hence North Atlantic Deep Water, which is formed from a variety of water masses in the subpolar North Atlantic (see section 4.2), mixed in the subpolar gyre, and exported to the rest of the global ocean. In the Atlantic Ocean, NADW is characterised by a prominent salinity maximum between 2000 to 3000 m (Schmitz 1996). Salinity, as temperature, is one of the so-called conservative properties of seawater, which are used by oceanographers to identify water masses. A *conservative* property is altered only by processes occurring at the boundaries of the ocean, and hence, within the ocean, changes occur only as a result of mixing with water masses with different characteristics. On the other hand, a *non-conservative* property will be subject to alteration due to internal processes (e.g., physical, chemical or biological processes occurring within the ocean). Prominent examples are concentrations of the macro-nutrients silicate, nitrate, and phosphate, which are all majorly governed by uptake by marine organism and release upon regeneration in the water column.

One of the major hurdles in reconstructing water masses and ocean circulation back in time is to find a proxy for a conservative water mass property such as salinity. The neodymium (Nd) isotopic composition of seawater has been suggested to be a strong candidate. The oceanic residence time of Nd is about 300-1000 years, which is shorter than the mean oceanic mixing time (about 1500 years), and Nd isotopes seem to not be affected by biological fractionation (Piepgras et al. 1979; Piepgras and Wasserburg 1980; Tachikawa et al. 2003; Arsouze et al. 2009). Co-variation of seawater Nd isotopes and salinity in the Atlantic Ocean has furthermore created the notion of Nd isotopes being a 'quasi-conservative' tracer for ocean circulation (von Blanckenburg 1999; see also Goldstein and Hemming 2003). The term 'quasi-conservative' goes back to the fact that dissolved Nd isotopes seem to behave conservatively in the ocean, but that concentration profiles of Nd

resemble nutrient-type behaviour, and that exchange with margins can lead to additional modification (i.e. non-conservative components). This so-called 'Nd paradox' (decoupling of Nd isotopes and concentrations; Goldstein and Hemming, 2003) will be discussed in more detail in Chapter 5.

Neodymium belongs to the group of rare earth elements (REE) and is mostly found in dissolved form in the ocean with concentrations in the order of ppt [ng/kg; ~15-45 pmol/kg] (Goldstein and Hemming 2003; Lacan et al. 2012). The Nd isotopic composition is expressed as

$$\varepsilon_{Nd} = \left[\frac{\left(\frac{^{143}Nd}{^{144}Nd}\right)_{Sample}}{\left(\frac{^{143}Nd}{^{144}Nd}\right)_{CHUR}} - 1 \right] \times 10^4 \quad (4.1)$$

where CHUR (Chondritic Uniform Reservoir) represents a present day average earth value $((^{143}Nd/^{144}Nd)_{CHUR} = 0.512638$ (Jacobsen and Wasserburg 1980)). The major source of Nd to the ocean is the continents, and the Nd isotopic composition of seawater hence reflects age and lithology of the surrounding continents: $\varepsilon_{Nd} \approx$ -10 to -25 in the North Atlantic to $\varepsilon_{Nd} \approx 0$ to -5 in the Pacific (Goldstein and Hemming 2003; Lacan et al. 2012).

However, our understanding of the modern distribution of Nd isotopes in the ocean relies on a relatively limited observational data base. For example, only ~90 measurements exist on seawater in the North Atlantic Subpolar Gyre, including the Labrador Sea, and less than 40 data points are available for the entire western subtropical North Atlantic. For seawater Nd isotopes to be used as a proxy for past ocean circulation, its behaviour and geochemical cycle in the modern ocean needs to be better constrained.

With this motivation in mind, we present twelve depth profiles of seawater Nd isotopic compositions along the flow path of NADW in the western Atlantic Ocean, from Iceland in the north, to the equator in the south. Six profiles of 10 to 13 water depths each were taken in the subpolar North Atlantic, thus almost doubling the available dataset, whereas the rest of the profiles are from the western subtropical Atlantic, hence tripling the number of data available in this area. Improved vertical sampling resolution as well as analytical precision allows us to reassess the Nd isotopic composition of NADW and the assumption that Nd isotopes behave like a quasi-conservative tracer of water masses away from continental inputs (von Blanckenburg 1999; van de Flierdt and Frank 2010). Our new results confirm that

water masses in the North Atlantic can be depicted based on their Nd isotopic composition, except in some areas where vigorous bottom currents lead to sediment resuspension. Our data furthermore reveal for the first time a clearly resolvable difference between upper-NADW and lower-NADW in the western Atlantic Ocean, with the value for lower-NADW deviating markedly from the commonly used values for NADW (ε_{Nd} = -13.5; Piepgras and Wasserburg, 1987). Comparison to more traditionally used water mass tracers in the modern ocean highlights the utility of the Nd isotopic composition of seawater as a water mass tracer in the strongly advecting western Atlantic Ocean to an unprecedented level of detail.

Whereas the present chapter deals with the Nd isotopic composition measured for the water masses constituting NADW, Chapter 5 is complementary and contains the Nd concentrations corresponding to the present samples as well as Nd isotope and concentration data for the surface waters of the studied profiles. We chose to separate our data set in this way because the focus of the present chapter is (i) to evaluate if Nd isotopes behave conservatively in deep waters away from ocean margin, (ii) to determine whether Nd isotopes feature the same behaviour in the subpolar formation region of NADW constituents compared to the export area, and (iii) to assess the ability of the Nd isotopic composition of seawater to trace water masses. Chapter 5 will subsequently use the Nd concentration results to investigate other questions, such as the "Nd paradox" (see Chapter 5).

4.2. Hydrological context

The cruise track for GA02 followed the deepest part of the North Atlantic Ocean and the flow path of NADW (Fig. 4.1), starting from the Irminger Sea (station 2: 64.00˚ N, 34.25˚W) down to the south of the Sargasso Sea (station 30: 18.57˚ N, 57.61˚W) (Table 4.2). Below we will outline the major hydrology of the area as constructed from the literature. We will focus our discussion on intermediate, deep, and bottom water masses. Surface currents will be discussed elsewhere (Chapter 5).

4.2.1. North Atlantic Deep Water (NADW) and its constituents

In the subtropical western Atlantic Ocean, NADW is subdivided into three main layers: upper-, middle-, and lower-NADW (Schmitz 1996). These three components refer to the source water masses which constitute NADW and are formed in the subpolar region. The

name NADW is used for intermediate to deep waters once they leave the mixing area of the subpolar gyre and are advected south in the deep western boundary current.

Table 4.1: Abbreviations of names of water masses and surface water currents.

Abbreviations	Full name
AABW	Antarctic Bottom Water
AAIW	Antarctic Intermediate Water
AW	Atlantic Water
CC	Canary Current
DSOW	Denmark Strait Overflow Water
DWBC	Deep Western Boundary Current
EDW	Eighteen Degree Water (also called STMW)
EGC	East Greenland Current
FC	Florida Current
GS	Gulf Stream
IC	Irminger Current
ISOW	Iceland Scotland Overflow Water
LC	Labrador Current
LDW	Lower Deep Water
LSW	Labrador Sea Water
MOW	Mediterranean Outflow Water
NAC	North Atlantic Current
NADW	North Atlantic Deep Water
NAO	North Atlantic Oscillation
NC	Norwegian Current
NEADW	North East Atlantic Deep Water
NEC	North Equatorial Current
NWABW	North West Atlantic Bottom Water
OW	Overflow Waters
SPMW	Subpolar Mode Water
STMW	Subtropical Mode Water (also called EDW)
ULSW	Upper Labrador Sea Water
WGC	Western Greenland Current

4.2.1.1. Upper-NADW

The least dense components of NADW in the northern North Atlantic are the two classes of Labrador Sea Water: Upper-LSW (ULSW) and Classical-LSW (which will be called LSW hereafter). Upper Labrador Sea Water is formed every winter by convection in newly generated eddies in the southern, central and northern Labrador Sea (Smethie et al. 2000;

Stramma et al. 2004; Kieke et al. 2006). ULSW is less dense than LSW and shows higher CFC concentrations indicating that it was ventilated more recently (Swift 1984; Smethie et al. 2000; Steinfeldt and Rhein 2004; Stramma et al. 2004; Kieke et al. 2006).

Labrador Sea Water is formed by deep convection due to surface water cooling during winter time in the central Labrador Sea (Talley and McCartney 1982; Sy et al. 1997; Yashayaev and Loder 2009). It is characterised by low salinity, high oxygen content and high anthropogenic chlorofluorocarbons (CFC) concentrations, and a potential density centred at $\sigma_\theta \approx 27.78$ kg/m^3. It can be distinguished from ULSW by an O_2 maximum (Talley and McCartney 1982; Swift 1984; Sy et al. 1997; Smethie et al. 2000; Steinfeldt and Rhein 2004; Kieke et al. 2006). Since the formation process of LSW is coupled to climatic conditions, such as the strength of the North Atlantic Oscillation (NAO), the depth to which this water mass is convected may change from one year to another, including years with absent LSW convection (Smethie et al. 2000). The thickness of LSW is anticorrelated to that of ULSW (Kieke et al. 2006). Both ULSW and LSW spread at mid-depth in three principal directions in the North Atlantic Ocean: northeastward into the Irminger Basin, southeastward across the Mid Atlantic Ridge, and south within the deep western boundary current (Lavender et al. 2000; Kieke et al. 2006; Kieke et al. 2009; Rhein et al. 2011) (Fig. 4.1). Labrador Sea Water (LSW) is considered to be the densest variety of Subpolar Mode Water (SPMW), followed by ULSW. At latitudes south of 35°N, Mediterranean Outflow Water (MOW), characterised by high salinity and high potential temperature, mixes with both ULSW and LSW to form 4 Sv of the water mass called upper-NADW (Schmitz 1996).

4.2.1.2. Middle-NADW

Middle-NADW is called North East Atlantic Deep Water (NEADW) in the northern North Atlantic, and it is a mixture of 2 Sv Iceland Scotland Overflow Waters (ISOW), 2 Sv Lower Deep Water (LDW), and 2 Sv of a mixture of Atlantic Water (AW) and LSW (Schmitz 1996). Dense water masses formed in the Greenland and Norwegian Seas overflow the Faroe Bank Channel and the Iceland-Faroe Ridge (Fig. 4.1). While sinking into the Iceland Basin due to their high density, the Overflow Waters (OW) drag saltier Atlantic Water (coming from the Subtropical Atlantic) and LSW along and form the so-called ISOW (Swift 1984; Dickson and Brown 1994; Smethie et al. 2000). ISOW then splits and one part flows through the Charlie Gibbs Fracture Zone into the Irminger Sea while the other part recirculates in the Iceland and West Europe Basin, where it mixes with LSW and Lower Deep Water (LDW) to
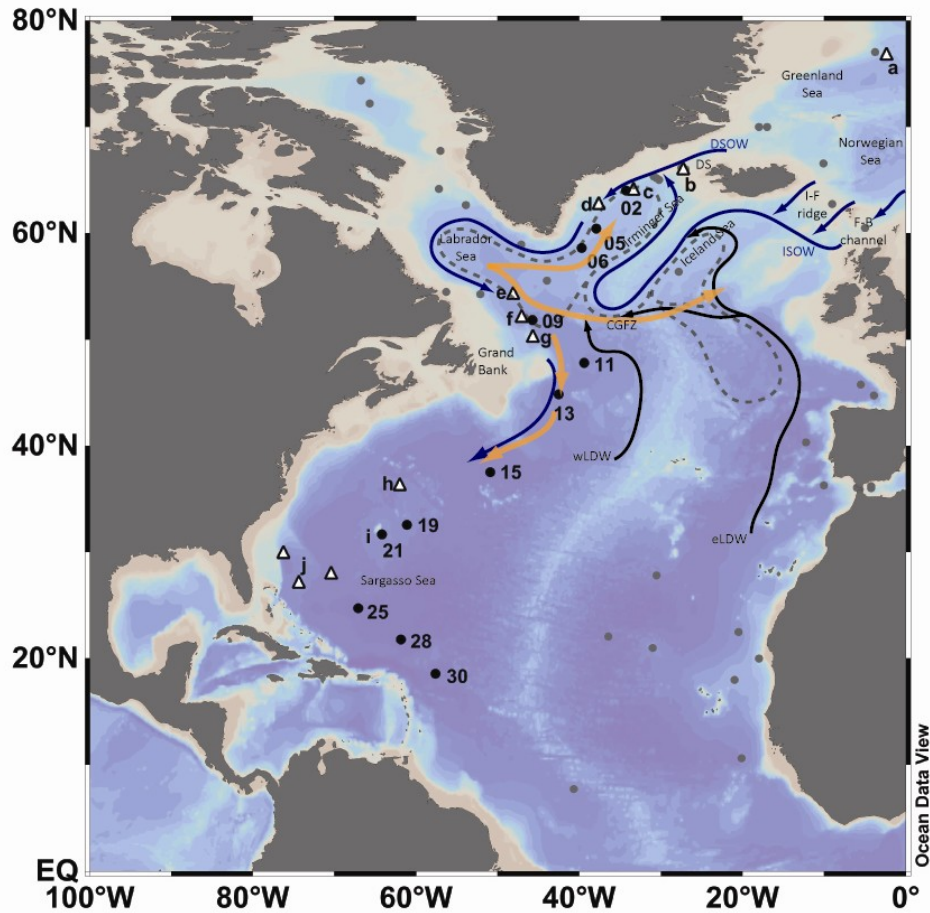
Figure 4.1: Map of the North Atlantic Ocean indicating the location of seawater profiles used in this study and the literature. Black dots with numbers stand for the stations where seawater was collected for this study (Table 4.2). White triangles with letters refer to stations from the literature, the data of which are used for comparison in this study. a: Signature station 30 (Lacan and Jeandel 2004a); b: Signature station 55 (Lacan and Jeandel 2004a); c: TTO/NAS station 167 (Piepgras and Wasserburg 1987); d: Signature station 9 (Lacan and Jeandel 2005b); e: Thalahassa station 15 (Rickli et al. 2009); f: Hudson 83-036 station 11 (Piepgras and Wasserburg 1987); g: Signature station 6 (Lacan and Jeandel 2005b); h: AII 109-1 station 30 (Piepgras and Wasserbug, 1987); i: BATS (Pahnke et al. 2012); j: OCE 63 station 1-4 (Piepgras and Wasserburg, 1980, 1987). The grey dots represent literature data where at least three depths were sampled for Nd isotopic compositions, but which are not further discussed in this chapter.

Purple (thicker) arrows represent schematically the spreading of Labrador Sea Water (LSW). Blue (thinner) arrows symbolise overflow of waters from the Greenland and Norwegian Seas (DSOW: Denmark Strait Overflow Water; ISOW: Iceland-Scotland Overflow Water). Black (thinner) arrows mark the northward flow of southern-derived water masses (w-LDW and e-LDW: western and eastern Lower Deep Water, respectively). Dotted grey lines represent deep recirculation cells. DS: Denmark Strait; I-F ridge: Iceland Faroe ridge; F-B channel: Faroe Bank channel; CGFZ: Charlie Gibbs Fracture Zone.

Map done with the software ODV, available at http://odv.awi.de/ (Schlitzer 2012).

become North East Atlantic Deep Water (NEADW) (LDW is the name for modified AABW, after its northward flow through the Atlantic Ocean). The characteristics of NEADW are a salinity maximum (due to the Atlantic Water coming from the Subtropical Atlantic), an oxygen minimum (due to the LDW), a CFC concentration lower than LSW and Denmark Strait Overflow Water (DSOW; see next section) and an intermediate potential density between LSW and North West Atlantic Bottom Water (NWABW) (Swift 1984; Dickson and Brown 1994; Smethie et al. 2000; Stramma et al. 2004).

4.2.1.3. Lower-NADW

Lower-NADW originates in the northern North Atlantic as North West Atlantic Bottom Water. Its main contributor is Denmark Strait Overflow Water (DSOW), a dense water mass that overflows the Denmark Strait (sill depth of ~600 m, Fig. 4.1). When sinking to the bottom of the Irminger Sea, DSOW entrains LSW and SPMW, to become NWABW. This water mass is the densest component of NADW, and is characterized by a salinity minimum, an oxygen maximum, and high CFC content (Swift 1984; Dickson and Brown 1994; Smethie et al. 2000; Stramma et al. 2004). In the subpolar Atlantic, NWABW is composed of 3 Sv DSOW, 3 Sv of entrained LSW and SPMW, and 1 Sv western LDW joining at about 50˚N. Further south, in the Subtropical Atlantic, another 1 Sv of western LDW mixes with NWABW around 30˚N, forming 8 Sv lower-NADW (Schmitz 1996).

4.2.2. Southern Ocean water masses: AAIW and AABW

Antarctic Intermediate Water (AAIW) and Antarctic Bottom Water (AABW) are both formed in the Southern Ocean and exported northward in all ocean basins. AAIW is formed in the southeast Pacific and southwest Atlantic Ocean from subduction of Antarctic surface waters at the Subantarctic Front (Sloyan and Rintoul 2001; Hartin et al. 2011). The subduction of Antarctic surface water to intermediate depths is linked with the deep winter mixed layer (>500 m), but the exact processes implicated are not fully understood, and they encompass convection driven by air-sea fluxes, eddy and turbulent mixing, Ekman transport, and mixing at the base of the mixed layer (Bostock et al. 2013). Due to its recent ventilation age, AAIW is characterised by a relative maximum in dissolved oxygen content. In the Atlantic Ocean it can be depicted as a tongue of low salinity and high nutrients (phosphate, nitrate and silicate) water spreading northwards at about 1000 m depth up to ~25-30˚N.

Antarctic Bottom Water is formed over the Antarctic continental shelf as well as in deeper water. South of 60˚S, there is only a slight difference in density between the surface layer, which is cold and fresh, and the underlying layer, which is warmer and more saline (Antarctic Circumpolar Water), and therefore the stratification is easily destabilized, by mixing due to strong winds for example. When this mixing is combined with increase in density of the surface layer, due to heat loss and sea-ice formation that rejects salt, or from surface water cooling in open ocean polynas, which are areas of open water surrounded by sea ice, then a dense water mass is produced, and it sinks and mixes with underlying waters to form AABW (England 1992; Brown et al. 2001). In the Atlantic sector of the Southern Ocean, the Weddell Sea is the major location of AABW formation. Northward advection of AABW into the Atlantic Ocean (up to 45˚N) can typically be recognised by relative high nutrient contents and by a low salinity.

4.3. Samples

Twelve depth profiles of seawater samples were collected for Nd concentrations and isotopes on the RV Pelagia during the first two legs of the Dutch GEOTRACES cruise GA02 (PE319 and PE321), that took place between the 28th of April and the 8th of July 2010 from Scrabster (Scotland) to Fortaleze (Brazil), via Bermuda (Fig. 4.1). Seawater samples for Nd isotope and concentration measurements were collected using either an ultraclean all-titanium frame CTD system (24 x 27L), or a Niskin-type sampler mounted on a stainless steel rosette (24 x 25L), and between 10 and 13 depths were sampled for Nd. During the GEOTRACES intercalibration exercise it was shown that Niskin-type samples are sufficiently clean for sampling seawater for REE concentrations and Nd isotopic compositions (Pahnke et al. 2012). Ten litres samples were filtered on board of the Pelagia using 0.2 μm Sartorius Sartoban 300 cartridges filters, which were rinsed with several litres of seawater prior to use. The samples were acidified on board to pH ~2 with subboiled distilled HCl (2 mL/L). Back in the home laboratory, between five and ten litres of seawater were weighted, spiked with ^{150}Nd spike, and equilibrated for at least one week. Details on sample treatment, purification and measurement techniques are provided in Chapter 3.

The filtration step was not tested in Chapter 3. However, extensive filtration tests were carried out as part of the international GEOTRACES intercalibration (Pahnke et al., 2012). While these tests revealed that the choice of filter has no effect on Nd isotope and

concentration measurements, the fact whether filtration altogether is necessary or not has to be evaluated on a case by case basis. This topic is revisited in paragraph 4.6.

4.4. Results

The Nd isotopic compositions and hydrological characteristics (salinity, potential temperature, potential density, and oxygen content) for all samples are reported in Table 4.2, and sections for ε_{Nd} and salinity for the whole transect can be found in Figure 4.2. θ-S plots for every station are shown in Figure 4.3. Surface and upper-ocean water masses, as well as bottom waters and Nd concentrations, will be discussed elsewhere (Chapter 5). In the following we will focus our discussion on NADW-relevant layers and their Nd isotopic composition.

In the present study, we chose water mass boundaries based on potential density (σ_{θ}) following Rhein et al. (2011) (Tables 4.2 and 4.3). In general, potential density ranges can vary depending on the area or the time of the year during which sampling happens. We chose to follow Rhein et al. (2011) because (i) the data set these authors used is recent (until 2009) (ii) the same density boundaries were used in previous publications (Rhein et al. 2002; Stramma et al. 2004; Kieke et al. 2006; Rhein et al. 2011) (iii) other observed physical characteristics (e.g., salinity maximum, O_2 minimum) of the water masses encountered during our cruises agree quite well with these boundaries. We are aware that the density ranges chosen are broad and can therefore overestimate the thickness of certain water masses, e.g., LSW (Yashayaev et al. 2007). However, the idea was to assign every sample measured in the present study to a water mass.

Table 4.2: Location, depth, hydrological properties and Nd isotopic composition for 12 depth profiles collected on GEOTRACES cruise GA02 on the Pelagia in 2010.

Sample depth [m]	Salinity[a]	Pot. Temp. (θ) [°C][a]	Pot. Dens. (σ_θ) [kg/m³]	O₂ [μmol/ kg][a]	^{143}Nd/^{144}Nd[b]	ε_{Nd}[c]	2se (int.)[d]	2sd (ext.)[e]	Water mass
Station 2 (2 May 2010; 64.0003°N – 34.2505°W; 2215 m)									
802	34.932	4.10	27.726	269.4	0.511920	-14.00	0.24	0.14	ULSW
1000	34.927	3.86	27.745	264.4	0.511950	-13.42	0.33	0.14	LSW
1901	34.929	3.02	27.830	271.3	0.512009	-12.28	0.25	0.15	NEADW
2151	34.880	1.85	27.891	295.7	0.512038	-11.70	0.42	0.15	NWABW
2206	34.884	1.26	27.938	301.6	0.512057	-11.33	0.62	0.15	NWABW
Station 5 (4 May 2010; 60.4277°N – 37.9078°W; 2943 m)									
417	34.920	4.19	27.705	269.0	0.511915	-14.11	0.10	0.14	ULSW
1001	34.878	3.55	27.738	273.8	0.511915	-14.11	0.13	0.14	ULSW
1502	34.919	3.44	27.782	267.2	0.511959	-13.25	0.09	0.14	LSW
2001	34.924	3.08	27.821	272.0	0.511992	-12.60	0.10	0.14	NEADW
2499	34.928	2.68	27.860	274.4	0.512006	-12.33	0.09	0.14	NEADW
2799	34.899	2.01	27.893	288.0	0.512054	-11.39	0.11	0.14	NWABW
2924	34.888	1.23	27.943	298.2	0.512086	-10.76	0.20	0.14	NWABW
Station 6 (5 May 2010; 58.6027°N – 39.7064°W; 3101 m)									
399	34.908	4.08	27.707	268.8	0.511910	-14.20	0.12	0.06	ULSW
801	34.863	3.54	27.726	277.3	0.511908	-14.24	0.09	0.06	ULSW
1499	34.914	3.43	27.778	267.0	0.511962	-13.19	0.08	0.06	LSW
1998	34.919	3.03	27.821	271.8	0.511984	-12.75	0.12	0.06	NEADW
2495	34.931	2.71	27.860	274.2	0.512019	-12.08	0.08	0.06	NEADW
2999	34.891	1.66	27.914	294.3	0.512064	-11.20	0.11	0.06	NWABW
3086	34.884	1.25	27.938	297.8	0.512092	-10.64	0.10	0.06	NWABW
Station 9 (9 May 2010; 51.8203°N – 45.7325°W; 4052 m)									
805	34.901	3.96	27.715	263.6	0.511901	-14.38	0.12	0.20	ULSW
993	34.890	3.73	27.730	267.6	0.511905	-14.29	0.12	0.20	ULSW
1247	34.898	3.60	27.749	267.7	0.511911	-14.18	0.13	0.20	LSW
1735	34.914	3.31	27.790	269.9	0.511914	-14.13	0.16	0.20	LSW
2252	34.916	2.91	27.830		0.511978	-12.87	0.11	0.20	NEADW
2997	34.907	2.14	27.890	277.8	0.512014	-12.18	0.14	0.20	NWABW
3745	34.898	1.70	27.917	287.9	0.512034	-11.79	0.12	0.20	NWABW
4041	34.898	1.64	27.922	290.5	0.512031	-11.84	0.12	0.20	NWABW
Station 11 (11 May 2010; 47.7996°N – 39.4001°W; 4570 m)									
1001	34.966	4.60	27.697	243.4	0.511901	-14.38	0.16	0.13	ULSW
1501	34.927	3.80	27.752	261.1	0.511912	-14.15	0.35	0.13	LSW
1998	34.922	3.41	27.786	264.7	0.511954	-13.34	0.25	0.13	LSW
3000	34.919	2.74	27.847	271.8	0.511985	-12.74	0.41	0.14	NEADW
4000	34.899	1.99	27.896	275.5	0.511993	-12.58	0.23	0.14	NWABW
4251	34.895	1.90	27.900	275.2	0.512009	-12.28	0.38	0.14	NWABW
4547	34.895	1.84	27.905	278.9	0.511996	-12.52	0.33	0.14	NWABW

Table 4.2 (continued)

Sample depth [m]	Salinity[a]	Pot. Temp. (θ) [°C][a]	Pot. Dens. (σ_0) [kg/m³][a]	O₂ [μmol/kg][a]	$^{143}Nd/^{144}Nd$[b]	ε_{Nd}[c]	2se (int.)[d]	2sd (ext.)[e]	Water mass
Station 13 (13 May 2010; 44.8442˚N – 42.5260˚W; 4751 m)									
1003	34.977	4.68	27.696	240.1	0.511901	-14.38	0.18	0.28	ULSW
1256	34.973	4.28	27.738	248.7	0.511906	-14.28	0.15	0.28	ULSW
1750	34.942	3.70	27.774	258.9	0.511934	-13.73	0.22	0.28	LSW
3501	34.913	2.34	27.879	272.6	0.512012	-12.22	0.13	0.28	NEADW
4499	34.892	1.85	27.903	272.8	0.511991	-12.62	0.13	0.33	NWABW
4726	34.893	1.82	27.906	276.3	0.511986	-12.73	0.47	0.33	NWABW
Station 15 (19 May 2010; 37.5164˚N – 50.8906˚W; 5441 m)									
2003	34.949	3.49	27.801	257.2	0.511950	-13.41	0.13	0.08	uNADW (LSW)
3002	34.937	2.66	27.870	258.5	0.512011	-12.23	0.12	0.08	mNADW (NEADW)
3999	34.896	1.96	27.898	262.0	0.511991	-12.62	0.10	0.20	lNADW (NWABW)
5001	34.877	1.76	27.900	255.5	0.511989	-12.66	0.12	0.20	modified-AABW
5364	34.870	1.71	27.899	250.4	0.511997	-12.50	0.12	0.06	modified-AABW
5414	34.869	1.70	27.899	250.3	0.511997	-12.50	0.11	0.06	modified-AABW
Station 19 (23 May 2010; 32.5514˚N – 61.0986˚W; 4683 m)									
149	36.627	18.76	26.331	193.6	0.512148	-9.56	0.09	0.06	STMW
251	36.588	18.33	26.411	193.1	0.512143	-9.66	0.08	0.06	STMW
401	36.541	17.88	26.487	189.1	0.512142	-9.67	0.08	0.06	STMW
866	35.261	9.47	27.250	138.2	0.512038	-11.71	0.13	0.06	
1001	35.120	7.25	27.482	168.6	0.511971	-13.01	0.08	0.06	
1251	35.055	5.18	27.701	221.4	0.511929	-13.84	0.12	0.06	uNADW (ULSW)
1750	34.983	3.92	27.784	248.4	0.511944	-13.54	0.07	0.06	uNADW (LSW)
2500	34.959	3.10	27.847	254.2	0.511991	-12.62	0.11	0.06	mNADW (NEADW)
3501	34.907	2.14	27.891	263.0	0.511994	-12.56	0.07	0.06	lNADW (NWABW)
4250	34.890	1.89	27.898	261.4	0.511986	-12.72	0.09	0.06	lNADW (NWABW)
4655	34.881	1.81	27.899	257.5	0.511985	-12.74	0.09	0.06	modified-AABW

Table 4.2 (continued)

Sample depth [m]	Salinity[a]	Pot. Temp. (θ) [°C][a]	Pot. Dens. (σ_0) [kg/m³]	O_2 [µmol/ kg][a]	$^{143}Nd/^{144}Nd$[b]	ε_{Nd}[c]	2se (int.)[d]	2sd (ext.)[e]	Water mass
Station 21 (BATS; 13 June 2010; 31.6669˚N – 64.1664˚W; 4567 m)									
75	36.613	18.70	26.335	223.4	0.512148	-9.56	0.09	0.06	STMW
201	36.566	18.05	26.464	210.8	0.512154	-9.44	0.18	0.33	STMW
297	36.521	17.74	26.507	207.3	0.512149	-9.55	0.13	0.33	STMW
500	36.298	16.54	26.626	192.0	0.512124	-10.03	0.12	0.33	
1001	35.071	6.03	27.608	207.1	0.511949	-13.44	0.56	0.33	
1249	35.008	4.64	27.726	243.7	0.511933	-13.75	0.13	0.33	uNADW (ULSW)
1749	34.968	3.71	27.793	258.4	0.511951	-13.39	0.11	0.33	uNADW (LSW)
2501	34.962	2.99	27.859	254.7	0.512022	-12.01	0.26	0.33	mNADW (NEADW)
3500	34.902	2.04	27.895	263.3	0.511995	-12.54	0.23	0.33	lNADW (NWABW)
4249	34.885	1.84	27.899	259.3	0.512003	-12.40	0.27	0.33	lNADW (NWABW)
4474	34.877	1.77	27.898	256.0	0.512009	-12.28	0.23	0.33	modified-AABW
Station 25 (17 June 2010; 24.7147˚N – 67.0728˚W; 5575 m)									
767	35.289	9.86	27.206	138.6	0.512073	-11.02	0.10	0.14	modified-AAIW
1250	35.062	5.27	27.696	217.4	0.511990	-12.64	0.12	0.14	uNADW (ULSW)
1751	34.994	3.82	27.803	251.1	0.511964	-13.14	0.08	0.14	uNADW (LSW)
2500	34.961	2.94	27.863	250.6	0.512006	-12.34	0.09	0.14	mNADW (NEADW)
3499	34.912	2.19	27.891	258.8	0.512007	-12.31	0.11	0.14	lNADW (NWABW)
4500	34.890	1.87	27.900	258.8	0.511988	-12.68	0.08	0.08	lNADW (NWABW)
5551	34.852	1.57	27.896	247.1	0.512034	-11.79	0.11	0.08	modified-AABW

Table 4.2 (continued)

Sample depth [m]	Salinity[a]	Pot. Temp. (θ) [°C][a]	Pot. Dens. (σ₀) [kg/m³]	O₂ [μmol/ kg][a]	^{143}Nd/^{144}Nd[b]	ε_{Nd}[c]	2se (int.)[d]	2sd (ext.)[e]	Water mass
Station 28 (20 June 2010; 21.7764°N – 61.8438°W; 5795 m)									
785	35.106	8.27	27.321	133.5	0.512069	-11.09	0.09	0.13	modified-AAIW
998	34.995	6.30	27.514	160.8	0.512057	-11.33	0.10	0.13	modified-AAIW
1752	34.984	3.70	27.808	253.3	0.511968	-13.08	0.10	0.13	uNADW (LSW)
2501	34.952	2.84	27.866	253.3	0.512008	-12.29	0.09	0.13	mNADW (NEADW)
3499	34.907	2.11	27.893	259.8	0.511999	-12.46	0.09	0.13	lNADW (NWABW)
4501	34.891	1.87	27.901	259.4	0.511994	-12.57	0.09	0.14	lNADW (NWABW)
5775	34.845	1.50	27.896	244.9	0.512045	-11.57	0.09	0.14	modified-AABW
Station 30 (22 June 2010; 18.5724°N – 57.6121°W; 5280 m)									
1250	35.028	4.97	27.704	216.0	0.512012	-12.21	0.30	0.15	uNADW (ULSW)
1749	34.997	3.81	27.806	247.4	0.511971	-13.00	0.12	0.08	uNADW (LSW)
2502	34.951	2.83	27.866	249.9	0.512012	-12.21	0.15	0.08	mNADW (NEADW)
3500	34.909	2.16	27.891	256.7	0.511999	-12.46	0.09	0.08	lNADW (NWABW)
4499	34.871	1.73	27.896	250.7	0.512016	-12.13	0.10	0.08	modified-AABW
5067	34.837	1.45	27.892	242.0	0.512053	-11.42	0.11	0.08	modified-AABW

a Hydrological properties measured on board the Pelagia by H. M. van Aken (Royal NIOZ).

b Normalized to 5 analyses of JNdi relative to JNdi value of 0.512115 (Tanaka et al., 2000).

c εNd values were calculated relative to a CHUR of 0.512638 (Jacobsen and Wasserburg, 1980).

d The internal errors are derived from the 2 sigma standard error on the measurement (maximum 360 cycles).

e External errors are the two sigma standard deviations derived from repeat analyses of Nd standard JNdi (n = 5).

The uncertainty plotted and quoted in the text is the larger one between internal and external error.

4.4.1. Upper-NADW

4.4.1.1. Subpolar – source area (ULSW, LSW)

In the Irminger Basin (stations 2, 5 and 6, Fig. 4.1), the potential density range corresponding to ULSW ($27.68 < \sigma_\theta < 27.74$ kg/m^3) is situated at a depth of 800 m (station 2), and at depths between 300 m and 1000 m (stations 5 and 6; Tables 4.2 and 4.3). This corresponds to a well-defined salinity minimum (34.90 ± 0.02 (1sd), n = 14) and a potential temperature of 3.92 ± 0.29°C (1sd) (Fig. 4.3a), and a small but resolvable O_2 maximum. The Nd isotopic composition measured for this water mass is -14.13 ± 0.19 (2sd, n = 5).

At station 9, located in the southeastern part of the Labrador Sea, ULSW is found between 800 and 1000 m, with S = 34.90 ± 0.01 (1sd), $\theta \approx 3.84 \pm 0.16$°C (1sd) and a Nd isotopic composition of -14.38 ± 0.20 (800 m) and -14.29 ± 0.20 (1000 m, Table 4.2) .

East of the Grand Bank (stations 11 and 13), ULSW flows between 1000 m and 1250 m and features a higher salinity (34.97 ± 0.01, 1sd) and potential temperature (4.52 ± 0.21°C, 1sd) compared to the southeastern Labrador Sea station (Tables 4.2 and 4.3). Its Nd isotopic composition ranges between -14.38 ± 0.28 and -14.28 ± 0.28.

Overall, ULSW in the subpolar region of the present study is characterised by a Nd isotopic composition of -14.24 ± 0.26 (2sd, n = 10, Table 4.3).

The layer corresponding to LSW ($27.74 < \sigma_\theta < 27.809$ kg/m^3) is found in the Irminger Basin at depths between 1000 and 1500 m (station 2) and between 1250 and 1750 m southeast of Greenland (stations 5 and 6, Tables 4.2 and 4.3). The salinity ranges from 34.89 to 34.96 and the potential temperature between 3.20 and 3.86°C (Fig. 4.3a). The Nd isotopic composition ranges from -13.42 to -13.19 (Table 4.2).

In the southeastern Labrador Sea (station 9), the potential density of LSW was sampled between 1250 and 2000 m, and S $\approx$ 34.91 and $\theta \approx$ 3.11 to 3.60°C (Fig. 4.3a). The Nd isotopic composition measured is -14.18 ± 0.20 at 1250 m and -14.13 ± 0.20 at 1735 m (Table 4.2).

East of Grand Bank (stations 11 and 13), LSW is found at depths between 1500 and 2000 m, and is characterized by S = 34.92 to 34.95 and θ = 3.41 to 3.95°C (Fig. 4.3a). The Nd isotopic composition is ranging from -14.15 to -13.34 (Table 4.2), with the deeper sample being the less radiogenic (lower) one. This is in agreement with the results for station 9 and mixing with less radiogenic NEADW flowing beneath LSW (see below).

Overall, the LSW Nd signature in the subpolar area of the present study is -13.67 ± 0.86 (2sd, n = 8).
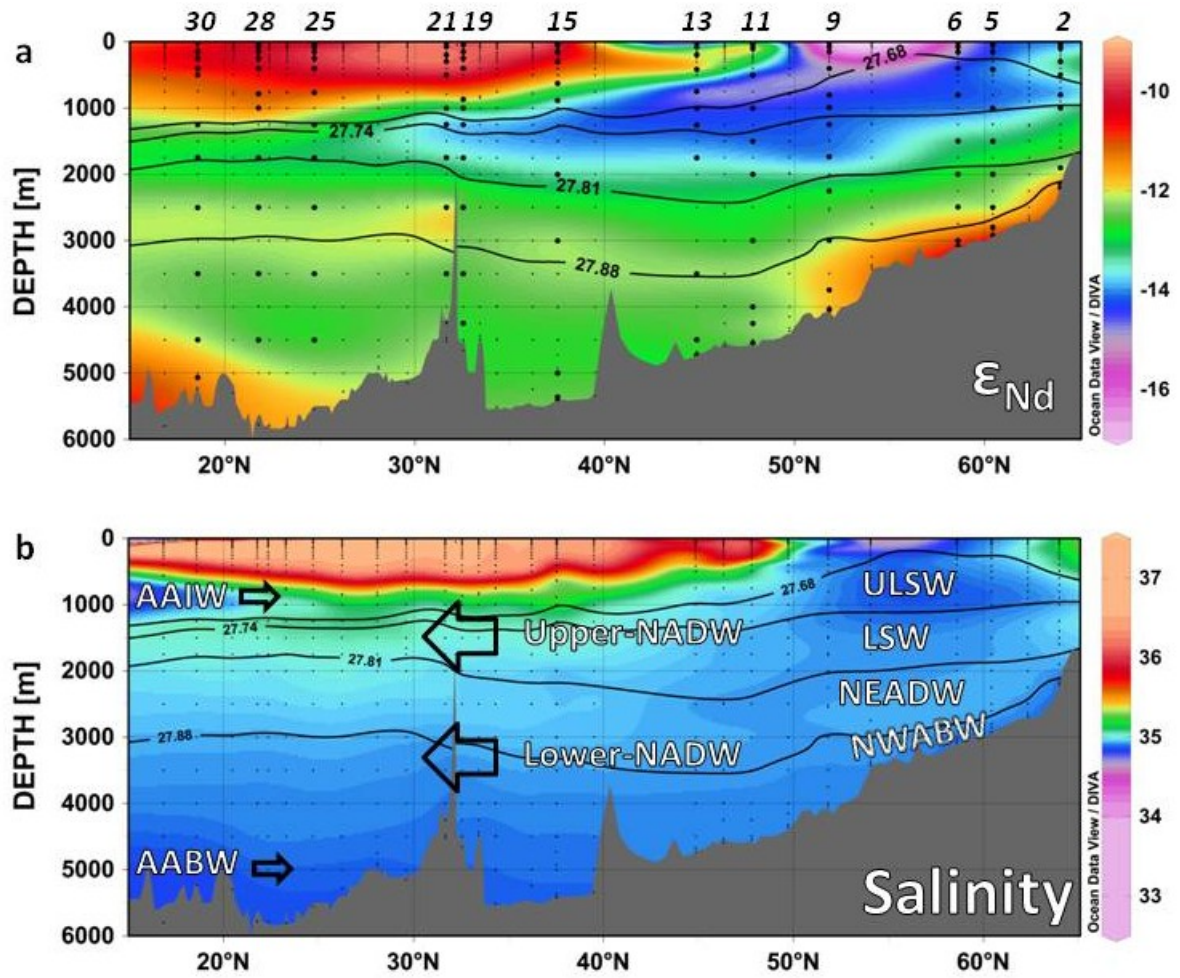
Figure 4.2: (a) Neodymium isotopic composition and (b) salinity section for the north to equatorial western Atlantic Ocean (this study). The black lines are the isopycnals σ_θ 27.68, 27.74, 27.81 and 27.88 kg/m^3 defining water mass boundaries (Table 4.3). The principle water masses are quoted on the salinity section, which is based on all 39 stations collected between Scrabster (Scotland) and Fortaleza (Brazil) during the two first legs of the Dutch GEOTRACES section GA02 (39 in comparison to 12 stations sampled for Nd isotopes and concentrations).

4.4.1.2. Subtropics – *downstream area (upper-NADW)*

At station 15, south of the Grand Bank, the density range of ULSW was not sampled, since no samples were taken between 800 m and 2000 m (Table 4.2). In the Sargasso Sea, the density layer of ULSW was sampled at 1250 m (stations 19 to 30, Fig. 4.1, Tables 4.2 and 4.3), lying below the well-defined silicate maximum corresponding to AAIW. In this area, ULSW is characterized by S = 35.04 ± 0.02 (1sd) and θ = 5.02 ± 0.24˚C (1sd) (Fig. 4.3b). The
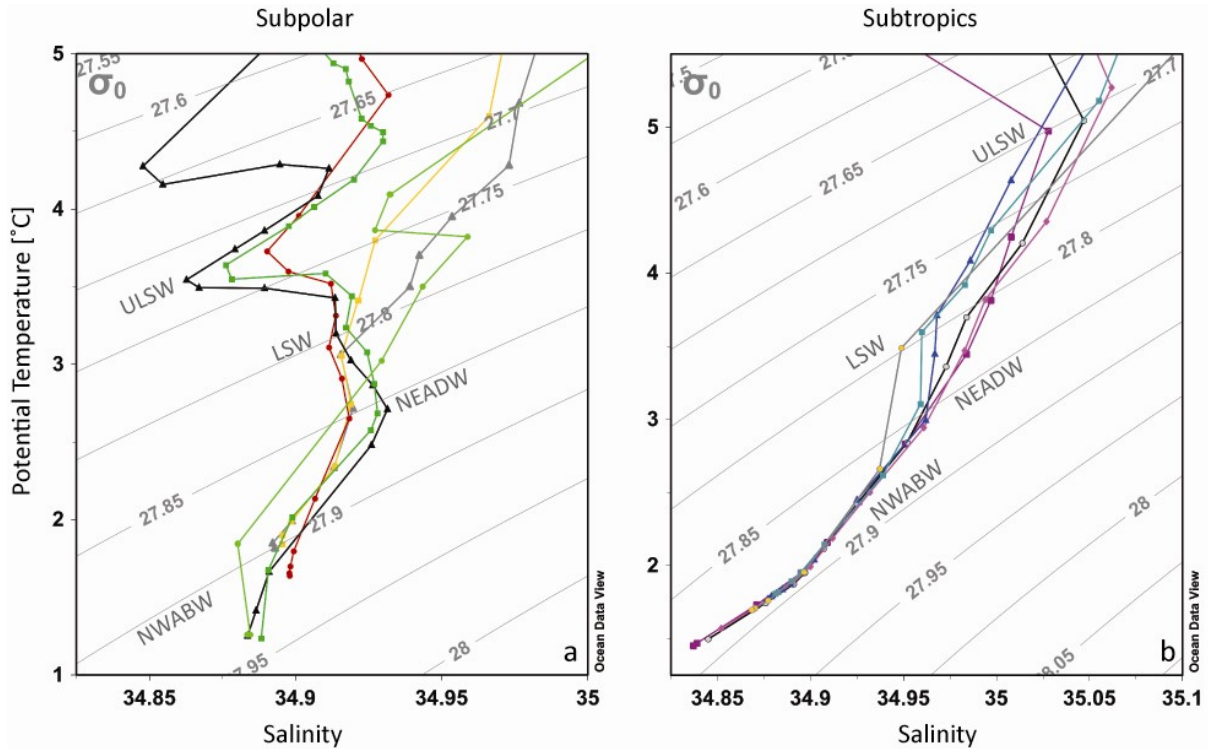
Figure 4.3: Potential temperature – salinity diagrams for (a) subpolar and (b) subtropical stations of the present study. a: light green dots = station 2; green squares = station 5; black triangles = station 6; red dots = station 9; orange squares = station 11; and grey triangles = station 13. b: yellow dots = station 15; turquoise squares = station 19; blue triangles = station 21; pink diamonds = station 25; grey dots = station 28; and purple squares = station 30. Diagrams done with the software ODV, available at http://odv.awi.de/ (Schlitzer 2012).

Nd isotopic composition is getting progressively more radiogenic when flowing southward, from -13.84 ± 0.12 at station 19 to -12.21 ± 0.30 at station 30.

In the Subtropical section of the Pelagia cruise, the LSW density range is found at depths between 1500 and 2000 m, and a small, but resolvable, O_2 maximum is observed. The salinity ranges from 34.95 to 35.03 and the potential temperature from 3.49 to 4.35˚C (Table 4.2, Fig. 4.3b). The Nd isotopic composition of LSW is -13.26 ± 0.43 (2sd, n = 6), and as for ULSW it is getting slightly more radiogenic when flowing southward.

Overall, the Nd isotopic signature of upper-NADW, encompassing ULSW and LSW in the subtropical North Atlantic, is -13.20 ± 1.00 (2sd, n = 10).

4.4.2. Middle-NADW

4.4.2.1. Subpolar – source area (NEADW)

In the Irminger Basin, NEADW ($27.809 < \sigma_\theta < 27.88$ kg/m^3) is detected at 1900 m (station 2) and between 2000 and 2750 m (stations 5 and 6; Fig. 4.1, Table 4.2). Even though the typical salinity maximum is less pronounced at station 2, it can be clearly observed at station 5 and 6 at $\sigma_\theta \approx 27.86$ kg/m^3 (Fig. 4.3a). The salinity measured for this water mass in the Irminger Sea is around 34.93 and $\theta = 2.81 \pm 0.21$°C (1sd). The Nd isotopic composition ranges from -12.75 ± 0.12 to -12.08 ± 0.08, and for the stations where two depths have been sampled, the shallower one is less radiogenic, probably due to mixing with overlying LSW.

At station 9 (southeastern Labrador Sea), NEADW is found between 2250 and 2550 m and features a salinity of 34.92, a potential temperature of 2.78 ± 0.18°C (1sd) and an ε_{Nd} value of -12.87 ± 0.20 (Nd sample collected only at 2250 m, Table 4.2).

NEADW is found at deeper depth east of the Grand Bank (between 2500 and 3500 m) compared with the southeastern Labrador Sea (station 9), and has the following characteristics: S ≈ 34.92, $\theta = 2.71 \pm 0.32$°C (1sd), Nd isotopic composition between -12.74 ± 0.41 (station 11, 3000 m) and -12.22 ± 0.28 (station 13, 3500 m), in good agreement with the Nd signature observed at station 9 (Table 4.2).

In summary, NEADW is recognised in the subpolar area of the Pelagia cruise by a salinity maximum at $\sigma_\theta \approx 27.85$ to 27.86 kg/m^3 (Fig. 4.3a) and features $\varepsilon_{Nd} = -12.48 \pm 0.59$ (2sd, n = 8).

4.4.2.2. Subtropics – downstream area (middle-NADW)

In the Subtropical area (stations 15 to 30, Fig. 4.1, Table 4.2), middle-NADW is flowing between 2000 and 3000 m depth and is characterised by a small O$_2$ minimum. It is slightly saltier than in the subpolar area (S $= 34.96 \pm 0.02$ (1sd)), and has a potential temperature of 2.99 ± 0.35°C (1sd). Its Nd isotopic composition is -12.28 ± 0.40 (2sd, n = 6).

4.4.3. Lower-NADW

4.4.3.1. Subpolar - source area

In the subpolar stations, NWABW is found between NEADW and the seafloor ($\sigma_\theta > 27.88$ kg/m^3, Fig. 4.3a), and is characterised by higher O$_2$ concentrations due to the presence of

recently ventilated DSOW. It has a salinity about 34.89 ± 0.01 (1sd) and $\theta = 1.55 \pm 0.30°C$ (1sd) in the Irminger Sea. Neodymium isotopic compositions measured range between -11.70 and -10.64 (n = 6), with the sample closer to the bottom being more radiogenic at all three stations (Table 4.2).

North West Atlantic Bottom Water can be found at station 9 (southeastern of Labrador Sea) with a salinity of 34.90 ± 0.00 (1sd), a potential temperature of $1.79 \pm 0.20°C$ (1sd), and a Nd isotopic composition of -11.94 ± 0.43 (2sd, n = 3, Table 4.2).

East of the Grand Bank the potential temperature is slightly warmer ($\theta = 1.88 \pm 0.07°C$) and the Nd isotopic composition less radiogenic ($\varepsilon_{Nd} = -12.54 \pm 0.34$; 2sd, n = 5). These results are consistent, within error, with the values obtained for NWABW in the southeastern Labrador Sea.

Overall, the Nd isotopic composition of NWADW in the subpolar area of the present study is -11.82 ± 1.38 (2sd, n = 14).

4.4.3.2. Subtropics – downstream area

In the subtropical area, lower-NADW flows below middle-NADW and above modified-AABW, at depths between 3000 and 4500 m. It is characterised by a small, but resolvable, O_2 maximum. The boundary between lower-NADW and modified-AABW in the present study is defined by $\theta > 1.82°C$ (van Aken 2010). The salinity and potential temperature measured are very similar to that found in the subpolar area (S= 34.90 ± 0.01 and $\theta = 1.88 \pm 0.07°C$, 1sd), as is the Nd isotopic composition ($\varepsilon_{Nd} = -12.53 \pm 0.25$, 2sd, n = 10). The deepest samples of this water mass are getting slightly more radiogenic when flowing southward (Table 4.2), probably due to mixing with the underlying, northward flowing AABW ($\varepsilon_{Nd} = -8.5 \pm 0.3$ in the South Atlantic, Jeandel 1993).

The Nd isotopic composition of lower-NADW is -12.53 ± 0.25 (n = 10). Since this average value is within error the same as the one derived for middle-NADW ($\varepsilon_{Nd} = -12.28 \pm 0.40$, 2sd, n = 6), we will combine them in the following under the name of lower-NADW with a Nd isotopic composition of -12.44 ± 0.39 (2sd, n = 16).

Table 4.3: Water masses encountered in the present study together with their characteristics. Grey areas represent locations closest to the formation areas of the respective water masses.

Water Mass	σ(θ) range [kg/m³]	Location	Salinity (1sd)	θ [˚C] (1sd)	Depth range [m]	ε_{Nd} (2sd)	Stations	Remarks
ULSW (u-NADW)	27.68-27.74	Irminger Sea	34.90 (0.02)	3.92 (0.29)	800 (st. 2) 300 – 1000 (st. 5&6)	-14.13 (0.19; n = 5)	2, 5, 6	ε_{Nd} subpolar -14.24 (± 0.26; n = 10)
		SE Labrador Sea	34.90 (0.01)	3.84 (0.16)	800-1000	-14.38 to -14.29	9	
		East Grand Bank	34.97 (0.01)	4.52 (0.21)	1000 - 1250	-14.38 to -14.28	11, 13	
		Sargasso Sea	35.04 (0.02)	5.02 (0.24)	1250	-13.84 to -12.21	15 to 30	St. 15 & 28 no ULSW, n = 4
LSW (u-NADW)	27.74 – 27.809	Irminger Sea	34.92 (0.02)	3.51 (0.23)	1000-1500 (st. 2) 1250-1750 (st. 5&6)	-13.42 to -13.19	2, 5, 6	ε_{Nd} subpolar -13.67 (± 0.86, n = 8)
		SE Labrador Sea	34.91 (0.01)	3.38 (0.22)	1250-2000	-14.13 to -14.18	9	
		East Grand Bank	34.93 (0.01)	3.63 (0.22)	1500-2000	-14.15 to -13.34	11, 13	
		Sargasso Sea	34.99 (0.02)	3.94 (0.29)	1500-2000	-13.26 (0.43, n = 6)	15 to 30	ε_{Nd} u-NADW -13.20 (± 1.00, n = 10)
NEADW (m-NADW)	27.81 – 27.88	Irminger Sea	34.93 (0.00)	2.81 (0.21)	1900 (st. 2) 2000-2750 (st. 5&6)	-12.75 to -12.08	2, 5, 6	ε_{Nd} subpolar -12.48 (± 0.59, n = 8)
		SE Labrador Sea	34.92 (0.00)	2.78 (0.18)	2250-2550	-12.87	9	
		East Grand Bank	34.92 (0.00)	2.71 (0.32)	2500-3500	-12.74 (st 11, 3000 m) -12.22 (st 13, 3500 m)	11, 13	
		Sargasso Sea	34.96 (0.02)	2.99 (0.35)	2000-3000	-12.28 (0.40, n = 6)	15 to 30	

Table 4.3 (continued)

Water Mass	σ(θ) range [kg/m³]	Location	Salinity (1sd)	θ [°C] (1sd)	Depth range [m]	ε_{Nd} (2sd)	Stations	Remarks
NWABW (l-NADW)	> 27.88	Irminger Sea	34.89 (0.01)	1.55 (0.30)	< 1900 (st. 2) < 2600-2750 (st. 5&6)	-11.70 to -10.64	2, 5, 6	
		SE Labrador Sea	34.90 (0.00)	1.79 (0.20)	Below 2550	-11.94 (0.43, n = 3)	9	ε_{Nd} subpolar -11.82 (± 1.38, n = 14)
		East Grand Bank	34.90 (0.00)	1.88 (0.07)	Below 3500	-12.54 (0.34, n = 5)	11, 13	
		Sargasso Sea	34.90 (0.01)	2.06 (0.21)	3000 – 4000 3500 - 4500	-12.53 (0.25, n = 10)	15 to 30	ε_{Nd} m- and l-NADW -12.44 (± 0.39, n = 16)
STMW	26.33 – 26.55	Sargasso Sea	36.57 (0.05)	18.13 (0.42)	150-500 m (st. 19) 75-400 m (st. 21)	-9.57 (0.17, n = 6)	19 and 21	
Modified-AAIW	27.21 – 27.54	Sargasso Sea	35.07 (0.14)	7.35 (1.70)	750-1000 m	-11.15 (0.32, n = 3)	25 to 30	
Modified-AABW	27.89 – 27.90	Sargasso Sea	34.87 (0.01)	1.68 (0.12)	Below l-NADW	-12.18 (0.96, n = 9)	15 to 30	θ < 1.82°C

4.4.4. Other water masses encountered in the present study

4.4.4.1. Subtropical Mode Water (STMW)

In the present study, STMW is only observed at station 19 (150-500 m, Table 4.2) and station 21 (75 to 400 m, Table 4.2). The salinity for this water mass is 36.57 ± 0.05 (1sd) and the potential temperature is 18.13 ± 0.42˚C (1sd, Table 4.2). The Nd isotopic composition measured is -9.57 ± 0.17 (2sd, n = 6, Tables 4.2 and 4.3).

4.4.4.2. Modified-AAIW

Modified-AAIW is recognised at stations 25 to 30 (Fig. 4.1) by a maximum in silicate, nitrate and phosphate concentrations above upper-NADW at a depth between 750 and 1000 m. It is characterised by a salinity ranging from 34.94 and 35.29 and a potential temperature ranging from 5.70 to 9.86˚C. Deeper samples are colder and less salty, and for the same water depth, samples show warmer temperatures and higher salinities when flowing northwards, suggesting dilution of the AAIW characteristics through mixing with NADW. Only three samples were collected for Nd in this water mass, and the Nd isotopic composition measured is -11.15 ± 0.32 (2sd, n = 3, Tables 4.2 and 4.3).

4.4.4.3. Modified-AABW

Modified-AABW flows below lower-NADW, and is characterised by a high content in silicate and phosphate, an increase in oxygen concentrations toward the bottom and a potential temperature below 1.82˚C (van Aken 2010). This water mass is found in the whole subtropical area of the present study at depths below about 4500 m. The salinity measured is 34.87 ± 0.01 (1sd) and the potential temperature is 1.68 ± 0.12˚C (1sd, Tables 4.2 and 4.3). The Nd isotopic composition is -12.18 ± 0.96 (2sd, n = 9, Tables 4.2 and 4.3), and it becomes progressively less radiogenic towards the north.

4.4.5. Neodymium isotope depth profiles

In sections 4.4.1 to 4.4.4, the Nd isotopic composition of each water mass of interest was stated. Here, a brief description of the Nd isotope depth profiles will be presented. For this purpose, the data set will be split according to the general overall shape of the isotopic profiles:

<u>Type I:</u> Irminger Sea (stations 2 to 6, Figs. 4.1 and 4.4a).

All three stations show a smooth trend in Nd isotopes from less radiogenic surface water values around -15.2 to -14.2 to more radiogenic bottom water values of -11.3 to -10.6. A relative hold or a reversal of the trend can be observed in the depth range of ULSW (300-1000 m). Furthermore all three profiles show a more rapid evolution towards more radiogenic values in the lowermost 500 m of the profiles (Fig. 4.4a).

<u>Type II:</u> Southeastern Labrador Sea and Grand Bank (stations 9 to 13, Figs. 4.1 and 4.4b).

These three stations show Nd isotope depth profiles with a great amount of variability in the uppermost 1000 m of the water column ($\varepsilon_{Nd} \approx$ -17.0 to -11.5), relatively constant Nd isotopic compositions from 1000 m to 2000 m depth in the depth range of ULSW and LSW ($\varepsilon_{Nd} \approx$ -14), a slight increase towards more radiogenic values down to about 3500 m (NEADW; $\varepsilon_{Nd} \approx$ -12.6), and a shift to slightly less radiogenic values at the very bottom (Fig. 4.4b).

<u>Type III</u>: Sargasso Sea (stations 15 to 30, Figs.4.1 and 4.4c)

In the subtropics, seawater from the six depth profiles analysed for Nd isotopic composition feature similar trends (Fig. 4.4c). The Nd isotopic composition is relatively constant for the upper 500 m ($\varepsilon_{Nd} \approx$ -10) and shifts to less radiogenic values of -13.8 to -12.2 in the depth range of upper-NADW (~ 1000 to 2000 m depth, Fig. 4.4c). Below this depth, seawater Nd isotopes display a trend towards more radiogenic values down to ~ 2500 m, and stay relatively constant for the next 2000 m (lower-NADW, $\varepsilon_{Nd} \approx$ -12.4, Fig. 4.4c), before becoming slightly more radiogenic closer to the bottom (modified-AABW, Fig. 4.4c).
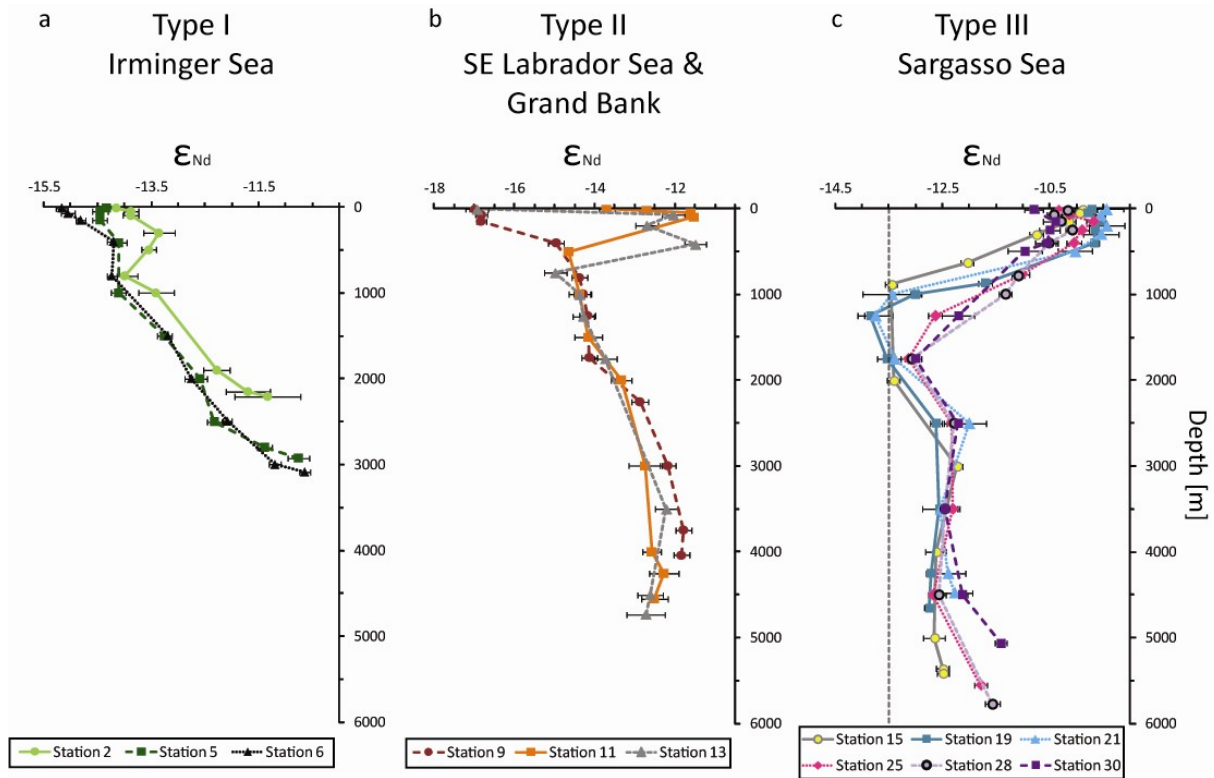
Figure 4.4: Neodymium isotope ratios versus depth [m] (a) in the Irminger Sea (Type I), (b) in the southeastern Labrador Sea and around Grand Bank (Type II), and (c) in the Sargasso Sea (Type III). Error bars represent the largest uncertainty between internal and external errors (see Table 4.2). The grey dotted line in (c) represents the accepted value of NADW (ε_{Nd} = -13.5; Piepgras and Wasserburg, 1987). Note the change of scale in the x-axis.

4.5. Discussion

4.5.1. Assessment of the Nd isotopic composition of seawater as a water mass proxy

In this section, the question whether the Nd isotopic composition of seawater can be used as a quasi-conservative water mass tracer will be further discussed. To test this hypothesis, we will discuss our new Nd isotopic data in relation to (i) distance from the source region of the principle water masses constituting NADW, (ii) previously published Nd isotopic compositions of deep waters from the whole Atlantic Ocean, and (iii) conservative and non-conservative seawater properties such as salinity and silicate concentrations.

4.5.1.1. Evolution of the Nd isotope signature with distance from the source area

When a water mass, such as NADW, leaves its formation region and is advected into the global ocean, it gradually mixes with surrounding water masses, leading to a loss of its original characteristics. While, for example, the core of NADW is still characterised by a salinity maximum in the South Atlantic (Schmitz 1996; Lacan and Jeandel 2005b), Figures 4.2b and 4.5a show that already in the relatively small area investigated here, LSW shows an increase in salinity from close to its source area in the southeastern Labrador Sea (station 9, ~52°N; S = 34.91) to the subtropics (station 30, ~19°N; S = 35.00).

If truly conservative, the Nd isotope characteristics of a water mass should be equally fading when flowing away from its source region through mixing with surrounding waters. A prime example for this from our new data is the evolution of the Nd isotopic composition of ULSW with latitude (Fig. 4.5b). Indeed, in the southeastern Labrador Sea, close to the source region of ULSW, the Nd isotopic composition of this water mass is ~ -14.3 (station 9, Tables 4.2 and 4.3, Fig. 4.5b). ULSW subsequently enters the subpolar gyre, and is ultimately exported within the western boundary current as part of upper-NADW (Fig. 4.1). When flowing northeastwards towards the Irminger Sea, the Nd isotopic composition of ULSW gets slightly more radiogenic and reaches a value of -14.00 ± 0.24 at station 2, which is the northernmost station of the present study. The same is true - and far more pronounced - when observing the southward spread of ULSW. The Nd isotopic composition changes by ~2 epsilon units from station 9 at ~52°N to station 30 at ~19°N (ε_{Nd} = 12.21 ± 0.30, Table 4.2). This Nd isotope evolution is consistent with fading of the ULSW signal on the one hand, and mixing with more radiogenic AAIW on the other hand. AAIW has an isotopic composition of about -8.7 in the South Atlantic (Jeandel 1993) close to its source region, but by the time it reaches 9°N the signal is -10.1 (Huang et al. 2014). Labrador Sea Water (LSW) on the other hand shows a similar, though less pronounced, evolution from $\varepsilon_{Nd} \approx$ -14.2 close to its source region (station 9, Table 4.2) to ε_{Nd} = -13.00 ± 0.12 in the subtropics as component of upper-NADW (station 30) (Fig. 4.5b).

Regarding the two source components of lower-NADW, NWABW and NEADW (Fig. 4.5c), we observe less of an evolution with latitude, but rather a drastic change for NWABW from its values close to the source region (e.g., stations 2 to 6, ε_{Nd} = -11.7 to -10.6, n = 6, Table 4.2; for comparison the main component of NWABW, Denmark Strait Overflow Water (DSOW), has a Nd isotope signature of ε_{Nd} = -8.4 ± 1.4; Lacan and Jeandel, 2004a) to values outside the Irminger Sea (ε_{Nd} = -12.44 ± 0.54, 2sd, n = 18). Indeed, NWABW displays ~1.1
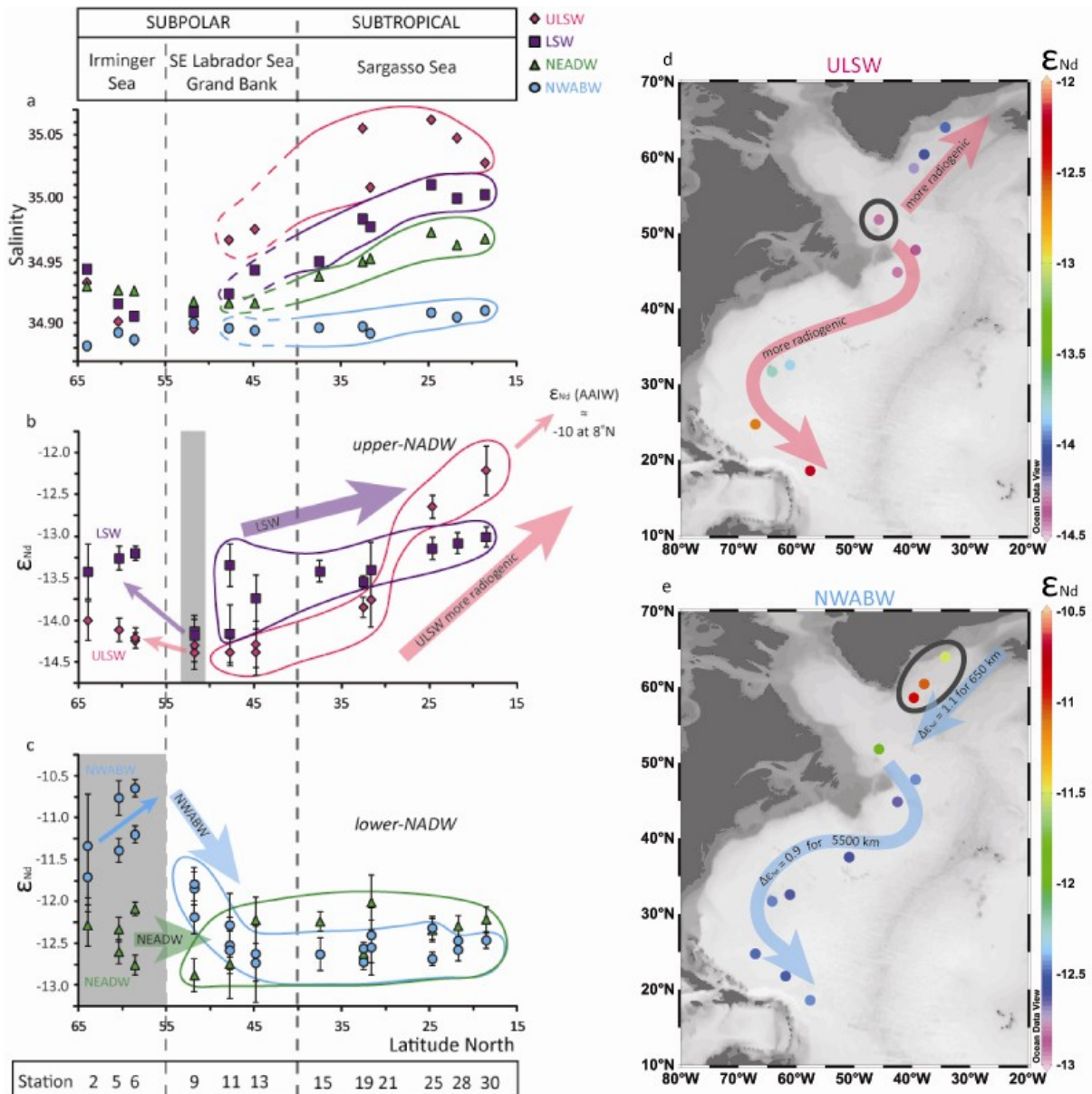
Figure 4.5: (a) Latitude vs. salinity for all intermediate and deep waters collected during this study. Samples are assigned to water masses according to Table 4.3. The study area can be separated in three distinct areas: (i) Irminger Sea, (ii) southeastern Labrador Sea and area around Grand Bank, and (iii) Sargasso Sea. (b) Latitude vs. Nd isotopic composition for ULSW (pink diamonds) and LSW (purple squares) samples. (c) Latitude vs. Nd isotopic composition for NEADW (green triangles) and NWABW (blue circles) samples. Thick stippled line separates the subtropical Atlantic to the right from the subpolar gyre area to the left. Accordingly sample locations to the right are labelled with upper- and lower-NADW and sample locations to the left are labelled with the name of the original source water masses. Grey shaded areas in both panels mark the sample locations closest to the formation areas of the respective water masses (e.g., station 9 in the southeastern Labrador Sea for ULSW and LSW in panel b and stations 2, 5 and 6 in the Irminger Sea for NEADW and NWABW in panel c). Note that the Irminger Sea samples were collected proximal to the overflow of DSOW, but

not in the direct influence of ISOW, the major constituent of NEADW. ULSW = pink diamonds, LSW = purple squares, NEADW = green triangles, NWABW = blue circles. Neodymium isotopic composition (expressed as ε_{Nd}) for the density layer of (d) ULSW and (e) NWABW. The grey circles mark the sample locations closest to the formation areas, and the arrows shows the direction of the flow path of the respective water masses.

epsilon unit variation for a flow path of ~650 km from station 2 to 6 in the Irminger Basin (Fig. 4.1) whereas only a ~0.9 epsilon unit change over about 5500 km from station 9 to 30. This observation is in agreement with constant salinity values for NWABW throughout the North Atlantic (Fig. 4.5a) and indicates that efficient mixing with overlying and less radiogenic water masses already happens in the subpolar gyre prior to export as part of lower-NADW. North East Atlantic Deep Water (NEADW) on the other hand shows a rather constant Nd isotopic composition throughout the study area (ε_{Nd} = -12.40 ± 0.54, 2sd, n = 14; all stations in subpolar and subtropical areas). The most likely explanation for this observation is that none of our stations lie close to the actual source areas of the main component of NEADW, Iceland-Scotland Overflow Water (ISOW; ε_{Nd} = -8.2 ± 0.6; Lacan and Jeandel, 2004b). Hence we are already recording a mixed signature as also evidenced by the relatively weak salinity maximum of this water mass (Fig. 4.3).

It should be noted that the influence of MOW, characterised by higher salinity, higher potential temperature, and a more radiogenic Nd isotopic composition (ε_{Nd} ≈ -9.4 when leaving the Mediterranean Sea, Spivack and Wasserburg 1988) does not feature prominently in the physical properties and Nd isotopic compositions for any of our stations (Tables 4.2 and 4.3). The only indication for MOW being present in the western North Atlantic during the time period of sampling is a small salinity maximum detected at station 19 (S = 35.055, 1250 m, Table 4.2, Fig. 4.3b), which goes with a slightly less radiogenic Nd isotopic composition (-13.84 ± 0.12 at 1250 m, Table 4.2) compared to the same water depths at neighbouring stations (e.g., ε_{Nd} = -14.28 ± 0.28 at 1250 m at station 13).

4.5.1.2. New data set in comparison to existing Atlantic Ocean data

Conservative behaviour of Nd isotopes in Atlantic seawater has been suggested for deep waters below 2500 m by correlation with salinity (see Figs. 9 and 10 in Goldstein and Hemming, 2003). Figure 4.6a shows an updated version of this figure, including our new deep water data (>2500 m) from all stations in comparison to previously published data. As

Figure 4.6: Neodymium isotope ratios versus (a) salinity, (b) potential temperature [˚C], and (c) silicate concentrations [µmol/kg]. The grey lines show the mixing envelope between a northern end-member ($\varepsilon_{Nd} \approx$ -13.5, S $\approx$ 34.95, $\theta \approx$ 3˚C and [SiO_2] $\approx$ 12 µmol/kg) and a southern end-member ($\varepsilon_{Nd} \approx$ -8.5, S $\approx$ 34.65, $\theta \approx$ -0.5˚C and [SiO_2] $\approx$ 125 µmol/kg). Diamonds are data from the literature, and blue dots are data from this study. All samples are from water depths > 2500 m. Figure adapted from Goldstein and Hemming (2003). Neodymium data sources: (Piepgras and Wasserburg 1983; Piepgras and Wasserburg 1987; Spivack and Wasserburg 1988; Jeandel 1993; Lacan and Jeandel 2005b; Godfrey et al. 2009; Rickli et al. 2009; Copard et al. 2011; Pahnke et al. 2012; Stichel et al. 2012; Garcia-Solsona et al. 2014). Note that data from the Mediterranean Sea, the Nordic Seas and Baffin Bays were not included.
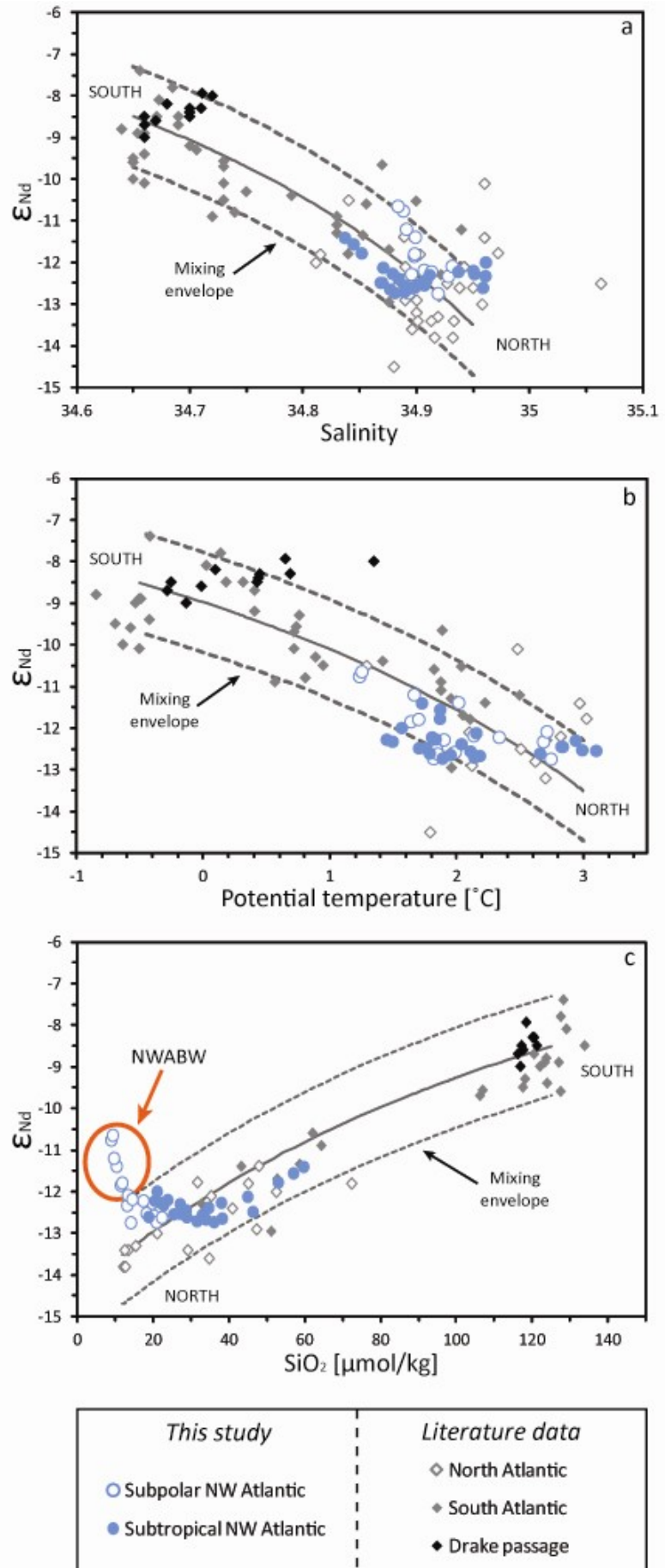
can be seen, all of the deep water data from the subpolar and subtropical North Atlantic fall within the mixing envelop defined by Southern Ocean water ($\varepsilon_{Nd} \approx$ -8.5) and North Atlantic Deep Water ($\varepsilon_{Nd} \approx$ -13.5). The utilisation of the latter, however, highlights that the approach is problematic when considering data from subtropical and subpolar areas, which encompass the various source components of NADW. For example, data for shallower ULSW wouldplot outside the mixing envelop, as these waters are (i) fresher in the subpolar area and (ii) saltier in the subtropical region for a given Nd isotopic composition as expected from the mixing relationship. Another interesting correlation is the one observed between Nd isotope ratios and potential temperature (Fig. 4.6b). Like salinity, potential temperature is a conservative water mass property, and Figure 4.6b shows that the data of the present data set fall within the mixing envelope defined by a northern end member and southern end member for water depths below 2500 m. As for the relationship with salinity, results for the shallower ULSW would plot outside the mixing array due to higher temperature for a given Nd isotopic composition measured for this water mass.

It is furthermore interesting to repeat the exercise done in Goldstein and Hemming (2003) to plot seawater Nd isotopic compositions versus silicate concentrations for waters below 2500 m (Fig. 4.6c). Since silicate is a macro-nutrient, its concentration in the upper part of the water column is governed by biological uptake. Concentrations in deeper waters are a function of remineralised silicate, and show an increase along the global conveyor belt due to the increasing age of water masses. For the Atlantic Ocean, two simple endmembers can be assumed: one that shows high nutrient (and hence silicate) concentrations and relatively radiogenic Nd isotopic compositions and is sourced in the south (AABW; $\varepsilon_{Nd} \approx$ -8.5 and $[SiO_2] \approx$ 125 µmol/kg) and one that shows lower nutrient concentrations and lower Nd isotopic compositions and reflects NADW exported from the subpolar gyre ($\varepsilon_{Nd} \approx$ -13.5 and $[SiO_2] \approx$ 12 µmol/kg). The samples from our data set that plot outside the mixing envelop in Figure 4.6c can be assigned to NWABW (Tables 4.2 and 4.3). There is, furthermore, considerable structure to the data set, which will be discussed in detail below.

4.5.1.3. Relationship of seawater Nd isotopes and silicate concentrations

Figure 4.7 provides a closer look at the correlation between ε_{Nd} and silicate for all intermediate to deep waters analysed in this study. Figure 4.7a highlights the source composition of all water masses that contribute to the different individual components and that are exported as NADW in terms of their Nd isotopic compositions and silicate

Figure 4.7: Neodymium isotope ratios (expressed as ε_{Nd}) versus silicate [µmol/kg].

(a) represents the data of the present study for the subpolar and subtropical regions (black diamonds) as well as some end member water masses; (b) data of the present study, but only for the subpolar area, and (c) data of the present study for the subtropical area.

(a) End members: pink circle: ULSW; purple circle: LSW; green circle: ISOW; blue circle: DSOW; yellow circle: MOW. (b) pink diamonds: ULSW; purple squares: LSW; green triangles: NEADW; and blue dots: NWABW. (c) lilac diamonds: upper-NADW; turquoise triangles: lower-NADW; and orange squares: modified-AABW. Note the different x-scale in (b).

References for the water masses end-members: ULSW: AE7W Line (southeastern half) and this study; LSW: (Tanhua et al. 2005) and this study; ISOW: (Fogelqvist et al. 2003) and (Lacan and Jeandel 2004b); DSOW: (Tanhua et al. 2005) and (Lacan and Jeandel 2004a); AABW: WOCE A07 station 76 (1993) and (Jeandel 1993); MOW: WOCE A03 station 6 (1993) and (Spivack and Wasserburg 1988)). Please note that the Nd isotopic composition of ULSW and LSW are taken from this study (station 9, southeastern Labrador Sea). We are aware that our samples were not collected in pure ULSW and LSW. However, there is no literature data available for pure ULSW or LSW either.
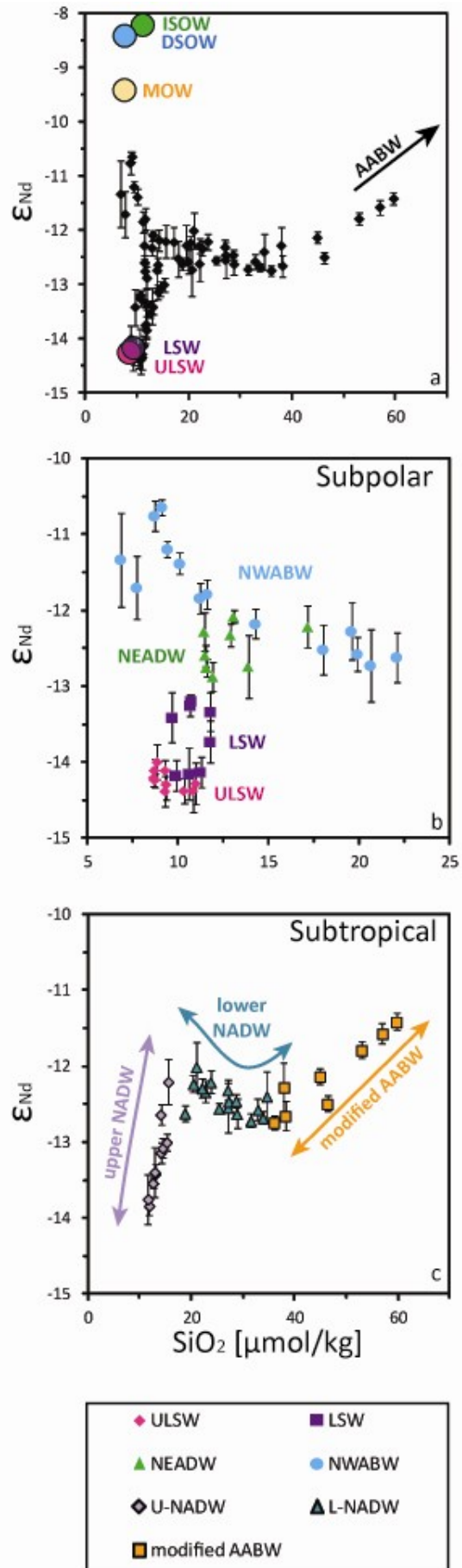
concentrations (see figure caption for more detail). It illustrates that all known endmembers encapsulate our data. In detail, there are three different trends visible: (i) NWABW samples trending towards the overflow sources (DSOW and ISOW), with a broad spread in silicate concentration (~7 µmol/kg at station 2 to ~21 µmol/kg at station 13) and Nd isotope ratios (~ -11.5 to ~ -12.7 for stations 2 and 13 respectively; Fig. 4.7b and Table 4.2). This contrasts with (ii) ULSW and LSW, for which the spread in silicate concentrations (between 8 and 11 µmol/kg, Table 4.2) and Nd isotope values (Fig. 4.7b) is small. In the subtropical area, upper-NADW still trends towards the NW Atlantic sources, as these are partially exported southward on a direct trajectory (see Fig. 4.1), but lower-NADW samples now point more in the direction of western Lower Deep Water (w-LDW) and ultimately AABW (Fig. 4.7c).

The fact that the NWABW samples from the Irminger Sea align with the endmember even though they extend beyond the global mixing array defined for the Atlantic Ocean (Fig. 4.6c) may seem contradictory. However, the Nd isotopic signature of the endmember DSOW was taken from Lacan and Jeandel (2004a), because this water mass was not sampled directly in the present study. The Nd isotopic composition of DSOW is $\varepsilon_{Nd} = -8.4 \pm 1.2$ (2sd, n = 4), measured in the bottom most samples collected in the Denmark Strait, where the current is vigorous and where exchange processes with sediments occur (Lacan and Jeandel 2004a; Lacan and Jeandel 2005b).

In summary, Figures 4.6a and 4.6b demonstrate that the Nd isotopic composition of seawater correlates with salinity and potential temperature for water depth below 2500 m, even in the subpolar area of the present study (e.g., close to the formation areas of some water masses), thereby showing the ability of Nd isotopic composition of seawater to trace water masses. A correlation is also observed for deep waters between their Nd isotopic composition and silicate (Figs. 4.6c and 4.7), with the exception of NWABW close to its source area, due to boundary exchange with the nearby margin.

4.6. Did Nd isotopic composition of seawater change over the last decades due to climatic changes or due to changes in boundary exchange?

The properties of the water masses constituting NADW change over time (Sy et al. 1997; Curry et al. 1998; Dickson et al. 2002; Curry et al. 2003; Stramma et al. 2004; Sarafanov et al. 2007; Yashayaev and Loder 2009; Lozier et al. 2010; Sarafanov et al. 2010). The changes in LSW have been shown to be related to changes in North Atlantic Oscillation (NAO) index,

with about 1 year delay: a negative NAO index leads to warmer, saltier and thinner LSW, while a positive NAO enhances the deep convection forming cooler, fresher and thicker LSW (Dickson et al. 2002; Stramma et al. 2004; Yashayaev and Clarke 2006). Overall, LSW has been getting cooler and fresher since the mid-1960s to the mid-1990s, and warmer and saltier since the mid-1990s to the present days (Dickson et al. 2002).

The same trends have been noticed for ISOW and DSOW, with an overall freshening between the 1960s and 1990s. This tendency has also been associated with the NAO, leading, for example, to an increased export of sea ice from the Arctic Ocean and to an augmentation of precipitation along the Norwegian Atlantic Current, causing a freshening of the upper layer of the Nordic Seas (Dickson et al. 2002).

In the following we will compare our new Nd isotope data from the subpolar and subtropical North Atlantic with available literature data in order to determine if changes in physical water mass properties did affect the Nd isotopic composition of seawater. We will furthermore consider boundary exchange, with oceanic margins as well as with suspended particles in the nephloid layer, as an alternative mechanism to explain offsets between our new data set and previously published results.

4.6.1. Subpolar region – source areas of North Atlantic Deep Water

4.6.1.1. Stations 2, 5 and 6 – Irminger Sea (Fig. 4.8a)

The values measured in the Irminger Basin (stations 2 to 6) are less radiogenic (ϵ_{Nd} from -11.70 to -10.64, Tables 4.2 and 4.3; Fig. 4.8a) than what can be found in the literature for NWABW in the Irminger Sea: ϵ_{Nd} = -8.6 ± 0.5, 2310 m, station TTO/NAS 167 (64.05°N – 33.33°W, triangle c in Fig. 4.1; Fig. 4.8a; Piepgras and Wasserburg (1987) and ϵ_{Nd} = -9.5 ± 0.4, 2100 m, station Signature 9 (triangle d on Fig. 4.1; Fig. 4.8a; 62.7°N – 37.59°W, Lacan and Jeandel (2005b)). The samples of these two studies were not filtered, whereas the ones from the present study were. It is also worth noting that both of the literature studies, as well as our station 2 are located closer to the continental shelf of Greenland than stations 5 and 6. The Nd isotope signature of surface sediment in the Irminger Basin is -7.9 ± 0.2 (station 91-51, 60°N - 38°W, Innocent et al. 1997), and this could explain the shift towards the more radiogenic values of Piepgras and Wasserburg (1987) and Lacan and Jeandel (2005b). Indeed, the Nd isotopic signature of DSOW in the Denmark Strait sill is very heterogeneous (ϵ_{Nd} ranges from -10.0 to -7.2, n = 4, unfiltered samples, Lacan and Jeandel 2004a), even
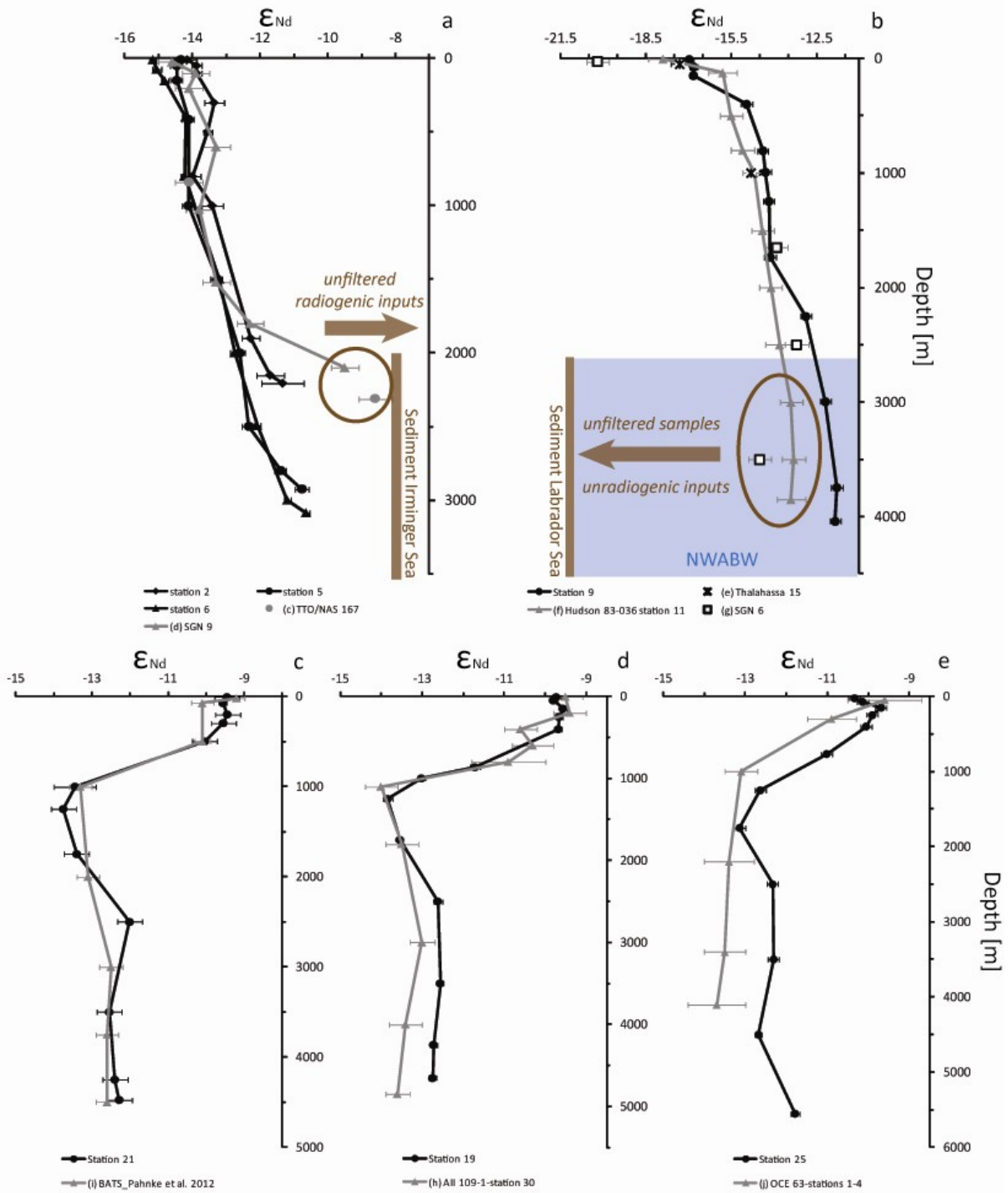
Figure 4.8: Seawater Nd isotopes ratio depth profiles at (a) stations Pelagia 2, 5 and 6 (black circles, see Table 4.2 and Fig. 4.1 for locations), TTO/NAS station 167 (grey dots, triangle c on Fig. 4.1, Piepgras and Wasserburg, 1987) and station Signature (SGN) 9 collected in July 1999 (grey triangle, triangle d on Fig. 4.1, Lacan and Jeandel, 2005b) (b) station Pelagia 9 (black circles), station Thalahassa 15 collected in July 2005 (black crosses, triangle e on Fig. 4.1, Rickli et al., 2009), Hudson 83-036 station 11 collected in November-December 1983 (grey triangles, triangle f on Fig. 4.1. Piepgras and Wasserburg, 1987), and station Signature (SGN) 6 collected in July 1999 (empty squares, triangle g on Fig. 4.1, Lacan and Jeandel, 2005b) (c) station BATS from the present study

(black circles) and station BATS from Pahnke et al (2012) (grey triangle, dot i on Fig. 4.1) (d) station Pelagia 19 (black circles) and AII 109-1-Station 30 collected in June-July 1981 (grey triangles, triangle h on Fig. 4.1, Piepgras and Wasserburg, 1987) (e) station Pelagia 25 (black circles) and OCE63-Stations 1-4 collected in May 1979 (grey triangle, triangles j on Fig. 4.1, Piepgras and Wasserburg, 1980, 1987). Errors plotted for our own data are either internal two sigma standard errors or external two sigma standard deviations, depended on which one is larger (this study, see Table 4.2). For literature results the external two sigma standard deviations are given. In (a) and (b), the brown bars represents the Nd isotopic composition of sediment collect in the area of the plotted stations (e.g., south-western Irminger Sea in (a) and southeastern Labrador Sea in (b)).

though the East Greenland Current precursor is homogenous (ε_{Nd} = -10.9 ± 0.2, n = 11, Lacan and Jeandel 2004a). Lacan and Jeandel (2004a) explained this heterogeneity by resuspension of sediments of different origin: whereas the DSOW from a station on the western side of the sill is influenced by unradiogenic sediments due to the presence of granitic Precambrian formations, the station on the eastern side features radiogenic enrichments from basaltic material (Lacan and Jeandel 2004a). Furthermore, these authors noticed a difference of ~2 epsilon unit in Nd isotope signature between filtered and unfiltered samples. Alibo and Nozaki (1999) found a difference of about 0.8 ppt in Nd concentration between filtered (0.04 µm) and unfiltered seawater samples collected close to the bottom of the water column in the western north Pacific near Japan, where particulate abundance was large (Alibo and Nozaki 1999). This corroborates that the discrepancy between our results and previously published data is most likely due to the fact that our samples were filtered and previous results were not.

The Nd released from the particulate phase can be calculated as follow:

$$Nd\ _{released}\ =\ Nd\ _{final}\ -\ Nd\ _{initial}\ \text{(4.2)}$$

where "final" refers either to Piepgras and Wasserburg (1987) TTO/NAS 167 (2310m, [Nd] = 3.0 ppt), or to Lacan and Jeandel (2005b) SGN 9 (2100m, [Nd] = 3.4 ppt) and the values for the "initial" constituent are the data from either our station 2 (2206m, [Nd] = 2.34 ppt, Chapter 5) or from our station 5 (2924m, 2.27 ppt, Chapter 5). Using equation 4.2, the Nd released from the particulate phase is 0.6 ppt for TTO/NAS 167 and station Pelagia 2, and 1.1 ppt for SGN 9 and station Pelagia 5.

4.6.1.2. Station 9 – southeastern Labrador Sea (Fig. 4.8b)

At station 9 in the southeastern Labrador Sea we see a clear offset between our samples and the results obtained by Piepgras and Wasserburg (1987) and Lacan and Jeandel (2005b) (Fig. 4.8b), whereby the latter are less radiogenic (e.g., systematic offset below 2500 m of up to ~2.5 epsilon). Before exploring this offset, it is worth mentioning that all four studies so far conducted in the area show an excellent agreement in seawater Nd isotopic compositions between ~1000 and ~2500 m water depth (this study; Piepgras and Wasserburg, 1987; Lacan and Jeandel, 2005b, Rickli et al., 2009). Following the water mass assignment performed in section 4.4, the lowermost three samples at our station 9 are associated with NWABW (S = 34.90-34.91), which is lower in salinity compared to samples collected at similar depth in the 1980s (Piepgras and Wasserburg, 1987; S = 34.92), but more salty than the samples collected in 1999 (Lacan and Jeandel, 2005b; S = 34.88). Even though this observation is in accord with the global freshening of ISOW and DSOW in the subpolar North Atlantic until the early 2000s (Dickson et al. 2002), and reversal of this trend from there on (Sarafanov et al. 2010), we do not consider such small shifts in salinity to be capable of creating significant differences in Nd isotopic compositions. As discussed in the previous section, our preferred interpretation is that the offset is related to the fact that many of the historical seawater Nd isotope analyses were performed on unfiltered samples. Even though Pahnke et al. (2012) have demonstrated that lack of filtration may not alter dissolved Nd isotopic compositions in deep waters away from continental margins (i.e. BATS, 2000 m), this may not be true for more continent-proximal locations and in areas with high particulate concentrations. Surface sediments (< 2 µm), collected from the bottom of the southeastern Labrador Sea, feature ε_{Nd} = -20.1 ± 0.1 and a Nd content of 29.23 ppm (station 91-93, Innocent et al. 1997). To investigate if dissolution of resuspended sediments could explain the discrepancy between the data of the present study and the literature results, the boundary exchange equation defined by Lacan and Jeandel (2004a) is used:

$$\varepsilon_{Nd}^{input} = \frac{\varepsilon_{Nd}^{final} \cdot Nd_{final} - \varepsilon_{Nd}^{initial} \cdot Nd_{initial}}{Nd_{final} - Nd_{initial}} \qquad (4.3)$$

where "final" refers to Piepgras and Wasserburg (1987) Hudson 83-036 station 11 (3850 m: ε_{Nd} = -13.4 ± 0.5; [Nd] = 2.8 ppt), and the values for the "initial" component are the data from our station 9 (4041 m: ε_{Nd} = -11.84 ± 0.20, Table 4.2; [Nd] = 2.46 ppt, Chapter 5). The

calculated Nd signature for the input sediment is ε_{Nd} = -24.5 ± 4.3, which is, within error, the same as the sediment measured around the studied area (e.g., ε_{Nd} = -20.1 ± 0.1, Innocent et al. 1997). Using equation 4.2, the Nd released from the particulate phase is 0.3 ppt.

4.6.2. Subtropics – downstream area

Prior to our study there were only limited data available for seawater Nd isotopes in the subtropical western North Atlantic Ocean. A 'baseline' profile for Nd isotopes was recently published for the Bermuda Atlantic Time-Series Study site (BATS, corresponding to station 21 in the present study, Table 4.2; Pahnke et al. (2012), dot i on Fig. 4.1; Fig. 4.8c), which serves as a cross-over station for GEOTRACES cruises GA02 (this study) and GA03 (US section). Intercalibration samples were collected in June-July 2008, and the results are in excellent agreement with results from our study (Fig. 4.8c). The only other Nd isotope data available for the subtropical western North Atlantic were measured by Piepgras and Wasserburg (1980, 1987), and their samples were collected in the early 1980s. Here, it is possible to compare station Pelagia 19 (32.55°N – 61.10°W, Table 4.2, Figs. 4.1 and 4.8d) with AII 109-1-Station 30 collected in June-July 1981 (36.25°N – 61.97°W, triangle h on Fig. 4.1; Fig. 4.8d, Piepgras and Wasserburg 1987) and station Pelagia 25 (24.71°N – 67.07°W, Table 4.2, Figs. 4.1 and 4.8e) with OCE63-Stations 1-4 collected in May 1979 (between 27.02 and 29.88°N – 70.38 and 76.23°W, triangle j on Fig. 4.1; Fig. 4.8e, Piepgras and Wasserburg, 1980, 1987).

In the literature, the Nd isotopic composition of NADW in the subtropical area (referred to as "mature-NADW") is characterized by ε_{Nd} = -13.5 ± 0.5 (Piepgras and Wasserburg 1987; von Blanckenburg 1999). However, no difference is made between the Nd signature of upper-NADW and lower-NADW. As shown previously, in the subtropical area of this study, the Nd isotopic composition of ULSW is -13.11 ± 1.63 (2sd, n = 4) and that of LSW is -13.26 ± 0.43 (2sd, n = 6), leading to a upper-NADW Nd isotopic signature of -13.20 ± 1.00 (2sd, n = 10). The large uncertainty on the upper-NADW Nd isotopic composition reflects the variability of Nd characteristics in ULSW, the signature of which is progressively diluted when flowing southward, primarily due to mixing with AAIW (see paragraph 4.5.1.1). The Nd isotopic signature in the subtropics of middle- and lower-NADW combined is -12.44 ± 0.39 (2sd, n = 16).

111

The values measured for upper-NADW match well the results of the present study for both AII 109-1-Station 30 and OCE63-Stations 1-4, even though these samples were collected about 30 years apart. This suggests that the Nd isotopic signature of ULSW and LSW were not affected by the changes in physical characteristics observed for these two water masses.

The samples encompassed in lower-NADW are, however, less radiogenic in the study of Piepgras and Wasserburg (1980, 1987) compared with the present data set (Figs. 4.8d and e). There is no salinity, temperature or nutrient data available for the seawater collected at the OCE 63 stations to compare with station Pelagia 25. However, salinity, oxygen and nutrients data are available for station AII 109-1-Station 30 (Piepgras and Wasserburg 1987), and the water mass sampled below 2000 m depth by these authors was slightly saltier, more oxygenated and had a lower phosphate content compared to the samples collected in the present study (Table 4.2). These changes in the water mass properties are similar to the ones measured for NEADW and NWABW in the southeastern Labrador Sea, except for the phosphate content. However, as shown in section 4.6.1.2, the Nd isotopic composition from Piepgras and Wasserburg (1987) was already less radiogenic in the southeastern Labrador Sea than the ones measured in the present study, and this was explained by sediment resuspension having a more pronounced effect on their unfiltered samples than on the filtered samples of this study. Moreover, the Nd concentration of the deepest sample from Piepgras and Wasserburg ([Nd] = 9 ppt) is about twice as high as that of the bottom sample from Pelagia station 19 ([Nd] = 4.27 ppt, Chapter 5), suggesting a thicker nepheloid layer and more interaction with bottom sediment. Using equation 4.3, the Nd isotopic composition of the input required is -14.4 ± 0.8, which is in agreement with sediment collected in the Sargasso Sea (ε_{Nd} = -13.3 ± 0.2, 36°N - 66°W, Jeandel et al. 1995).

In summary, even though changes in the water mass properties of ULSW, LSW, NEADW and NWABW can be observed over the past 30 years, the changes do not seem to have a measurable effect on the Nd isotope signature of the water masses. Furthermore, the present data set allows us to redefine the Nd isotopic signature of NADW, and moreover to distinguish between upper-NADW, with ε_{Nd} = -13.20 ± 1.00, and lower-NADW, featuring ε_{Nd} = -12.44 ± 0.39.

4.7. Conclusion

We presented new results on the Nd isotopic composition of seawater for twelve depth profiles from the north to equatorial western Atlantic Ocean. Improved analytical precision on seawater Nd isotope analyses (see Chapter 3), compared to pioneering studies in the 1980s, allow us to revisit the question of the Nd isotopic composition of North Atlantic Deep Water (NADW) and its precursor water masses in the subpolar North Atlantic.

Starting in the subpolar area, Upper Labrador Sea Water carries a very well defined Nd isotopic composition, while the original Labrador Sea Water (LSW) signature is being lost more rapidly upon advection away from its source area in the Labrador Sea. Our stations are not well situated to trace back North East Atlantic Deep Water (NEADW) to its formation area. We only encountered already diluted NEADW in the Irminger Sea and further downstream in the subpolar gyre. Resampling of stations in the Irminger Sea however reveals that sediment resuspension and exchange with the continental margin plays an important role in setting the Nd isotopic composition of the denser water masses NEADW and NWABW.

Leaving the subpolar gyre, exported North Atlantic Deep Water (NADW) can be separated based on our new data into upper- and lower-NADW, with distinct Nd isotopic compositions. While results for upper-NADW show excellent agreement with historical measurements, our data for lower-NADW tend to be more radiogenic, most likely due to a combination of procedural differences in sample collection (e.g., filtration vs. unfiltered samples) and extent of boundary exchange in the source region of NWABW.

Overall, our new data reemphasise (at unprecedented resolution in the NW Atlantic) that the Nd isotopic composition of seawater can serve as an excellent water mass tracer, if sampled in areas away from oceanic margin, and particularly in areas of strong advection (i.e., deep western boundary current). Our new results should not only aid to improve our understanding of the marine biogeochemical cycle of Nd (see also Chapter 5) but provide a more detailed framework for using the Nd isotopic composition of seawater to investigate past variations of the global thermohaline circulation.

Acknowledgements

A particular thanks to our colleagues at the Imperial College MAGIC labs for their help and support, especially to Maxence Paul. We are grateful to the Captain and the crew of the

Chapter 5

NEODYMIUM GEOCHEMICAL CYCLING IN THE WESTERN NORTH ATLANTIC OCEAN

Abstract

The biogeochemical cycle of neodymium (Nd) in the modern ocean is not fully understood. While the Nd isotopic composition of seawater traces water masses and the composition of the continental margins, Nd concentrations in the open ocean feature an increase with depth, as well as an increase along the global conveyor belt, similar to the behaviour of the nutrient silicate. In order to further illuminate and understand this 'Nd paradox' we here present Nd concentration data for twelve seawater depth profiles collected in the equatorial to north western Atlantic Ocean during the Dutch GEOTRACES cruise GA02 in 2010. We furthermore report the Nd isotopic compositions for the surface and bottom layers of all profiles, thus allowing an assessment of the Nd sources and sinks in the studied area. Comparison between the new concentration profiles and the corresponding Nd isotope profiles (Chapter 4) provides novel insights into the geochemical cycle of Nd and reveals that different processes are necessary to account for the observed Nd characteristics. Surface samples show that riverine inputs are important for the Nd budget in the Irminger Basin and in the southern subtropical gyre. No direct proximal input sources need to be invoked to account for the Nd characteristics in the vicinity of the Grand Bank and in the northern subtropical gyre. Boundary exchanges is shown to act as a sink for Nd in the subpolar area close to the East Greenland margin, and release of Nd from resuspended sediments is observed in subtropical areas with a pronounced nepheloid layer. Whereas boundary exchanges are required to account for the observed Nd isotope and concentration profiles in subpolar regions, the profiles are decoupled in the open western North Atlantic, where the prevailing process seems to be release from sinking particles (reversible scavenging), except in the deep water layer of maximal lateral transport.

5.1. Introduction

The rare earth element (REE) neodymium (Nd) is mostly found in dissolved form in the ocean and has concentrations in the order of ppt [ng/kg; ~15 - 45 pmol/kg] (Goldstein and Hemming 2003).

The Nd isotopic composition is expressed as

$$\varepsilon_{Nd} = \left(\frac{\frac{^{143}Nd}{^{144}Nd}_{Sample}}{\frac{^{143}Nd}{^{144}Nd}_{CHUR}} - 1 \right) \times 10^4 \quad (5.1)$$

where CHUR (Chondritic Uniform Reservoir) provides an estimate for the average composition of the present day bulk (silicate) earth: $(^{143}Nd/^{144}Nd)_{CHUR} = 0.512638$ (Jacobsen and Wasserburg 1980). The radioactive decay of ^{147}Sm to ^{143}Nd ($t_{1/2}(^{147}Sm) = 1.06 \cdot 10^{11}$ years) leads to changes in the $^{143}Nd/^{144}Nd$ ratio with time, leading to a range of solid earth Nd isotopic compositions from $\varepsilon_{Nd} \approx -45$ for old granitic cratons to $\varepsilon_{Nd} \approx +12$ for young mid-oceanic ridge basalts (Goldstein and Hemming 2003).

Sources of dissolved Nd to the ocean encompass river runoff (6%), aeolian inputs (4%) and dissolution of Nd from margin sediments (90%, Rempfer et al. 2011). The latter source is referred to as boundary exchange, which is the strong interactions between continental margins and water masses by co-occurrence of sediment dissolution and boundary scavenging (Lacan and Jeandel 2005a). The continental margin includes the continental shelf, the continental slope and the continental rise, and hence encompasses solid material delivered by rivers through estuaries (Chester 2000).

The Nd isotopic composition of seawater reflects the age of the surrounding continents, with $\varepsilon_{Nd} \approx -10$ to -25 in the North Atlantic to $\varepsilon_{Nd} \approx 0$ to -5 in the Pacific (see Chapter 4 and Goldstein and Hemming (2003); Lacan et al. (2012)). Away from continental sources, seawater Nd isotopic compositions seem to behave conservatively and can be used as a water mass tracer (Piepgras and Wasserburg 1987; Lacan and Jeandel 2004a; Lacan and Jeandel 2004b; Lacan and Jeandel 2004c; Lacan and Jeandel 2005; Lacan et al. 2012). This behaviour is, however, at odds with Nd concentrations profiles in the ocean, which are clearly decoupled, an observation that has been termed the 'Nd paradox' (e.g., Jeandel et al. (1995); Tachikawa et al. (2003); Siddall et al. (2008)). In detail, Nd concentration depth profiles resemble silicate profiles in the open ocean, showing depletions at the surface and enrichments with depth as well as an increase in bottom water concentrations along the conveyor belt (Elderfield and Greaves 1982; de Baar et al. 1985; Elderfield 1988; Bertram and Elderfield 1993). This type of behaviour is strongly suggestive of additional processes, other than inputs to the surface and ocean boundaries, that influence the vertical cycling of Nd in the ocean. Previous work suggested that Nd is scavenged at the surface, sinks with the

particulate phase, and is released at depth, a process commonly called reversible scavenging (Nozaki and Alibo 2003; Siddall et al. 2008; Arsouze et al. 2009; Oka et al. 2009).

However, most of the above cited studies on the problem are modelling studies, not at least because observational data from the ocean are still sparse (i.e., 880 results for Nd isotopes in September 2011, (Lacan et al. 2012)). Together, these studies have so far yielded a number of important observations on the behaviour of Nd in the ocean: (i) hydrothermal vent are considered as a negligible Nd source, but their impact on the Nd isotopic signature may be important (Jeandel et al. 2013); (ii) submarine groundwater fluxes may be significant Nd sources (Tachikawa et al. 2003; Johannesson and Burdige 2007; Arsouze et al. 2009)); (iii) atmospheric and riverine Nd fluxes into the oceans are not sufficient to explain oceanic budgets, and the missing flux is most likely provided by continental margin inputs, representing about 90% of the total Nd flux (Tachikawa et al. 2003; Arsouze et al. 2009; Rempfer et al. 2011)); (iv) vertical cycling (scavenging and remineralisation) is necessary to balance both the marine Nd concentration and isotope budget (Siddall et al. 2008; Arsouze et al. 2009; Oka et al. 2009; Rempfer et al. 2011); (v) to understand vertical cycling in detail, it will be important to consider the effects of particle size and type (Siddall et al. 2008; Arsouze et al. 2009)).

In order to shed further light on the vertical cycling of Nd in the water column, as well as its input and output fluxes, we here present Nd concentration data for twelve depths profiles from the north to equatorial western Atlantic Ocean. Surface and bottom waters are specifically inspected for their Nd isotope compositions. The isotope signature of the remainder of the water column was discussed in Chapter 4. Our results show that the processes governing the geochemical cycling of Nd are different in the subpolar and subtropical western North Atlantic Ocean. Indeed, one of the major differences is not the latitudinal position, but rather the proximity of the sampling location to the continental margin (Fig. 5.1a). For the subpolar stations, boundary exchange with the margins is necessary to explain the observed Nd isotope and concentration values. In the subtropical area, the Nd isotopic composition and concentration profiles are decoupled. Release from suspended particles seems to account for the increase in Nd concentration with depth. However, at depth where the maximum velocity of deep water masses is encountered, strong lateral advection hinders the release of Nd from particles.

5.2. Hydrological context

The cruise track for GA02 followed the deepest part of the North Atlantic Ocean and the flow path of NADW (Fig. 5.1a), starting from the Irminger Sea (station 2: 64.00° N, 34.25°W) down to the south of the Sargasso Sea (Station 30: 18.57° N, 57.61°W) (Table 5.1). Below we outline the major hydrology of surface currents as constructed from the literature and direct seaboard measurements of physical properties (Fig. 5.1b). Intermediate and deep water masses were dealt with in Chapter 4. The abbreviations for the water masses and current names can be found in Table 4.1 of Chapter 4.

5.2.1. Surface and upper-layer water masses

5.2.1.1. Subpolar Area

The most prominent current in the subpolar North Atlantic is the North Atlantic Current (NAC), the northeastward extension of the Gulf Stream, which brings warm and salty water of subtropical origins into the subpolar North Atlantic (Fig. 5.1b). West of Scotland, the NAC splits into the Irminger Current (IC), which flows south of Iceland, and into a second branch that continues its flow northeastward to become the Norwegian Current (NC). East of Greenland, the subtropical waters brought northward into the Irminger Sea by the IC are mixed with cold and fresh polar water carried southward in the East Greenland Current (EGC). This current follows the Greenland coast in westward direction all the way up to Baffin Bay under the name West Greenland Current (WGC). It then becomes the Labrador Current (LC) for its southward return journey along the Labrador coast. Upon arrival in the Newfoundland Basin the LC splits, with one part of it flowing southwards, while another part flows east and rejoins the NAC, closing the loop of anti clockwise surface water flow, which is called the North Atlantic Subpolar Gyre (Fig. 5.1b; (Schmitz 1996; Lacan and Jeandel 2004c)).

The subsurface layer (between 200 and 1000 m) of the subpolar gyre is composed of Subpolar Mode Water (SPMW). This is formed by mixing of subtropical and polar water masses followed by winter time convection, and is the precursor of Labrador Sea Water (McCartney and Talley 1982; Hanawa and Talley 2001).
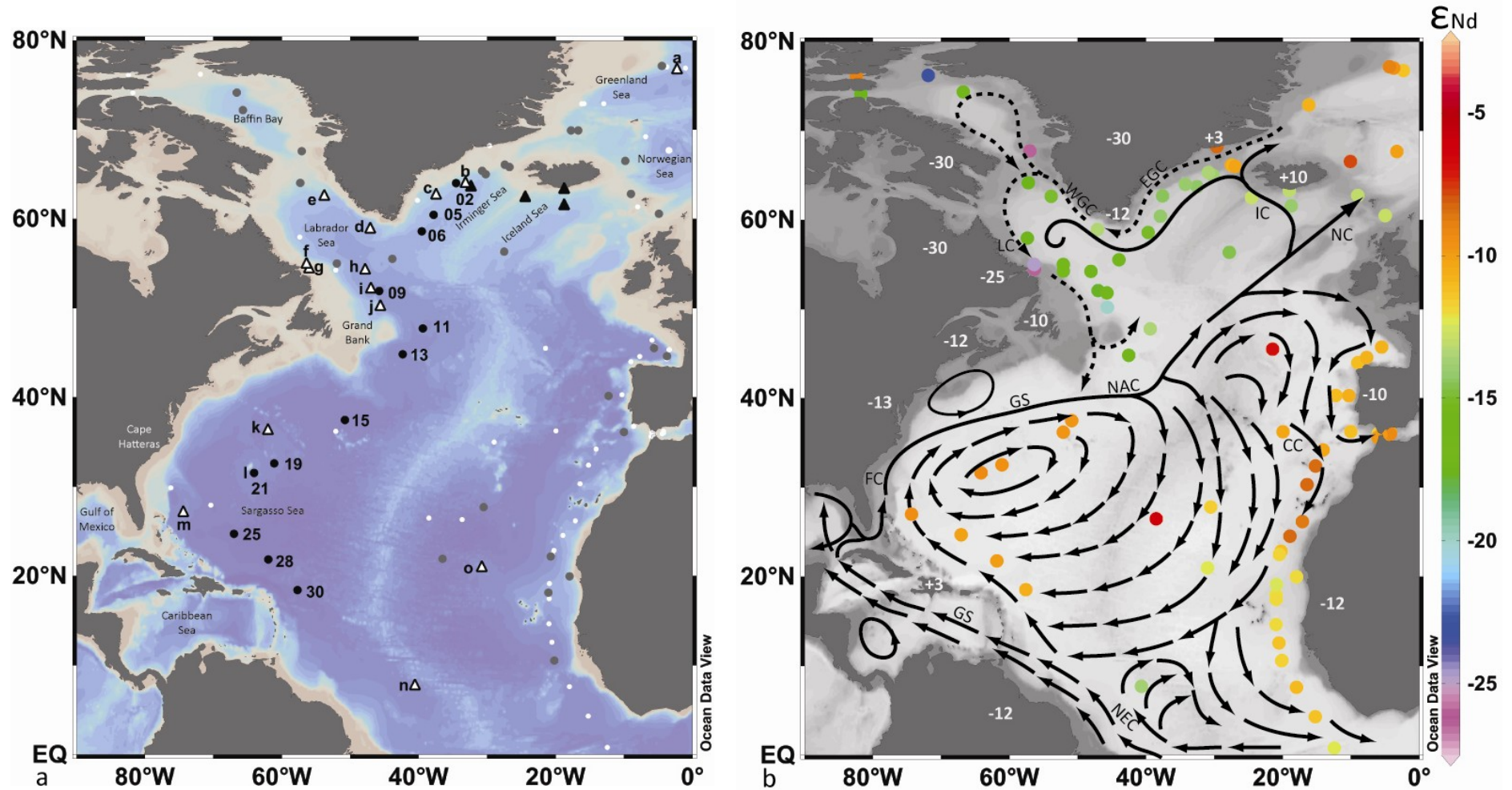
Figure 5.1: (a) Map indicating samples locations in the North Atlantic. The black dots with numbers stand for the Pelagia stations (this study, Table 5.1). The black triangles represent additional FISH samples collected for this study (Table 5.2). The grey dots represent literature data where at least three depths throughout the water column were sampled for Nd isotopic composition, whereas the white dots represent literature data where less than three depths where

sampled. White triangles with associated letters represent stations that are discussed in the text. a: Signature station 30 (Lacan and Jeandel 2004a); b: TTO/NAS station 167 (Piepgras and Wasserburg, 1987); c: Signature station 9; d: Signature station 2; e: Signature station 3; f: Signature station 5; g: Hudson 83-036 LC (Piepgras and Wasserburg, 1987); h: Thalahassa station 15 (Rickli et al. 2009); i: Hudson 83-036 station 11 (Piepgras and Wasserburg, 1987); j: Signature station 6; k: AII 109-1 station 30; l: BATS (Pahnke et al. 2012); m: OCE 63 station 4 (Piepgras and Wasserburg, 1980, 1987); n: TTO/TAS station 63 (Piepgras and Wasserburg, 1987); o: NE Atl. E3 O (Tachikawa et al. 1999). Where not specified, station data are from Lacan and Jeandel (2005b) (Signature stations). (b) Nd isotopic composition (expressed as ε_{Nd}) for the surface most samples (max depth = 100 m) of the present study and from the literature. The arrows represent surface currents (dashed lines for colder waters), and the numbers represent the approximate Nd isotopic signature of the continents. Map drawn after Schmitz, 1996. Currents names abbreviations: NC: Norwegian Current; IC: Irminger Current; EGC: East Greenland Current; WGC: West Greenland Current; LC: Labrador Current; NAC: North Atlantic Current; CC: Canary Current; NEC: North Equatorial Current; FC: Florida Current; GS: Gulf Stream. Maps were realised using the ODV software (Schlitzer 2012).

5.2.1.2. Subtropical Area

In contrast to the subpolar gyre, the subtropical gyre circulates clockwise, and occupies the latitudes from ~10˚N to ~40˚N in the North Atlantic basin. Its most prominent current is the Gulf Stream (GS), which forms the western and northern part of the gyre. The Gulf Stream is fed by warm and salty waters from the Gulf of Mexico. The western limb of the Gulf Stream between the Gulf of Mexico and Cape Hatteras (~ 35˚N) is constituted by the Florida Current (FC), which separates from the coast at ~ 35˚N. While part of it is recirculated southward to rejoin the Gulf Stream, another part flows eastward and becomes the NAC. Much of the water in the NAC turns south-eastwards to contribute to the Canary Current (CC), which flows down the western margin of Southern Europe and western Africa (Fig 5.1b) (Reid 1994; Schmitz 1996). Ultimately the waters turn across the Atlantic again to join the North Equatorial Current (NEC), most of which enters the Gulf of Mexico.

Below the surface layer of the northwestern part of the subtropical gyre, North Atlantic Subtropical Mode Water (STMW), which is often called 'Eighteen Degree Water' (EDW, (Worthington 1958)), is found as a vertically homogeneous water mass. It is formed each year by winter convection south of the northern part of the Gulf Stream (~35˚N), and subsequently travels southwards, occupying water depths from ~50 m to ~500 m in the western subtropical gyre. Variations in the STMW properties are associated with the North

Atlantic Oscillation (NAO), and low NAO corresponds to strong STMW (Worthington 1958; Hanawa and Talley 2001; Davis et al. 2013).

5.3. Samples

Twelve seawater depth profiles were collected for Nd concentrations (and isotopes) on the RV Pelagia during the first two legs of the Dutch GEOTRACES cruise GA02 (PE319 and PE321), that took place between the 28th of April and the 8th of July 2010 from Scrabster (Scotland) to Fortaleze (Brazil), via Bermuda (Fig. 5.1a). Details about the sampling protocol are given in Chapter 4, and details on sample treatment, purification and measurement techniques are provided in Chapter 3.

5.4. Results and discussion

In order to investigate the entire new dataset, we break down our observations and the discussion into four major sections. Firstly, a Nd concentration section of the studied area is presented and described in order to provide an overview of the data set (Fig. 5.2). Secondly, the Nd isotopes and concentrations of the surface samples are presented, thus allowing investigation of the Nd sources and transport at the surface of the North Atlantic Ocean. Then, the Nd isotopic compositions and concentrations are discussed for the bottom water samples in order to assess the Nd sources and sinks in the bottom layer of the studied area. Finally, the Nd concentrations profiles are presented, and they are compared to the Nd isotope profiles depicted in Chapter 4, enabling a discussion of the geochemical cycle of Nd in both the subpolar and the subtropical western North Atlantic Ocean. Neodymium concentrations for every sample and Nd isotopic data for the surface and subsurface layers can be found in Table 5.1, together with hydrological properties and nutrient concentrations. In Figure 5.3, θ-S plots are presented for every station.

5.4.1. Neodymium concentration section: overview of the present data set

Figure 5.2 presents the Nd concentrations for the entire study area in a section view. Overall most of the section is dominated by Nd concentrations in the range of 2.4 to 2.9 ppt. In detail, the northernmost profiles (e.g., north of 40˚N) show a relatively small gradients in

Nd concentrations from top to bottom, with the lowest concentrations being found in the deep and bottom waters in the Irminger Basin (stations 2 to 6, [Nd] ≈ 2.3 ppt) and the highest values in the surface and subsurface of the Labrador Sea (station 9; [Nd] ≈ 3.1 ppt) (Figs. 5.1a and 5.2). Stronger gradients in Nd concentrations and a first order increase of values from top to bottom can be found in all stations of the western North Atlantic (stations 15 to 30; [Nd] ≈ 1.9 ppt in surface waters, [Nd] ≈ 4.6 ppt in bottom waters). As will be discussed later in more detail, this increase is, however, not linear as constant Nd concentrations can be found at intermediate to deep levels in the water column (1000-2500 m) (Fig. 5.2).
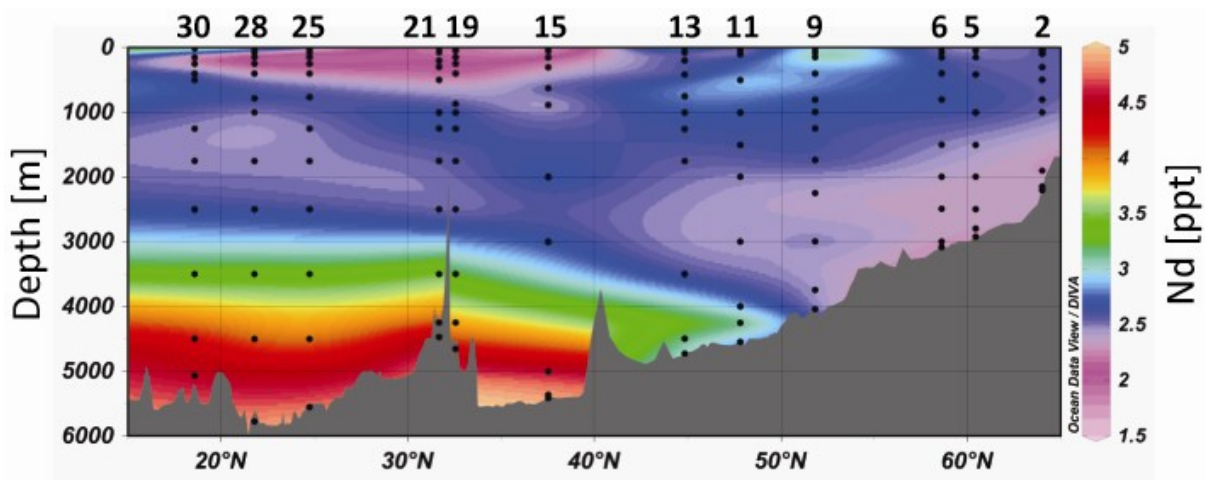
Figure 5.2: Neodymium concentration section for the north to equatorial western Atlantic Ocean (this study). The black dots represent the location of actual samples which were analysed, and the numbers above the section denote the station numbers (see Table 5.1).

5.4.2. Surface waters

In order to evaluate the importance of Nd inputs to the surface ocean, we will discuss surface samples only in this section. The Nd isotopic compositions of the surface samples of the present study are presented in Figure 5.1b, together with previously published data for the North Atlantic Ocean. Overall, this map highlights that the subpolar gyre in the North Atlantic is rather homogenous (ε_{Nd} ≈ -15) and less radiogenic in its Nd isotopic composition than the subtropical gyre (ε_{Nd} ≈ -10).

5.4.2.1. Subpolar area

5.4.2.1.1. Irminger Basin (stations 2 to 6)

Following surface waters in the Irminger Basin in southward direction, the water becomes progressively less radiogenic, ranging from ε_{Nd} = -14.15 ± 0.29 at station 2 to ε_{Nd} = -15.17 ± 0.11 at station 6, and the concentrations are identical within external reproducibility (2.54 - 2.46 ppt, Table 5.1).

The Nd isotopic compositions measured for the surface water of the Irminger Basin are in agreement with previous results (ε_{Nd} = -14.6 ± 0.4 at 25 m depth; station Signature 9, triangle c on Fig. 5.1a, Lacan and Jeandel 2005b). The Nd concentrations, however, are systematically lower in the present study. This can be explained by the fact that the samples of Lacan and Jeandel (2005b) were not filtered, whereas the ones in the present investigation were. Indeed, when Lacan and Jeandel (2004a) compare the Nd concentrations for a filtered and an unfiltered sample from the same station and same depth (station Signature 30; triangle a in Fig. 5.1a, 1840 m), these authors find that only 93% of the Nd is present in the filtered sample, Lacan and Jeandel 2004a). Assuming that the data of Lacan and Jeandel (2005b) show similar difference in Nd concentrations between hypothetical filtered seawater and unfiltered seawater collected at station Signature 9, the calculated concentration is 2.51 ppt, which is in good agreement with the samples of the present study.

Along with a decrease in the Nd isotopic composition, the salinity of surface waters also decreases southwards in the Irminger Basin (35.13 at station 2 to 34.81 at station 6, all samples from 10 m depth, Table 5.1, Fig. 5.3a). The potential temperature is highest at station 2 (θ = 6.78 ˚C) and lowest at station 5 (θ = 5.39˚C), whilst the oxygen content features the opposite trend (Table 5.1). These relatively high salinity and temperature characteristics show that the samples from stations 2 to 6 were taken in the Irminger Current (IR) rather than in the East Greenland Currant (EGC) (Fig. 5.1b). The coupled trend of decreasing salinity alongside less radiogenic Nd isotopic compositions hints at the addition of an unradiogenic riverine source. This idea is corroborated by both dissolved and particulate Nd isotopic compositions from west Greenland rivers, which have been shown to be highly unradiogenic (ε_{Nd} = -43.3 ± 1.25, 2sd, n = 3, (Goldstein and Jacobsen 1987) and ε_{Nd} = -41.5 ± 2.72, 2sd, n = 3, (Goldstein and Jacobsen 1988)) respectively).

Table 5.1: Location, depth, hydrological properties, nutrient concentration, Nd concentrations and Nd isotopic compositions (in italic are the values already presented in Chapter 4) for the 12 depth profiles collected on the GEOTRACES cruise GA02 on the Pelagia in 2010.

Sample depth [m]	Salinity[a]	Pot. Temp. (Θ) [°C][a]	Pot. Dens. (σ_θ) [kg/m^3]	O$_2$ [µmol/kg][a]	Phosphate [µmol/kg][b]	Silicate [µmol/kg][b]	Nitrate [µmol/kg][b]	^{143}Nd/^{144}Nd[c]	ε_{Nd}[d]	2se (int.)[e]	2sd (ext.)[f]	Nd [ppt][g]	Water mass
Station 02 (2 May 2010; 64.0003°N – 34.2505°W; 2215m)													
10	35.131	6.78	27.554	273.6	0.89	6.37	13.64	0.511912	-14.15	0.29	0.14	2.54	
50	35.149	6.71	27.579	268.8	0.91	6.32	13.98	0.511926	-13.88	0.12	0.14	2.54	
100	35.148	6.69	27.581	268.4	0.93	6.35	14.13	0.511926	-13.88	0.08	0.14	2.54	
302	35.100	6.15	27.616	269.0	0.99	7.23	15.31	0.511953	-13.36	0.29	0.14	2.54	
499	35.022	5.26	27.667	245.4	1.10	9.21	16.67	0.511944	-13.55	0.14	0.14	2.54	
802	34.932	4.10	27.726	269.4	1.08	8.88	16.46	*0.511920*	*-14.00*	*0.24*	*0.14*	2.55	ULSW
1000	34.927	3.86	27.745	264.4	1.09	9.69	16.63	*0.511950*	*-13.42*	*0.33*	*0.14*	2.51	LSW
1901	34.929	3.02	27.830	271.3	1.08	11.46	16.31	*0.512009*	*-12.28*	*0.25*	*0.15*	2.30	NEADW
2151	34.880	1.85	27.891	295.7	0.91	7.74	13.67	*0.512038*	*-11.70*	*0.42*	*0.15*	2.36	NWABW
2206	34.884	1.26	27.938	301.6	0.87	6.85	13.06	*0.512057*	*-11.33*	*0.62*	*0.15*	2.34	NWABW
Station 05 (4 May 2010; 60.4277°N – 37.9078°W; 2943m)													
10	34.892	5.39	27.546	298.5	0.81	4.17	12.10	0.511903	-14.34	0.12	0.14	2.51	
50	34.913	4.94	27.616	295.1	0.85	4.66	12.99	0.511897	-14.45	0.12	0.14	2.49	
150	34.923	4.58	27.664	280.6	1.02	7.49	15.55	0.511897	-14.46	0.11	0.14	2.54	
417	34.920	4.19	27.705	269.0	1.08	8.73	16.46	*0.511915*	*-14.11*	*0.10*	*0.14*	2.59	ULSW
1001	34.878	3.55	27.738	273.8	1.08	9.32	16.52	*0.511915*	*-14.11*	*0.13*	*0.14*	2.61	ULSW
1502	34.919	3.44	27.782	267.2	1.10	10.69	16.65	*0.511959*	*-13.25*	*0.09*	*0.14*	2.44	LSW
2001	34.924	3.08	27.821	272.0	1.09	11.52	16.57	*0.511992*	*-12.60*	*0.10*	*0.14*	2.36	NEADW
2499	34.928	2.68	27.860	274.4	1.08	12.91	16.16	*0.512006*	*-12.33*	*0.09*	*0.14*	2.36	NEADW
2799	34.899	2.01	27.893	288.0	0.99	10.11	14.78	*0.512054*	*-11.39*	*0.11*	*0.14*	2.35	NWABW
2924	34.888	1.23	27.943	298.2	0.93	8.71	13.80	*0.512086*	*-10.76*	*0.20*	*0.14*	2.27	NWABW

Table 5.1 (continued)

Sample depth [m]	Salinity[a]	Pot. Temp. (Θ) [°C][a]	Pot. Dens. (σ_0) [kg/m³]	O$_2$ [µmol/kg][a]	Phosphate [µmol/kg][b]	Silicate [µmol/kg][b]	Nitrate [µmol/kg][b]	^{143}Nd/^{144}Nd[c]	ε_{Nd}[d]	2se (int.)[e]	2sd (ext.)[f]	Nd [ppt][g]	Water mass
Station 06 (5 May 2010; 58.6027°N – 39.7064°W; 3101m)													
10	34.811	5.84	27.426	287.5	0.82	4.71	12.01	0.511861	-15.17	0.11	0.06	2.46	
74	34.839	5.20	27.526	286.7	0.89	5.27	12.89	0.511866	-15.05	0.12	0.06	2.47	
152	34.848	4.27	27.638	283.4	0.99	7.01	15.04	0.511878	-14.82	0.09	0.06	2.54	
399	34.908	4.08	27.707	268.8	1.06	8.69	16.59	*0.511910*	*-14.20*	*0.12*	*0.06*	2.61	ULSW
801	34.863	3.54	27.726	277.3	1.05	8.74	16.31	*0.511908*	*-14.24*	*0.09*	*0.06*	2.66	ULSW
1499	34.914	3.43	27.778	267.0	1.10	10.74	16.92	*0.511962*	*-13.19*	*0.08*	*0.06*	2.48	LSW
1998	34.919	3.03	27.821	271.8	1.09	11.59	16.52	*0.511984*	*-12.75*	*0.12*	*0.06*	2.37	NEADW
2495	34.931	2.71	27.860	274.2	1.08	13.09	16.45	*0.512019*	*-12.08*	*0.08*	*0.06*	2.31	NEADW
2999	34.891	1.66	27.914	294.3	0.97	9.44	14.68	*0.512064*	*-11.20*	*0.11*	*0.06*	2.32	NWABW
3086	34.884	1.25	27.938	297.8	0.94	9.12	14.14	*0.512092*	*-10.64*	*0.10*	*0.06*	2.27	NWABW
Station 09 (9 May 2010; 51.8203°N – 45.7325°W; 4052m)													
10	34.819	9.16	26.954	261.7	0.42	1.85	5.56	0.511768	-16.98	0.11	0.14	2.97	
75	34.902	8.39	27.141	253.0	0.70	4.86	9.68	0.511776	-16.82	0.09	0.14	3.12	
149	34.742	6.83	27.242	244.4	0.86	6.12	12.54	0.511775	-16.83	0.12	0.06	3.14	
400	34.923	4.97	27.621	231.3	1.13	9.74	17.39	0.511871	-14.96	0.14	0.20	2.79	
805	34.901	3.96	27.715	263.6	1.09	9.31	16.81	*0.511901*	*-14.38*	*0.12*	*0.20*	2.67	ULSW
993	34.890	3.73	27.730	267.6	1.09	9.38	16.72	*0.511905*	*-14.29*	*0.12*	*0.20*	2.65	ULSW
1247	34.898	3.60	27.749	267.7	1.10	9.89	16.88	*0.511911*	*-14.18*	*0.13*	*0.20*	2.61	LSW
1735	34.914	3.31	27.790	269.9	1.11	11.26	17.08	*0.511914*	*-14.13*	*0.16*	*0.20*	2.61	LSW
2252	34.916	2.91	27.830		1.09	11.95	16.48	*0.511978*	*-12.87*	*0.11*	*0.20*	2.39	NEADW
2997	34.907	2.14	27.890	277.8	1.06	14.29	15.97	*0.512014*	*-12.18*	*0.14*	*0.20*	2.50	NWABW
3745	34.898	1.70	27.917	287.9	0.98	11.61	14.78	*0.512034*	*-11.79*	*0.12*	*0.20*	2.46	NWABW
4041	34.898	1.64	27.922	290.5	0.98	11.22	14.71	*0.512031*	*-11.84*	*0.12*	*0.20*	2.46	NWABW

Table 5.1 (continued)

Sample depth [m]	Salinity[a]	Pot. Temp. (Θ) [°C][a]	Pot. Dens. (σ₀) [kg/m³]	O₂ [μmol/ kg][a]	Phosphate [μmol/ kg][b]	Silicate [μmol/ kg][b]	Nitrate [μmol/ kg][b]	¹⁴³Nd/¹⁴⁴Nd[c]	ε_Nd[d]	2se (int.)[e]	2sd (ext.)[f]	Nd [ppt][g]	Water mass
Station 11 (11 May 2010; 47.7996˚N – 39.4001˚W; 4570m)													
9	35.596	15.20	26.419	259.5	0.03	0.05	0.36	0.511936	-13.70	0.13	0.20	2.55	
23	35.886	14.87	26.689	237.9	0.06	0.20	2.66	0.511987	-12.70	0.13	0.20	2.46	
50	36.026	15.06	26.754	219.9	0.25	1.72	3.97	0.512043	-11.61	0.10	0.08	2.39	
101	36.004	14.56	26.848	212.6	0.38	2.58	6.30	0.512047	-11.53	0.11	0.08	2.41	
502	35.003	8.07	27.270	160.8	1.28	11.07	21.02	0.511887	-14.65	0.13	0.08	2.94	
1001	34.966	4.60	27.697	243.4	1.12	10.34	17.17	*0.511901*	*-14.38*	*0.16*	*0.13*	2.70	ULSW
1501	34.927	3.80	27.752	261.1	1.13	10.63	17.06	*0.511912*	*-14.15*	*0.35*	*0.13*	2.60	LSW
1998	34.922	3.41	27.786	264.7	1.13	11.81	17.37	*0.511954*	*-13.34*	*0.25*	*0.13*	2.47	LSW
3000	34.919	2.74	27.847	271.8	1.10	13.90	16.69	*0.511985*	*-12.74*	*0.41*	*0.14*	2.40	NEADW
4000	34.899	1.99	27.896	275.5	1.12	19.92	16.66	*0.511993*	*-12.58*	*0.23*	*0.14*	2.82	NWABW
4251	34.895	1.90	27.900	275.2	1.12	19.59	16.64	*0.512009*	*-12.28*	*0.38*	*0.14*	3.24	NWABW
4547	34.895	1.84	27.905	278.9	1.09	18.03	16.33	*0.511996*	*-12.52*	*0.33*	*0.14*	2.82	NWABW
Station 13 (13 May 2010; 44.8442˚N – 42.5260˚W; 4751m)													
10	35.112	13.21	26.440	270.2	0.04	0.18	0.00	0.511770	-16.93	0.13	0.28	3.04	
77	35.934	14.69	26.766	220.5	0.26	1.44	4.04	0.512021	-12.04	0.18	0.28	2.48	
198	35.654	13.23	26.859	199.0	0.58	3.79	9.40	0.511987	-12.71	0.11	0.28	2.63	
418	35.313	10.24	27.160	126.9	1.39	11.86	22.32	0.512049	-11.49	0.10	0.28	2.54	
750	34.992	5.61	27.598	210.8	1.23	11.58	18.90	0.511870	-14.98	0.15	0.28	2.81	
1003	34.977	4.68	27.696	240.1	1.15	10.85	17.80	*0.511901*	*-14.38*	*0.18*	*0.28*	2.70	ULSW
1256	34.973	4.28	27.738	248.7	1.15	11.01	17.63	*0.511906*	*-14.28*	*0.15*	*0.28*	2.63	ULSW
1750	34.942	3.70	27.774	258.9	1.14	11.78	17.58	*0.511934*	*-13.73*	*0.22*	*0.28*	2.54	LSW
3501	34.913	2.34	27.879	272.6	1.11	17.20	16.82	*0.512012*	*-12.22*	*0.13*	*0.28*	2.58	NEADW
4499	34.892	1.85	27.903	272.8	1.15	22.10	17.09	*0.511991*	*-12.62*	*0.13*	*0.33*	3.11	NWABW
4726	34.893	1.82	27.906	276.3	1.11	20.65	16.72	*0.511986*	*-12.73*	*0.47*	*0.33*	3.04	NWABW

Table 5.1 (continued)

Sample depth [m]	Salinity[a]	Pot. Temp. (Θ) [°C][a]	Pot. Dens. (σ₀) [kg/m³]	O₂ [μmol/kg][a]	Phosphate [μmol/kg][b]	Silicate [μmol/kg][b]	Nitrate [μmol/kg][b]	$^{143}Nd/^{144}Nd$[c]	ε_{Nd}[d]	2se (int.)[e]	2sd (ext.)[f]	Nd [ppt][g]	Water mass
Station 15 (19 May 2010; 37.5164°N – 50.8906°W; 5441m)													
11	36.428	17.79	26.424	216.3	0.02	0.17	0.28	0.512131	-9.90	0.14	0.08	1.74	
52	36.428	17.76	26.429	214.5	0.03	0.18	0.34	0.512128	-9.96	0.11	0.08	1.75	
153	36.385	16.84	26.621	197.7	0.34	2.05	6.36	0.512117	-10.16	0.14	0.08	2.12	
304	36.152	15.74	26.699	180.3	0.51	3.04	8.90	0.512087	-10.75	0.13	0.08	2.27	
629	35.310	9.88	27.218	143.3	1.37	11.75	21.78	0.512021	-12.04	0.12	0.08	2.56	
885	35.202	6.97	27.591	186.1				0.511948	-13.45	0.11	0.08	2.40	
2003	34.949	3.49	27.801	257.2	1.16	13.10	17.68	*0.511950*	*-13.41*	*0.13*	*0.08*	2.68	uNADW (LSW)
3002	34.937	2.66	27.870	258.5	1.20	20.40	18.15	*0.512011*	*-12.23*	*0.12*	*0.08*	2.69	mNADW (NEADW)
3999	34.896	1.96	27.898	262.0	1.26	28.8	18.68	*0.511991*	*-12.62*	*0.10*	*0.20*	3.65	lNADW (NWABW)
5001	34.877	1.76	27.900	255.5	1.37	38.19	20.12	*0.511989*	*-12.66*	*0.12*	*0.20*	4.57	modified-AABW
5364	34.870	1.71	27.899	250.4				*0.511997*	*-12.50*	*0.12*	*0.06*	4.87	modified-AABW
5414	34.869	1.70	27.899	250.3	1.47	46.3	21.54	*0.511997*	*-12.50*	*0.11*	*0.06*	4.86	modified-AABW
Station 19 (23 May 2010; 32.5514°N – 61.0986°W; 4683m)													
10	36.795	21.96	25.598	196.4	0.01	0.61	0.00	0.512139	-9.72	0.10	0.06	1.96	
50	36.762	20.72	25.917	200.4	0.01	0.61	0.01	0.512136	-9.80	0.10	0.06	1.93	
149	36.627	18.76	26.331	193.6	0.05	0.75	1.60	*0.512148*	*-9.56*	*0.09*[e]	*0.06*[f]	1.99	STMW
251	36.588	18.33	26.411	193.1	0.10	0.94	2.61	*0.512143*	*-9.66*	*0.08*	*0.06*	2.04	STMW
401	36.541	17.88	26.487	189.1	0.18	1.29	3.89	*0.512142*	*-9.67*	*0.08*	*0.06*	2.10	STMW
866	35.261	9.47	27.250	138.2	1.40	12.29	22.39	*0.512038*	*-11.71*	*0.13*	*0.06*	2.52	
1001	35.120	7.25	27.482	168.6	1.39	13.12	21.60	*0.511971*	*-13.01*	*0.08*	*0.06*	2.63	
1251	35.055	5.18	27.701	221.4	1.22	11.90	18.71	*0.511929*	*-13.84*	*0.12*	*0.06*	2.63	uNADW (ULSW)
1750	34.983	3.92	27.784	248.4	1.17	12.60	17.93	*0.511944*	*-13.54*	*0.07*	*0.06*	2.55	uNADW (LSW)
2500	34.959	3.10	27.847	254.2	1.21	18.77	18.30	*0.511991*	*-12.62*	*0.11*	*0.06*	2.48	mNADW (NEADW)
3501	34.907	2.14	27.891	263.0	1.22	25.35	18.30	*0.511994*	*-12.56*	*0.07*	*0.06*	3.23	lNADW (NWABW)

Table 5.1 (continued)

Sample depth [m]	Salinity[a]	Pot. Temp. (Θ) [°C][a]	Pot. Dens. (σ₀) [kg/m³]	O_2 [μmol/ kg][a]	Phosphate [μmol/ kg][b]	Silicate [μmol/ kg][b]	Nitrate [μmol/ kg][b]	$^{143}Nd/^{144}Nd$[c]	ε_{Nd}[d]	2se (int.)[e]	2sd (ext.)[f]	Nd [ppt][g]	Water mass
Station 19 (continued)													
4250	34.890	1.89	27.898	261.4	1.28	31.51	19.00	*0.511986*	*-12.72*	*0.09*	*0.06*	3.85	lNADW (NWABW)
4655	34.881	1.81	27.899	257.5	1.33	36.01	19.75	*0.511985*	*-12.74*	*0.09*	*0.06*	4.27	modified-AABW
Station 21 (BATS; 13 June 2010; 31.6669˚N – 64.1664˚W; 4567m)													
9	36.699	23.78	24.995	212.7	0.02	0.43	0.01	0.512154	-9.45	0.16	0.33	1.88	
75	36.613	18.70	26.335	223.4	0.01	0.46	0.19	*0.512148*	*-9.56*	*0.09*	*0.06*	1.88	STMW
201	36.566	18.05	26.464	210.8	0.14	1.10	3.17	*0.512154*	*-9.44*	*0.18*	*0.33*	2.09	STMW
297	36.521	17.74	26.507	207.3	0.20	1.34	4.06	*0.512149*	*-9.55*	*0.13*	*0.33*	2.12	STMW
500	36.298	16.54	26.626	192.0	0.41	2.39	7.46	*0.512124*	*-10.03*	*0.12*	*0.33*	2.27	
1001	35.071	6.03	27.608	207.1	1.34	12.78	20.55	*0.511949*	*-13.44*	*0.56*	*0.33*	2.66	*uNADW*
1249	35.008	4.64	27.726	243.7	1.20	11.67	18.42	*0.511933*	*-13.75*	*0.13*	*0.33*	2.64	uNADW (ULSW)
1749	34.968	3.71	27.793	258.4	1.16	12.95	17.97	*0.511951*	*-13.39*	*0.11*	*0.33*	2.53	uNADW (LSW)
2501	34.962	2.99	27.859	254.7	1.24	20.98	18.66	*0.512022*	*-12.01*	*0.26*	*0.33*	2.54	mNADW (NEADW)
3500	34.902	2.04	27.895	263.3	1.24	27.10	18.44	*0.511995*	*-12.54*	*0.23*	*0.33*	3.46	lNADW (NWABW)
4249	34.885	1.84	27.899	259.3	1.31	34.61	19.69	*0.512003*	*-12.40*	*0.27*	*0.33*	4.10	lNADW (NWABW)
4474	34.877	1.77	27.898	256.0	1.39	40.15	20.67	*0.512009*	*-12.28*	*0.23*	*0.33*	4.46	modified-AABW
Station 25 (17 June 2010; 24.7147˚N – 67.0728˚W; 5575m)													
25	36.570	25.87	24.262	205.4	0.01	0.98	0.00	0.512108	-10.34	0.14	0.14	2.53	
73	36.900	23.31	25.288	213.9	0.01	0.79	0.00	0.512118	-10.14	0.11	0.14	2.14	
150	36.725	20.19	26.031	210.6	0.01	0.74	0.01	0.512141	-9.69	0.10	0.14	1.90	
251	36.578	18.38	26.391	196.3	0.15	1.31	3.67	0.512130	-9.91	0.12	0.14	2.10	
400	36.405	17.19	26.552	187.0	0.34	2.10	6.58	0.512123	-10.05	0.11	0.14	2.26	

Table 5.1 (continued)

Sample depth [m]	Salinity[a]	Pot. Temp. (Θ) [°C][a]	Pot. Dens. (σ_0) [kg/m³]	O_2 [µmol/kg][a]	Phosphate [µmol/kg][b]	Silicate [µmol/kg][b]	Nitrate [µmol/kg][b]	$^{143}Nd/^{144}Nd$[c]	ε_{Nd}[d]	2se (int.)[e]	2sd (ext.)[f]	Nd [ppt][g]	Water mass
Station 25 (continued)													
767	35.289	9.86	27.206	138.6	1.49	12.99	24.19	*0.512073*	*-11.02*	*0.10*	*0.14*	2.61	modified-AAIW
1250	35.062	5.27	27.696	217.4	1.31	14.10	20.47	*0.511990*	*-12.64*	*0.12*	*0.14*	2.48	uNADW (ULSW)
1751	34.994	3.82	27.803	251.1	1.19	14.14	18.33	*0.511964*	*-13.14*	*0.08*	*0.14*	2.48	uNADW (LSW)
2500	34.961	2.94	27.863	250.6	1.25	22.69	19.17	*0.512006*	*-12.34*	*0.09*	*0.14*	2.59	mNADW (NEADW)
3499	34.912	2.19	27.891	258.8	1.25	27.05	18.84	*0.512007*	*-12.31*	*0.11*	*0.14*	3.32	lNADW (NWABW)
4500	34.890	1.87	27.900	258.8	1.32	33.85	19.58	*0.511988*	*-12.68*	*0.08*	*0.08*	4.03	lNADW (NWABW)
5551	34.852	1.57	27.896	247.1	1.53	52.95	22.51	*0.512034*	*-11.79*	*0.11*	*0.08*	4.75	modified-AABW
Station 28 (20 June 2010; 21.7764°N – 61.8438°W; 5795m)													
25	36.218	27.72	23.404	197.1	0.01	1.06	0.00	0.512117	-10.17	0.10	0.13	3.04	
74	36.887	23.51	25.218	210.2	0.01	0.75	0.00	0.512103	-10.43	0.09	0.13	2.20	
150	36.889	20.84	25.979	182.5	0.03	0.78	1.06	0.512110	-10.30	0.11	0.13	1.97	
251	36.575	18.23	26.424	188.2	0.20	1.41	4.39	0.512121	-10.09	0.12	0.13	2.15	
401	36.229	16.16	26.660	178.5	0.49	2.87	8.94	0.512099	-10.52	0.10	0.13	2.33	
785	35.106	8.27	27.321	133.5	1.71	16.53	27.03	*0.512069*	*-11.09*	*0.09*	*0.13*	2.63	modified-AAIW
998	34.995	6.30	27.514	160.8	1.71	18.94	26.36	*0.512057*	*-11.33*	*0.10*	*0.13*	2.47	modified-AAIW
1752	34.984	3.70	27.808	253.3	1.19	14.49	18.31	*0.511968*	*-13.08*	*0.10*	*0.13*	2.47	uNADW (LSW)
2501	34.952	2.84	27.866	253.3	1.24	22.08	18.69	*0.512008*	*-12.29*	*0.09*	*0.13*	2.62	mNADW (NEADW)
3499	34.907	2.11	27.893	259.8	1.25	27.23	18.65	*0.511999*	*-12.46*	*0.09*	*0.13*	3.34	lNADW (NWABW)
4501	34.891	1.87	27.901	259.4	1.30	32.88	19.24	*0.511994*	*-12.57*	*0.09*	*0.14*	4.07	lNADW (NWABW)
5775	34.845	1.50	27.896	244.9	1.59	56.98	23.29	*0.512045*	*-11.57*	*0.09*	*0.14*	4.83	modified-AABW
Station 30 (22 June 2010; 18.5724°N – 57.6121°W; 5280m)													
11	35.503	29.02	22.437	196.8	0.01	0.44	0.00	0.512084	-10.80	0.18	0.15	3.27	
152	37.224	22.90	25.654	190.1	0.02	0.60	0.25	0.512105	-10.40	0.23	0.15	2.18	
249	36.626	18.45	26.409	154.5	0.41	2.05	7.83	0.512099	-10.51	0.19	0.15	2.28	

Sample depth [m]	Salinity[a]	Pot. Temp. (Θ) [°C][a]	Pot. Dens. (σ_0) [kg/m^3]	O_2 [μmol/kg][a]	Phosphate [μmol/kg][b]	Silicate [μmol/kg][b]	Nitrate [μmol/kg][b]	$^{143}Nd/^{144}Nd$[c]	ε_{Nd}[d]	2se (int.)[e]	2sd (ext.)[f]	Nd [ppt][g]	Water mass
Station 30 (continued)													
402	35.914	14.36	26.821	133.5	0.95	5.36	16.55	0.512097	-10.56	0.21	0.15	2.61	
499	35.650	12.40	27.021	142.7	1.11	7.46	18.84	0.512076	-10.97	0.32	0.15	2.61	
1250	35.028	4.97	27.704	216.0	1.37	15.59	21.03	*0.512012*	*-12.21*	*0.30*	*0.15*	2.47	uNADW (ULSW)
1749	34.997	3.81	27.806	247.4	1.23	15.28	18.86	*0.511971*	*-13.00*	*0.12*	*0.08*	2.47	uNADW (LSW)
2502	34.951	2.83	27.866	249.9	1.27	23.77	19.30	*0.512012*	*-12.21*	*0.15*	*0.08*	2.64	mNADW (NEADW)
3500	34.909	2.16	27.891	256.7	1.27	28.65	19.06	*0.511999*	*-12.46*	*0.09*	*0.08*	3.32	lNADW (NWABW)
4499	34.871	1.73	27.896	250.7	1.45	44.89	21.38	*0.512016*	*-12.13*	*0.10*	*0.08*	4.24	modified-AABW
5067	34.837	1.45	27.892	242.0	1.61	59.67	23.75	*0.512053*	*-11.42*	*0.11*	*0.08*	4.52	modified-AABW

[a] Hydrological properties measured on board the Pelagia by H. M. van Aken (Royal NIOZ).

[b] Nutrients concentrations measured on board the Pelagia (within 3 hours after sampling) by K. Bakker (Royal NIOZ).

[c] Normalised relative to JNdi value of 0.512115 (Tanaka et al., 2000) using five runs of JNdi.

[d] ε_{Nd} values were calculated relative to a CHUR of 0.512638 (Jacobsen and Wasserburg, 1980).

[e] The internal errors are derived from the 2 sigma error on the instrument measurement (maximum 360 cycles).

[f] External errors are the two sigma standard deviations derived from repeat standard analyses of JNdi (n = 5).

The uncertainty plotted is the biggest between internal and external error.

[g] Concentration uncertainties were calculated using the propagated absolute 2 sigma error [ppt] taking into account the error on the weighing of the sample, the error on the weighing of the spike and the error on the data collection on the instrument (2se on up to 360 cycles). At a maximum they represent 0.03% of the samples concentrations and therefore are not represented here. The external 2 sigma error is 0.09 ppt, and was obtained by the repeated measurement of an in house seawater sample (n = 5). The external error is represented on the figures.

The fact that the Nd concentration does not increase from station 2 to station 6 is not in contradiction with riverine supply. Indeed, batch experiments performed with riverine particles and seawater have shown that the seawater Nd content decreases, even if the particles carry high Nd contents in the order of 10 ppm. This is thought to be due to the formation of secondary phases such as REE phosphate minerals (Pearce et al. 2013). Moreover, data for the beam attenuation coefficient, which is used as a measure of turbidity, shows that this is twice as large for the surface waters of stations 5 and 6 compared to station 2 (data not shown here). This supports the idea of a riverine Nd supply.

In summary, unradiogenic riverine input can account for the Nd characteristics observed in the surface waters of the Irminger Basin.
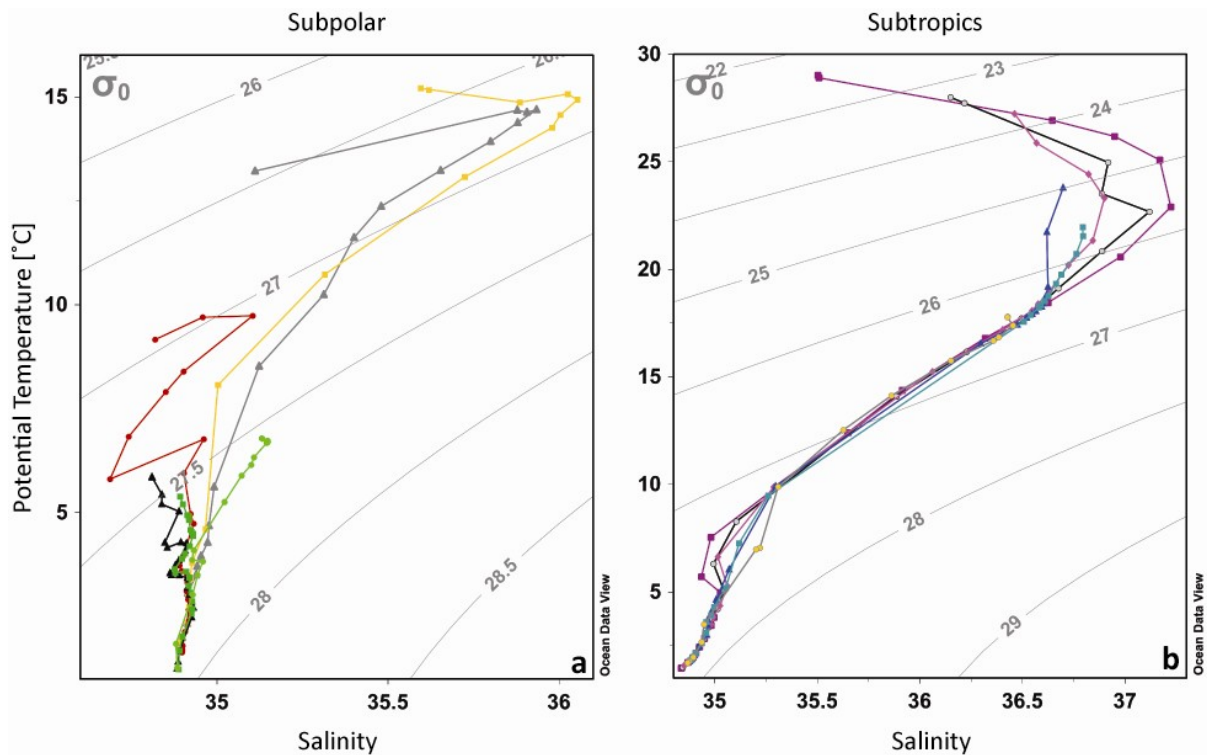
Figure 5.3: Potential temperature – salinity diagrams for (a) subpolar and (b) subtropical stations of the present study. a: light green dots = station 2; green squares = station 5; black triangles = station 6; red dots = station 9; orange squares = station 11; and grey triangles = station 13. b: yellow dots = station 15; turquoise squares = station 19; blue triangles = station 21; pink diamonds = station 25; grey dots = station 28; and purple squares = station 30. These diagrams were realised using the ODV software (Schlitzer 2012).

5.4.2.1.2. Around the Grand Bank (stations 9 to 13)

In the southeastern Labrador Sea and in the area east of Grand Bank (stations 9 to 13, Fig. 5.1a), the salinity is lowest at station 9 (S = 34.82), increasing to 35.60 at station 11 and is lower again at station 13 (S = 35.11, Fig. 5.3a). The potential temperature features the same trend (Fig. 5.3a), while dissolved oxygen shows the opposite trend (Table 5.1). This is due to the encounter of the Gulf Stream at stations 11 and 13, carrying warmer and saltier waters northward (van Aken 2010). The Nd isotopic composition is the same within error at stations 9 and 13 (ε_{Nd} = -16.98 ± 0.14 and ε_{Nd} = -16.93 ± 0.28 respectively, Table 5.1), but is more radiogenic at station 11 (ε_{Nd} = -13.70 ± 0.20). The Nd concentration is lowest at station 11 ([Nd] = 2.55 ppt), and it is 2.97 ppt at station 9 and 3.04 ppt at station 13 (Table 5.1).

When comparing these surface data to results published in the literature, a good linear correlation is obtained on a salinity vs. ε_{Nd} plot when the two following endmembers are used: the Labrador Current (Hudson 83-036 LC, triangle g on Fig. 5.1a, Piepgras and Wasserburg 1987) and modified Gulf Stream waters (Pelagia station 15, this study) (Fig. 5.4; r^2 = 0.98). However, conservative binary mixing should lead to a non-linear correlation on a salinity vs. ε_{Nd} plot (when the endmembers have different Nd concentrations) following the equation (Mariotti et al. 1988):

$$\varepsilon Nd_{Mix} = \frac{\varepsilon Nd_{SW1} \cdot Nd_{SW1} \cdot f_{SW1} + \varepsilon Nd_{SW2} \cdot Nd_{SW2} \cdot f_{SW2}}{f_{SW1} \cdot Nd_{SW1} + f_{SW2} \cdot Nd_{SW2}} \qquad (5.2)$$

Here, the subscripts 'Mix' refer to the mixture (stations Pelagia 9, 11 or 13), SW1 to the seawater component 1 (Labrador Current: ε_{Nd} = -26.0 ± 0.4, [Nd] = 4.3 ppt, assuming only 93% of the Nd would have been present in dissolved form following filtration, S = 32.69, Piepgras and Wasserburg 1987), and SW2 to the seawater component 2 (modified Gulf Stream water: ε_{Nd} = -9.90 ± 0.14, [Nd] = 1.74 ppt, S = 36.43, Pelagia station 15, this study). In addition, the parameter 'f' denotes the respective mass fractions (f_{SW1} + f_{SW2} = 1).

If the unradiogenic end-member with low salinity is not assumed to be the LC sample of Piepgras and Wasserburg (1987) (triangle (g) on Fig. 5.1a), a good candidate would be SGN 5 sample from Lacan and Jeandel (2005b) (triangle (f) on Fig. 5.1a), which is characterised by ε_{Nd} = -24.9 ± 0.4, [Nd] = 6.3 ppt and S = 30.6 (Lacan and Jeandel 2005b). Both stations were collected in close proximity, but during different times of the year (July for SGN5 and November-December for Hudson-83-036 LC (BIO 1984)). Hence, ice melting could explain

the lower salinity and higher Nd content measured in Lacan and Jeandel (2005b) sample. Several literature data as well as the values for station 9 to 13 (this study) show a good non-linear covariation on a salinity versus ε_{Nd} plot with Lacan and Jeandel (2005b) SGN 5 and Pelagia station 15 end-members (Fig. 5.4, $r^2 = 0.99$). Moreover, mixing calculations using equation 5.2 show that, within 10%, the results for the Nd isotopic composition, concentration and salinity of Pelagia stations 9 to 13 can be explained using these end-members. This shows that no external inputs, such as aerosols or rivers, are required to account for the observed Nd characteristics in this area.
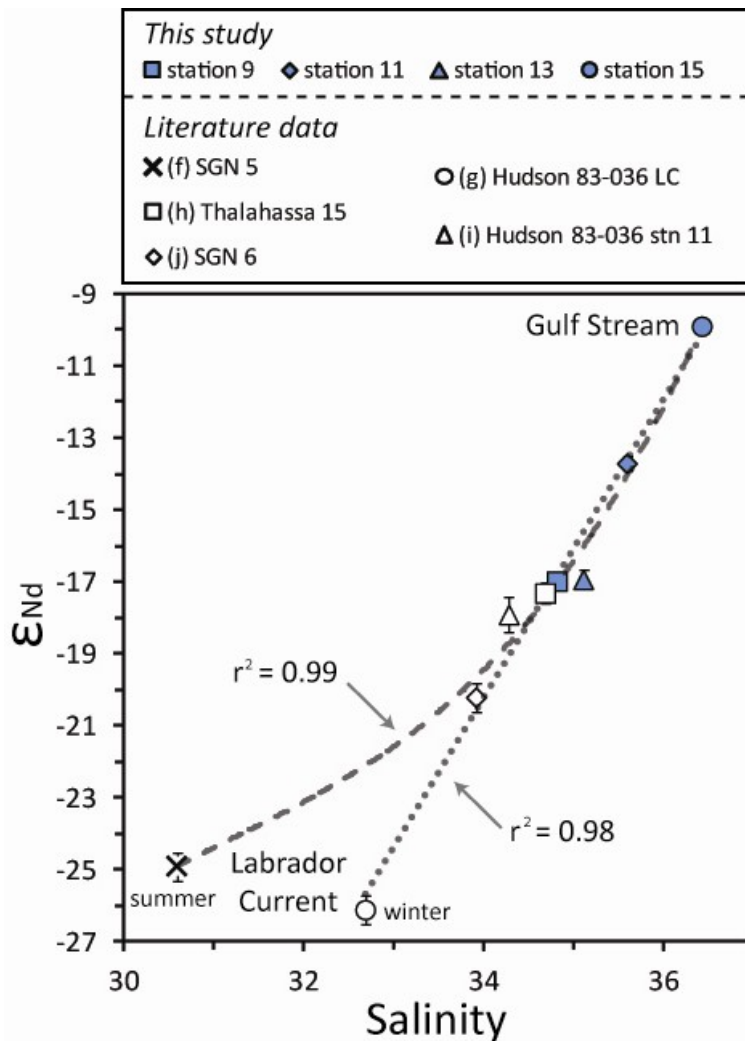
Figure 5.4: Neodymium isotopic composition versus salinity for surface samples in the southern Labrador Sea and in the vicinity of the Grand Bank. Blue filled symbols are data from the present study, and open symbols are data taken from the literature. For location of literature samples and references see Figure 5.1. For details about samples from this study (stations 9, 11, 13, and 15 annotated in the diagram) see Table 5.1. Some error bars are smaller than the size of the symbol.

Importantly, Figure 5.4 shows that even if the salinity of the Labrador Current end-member differs between summer (S = 30.6, SGN 5, Lacan and Jeandel 2005b) and winter (S = 32.7, Hudson 83-036 LC, Piepgras and Wasserburg 1987), the Nd isotopic composition remains similar (ε_{Nd} = -24.9 ± 0.4 in summer, versus ε_{Nd} = -26.0 ± 0.4 in winter). This suggests that the Nd isotope signature of the Labrador Sea source area is quite robust.

In summary, mixing between Labrador Current and Gulf Stream waters can explain the measured Nd data from the vicinity of the Grand Bank, and no external inputs are required.

5.4.2.2. Subtropical area

5.4.2.2.1. Northern subtropical gyre (stations 15 to 21)

In the northern subtropical gyre (stations 15 to 21, Fig. 5.1a, Table 5.1), the potential temperature and the potential density of the surface samples decrease when flowing northwards, whereas the highest salinity is encountered at station 19 (Fig. 5.3b). Whilst some Nd isotopic composition are identical within error, the data do show a gradual trend of less radiogenic ε_{Nd} values during the northward flowpath (ε_{Nd} = -9.90 ± 0.15 at station 15 and -9.45 ± 0.33 at station 21, Table 5.1). The lowest Nd concentration is observed at station 15 (1.74 ppt) and highest at station 19 (1.96 ppt), but the results are almost identical within external reproducibility (about ±0.09 ppt, 2sd) for these three stations. The lack of variability in the Nd isotope ratios and concentrations shows that the Nd properties of Gulf Stream waters are quite uniform. The surface water Nd isotope signatures measured in the present study are in accord with published data (Piepgras and Wasserburg 1987; Pahnke et al. 2012), but the Nd concentrations are lower and the salinities higher for the former samples (Pelagia station 21 (BATS): [Nd] = 1.88 ppt, S = 36.70 at 9 m depth, Table 5.1; Pahnke et al., (2012) BATS: [Nd] = 2.0 ppt, S = 36.52 at 20 m depth, dot l on Fig. 5.1a). The discrepancies are small, however, and they may be readily explained by natural variations in (sub)surface water properties during different sampling years (e.g., 2010 versus 2008).

In summary, the Nd properties of the Gulf Stream are quite uniform and do not show signs of direct external Nd inputs.

5.4.2.2.2. Southern subtropical gyre (stations 25 to 30)

In the southern subtropical gyre (station 25 to 30, Fig. 5.1a, Table 5.1), the surface water becomes saltier, denser and colder when flowing northwestwards (Fig. 5.3b). The Nd isotopic composition is -10.80 ± 0.18 at station 30, and is slightly more radiogenic at stations 25 and 28 (ε_{Nd} = -10.34 ± 0.14 and ε_{Nd} = -10.17 ± 0.13 respectively, Table 5.1). The Nd concentrations decrease from station 30 (3.27 ppt) to station 25 (2.53 ppt). In this region of the Sargasso Sea, there are several sources which may increase the seawater Nd concentration and affect the Nd isotope signature. These inputs are from the Caribbean volcanic arc,

Saharan dust deposition, and/or supply from the Amazon or Orinoco Rivers. These potential sources are discussed below in more detail.

Volcanic ash input

It is conceivable that the Nd concentration increase observed in the surface waters close to the Caribbean may be due to inputs from volcanic ash or from weathering of the Caribbean Island arc.

The Soufrière Hills volcano, on the Caribbean island of Montserrat, came back to activity in 1995, after having been dormant for centuries. In February 2010, an eruption sent large ash clouds eastwards, reaching Antigua and Guadeloupe. The only surface seawater measurement available for Nd in the vicinity of the Caribbean before 1995 is OCE 63-3, and it features ε_{Nd} = -9.6 ± 0.9 (no concentration data available, triangle m on Fig. 5.1a, Piepgras and Wasserburg 1987). In order to assess the potential impact of volcanic activity on seawater Nd, one surface seawater sample was collected under the ash plume of the Eyjafjallajökull 2010 volcanic eruption (Achterberg et al. 2013). The data for this sample were compared to surface seawater samples collected south of Iceland, outside the volcanic plume (Table 5.2, black triangles Fig. 5.1a).

The one sample analysed shows a clear Fe fingerprint from the volcanic eruption (Achterberg et al. 2013) and this features ε_{Nd} = -13.27 ± 0.13 and [Nd] = 2.63 ppt (Table 5.2, this study). The samples collected during the Pelagia cruise in the same area but outside the influence of the ash plume feature ε_{Nd} = -14.15 ± 0.14, [Nd] = 2.49 ppt and ε_{Nd} = -13.02 ± 0.16, [Nd] = 2.44 ppt. Importantly, all three samples have nearly identical Nd isotopic compositions within uncertainty. Moreover, the ε_{Nd} value for ash-affected surface waters is consistent with the overall Nd isotope signature measured for surface waters of the North Atlantic Subpolar Gyre (see Fig. 5.1b and Lacan and Jeandel 2004c). In contrast, tephra samples collected in Eyjafjallajökull 2010 feature ε_{Nd} values of about +7 (Sigmarsson et al. 2011). According to experiments performed by Pearce et al (2013), dissolution of basaltic material should lead to a more radiogenic Nd isotopic composition of seawater within 7 days. As our sample was collected about 3 weeks after the first main eruption, these results appear to suggest that volcanic ash does not influence the Nd signature of surface seawater. A similar conclusion is reached when returning to the surface water samples from stations 25 to 30, in the vicinity of the Caribbean, which were collected in June 2010 (Table 5.1) about four months after the Soufrière Hills volcano eruption. In detail, less radiogenic values were observed than expected for any impact of volcanic ash, which is characterised by ε_{Nd} = +6.2 ±

0.2 on Montserrat (Kumar et al. 2014). We hence conclude that volcanic ash dissolution has no significant impact on surface water Nd concentrations and isotopic compositions at stations 25 to 30. This inference may potentially apply globally, given our results for the seawater samples collected off Iceland.

Table 5.2: Location, collection date, Nd isotopic composition and concentration for seawater surface samples collected in the vicinity of Iceland during the 2010 Eyjafjallajökull volcano eruption.

Sample	Latitude [°N]	Longitude [°W]	Sampling date	^{143}Nd/^{144}Nd[a]	ε_{Nd}[b]	2se (int.)[c]	2sd (ext.)[d]	Nd [ppt][e]
Pelagia FISH	61.57	18.77	30/04/2010	0.511912	-14.15	0.14	0.06	2.49
Pelagia FISH	62.51	24.58	01/05/2010	0.511971	-13.02	0.16	0.06	2.44
Pelagia FISH	36.73	32.51	02/05/2010	0.511900	-14.40	0.24	0.06	2.47
Volcano ash plume	36.30	19.05	08/05/2010	0.511958	-13.27	0.13	0.06	2.63

[a] Normalised relative to JNdi value of 0.512115 (Tanaka et al. 2000) using five runs of JNdi.

[b] ε_{Nd} values were calculated relative to a CHUR of 0.512638 (Jacobsen and Wasserburg 1980).

[c] The internal errors are derived from the 2 sigma error on the instrument measurement (maximum 360 cycles).

[d] External errors are the two sigma standard deviations derived from repeat standard analyses of JNdi (n = 5).

[e] Concentration uncertainties were calculated using the propagated absolute 2 sigma error [ppt] taking into account the error on the weighing of the sample, the error on the weighing of the spike and the error on the data collection on the instrument (2se on up to 360 cycles). At a maximum they represent 0.03% of the samples concentrations and therefore are not represented here. The external 2 sigma error is 0.09 ppt, and was obtained by the repeated measurement of an in house seawater sample (n = 5).

Weathering from the Caribbean Island arc

It has been shown that weathering of volcanic islands can increase the Nd concentration of surface waters and shift the Nd isotope ratios towards more radiogenic values (Rickli et al. 2010). In the present study, no samples were collected directly upstream of the Caribbean volcanic islands to allow a direct comparison. However, Piepgras and Wasserburg (1987) collected a surface seawater sample at 40.7°N and 7.73°W (TTO/TAS station 63, triangle n, Fig. 5.1a), which features ε_{Nd} = -13.9 ± 0.5 and [Nd] = 2.6 ppt. Furthermore, Tachikawa et al. (1999) provide data for a sample from 50 m depth at 21°N - 31°W (NE Atl. E3O, triangle o on Fig. 5.1a) and this is characterised by ε_{Nd} = -12.5 ± 0.4 and [Nd] = 4.0 ppt. These results demonstrate that the samples of the present study do show a more radiogenic Nd isotopic

composition, whilst the concentrations are intermediate between samples upstream the North Equatorial Current and the subtropical gyre to the south. Furthermore, no decrease in salinity was observed for samples impacted by weathering in the study of Rickli et al. (2010), whereas the samples of the present study show a salinity minimum at the surface (see below).

Dust inputs

Another potential source of Nd to the subtropical gyre is dust input, either from North Africa or from the North American continent.

Dust input to the ocean is typically associated with elevated concentrations of dissolved aluminium in surface waters (Measures and Vink 2000). Dissolved Al concentrations for surface waters at stations 25 to 30 are between about 34 and 44 $nmol/dm^3$, suggesting a significant role of dust input (van Hulten et al. 2013). Similar Al concentrations are observed at stations 19 and 21 ([Al]diss $\approx$ 30 $nmol/dm^3$, van Hulten et al. 2013). These observations concur with the findings of Measures et al. (2008) that the surface water imprint of Saharan dust is stronger in the western Atlantic Ocean than it is in the eastern basin, and the observations of Kumar et al. (2014) that long range dust transport from the Sahara can be traced in the Caribbean area (Measures et al. 2008; Kumar et al. 2014). The latter study investigated the Nd isotopic composition of atmospheric total suspended particulates at three locations from both sides of the Atlantic (Mali, Tobago and the U.S. Virgin Islands) and found that summer dust reaching the Caribbean originates mainly from the Sahel region, together with some contributions from northern Saharan sources (Kumar et al. 2014). These authors also identified a temporal variability in the Nd isotope signature of the dust, and suggested that it was most likely due to mixing of dust from different source regions during transport as well as a shift in the origin of air masses (e.g., Sahel area versus the oceanic region adjacent to north-west Africa, Kumar et al. 2014).

Air mass back trajectories obtained from the NOAA Air Resources Laboratory (Hysplit model, Draxler and Rolph 1997) for the actual time of the Pelagia cruise show that stations 25 to 30 received dust from the oceanic region adjacent to north-west Africa, and not directly from the Sahel (Fig. 5.5a). In contrast, stations 15 to 21 appear to have rather received dust from the north-west (e.g., North America, Fig. 5.5b). This suggests that the higher Nd concentrations measured in the surface of stations 25 to 30 are not directly due to Saharan dust input. It does not, however, rule out that the entire subtropical gyre is influenced by such aeolian inputs. Indeed, the Nd isotopic composition of North African dust collected on land in the vicinity of the Sargasso Sea ranges from ε_{Nd} = -8.8 to -13.5 (Bermuda -13.2 (Jeandel et al.

1995); Barbados -12.2 (Grousset et al. 1988); Caribbean Virgin Islands from -9.1 to -13.5 and Tobago from -8.8 to -12.7 (Kumar et al. 2014)). For more labile Nd phases (leachable in 0.5N HBr), the ε_{Nd} values range from -11.4 to -13 on the Caribbean Virgin Islands and Tobago (Kumar et al. 2014). These values are consistent with the Nd isotopic signature measured in the surface waters of the subtropical gyre (Fig. 5.1b), where no additional inputs are encountered (as for example weathering from volcanic island, see Rickli et al. 2009).

In summary, the surface water samples of stations 25 to 30 are likely influenced by dust inputs, but another source is required to account for the elevated Nd concentrations and the shift toward slightly less radiogenic ε_{Nd} values.
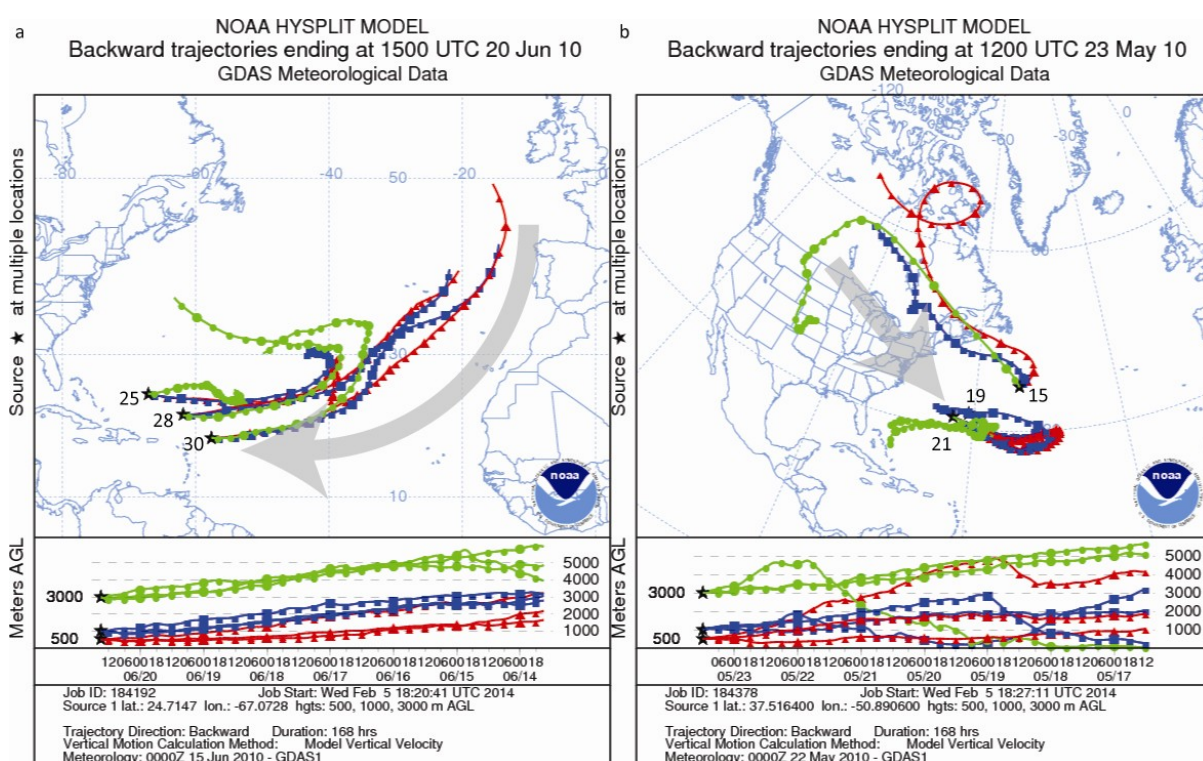
Figure 5.5: Air mass back trajectories obtained from NOAA Air Resources Laboratory (Hysplit model, (Draxler and Rolph 1997)) done on 168 hours (7 days) for (a) stations 25 to 30 and (b) stations 15 to 21. Note that the ending date was chosen as the date of the middle sample (e.g., (a) station 28, 20th of June 2010; (b) station 19, 23rd of May, 2010), but the back-trajectories were similar for other sampling dates.

Riverine inputs

The last potential source that could contribute to elevated Nd concentrations encountered in surface waters at stations 25 to 30 is input from the Orinoco and / or Amazon Rivers.

The Nd characteristics of dissolved Amazon River water are ε_{Nd} = -9.2 ± 0.4 and [Nd] = 48.5 ppt (TTO/TAS station 46, Stordal and Wasserburg 1986). Concerning the Orinoco River, only sediments samples have been analysed for their Nd isotopic composition and concentration (ε_{Nd} = -13.9 ± 0.4, [Nd] = 35.08 ppm, Goldstein et al. 1997)). Due to the prevailing clockwise water flow in the subtropical gyre, the Nd isotope signature of a potential riverine input source from the south would have to be more radiogenic than the values of Piepgras and Wasserburg (1987) TTO/TAS station 63 (ε_{Nd} = -13.9 ± 0.5) or Tachikawa et al. (1999) NE Atl E3 O (ε_{Nd} = -12.5 ± 0.4), as well as more radiogenic than what is measured at station 25 to 30 ($\varepsilon_{Nd} \approx$ -10.5). Therefore, the Orinoco River is not a good candidate to explain the present dataset. Assuming that 70% of dissolved Nd is removed from river waters in estuaries (Goldstein and Jacobsen 1987), mixing calculations using equation 5.2 show that the Nd isotope ratio of station 30 can be explained by mixing between 75% of seawater (TTO/TAS station 63 or NE Atl E3 O) and 25% of Amazon River water. Similarly, the Nd isotopic composition of stations 25 and 28 are in accord with a mixture consisting of ~ 90% seawater (Pelagia station 30, this study) and 10% Amazon River water. The calculated concentrations are, however, higher than the measured values. This may be due to the formation of REE phosphate minerals as this process may lower the actually observed Nd contents (Pearce et al. 2013). Furthermore, the calculated salinity is significantly lower than the measured one, e.g., $S_{calc} \approx$ 27 for 75% seawater (TTO/TAS station 63 or NE Atl E3 O) and 25% Amazon River water and $S_{calc} \approx$ 31 for 90% seawater Pelagia station 30 and 10% Amazon River water, whereas the measured salinity is 35.5 at station 30 and 36.2 at station 28. While the measured Nd characteristics and salinity measured in the surface waters of the southern subtropical gyre of the present study hint towards a riverine input, the mixing calculations show that the samples were probably collected too far from the Amazon mouth as to be directly influenced by the latter. Another, more proximal, riverine source may be from the Caribbean islands. Indeed, weathering of these volcanic islands by rivers could shift the Nd isotopic composition of the surface waters towards more radiogenic values while decreasing the salinity. However, to our knowledge, no Nd data are available in the literature for the Caribbean rivers, and therefore this hypothesis cannot be assessed with certainty.

In summary, aside from the background input of North African dust to the whole subtropical gyre, the riverine input, possibly from the Caribbean arc, appears to be an important Nd source for the southern subtropical gyre of the Atlantic Ocean.

5.4.3. Bottom layer

In order to assess Nd sources and sinks in the bottom layer of the study area, we will in the following discuss the Nd concentrations and isotopic compositions of bottom water samples. When considering our new results in the context of previously published data (see Lacan et al. (2012) for a recent summary), we observe a range of ε_{Nd} values from about -20 to -5 in the subpolar gyre, with very unradiogenic values in the northernmost Labrador Sea (e.g., $\varepsilon_{Nd} \approx$ -20, Stordal and Wasserburg 1986) and more radiogenic values around the ridges separating the Nordic Seas from the open subpolar North Atlantic (e.g., $\varepsilon Nd \approx$ -4 to -7, Lacan and Jeandel 2004a; Lacan and Jeandel 2004b). In contrast, the Nd isotopic compositions of bottom waters are rather homogenous in the subtropical gyre ($\varepsilon_{Nd} \approx$ -12, Piepgras and Wasserburg 1980; Piepgras and Wasserburg 1987; Spivack and Wasserburg 1988; Godfrey et al. 2009; Rickli et al. 2009; Pahnke et al. 2012)).

5.4.3.1. Subpolar area

The bottom most samples of the three stations located in the Irminger Sea (Pelagia 2, 5 and 6, Fig. 5.1a) feature the same Nd isotopic composition within error (ε_{Nd} = -11.33 ± 0.62 at station 2, ε_{Nd} = -10.76 ± 0.20 at station 5 and ε_{Nd} = -10.64 ± 0.10 at station 6, Table 5.1). The Nd concentration at station 2 is 2.34 ppt and slightly lower values are observed at stations 5 and 6 ([Nd] = 2.27 ppt at both stations). When taking into account the entire NWABW layer (depth > 1900 m, > 2600 m and > 2750 at station 2, 5 and 6, respectively, Chapter 4), the Nd isotopic compositions are systematically more radiogenic for samples collected closer to the bottom (e.g., station 6: ε_{Nd} = -11.20 ± 0.11 at 3000 m and ε_{Nd} = -10.64 ± 0.10 at 3086 m; Table 5.1). The Nd concentrations are, however, slightly lower for the bottom most samples, and the biggest difference is observed at station 5: [Nd] = 2.35 ppt at 2799 m and [Nd] = 2.27 ppt at 2924 m). Surface sediments (< 2 μm) collected in the Irminger Basin close to stations 5 and 6 (60° N –38° W) feature ε_{Nd} = -7.9 ± 0.2 and [Nd] = 30.33 ppm (Innocent et al. 1997). Therefore, remobilisation of surface sediments may explain the shift to more radiogenic Nd values for water samples collected near the sea floor. This is not in contradiction with the decrease in Nd content. Indeed, it has been shown that variations in Nd isotope signatures due to sediment remobilisation can be linked with Nd removal from seawater (boundary exchange; Lacan and Jeandel, 2005a, 2005b).

From station 6 in the south of the Irminger Basin (ε_{Nd} = -10.64 ± 0.11, [Nd] = 2.27 ppt, Table 5.1) to station 9 in the southeastern Labrador Sea (ε_{Nd} = -11.84 ± 0.20, [Nd] = 2.46 ppt, Table 5.1, Fig. 5.1a), the Nd isotopic composition of bottom waters (NWABW; Chapter 4) evolves to less radiogenic values by about 1 epsilon unit and the Nd concentrations increase by ~0.2 ppt. The Nd concentrations of the deepest samples continue to increase when flowing around the Grand Bank, with 2.82 ppt at station 11 and 3.04 ppt at station 13, whereas the Nd isotopic ratio is only slightly less radiogenic at station 11 (ε_{Nd} = -12.52 ± 0.33) but is identical within error further south (ε_{Nd} = -12.73 ± 0.47 at station 13, Table 5.1).

The process of boundary exchange has been shown to influence the Nd isotopic composition of water masses along the Greenland margin (Lacan and Jeandel 2005b). In the following, we explore whether the shift in Nd isotopic compositions from the southeastern Labrador Sea to the Grand Bank region (stations 9 to 11) could also be due to boundary exchange.

The external input flux of Nd required to influence the Nd isotope signature in the bottom water sample at station 9 can be calculated using the equation (Lacan and Jeandel, 2005b):

$$\varepsilon Nd_i \cdot Nd_i \cdot F_w + \varepsilon Nd_a \cdot F_a = \varepsilon Nd_f \cdot Nd_i \cdot F_w + F_a \qquad (5.3)$$

where εNd_i, εNd_f and εNd_a represent the Nd isotopic composition of the water mass before (i) and after (f) the external input and of the input material (a), respectively. $[Nd]_i$ is the Nd concentration of the water mass before the input and F_w the water mass flux. The external flux of Nd (F_a) can be calculated using the following values: εNd_i = -11.84 (Pelagia station 9, 4041 m, Table 5.1), εNd_f = -12.52 (Pelagia station 11, 4547 m, Table 5.1), εNd_a = -20.1 (local sediment around station 9; (Innocent et al. 1997)), $[Nd]_i$ = 2.46 ppt (Pelagia station 9, 4041 m, Table 5.1), and F_w = 7 Sv (3 Sv of DSOW, 3 Sv of entrained LSW and SPMW and 1 Sv of western LWD (Schmitz 1996)). With these values, the calculated external flux of Nd is (F_a) is 1.5 g/s.

To calculate the Nd flux corresponding to the sediment accumulation between stations 9 and 11 along the Labrador Shelf (Fig. 5.1a), we follow the reasoning of Lacan and Jeandel (2005b). To do so, the following values are used: the sediment accumulation rate in the deepest part of the Labrador Sea is about 40 cm/kyr (Innocent et al. 1997), the area of interaction between station 9 and 11 is about 95 550 km^2 (e.g., 637 km for the distance

between stations 9 and 11 and 150 km for the width of DWBC), the sediment density is about 2.5 g/cm³ (Jarrard et al. 1989), and the Nd sediment concentration is 29.23 ppm (Innocent et al. 1997). This calculation shows that sediment accumulation in the southeastern Labrador Sea corresponds to an Nd sink flux of about 88 g/s. This suggests that the remobilisation of only 2% of the sediment flux would be enough to account for the Nd input flux that is required to explain the changing Nd isotopic composition between stations 9 and 11.

Even though the above calculations encompass many assumptions, they show that sediment resuspension can easily explain the slightly altered Nd isotopic signature found for NWABW in the vicinity of the Grand Bank (stations 9 to 13). This finding is in agreement with the previous study of Lacan and Jeandel (2005b), who identified the southern tip of the Greenland margin as an area where boundary exchange happens. It should, however, be noted that the changes imposed onto bottom water samples by sediment-seawater interaction are relatively small in magnitude (~1 epsilon unit) in our study, whilst Lacan and Jeandel (2005b) observed a change of ~4 epsilon units along the Greenland margin.

5.4.3.2. Subtropics

In the subtropics, the Nd isotopic composition of the bottom most samples are assigned to modified-AABW, which evolves to less radiogenic values when flowing northward (Fig. 5.6a and Table 5.1). This observation is in good agreement with gradual dilution of the radiogenic AABW signature (ε_{Nd} (AABW) ≈ -8.5 ± 0.3 in the South Atlantic, Jeandel 1993) through mixing with overlying lower-NADW (ε_{Nd} = -12.44 ± 0.39, see Chapter 4). Neodymium concentrations do not follow this dilution trend. The bottom water Nd concentration at station 30 ([Nd] = 4.52 ppt) is lower than at station 28 ([Nd] = 4.83 ppt) and station 15 ([Nd] = 4.86 ppt), whereby the latter shows the highest Nd content of the study area (Fig. 5.6b, Table 5.1). In assessing Nd concentrations in bottom water samples it is important, however, to assess how far above the seafloor the samples were collected, and this varies from station to station. For example, the deepest sample of station 30 was collected more than 200 m above the ocean floor, whereas at other stations, the deepest samples are from within 30 m or 90 m (station 21) of the ocean floor (Table 5.1). Assuming a linear increase in Nd concentration with water depth (see section 5.4.4) we can extrapolate a Nd concentration of 4.73 ppt for station 30 at 30 m above the ocean floor. Figure 5.6b, however, highlights that even this revised concentration looks too low for the expected bottom water trend with latitude (Fig.

5.6b, empty square). So far, no suitable explanation could be found to explain why the concentration of this particular bottom water sample is much lower than expected.
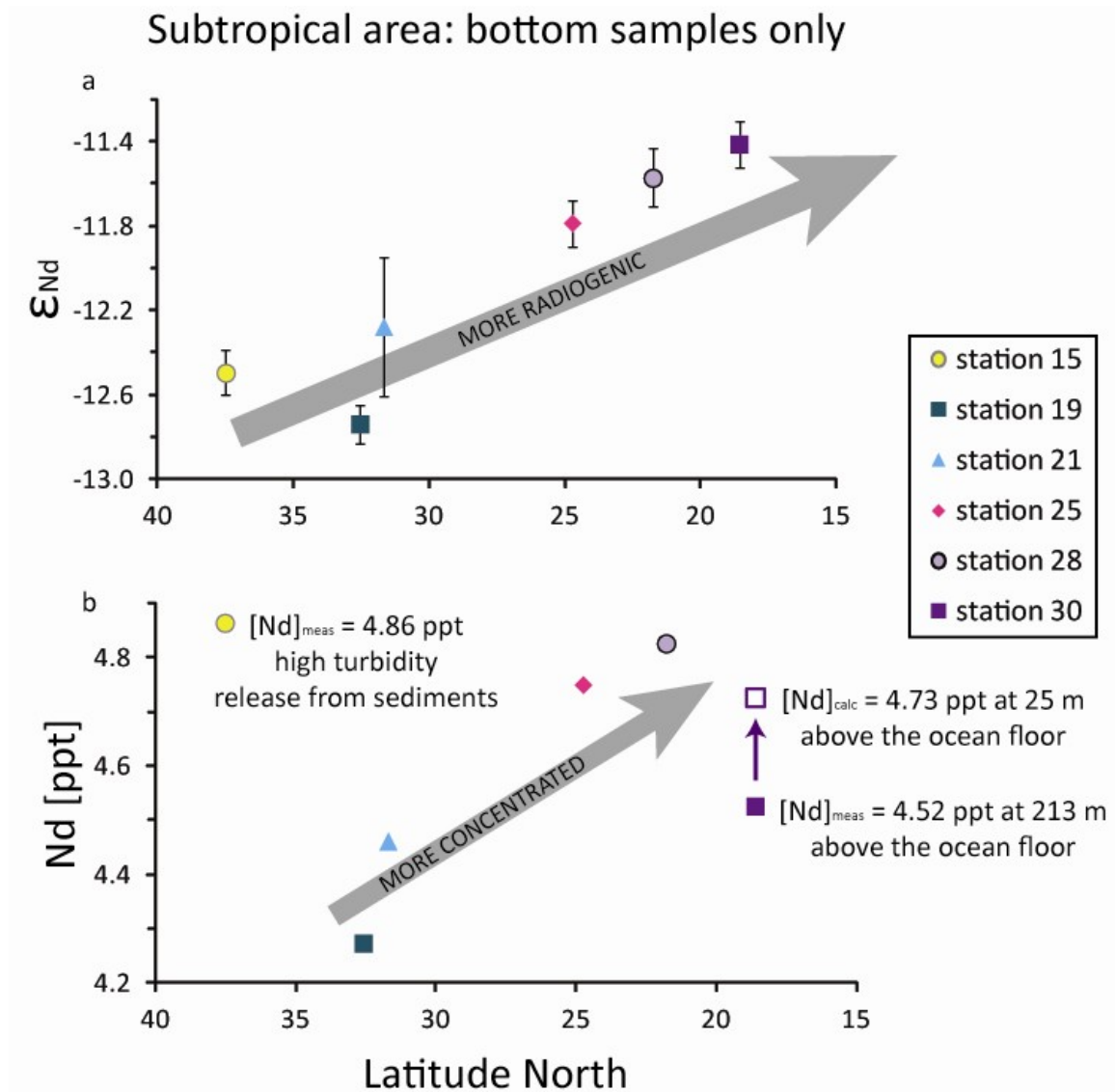
Figure 5.6: (a) Neodymium isotopic composition and (b) Nd concentration versus the latitude north for the bottom most sample from the subtropical area of the present study. Yellow dot: station 15; dark blue square: station 19; blue triangle: station 21; pink diamond: station 25; light purple dot: station 28; and purple square: station 30. The empty square in (b) represents the Nd concentration extrapolated assuming linear increase for a sample closer to the bottom floor.

Station 15, on the other hand, reveals a higher than expected Nd concentration in the bottommost seawater sample (Fig. 5.6b). In this case, however, a straightforward explanation is possible. The shipboard beam attenuation coefficient, as a measure of turbidity in the water

column, was very high with 0.23 m^{-1} at this location. In comparison, the beam attenuation coefficient was 0.07 m^{-1} and 0.04 m^{-1} at stations 19 and 28, respectively. This suggests that a pronounced nepheloid layer was present as a result of increased sediment resuspension. In an attempt to quantify the sediment input, we can use the boundary exchange equation from Lacan and Jeandel (2004a):

$$\varepsilon_{Nd}^{input} = \frac{\varepsilon_{Nd}^{final} \cdot Nd_{final} - \varepsilon_{Nd}^{initial} \cdot Nd_{initial}}{Nd_{final} - Nd_{initial}} \qquad (5.4)$$

where initial represents the bottom water sample at station 19 (ε_{Nd} = -12.74 ± 0.09 and [Nd] = 4.27 ppt, 4655 m, Table 5.1), and final represents the bottom water sample at station 15 (ε_{Nd} = -12.50 ± 0.11 and [Nd] = 4.86 ppt, 5414 m, Table 5.1). Station 19 was chosen as the initial station as it is located upstream of station 15 in terms of northward AABW flow. The calculated Nd isotopic composition of the input between station 19 and station 15 is ε_{Nd} = -10.7 ± 1.1, which is not too dissimilar to results obtained for surface sediments collected at 36°N and 66°W (ε_{Nd} = -13.3 ± 0.2 and [Nd] = 20.4 ppm, (Jeandel et al. 1995)). Therefore, sediment resuspension and Nd mobilisation within the nepheloid layer may explain the values measured for the deepest sample from Pelagia station 15.

Only two studies are available in the literature, which report Nd concentrations in bottom waters from the Sargasso Sea and the northwest Atlantic Ocean. For the GEOTRACES intercalibration exercise, BATS was sampled in June 2008, and the data reported by Pahnke et al. (2012) (dot l in Fig. 5.1a) ([Nd] = 4.0 ppt at 4280 m) agree well with the present study (station 21, [Nd] = 4.10 ppt at 4249 m and [Nd] = 4.46 ppt at 4474 m). Piepgras and Wasserburg (1987) published results for unfiltered samples from a station located north of Pelagia station 19 (AII 109-1 station 30, triangle k on Fig. 5.1a) and reported Nd contents of 3.8 ppt at 4000 m and 9.0 ppt at 4850 m. While the value at 4000 m agrees favourably with the present dataset (station Pelagia 19, [Nd] = 3.85 ppt at 4250 m, Table 5.1), the Nd concentration of the deepest sample exceeds our result by a factor of more than two. There are numerous possible explanations for this discrepancy making it impossible to pinpoint the cause at present. For example, the different Nd contents may be due to the occurrence of variable amounts of particles in the water column, whereby proximity to the ocean floor will have a larger impact on Nd concentrations in unfiltered versus filtered seawater samples (see section 5.4.2.1.1).

5.4.4. Cycling in the water column

This section focuses on the internal (bio)geochemical cycling of Nd in the water column rather than the effects which are imposed by external inputs to the surface or bottom layer. In order to do so, the present dataset is split in three areal groups, according to the overall shape of the Nd concentration depth profiles (Fig. 5.7):

- Type I: Irminger Sea (stations 2 to 6, Figs. 5.1a and 5.7a): relatively constant Nd concentration with depth, with a slight decrease visible only in the lowest 100 m.

- Type II: SE Labrador Sea and Grand Bank (stations 9 to 13, Figs. 5.1a and 5.7b): variable Nd concentrations in the uppermost 500 m of the water column, constant Nd concentrations for most of the intermediate to deep water column, and a sudden increase and decrease in Nd concentrations in the bottom ~500 m (for stations 11 and 13).

- Type III: Sargasso Sea (stations 15 to 30, Figs. 5.1a and 5.7c): increasing Nd concentrations down to ~1000 m, constant values from ~1000 m down to ~2500 m, and increasing values for the remainder of the water column (slope of Nd increase is identical for subsurface and deep waters).
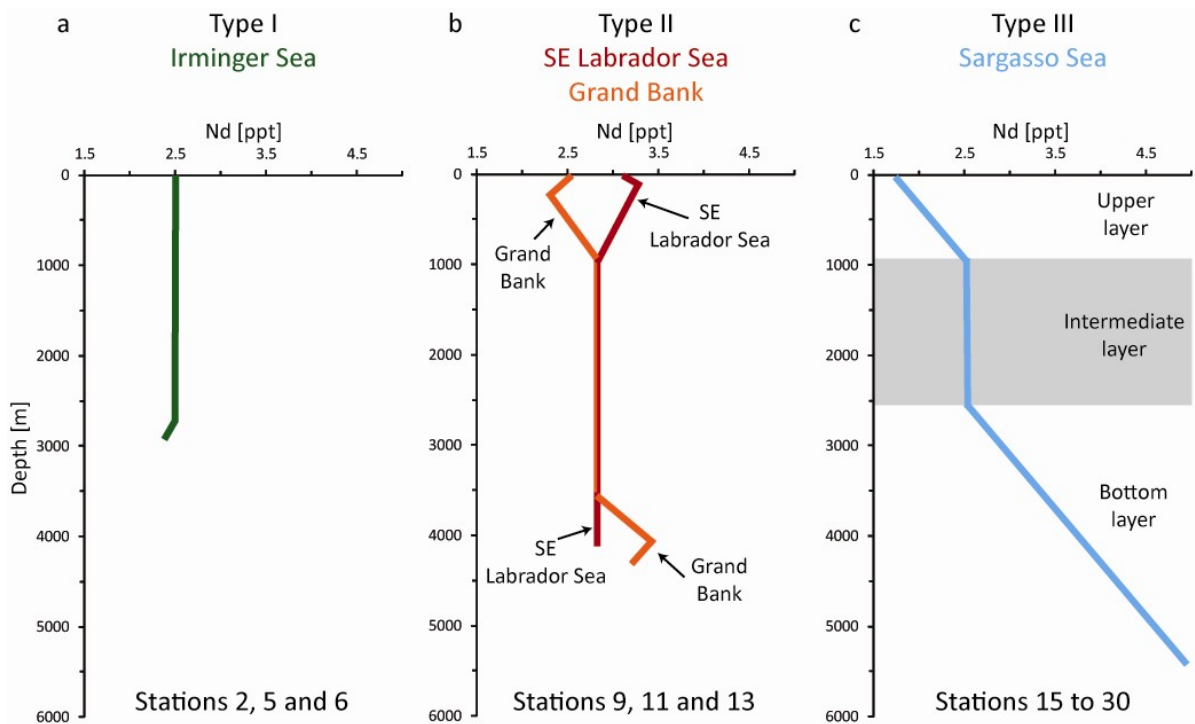
Figure 5.7: Nd concentration depth profiles schematised for (a) the Irminger Sea, Type I (see text), (b) south eastern Labrador Sea (red) and Grand Bank (orange), Type II, and (c) the Sargasso Sea, Type III.

5.4.4.1. Subpolar: Type I (Irminger Sea)

5.4.4.1.1. Profile description

In the Irminger Basin (stations 2 to 6, Figs. 5.1a and 5.8b), the three depth profiles for seawater Nd isotopes feature a similar overall shape. The surface samples have the least radiogenic values of the profile (ε_{Nd} = -14.15 to -15.17), and higher values are observed progressively down to 300 m (station 2) or to 500 m depth (stations 5 and 6). Between 300 and 800 m, station 2 shows an inverse trend in Nd isotopes, reaching near-surface values at 800 m (ε_{Nd} = -14.00 ± 0.24, Fig. 5.8b, Table 5.1). Stations 5 and 6 on the other hand feature a rather constant Nd isotopic composition down to 800 m and 1000 m respectively. Below these depths, all three profiles show a trend towards more radiogenic compositions with depth, reaching values of ε_{Nd} ≈ -11.3 (station 2) and ε_{Nd} ≈ -10.7 (station 5 and 6) at the bottom of the profiles.

Neodymium concentration profiles are relatively constant with depth (Fig. 5.7a and 5.8a), with the largest variations found at station 6 with $\Delta(Nd_{conc})$ = 0.39 ppt. In detail, Nd concentrations at station 2 are relatively constant down to 800 m ([Nd] ≈ 2.54 ppt, Table 5.1), decrease to 2.30 ppt at 1900 m, increase again to 2.36 ppt at 2150 m, and slightly decrease to 2.34 ppt at the bottom of the profile (Table 5.1, Fig. 5.8a). At stations 5 and 6, Nd concentrations increase from ~2.5 ppt at the subsurface to ~2.6 ppt at 1000 m and 800 m depth, respectively. Lower in the water column, Nd concentrations decrease down to 2000 m and 2500 m ([Nd] ≈ 2.33 ppt), respectively, stay constant for about 1000 m or 500 m, and finally decrease sharply for the last 100 m to reach bottom water concentrations of 2.27 ppt (Table 5.1, Fig. 5.8a).

In summary, Nd isotope variations of about 4.5 ε-units in the vertical water column of the Irminger Sea are not accompanied by large changes in Nd concentrations. The concentration profiles show rather small variations of up to $\Delta(Nd_{conc})$ = 0.39 ppt, in agreement with previous studies (Lacan and Jeandel, 2005b).
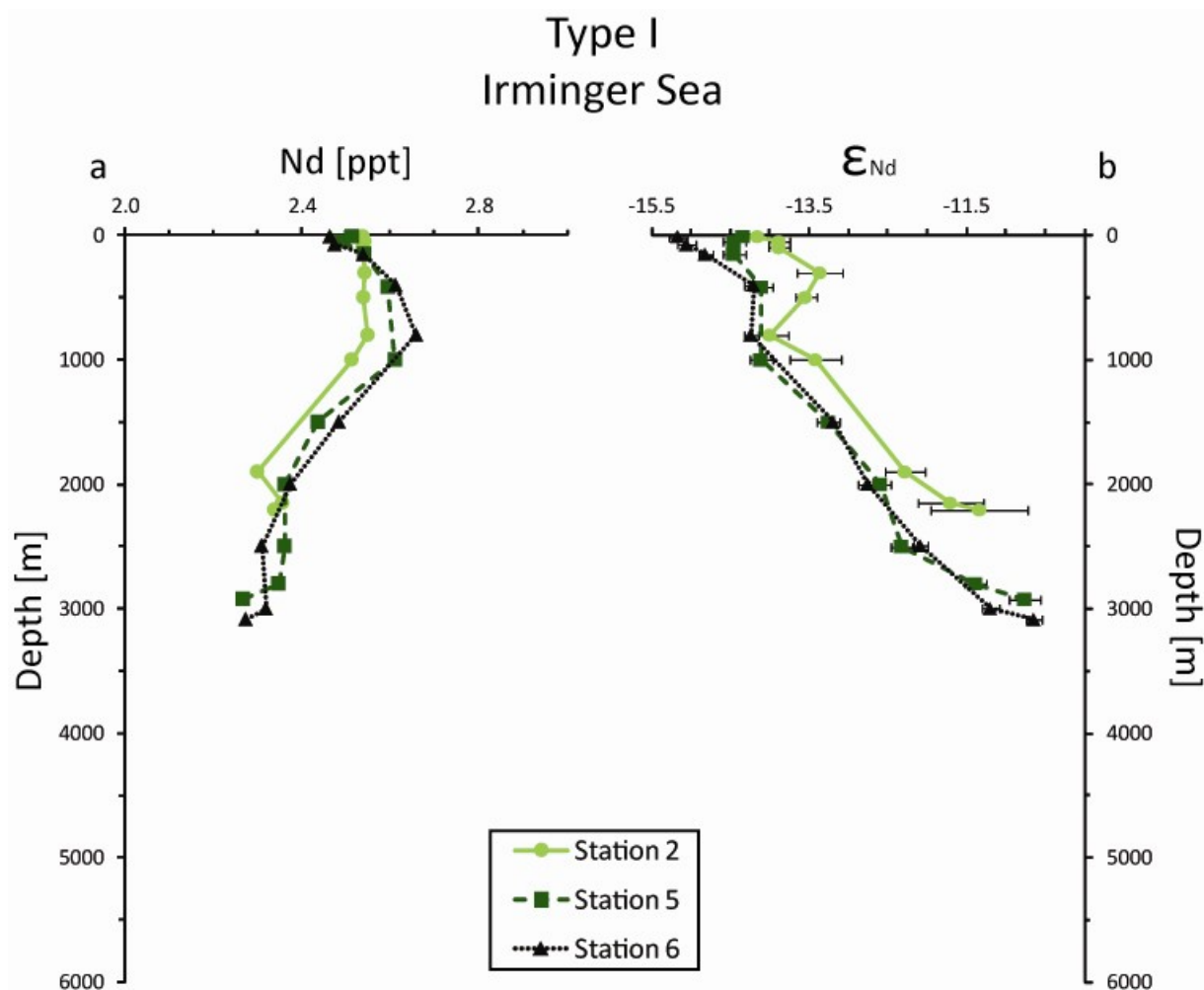
Figure 5.8: (a) Neodymium concentrations and (b) Nd isotopic composition depth profiles for the Irminger Sea (Type I). Light green dots: station 2; dark green squares: station 5; and black triangles: station 6. Note the scale on the concentration axis.

5.4.4.1.2. Discussion

When all the seawater samples from the Irminger Basin (stations 2, 5 and 6, Fig. 5.9a) are plotted on a graph of ε_{Nd} vs. 1/Nd (reciprocal of the Nd concentration), a good regression with a coefficient of $r^2 = 0.73$ is obtained. The positive correlation is best for stations 2 and 5 ($r^2 = 0.84$), whilst station 6 features $r^2 = 0.65$. Furthermore, a fairly good correlation is observed between Nd concentrations (and Nd isotope ratios) and potential temperature (Fig. 5.9b). However, other parameters such as salinity or nutrient concentrations do not yield significant correlations using the entire sample set from the Irminger Sea (i.e., when taking all water depths into account) nor when the seawater samples are grouped by water mass, as identified using hydrographic data (Table 4.3, Chapter 4). The latter approach is, however, hampered by the scarcity of data that can be applied to explore correlations (e.g., n = 5 for

ULSW, n = 3 for LSW, n = 5 for NEADW and n = 6 for NWABW). The good correlation between Nd isotope ratios and the reciprocal of the concentration suggests a coupling between these two chemical characteristics, as might be expected for areas where convection leads to efficient homogenisation of water mass properties such as salinity, potential temperature and potential density. However, the samples of the present study were collected in May, and the subpolar gyre was clearly stratified as seen in Figure 5.3. Therefore, another explanation is required to account for the observed correlation between the Nd concentrations and isotopes or temperature data; so far, no suitable explanation could be found.
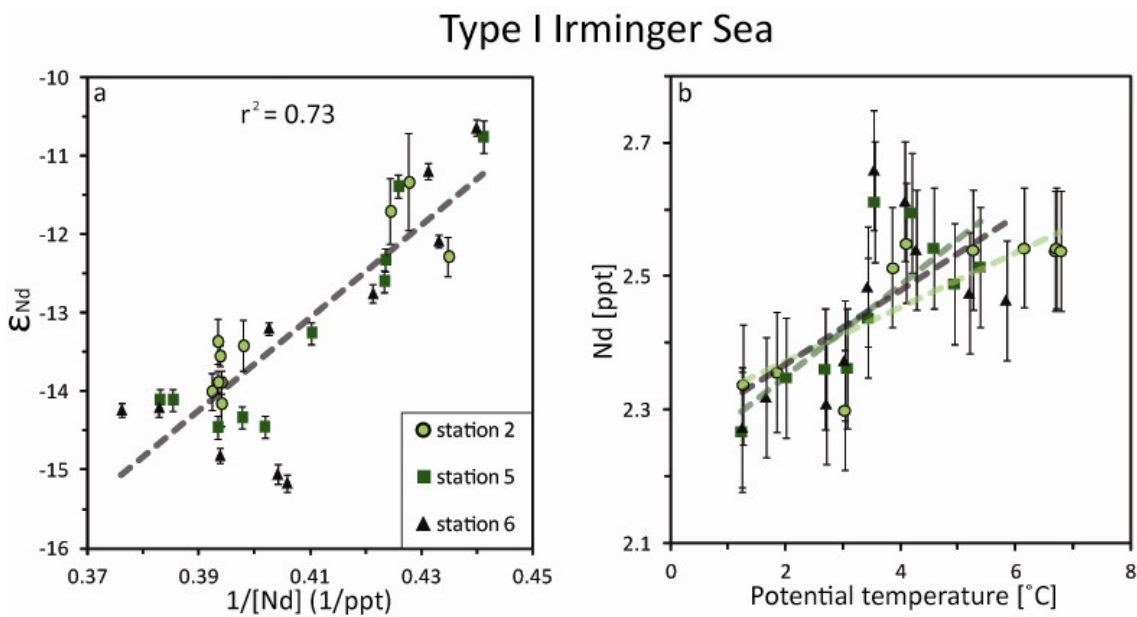
Figure 5.9: (a) Neodymium isotopic composition versus the reciprocal Nd concentration and (b) Nd concentration versus potential temperature for stations from the Irminger Sea (Type I). Light green dots: station 2; dark green squares: station 5; and black triangles: station 6. In (b), $r^2 = 0.68$ (station 2, light green line); $r^2 = 0.60$ (station 5, dark green line); and $r^2 = 0.37$ (station 6, grey line).

As expected, the Nd isotopic compositions of NEADW and NWABW in the Irminger Basin (station 2 to 6) can be explained by mixing between the different constituting water masses (e.g., NEADW = 2 ISOW + 2 LDW + 2 (AW + LSW) and NWABW = ½ DSOW + ½ (LSW + SPMW)) (see Chapter 4). However, these calculations generate Nd contents for NEADW and NWABW that are systematically higher than the measured concentrations for Irminger Basin samples (NEADW: $[Nd]_{calc} = 3.00$ ppt and $[Nd]_{meas} = 2.34 \pm 0.07$ ppt, 2sd n = 5, Table 5.1; NWABW: : $[Nd]_{calc} = 2.47$ ppt and $[Nd]_{meas} = 2.32 \pm 0.08$ ppt, n = 6, Table 5.1). This suggests that boundary exchange between seawater and continental margin acts as

a Nd sink in this area, in, agreement with the results of previous Nd studies for the Irminger Basin (Lacan and Jeandel 2005a; Lacan and Jeandel 2005b).

5.4.4.2. Subpolar: Type II (Grand Bank and southeastern Labrador Sea)

5.4.4.2.1. Profile description

In the southeastern Labrador Sea and around Grand Bank (stations 9, 11 and 13; Figs. 5.1a and 5.10b), the seawater Nd isotope profiles show very similar compositions between ~1000 m and the near bottom samples, whereby the latter feature a slight increase in ε_{Nd} from values of around -14.4 to about -12 (3500-4000 m). Deviations in the shape of the individual profiles can be found to some extend in the near bottom layer and, to a remarkable extent, in the upper part of the water column (0-1000 m). Stations 9 and 13 feature very unradiogenic surface water values ($\varepsilon_{Nd} \approx$ -16.9). While the Nd isotopic composition of seawater at station 9 shows constant values down to 150 m, followed by a sharp increase to more radiogenic values at 400 m ($\varepsilon_{Nd} \approx$ -15), station 13 exhibits a very rapid subsurface shift towards more radiogenic values of $\varepsilon_{Nd} \approx$ -12 at 77 m. Between 77 and 400 m, the ε_{Nd} of seawater at this location varies between -12.7 and -11.5 before returning to similar values of -14.4 at 800-1000 m water depth in all three depth profiles. Stations 11 and 13 feature a small (<2 epsilon unit) shift towards less radiogenic values in the lowest part of the water column.

Neodymium concentration profiles in the southeastern Labrador Sea and the Grand Bank region are more variable than in the Irminger Sea (Figs. 5.7b and 5.10a), with $\Delta(Nd_{conc}) =$ 0.63 to 0.85 ppt. Similar to the isotopic compositions, the Nd concentration profiles of the stations resemble each other at water depths between ~1000 m and ~3500 m, but deviate significantly in the upper 1000 m and towards the seafloor. In fact, the Nd concentration and isotope profiles are mirror images of each other for the upper 3500 m of the water column(Figs. 5.10a and b). Indeed, Nd concentrations return from a trend of slightly decreasing values in all three profiles to significantly higher concentrations in the deepest ~1500 m at stations 11 and 13 ([Nd] $\approx$ 3.2 ppt at 3000/3500 m and [Nd] = 2.82/3.04 ppt at the bottom of the profile).
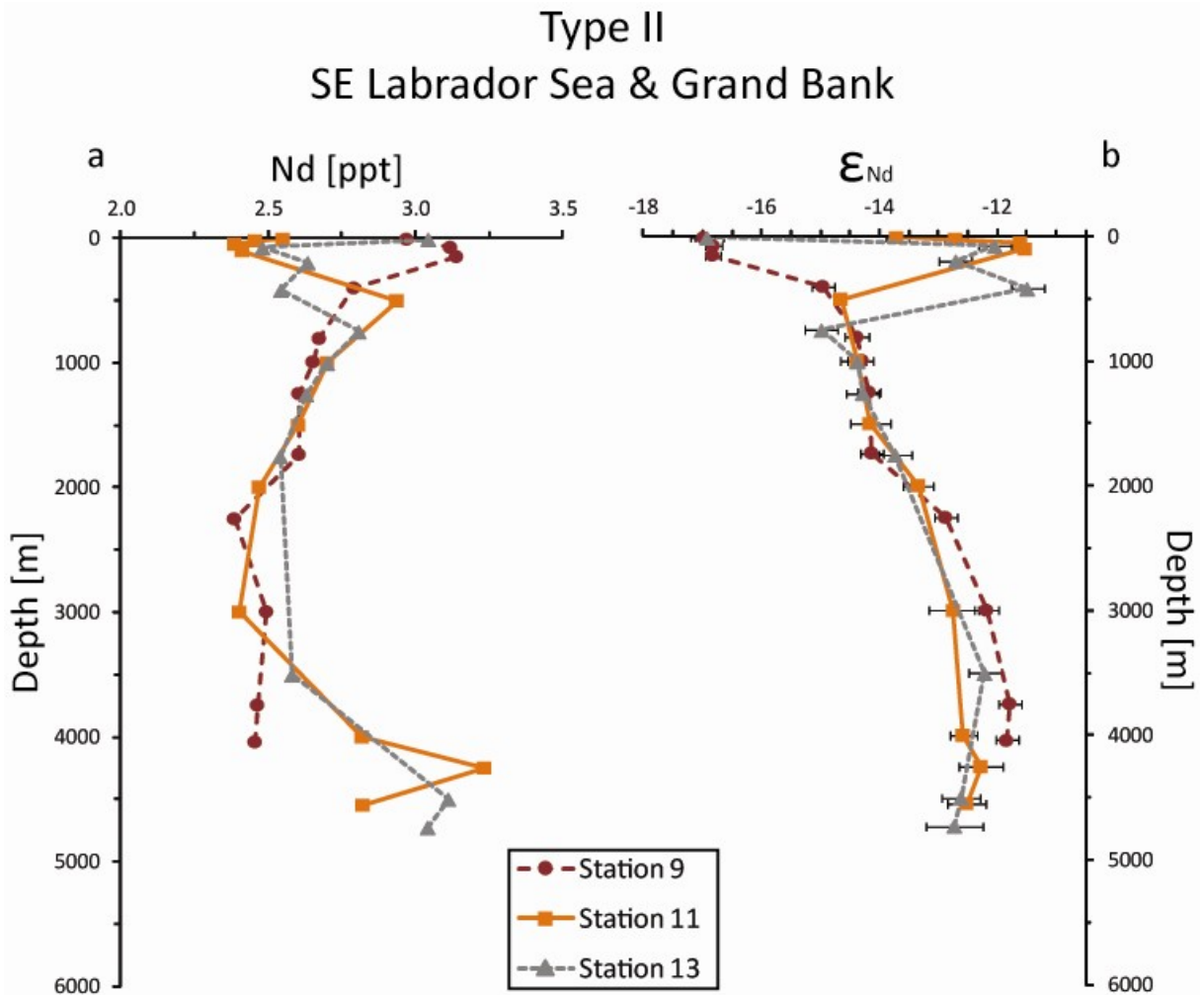
Figure 5.10: (a) Neodymium concentration and (b) Nd isotopic composition depth profiles for the stations around the Grand Bank (Type II). Red dots: station 9; orange squares: station 11; and grey triangles: station 13.

5.4.4.2.2. Discussion

As for the Irminger Sea, a covariation between the Nd isotopic composition of seawater and 1/[Nd] can be observed in Figure 5.11. For station 9 (southeast Labrador Sea, Fig. 5.1a), an overall correlation coefficient of $r^2 = 0.91$ is obtained when all samples from the water column are plotted (Fig. 5.11a). Stations 11 and 13 (from the Grand Bank area) show a relatively good correlation ($r^2 = 0.72$) for the samples from the surface down to 3500 m depth (corresponding to surface waters, ULSW, LSW, and NEADW), whereas the correlation for the deeper samples (NWABW) is very poor ($r^2 < 0.1$). The latter observation, however, is readily explained as the samples collected near the seafloor feature relatively constant Nd isotopic compositions but highly variable Nd concentrations (Fig. 5.11b).
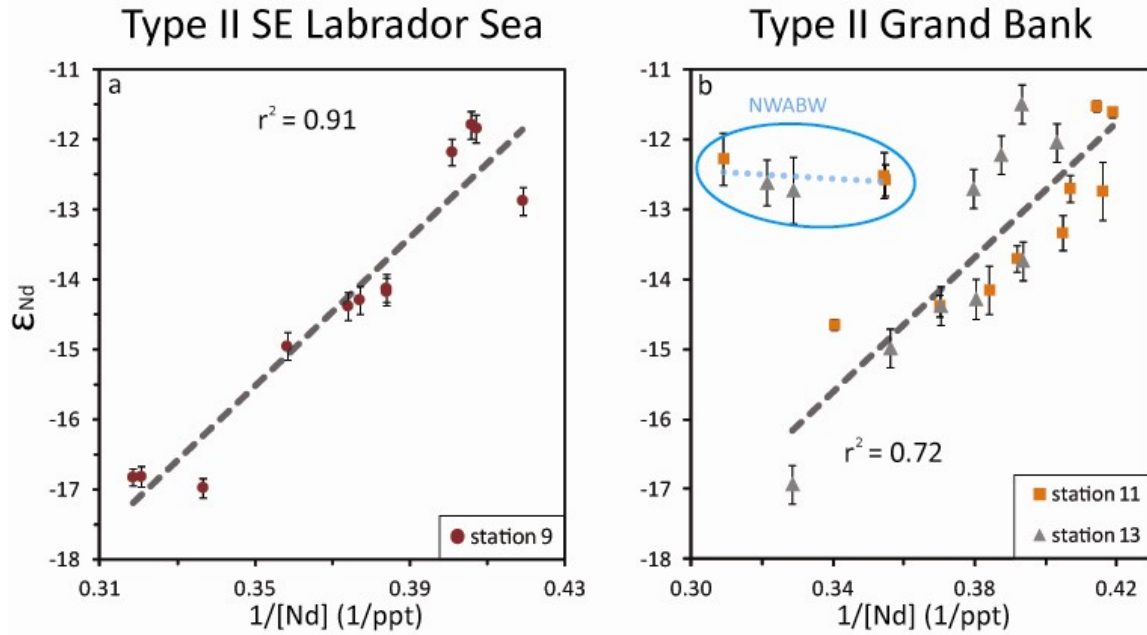
Figure 5.11: Neodymium isotopic composition versus the reciprocal Nd concentration for (a) south eastern Labrador Sea (station 9, red dots) and (b) the Grand Bank (orange squares: station 11; and grey triangles: station 13). The samples from the water mass NWABW were not included in the regression.

When considering other seawater parameters, such as salinity or silicate concentrations, no covariation with ε_{Nd} or Nd concentration is observed (not shown). An important exception is the good correlation of Nd concentrations ($r^2 = 0.85$) and isotope ratios ($r^2 = 0.98$) with potential temperature at station 9 (Fig. 5.12). The same positive correlation between potential temperature and ε_{Nd} is also observed for seawater from stations 11 and 13 (in the Grand Bank region) ($r^2 = 0.91$) when surface waters are excluded (e.g., using ULSW, LSW, NEADW and NWABW). The correlation with Nd concentrations is poor ($r^2 = 0.3$), however, as both surface and bottom waters do not fall on the trendline defined by the other samples. As noticed for the Irminger Basin samples (section 5.4.4.1.2), the θ-S plots (Fig. 5.3 and Fig. 4.3 Chapter 4) show that stations 9 to 13 are stratified. Therefore, the correlation observed between ε_{Nd} and $1/[Nd]$ cannot be explained by an homogenisation of the water column properties, such as what would be observed during convection.

Figure 5.12: (a) Neodymium concentrations [ppt] and (b) Nd isotopic composition (ε_{Nd}) versus potential temperature [˚C] for the stations around the Grand Bank (Type II). Red dots: station 9; orange squares: station 11; and grey triangles: station 13.

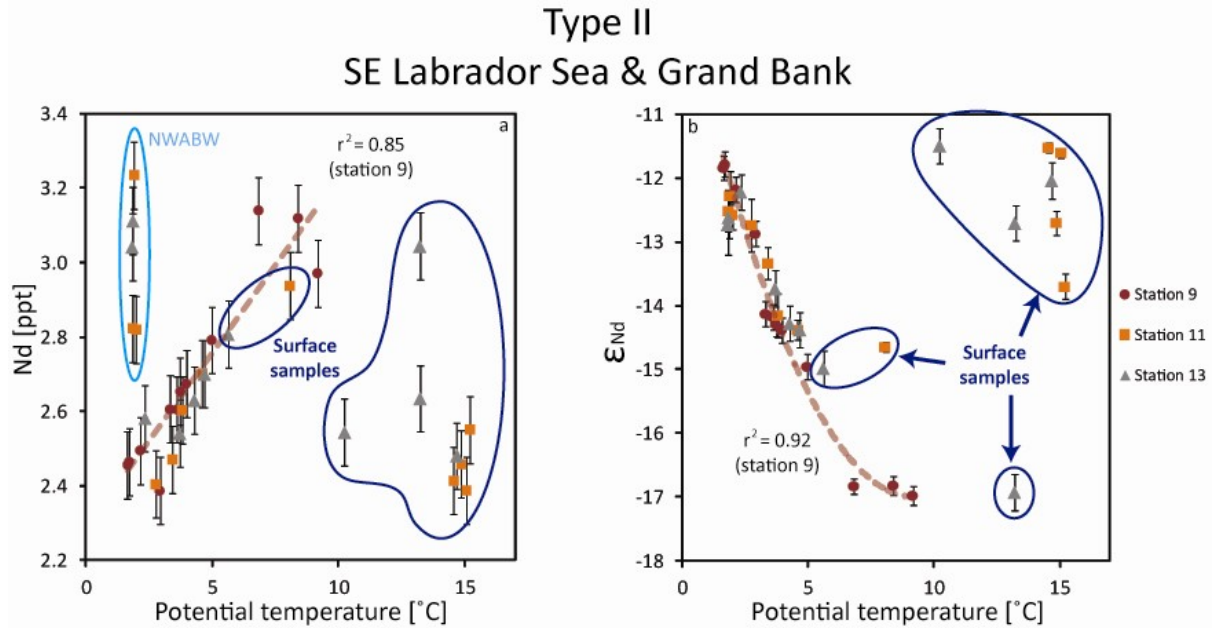As for the Irminger Sea, it was shown in Chapter 4 that the Nd isotope characteristics of the water masses from the southeaster Labrador Sea and the Grand Bank region are primarily a consequence of water mass mixing. However, the predicted Nd concentrations for NEADW are also systematically higher than the measured data, whilst the values calculated for NWABW are identical, within error, to the measured concentrations: [Nd]$_{calc}$ = 3.0 ± 0.4 ppt and [Nd]$_{meas}$ = 2.46 ± 0.22 ppt, 2sd, n = 3 for NEADW (Table 5.1); [Nd]$_{calc}$ = 2.5 ± 0.2 ppt and [Nd]$_{meas}$ = 2.47 ± 0.04 ppt, 2sd, n = 3 for NWABW at station 9; and [Nd]$_{calc}$ = 2.8 ± 0.4 and [Nd]$_{meas}$ = 3.01 ± 0.36 ppt, 2sd, n = 5 for NWABW at stations 11 and 13 (Table 5.1). This suggests that boundary exchange along the continental margins is also an important process at these stations.

In summary, the present dataset for the subpolar western North Atlantic Ocean lead to four main conclusions:

(i) dissolved Nd concentrations are relatively constant with water depth (Δ(Nd$_{conc}$) = 0.25 to 0.85 ppt), with the exception of samples from the (sub)surface and bottom layers of the Grand Bank region;

(ii) seawater Nd isotopic compositions show large variations within each profile according to vertical water mass structure. The within-profile variability ranges from 5.4 epsilon units at

station 13 in the Grand Bank region to a minimum of 2.8 epsilon units at station 2 in the northern Irminger Sea;

(iii) boundary exchange, acting as both a source and a sink of Nd, is necessary to explain seawater Nd characteristics of this region.

5.4.4.3. Subtropics – Type III

5.4.4.3.1. Profile description

In the subtropical area of the present study, the Nd isotope depth profiles show the same overall shape for all of the stations (15 to 30, Figs. 5.1a and 5.13b). The most radiogenic values are found at the surface, ranging from ε_{Nd} = -9.5 at station 21 to ε_{Nd} = -10.8 at station 30. Subsurface water depths (~100 to 500 m) at stations 19 and 21 are characterised by the presence of subpolar mode waters and relatively constant Nd isotope ratios ($\varepsilon_{Nd} \approx$ -9.6, STMW, see Chapter 4). Below this depth, a gradual decrease towards less radiogenic values of ε_{Nd} = -13.7 at ~1250 m is observed. At station 15, this decrease already starts below the surface layer and it reaches a minimum of ε_{Nd} = -13.5 at ~ 900 m, which is maintained to about 2000 m. The profiles of stations 25 to 30 show a slight deviation in that they exhibit a small (<0.5 epsilon unit) shift towards more radiogenic values in the subsurface (i.e., down to depths of ~150 m) before starting the same trajectory towards less radiogenic values, with a minimum being reached around ~ 1750 m (ε_{Nd} = -13). Below this depth, all the profiles show a shift towards more radiogenic Nd isotopic compositions at ~2500 m ($\varepsilon_{Nd} \approx$ -12.5 to -12.0), and stay relatively constant down to 4500 m, before some profiles show a small shift (≤ 1 epsilon unit) towards more radiogenic bottom water samples.

The Nd concentration profiles for all six stations in the Sargasso Sea are even more similar to each other than the Nd isotope profiles (Figs. 5.7c and 5.13a). The only exceptions to this observation are the surface waters at stations 25 to 30, where the Nd concentrations are higher than for the subsurface samples, due to influence of the Amazon River (see section 5.4.2.2). For stations 15 to 21, the concentrations are lowest at the surface ([Nd] $\approx$ 1.8 ppt) and increase gradually down to ~1000 m ([Nd] $\approx$ 2.5 ppt). At station 25 to 30, the concentrations first decrease down to ~150 m before increasing gradually to ~1000 m, where they reach Nd concentrations of 2.5 ppt, as observed at stations 15 to 21. Below this depth,
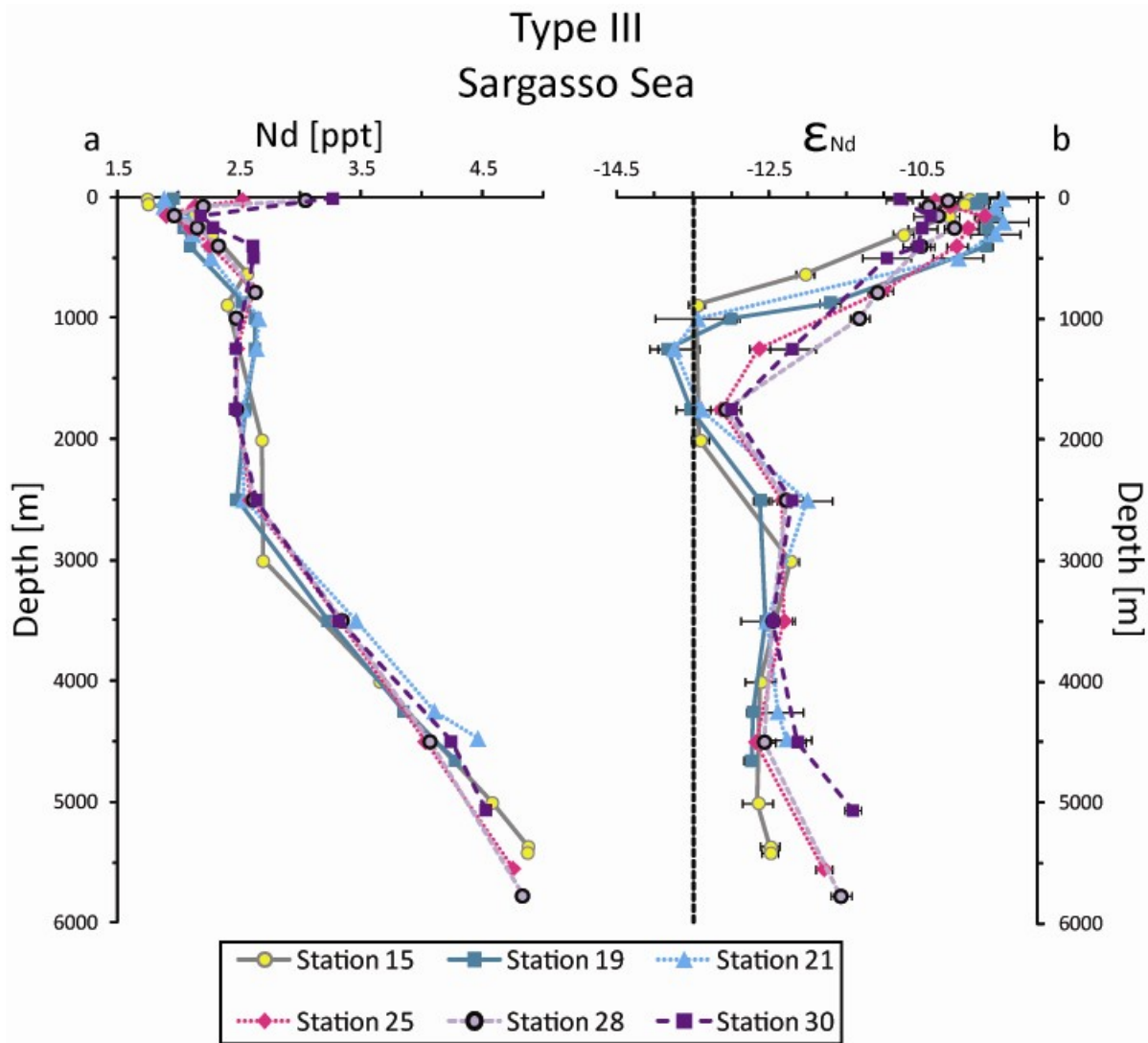
Figure 5.13: (a) Neodymium concentration in ppt and (b) Nd isotopic composition (expressed as ε_{Nd}) depth profiles for the stations from the subtropics. Yellow dots: station 15; dark blue squares: station 19; blue triangles: station 21; pink diamonds: station 25; light purple dots: station 28; and purple squares: station 30. The vertical dashed line in (b) stands for the historical value of NADW (ε_{Nd} = -13.5; Piepgras and Wasserburg, 1987).

the Nd concentrations remain constant down to ~2500-3000 m, but they then increase again to the bottom, where maximum Nd concentrations are reached for each profile, ranging from 4.27 ppt at station 19 to 4.86 ppt at station 15. It is worth mentioning that the slope of the concentration increase with depth is identical for the subsurface and the deep water layers. Notably, the Nd concentration data of the present study for the subtropical Atlantic are in good agreement with the results of previous investigations (Piepgras and Wasserburg 1987; Pahnke et al. 2012).

155

5.4.4.3.2. Discussion

Overall, the Nd concentration profiles of subtropical seawater show relatively large variations, from 2.34 ppt at stations 19 and 30 to 3.13 ppt at station 15. This observation stands in contrast to the relatively constant Nd concentration profiles for the subpolar gyre. Furthermore, the subtropical Nd isotope profiles show less variability compared to the profiles of the subpolar area. In detail, the subtropical profiles display a range in ε_{Nd} values that varies from 2.6 epsilon units at station 30 to 4.3 epsilon units at station 21. From these observation it is already obvious that Nd isotope and concentration profiles are decoupled, and the data exhibit poor correlation coefficients in plots of the seawater Nd isotopic composition versus 1/[Nd] ($r^2 \leq 0.5$ for all stations except station 19 ($r^2 = 0.6$) (Table 5.1).

In order to investigate what processes govern the Nd concentration profiles in the subtropical western Atlantic Ocean, the dataset was separated into three groups (Fig. 5.7c): (a) an upper layer, which encompasses the almost linear increase in Nd concentration with depth from the surface (or subsurface for stations 25 to 30) down to intermediate water levels, (b) a middle layer, with relatively constant Nd concentrations and (c) a bottom layer, which again shows a near linear increase in Nd concentrations.

Upper layer (0 – 400 m)

A fairly convincing positive linear regression is obtained in cross plots of Nd concentrations versus dissolved silicate, nitrate and phosphate concentrations ($r^2 = 0.72 – 0.75$, excluding the surface samples from stations 25 to 30, Figs. 5.14a and b). The correlation between [Nd] and salinity is, however, poor ($r^2 < 0.1$), and it is poor as well for ε_{Nd} versus 1/[Nd] ($r^2 \approx 0.3$). Together, these observations indicate that Nd displays a behaviour akin to nutrients in the upper 400 m of the water column and also argue against water mass mixing. It is important to note in this context, that in contrast to the nutrients, Nd is not highly depleted in surface waters (see also Akagi 2013), pointing to a different control on low Nd concentrations. We here suggest that the predominant process leading to low Nd concentrations in the (sub)surface ocean is adsorption of Nd onto suspended biogenic and detrital particles. The scavenged Nd is then successively released by desorption from the particles and during remineralisation of biogenic particulates. Such processes can explain the strong correlation of Nd with nutrients, even though Nd is not a nutrient element and is not actively utilised in the biological pump. Similar observations have been made in a number of
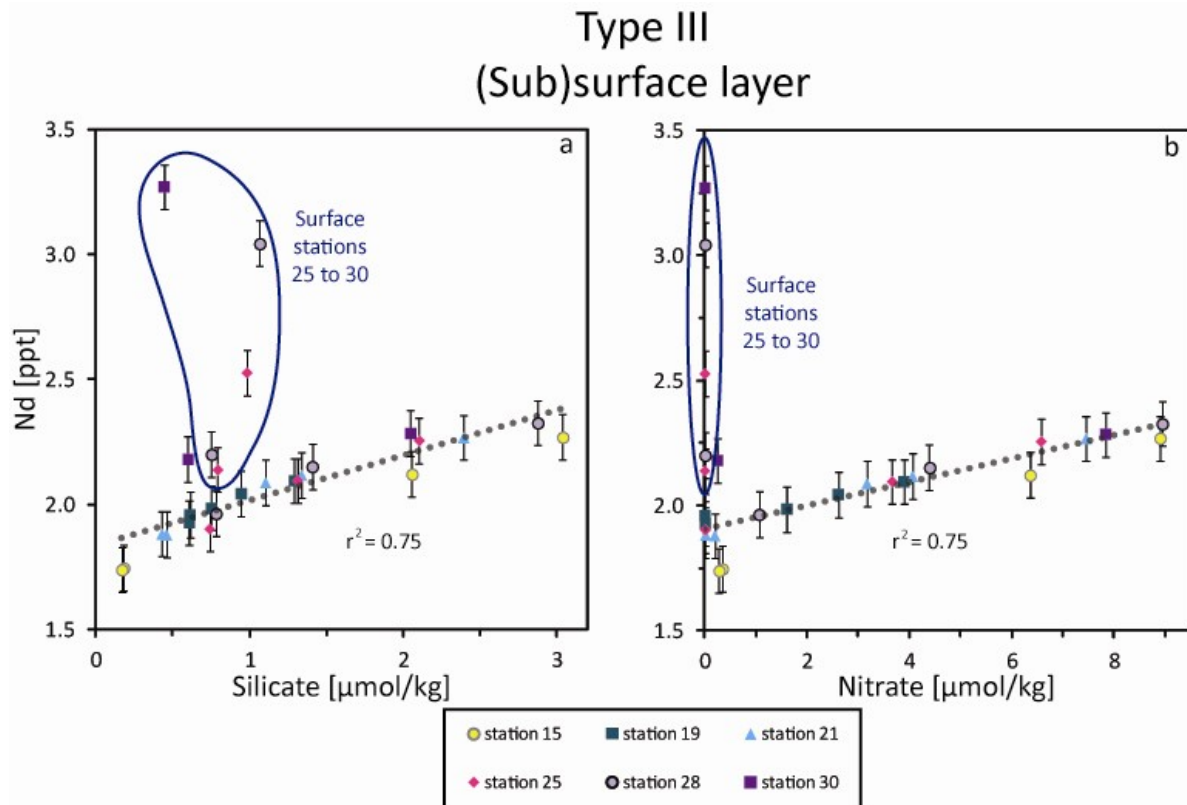
Figure 5.14: Neodymium concentrations versus (a) silicate concentrations and (b) nitrate concentrations for the surface waters of the subtropical western North Atlantic. Yellow dots: station 15; dark blue squares: station 19; blue triangles: station 21; pink diamonds: station 25; light purple dots: station 28; and purple squares: station 30. Circled samples represent the surface most samples of station 25, 28 and 30, and were not taken into account for the regression calculation due to additional external input (see text).

previous studies (Sholkovitz et al. 1994; Siddall et al. 2008; Arsouze et al. 2009; Oka et al. 2009; Rickli et al. 2009; Rempfer et al. 2011; Stichel et al. 2012; Akagi 2013). For example, Sholkovitz et al. (1994) suggested that Mn oxohydroxides are important for the removal/release of Nd in the upper water column, while Rickli et al. (2009), Stichel et al. (2012) and Akagi (2013) suggested that Nd is adsorbed onto diatom frustules in the surface ocean and released with depth upon remineralisation of the frustules.

Bottom layer (3000 m – bottom)

A very intriguing observation from this study is that the lowermost part of the water column in the northwest Atlantic Ocean shows a similar increase in Nd concentrations as the top part, and this similarity even extends to the slope of the increase with depths (Figs. 5.7c

and 5.13a). The samples of this 'bottom layer' encompass the water masses lower-NADW and modified-AABW (Table 5.1) at depths below ~2500 m. The properties of these water
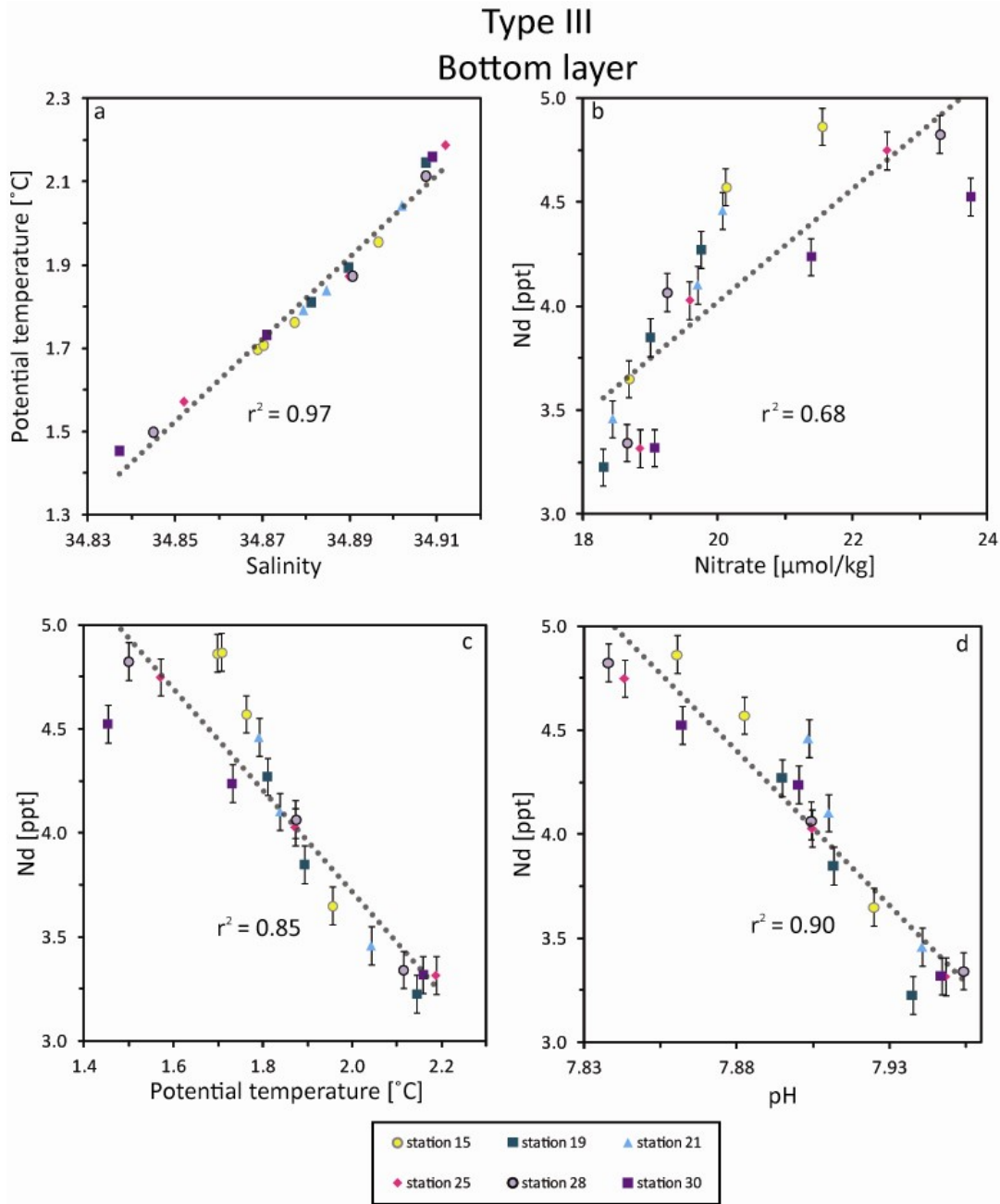
Figure 5.15: Potential temperature versus salinity (a), Nd concentration versus (b) nitrate concentration, (c) potential temperature, and (d) pH for the samples collected in the bottom water masses in the subtropical area of the present study. Yellow dots: station 15; dark blue squares: station 19; blue triangles: station 21; pink diamonds: station 25; light purple dots: station 28; and purple squares: station 30.

masses are controlled by water mass mixing, as is revealed by the excellent correlation defined by all samples in a θ vs. S diagram ($r^2 = 0.97$; Fig. 5.15a). However, as for the (sub)surface samples, a reasonable correlation is also obtained between seawater Nd concentrations and nutrients (silicate: $r^2 = 0.74$, nitrate: $r^2 = 0.68$, phosphate: $r^2 = 0.71$, Fig. 5.15b). In contrast to the (sub)surface samples, the deep and bottom water Nd concentrations also co-vary with salinity and potential temperature ($r^2 = 0.77$ and $r^2 = 0.85$ respectively, Fig. 5.15c), whilst these data exhibit only a poor correlation for the subsurface samples ($r^2 < 0.2$). Together, this suggests that Nd concentrations in the lower part of the water column are primarily controlled by binary water mass mixing. This interpretation is in accord with the nutrient data, as major nutrients are also known to display 'quasi-conservative' behaviour in deep waters (Goldstein and Hemming 2003).

Of further interest is the observation that seawater Nd concentrations are also highly correlated with the water pH value ($r^2 = 0.9$). This covariation is negative, which suggests that dissolved Nd contents increase with decreasing pH (Fig. 5.15d).

Bottom layer: comparison with other data set from the Atlantic Ocean

When the results of the present study are compared with published data for the Atlantic Ocean from below 2500 m water depth, it is obvious that the binary mixing trend defined by our new data (Figs. 5.15 a and c) clearly deviates from the overall mixing envelope that was previously identified for Atlantic Ocean deep waters (Fig. 5.16a). Indeed, mixing lines calculated between a northern water mass (with high salinity and low [Nd]) and a southern water mass (with low salinity and higher [Nd]), show that the Nd concentrations measured for the bottom layer of the present study have elevated Nd contents for a given salinity (Fig. 5.16a), thus suggesting additional input of Nd. Looking at the Nd isotope vs. concentration systematics for the Atlantic Ocean (Fig. 5.16b), our samples also fall outside the mixing array, but they feature Nd isotope ratios that are similar to samples that lie within the mixing envelope. Indeed, it was shown in Chapter 4 that in the subtropical North Atlantic Ocean, the Nd isotopic compositions of seawater from below 2500 m depth display conservative behaviour and are controlled by water mass mixing (see Fig. 4.6 in Chapter 4). Therefore, the present dataset reinforces earlier observations that Nd isotopes and concentrations display decoupled behaviour in the open ocean.
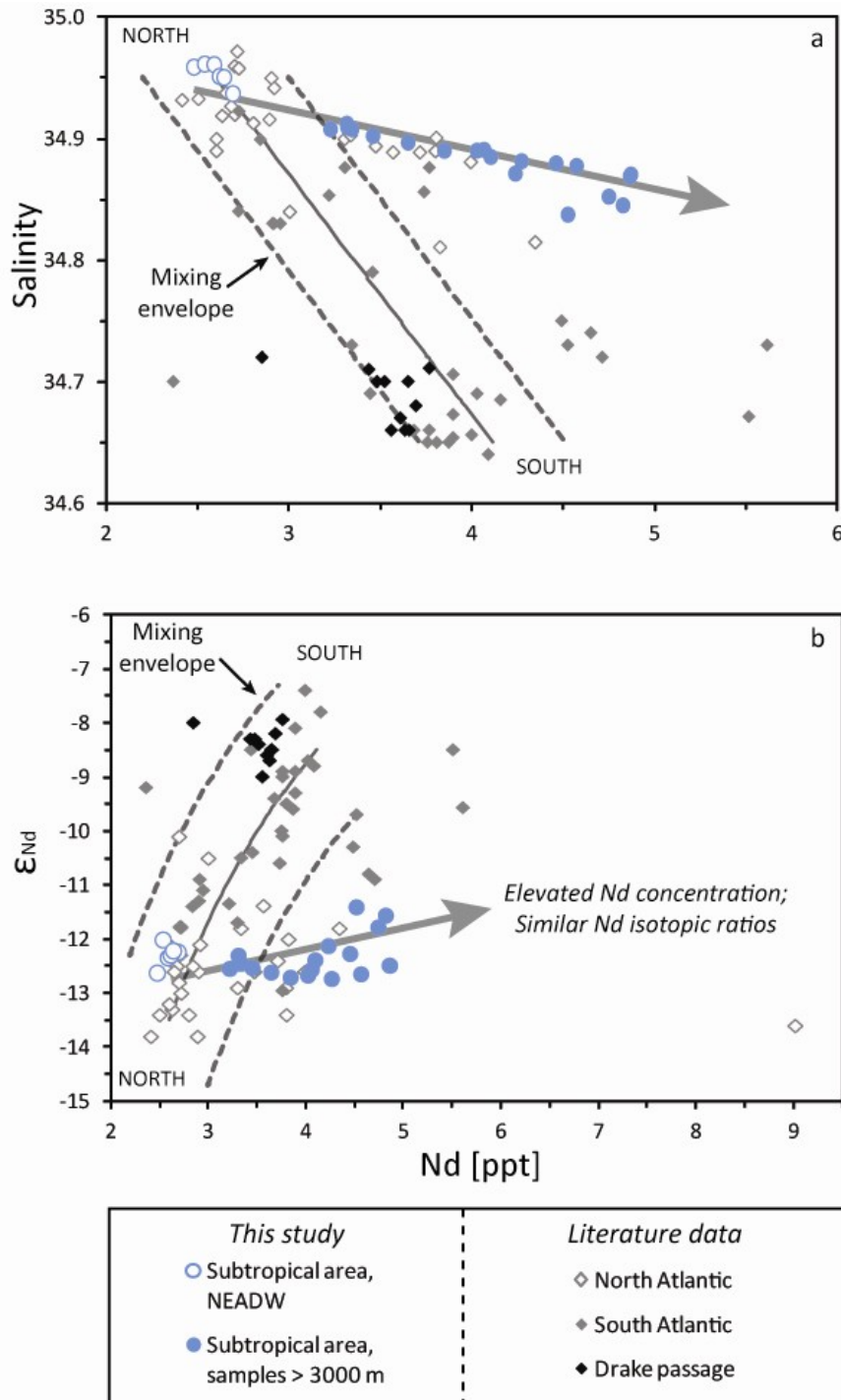
Figure 5.16: (a) Salinity and (b) Nd isotopic composition versus Nd concentration for samples collected at depth > 2500 m from the Atlantic Oceans. The grey lines show the mixing envelope between a northern end-member ([Nd] ≈ 2.6 ppt, S ≈ 34.95 and ε_{Nd} ≈ -13.5) and a southern end-member ([Nd] ≈ 4.1 ppt, S ≈ 34.65 and ε_{Nd} ≈ -8.5). Diamonds are data from the literature, and blue dots are data from this study. All samples are from water depths > 2500 m. The arrows show that at certain locations the Nd concentration is high for similar salinity (a) or Nd isotope (b) values. Figure adapted from Goldstein and Hemming (2003). Neodymium data sources: (Piepgras and Wasserburg 1983; Piepgras and Wasserburg 1987; Spivack and Wasserburg 1988; Jeandel 1993; Lacan and Jeandel 2005b; Rickli et al. 2009; Pahnke et al. 2012; Stichel et al. 2012; Garcia-Solsona et al. 2014). Please note that data from the Mediterranean Sea, the Nordic Seas and Baffin Bays were not included. Please note as well that the data of the present study represented in this diagram are all from the subtropics (and not from the subpolar area, as in Fig. 4.6 from Chapter 4), and the filled circles represent the results from the "bottom layer" (see paragraph 5.4.4.3.2.2) whereas the empty circles are the samples from NEADW (since this water mass is encountered below 2500 m depth, see text).

Several mechanisms could be responsible for the observed increase in Nd concentrations in the lower part of the water column and these are discussed below.

(a) Redissolution from bottom sediments

Redissolution of Nd from bottom sediments, followed by diffusion of Nd from the bottom into the overlying waters might be an explanation for the observed concentration trends. However, as outlined in section 5.4.3.2, the beam attenuation coefficient, a measure of turbidity, is only high for the bottom layer at one of the six stations (station 15). Even if sediment resuspension in an extended nepheloid layer is responsible for the slightly higher Nd concentrations measured at station 15, it seems unlikely that it could explain the increase encountered at other stations, as a significant source of Nd is needed.

(b) Boundary exchanges

Continuous exchange at the ocean-solid earth interface might be another explanation. Indeed, it has been shown that boundary exchange plays a prominent role for seawater Nd isotopes in the subpolar North Atlantic (this study; Lacan and Jeandel, 2005a,b). However, continuous release of Nd from the seafloor would need to be coupled with upward diffusion of the signal through the water column and, as outlined above, this would produce a concentration pattern, which differs from the observations of the present study.

Another way of thinking about the effect of boundary exchange on seawater Nd concentrations and isotopes is to consider potential boundary exchange in the source area of a water mass. The source areas can be identified by following the isopycnals in the region of interest back to the area where they crop out. In our specific case, this would involve a mix of southern and northern sources (Fig. 5.15a), and if boundary exchange does influence the Nd characteristics of the water masses in their formation region, it seems not likely that boundary exchanges take place in the Sargasso Sea itself between the water masses measured here and the margin in the vicinity. Indeed, the present Nd concentration profiles do not indicate that boundary exchange processes act as a direct Nd source (or sink) here, since the dissolved Nd concentration at stations 25 to 30 are not higher (or lower) compared to what is measured at stations 15 to 21 (Fig. 5.1a and 5.13a), even though the former stations are closer to a continental margin than the latter.
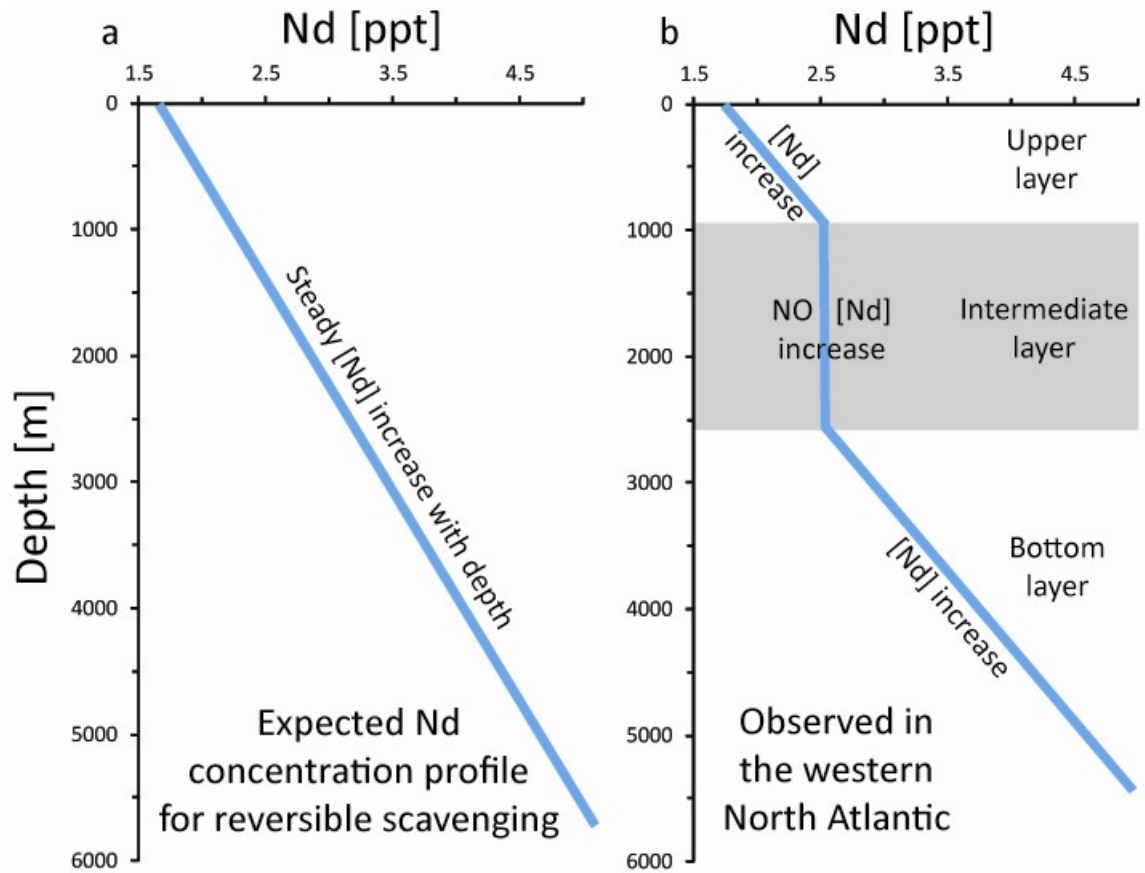
(c) Reversible scavenging

In our opinion, the higher Nd concentrations in the deeper layers of the western subtropical North Atlantic Ocean are most likely caused by the remineralisation of sinking particles. A modelling study by Siddall et al. (2008) suggested that remineralisation at depth can increase Nd concentrations without changing the isotopic compositions in areas of strong lateral advection, such as the Atlantic Ocean. In fact, these authors identified that Nd concentrations in the global ocean can only be successfully modelled if reversible scavenging is included. The process of reversible scavenging describes adsorption and desorption of elements on particle surfaces, or in other words, exchange between the dissolved and particulate elemental pools in the ocean. Initially formulated by (Bacon and Anderson 1982), the process was considered in the following to play a prominent role in the global Nd cycle (e.g., Bertram and Elderfield 1993; Nozaki and Alibo 2003; Tachikawa et al. 2003) but was only recently included in more elaborate modelling studies to simulate the biogeochemical cycle of Nd (e.g., Siddall et al. 2008; Arsouze et al. 2009; Oka et al. 2009; Rempfer et al. 2011). While it can be assumed that isotopic fractionation during adsorption / desorption can be neglected, it is less clear whether there is preferential scavenging of Nd onto specific particle types (see Siddall et al. (2008) for a discussion) and what role different particle sizes may play (Arsouze et al. 2009). In the end, it will be important to determine the compositions of relevant particles and their Nd concentration and ε_{Nd} value in order to better characterize and quantify the process. In the absence of such data, further efforts to identify the provenance of the Nd released at depth remain speculative.

Middle layer (1000 – 2500 m)

The middle layer (Fig. 5.7c) is characterized by relatively constant Nd concentrations with increasing depth and it can be assigned to the following water masses: modified-AAIW, ULSW, LSW and NEADW, or rather, since these samples are from the subtropical North Atlantic Ocean, upper-NADW and middle-NADW (see Chapter 4). It was shown previously that reversible scavenging is most likely responsible for the increasing Nd concentrations in the upper and bottom layers of the study area (Figs. 5.7c and 5.13a). This implies that reversible scavenging probably occurs throughout the water column and in an ideal scenario this would result in steadily increasing Nd concentrations with water depth. Such behaviour has been documented in other ocean basins (e.g., Nozaki and Alibo 2003; Stichel et al. 2012) and is shown in schematic form in Figure 5.17a. The middle layer with constant Nd

concentrations between ~1000 and ~2500-3000 m is hence a unique characteristic of the western North Atlantic Ocean.

Figure 5.17: Schematic Nd concentration depth profiles as (a) expected for steady reversible scavenging throughout the water column, and (b) observed in the subtropical North Atlantic.

A major difference between the western North Atlantic and other locations where a continuous increase of [Nd] with depth is observed (i.e., Pacific Ocean, Drake Passage), is the strong lateral advection of deep waters. This suggests that high water mass velocities may play a key role in generating the distinctive Nd concentration pattern (Fig. 5.17b) of the western North Atlantic. This interpretation is supported by the data of (Andrie et al. 1997), who performed direct velocity measurements in the Deep Western Boundary Current (DWBC) just to the south of the southernmost profile of the present study, at about 7˚N between the coast and 35˚W. These authors show that the upper core of the DWBC, between 1000 m and 3000 m depth, has a maximum velocity of more than 40 cm/s at a depth of about 1500 m. The lower core was found to be centred at 3500 m, with velocities lower than

20 cm/s. Furthermore, zonally integrated stream functions calculated from the WOCE hydrographic data suggest that the highest mass transport at about 20˚N in the Atlantic Ocean occurs between 1000 and 2000 m depth (Ganachaud 2003). We therefore propose that the release of Nd from particles witnessed in the upper and lower part of the water column is 'overruled' by fast lateral advection in the middle layer. In other words, lateral rather than vertical processes dominate the cycling and behaviour of Nd at water column depths of 1000 to 3000 m in the western North Atlantic.

5.5. Conclusions

The objectives of this study were to better characterise and constrain the sources, sinks and geochemical cycling of dissolved Nd in the modern ocean. To address this goal, we determined and investigated the Nd concentrations (and isotopic compositions) of 12 depth profiles in the north to equatorial western Atlantic Ocean.

Surface Ocean: Riverine inputs appear to dominate the Nd fingerprint of surface waters in the Irminger basin (stations 2 to 6) and in the southern subtropical gyre (stations 25 to 30). In the northern subtropical gyre (stations 15 to 21), the Nd isotopic compositions and concentrations are consistent with values obtained for the subtropical gyre, ultimately being influenced by dust input from the North Africa. In the southern Labrador Sea and around the Grand Bank (stations 9 to 13), mixing between the strong Labrador Current and the Gulf Stream, carrying quite distinct Nd isotopic compositions, can account for the observed signatures. None of the surface waters investigated, including a sample collected from under the ash plume of the large 2010 Iceland eruption, provides evidence for significant addition of Nd from volcanic ash to the surface ocean.

Bottom water layer: Sediment remobilisation was encountered in the subpolar North Atlantic of the present study, and the process of boundary exchange, acting as both a Nd source and sink, is required to account for the Nd concentrations determined for samples from the bottom water layer of this region. The impact of boundary exchanges on the Nd isotopic signature is relatively small in the vicinity of the Grand Bank (stations 9 to 13), but more pronounced in the Irminger Sea (stations 2 to 6). In the subtropical western Atlantic Ocean, most stations show no direct evidence for Nd inputs from or associated with bottom sediments. Only station 15 had a pronounced nepheloid layer, and this is hence the only station where sediment resuspension may act as a Nd source.

Vertical cycling of Nd: Different processes seem to govern the vertical cycling of Nd in the subpolar and subtropical western North Atlantic Ocean. In the subpolar North Atlantic Ocean, boundary exchanges with the proximal margin are required to account for the observed Nd isotope and concentration profiles. In contrast, the two Nd parameters are clearly decoupled in the subtropical region. Here, Nd concentrations generally increase with depth due to reversible scavenging but constant Nd contents are observed in the middle of the water column (1000 – 3000 m) because strong lateral advection dominates the cycling of Nd. Regardless of location and water depth, Nd isotopes were found to be a robust tracer for the main water masses encountered in the North Atlantic (see Chapter 4).

The present study fills an important gap in the global marine Nd database, in particular because Nd isotope and concentration data were especially scarce for the subtropical western North Atlantic Ocean. The new high quality results of this study, furthermore, provide new insights into the 'Nd paradox'. Further constraints to better understand the origin of the paradox will be available once the budget for the vertical cycling of Nd in the North Atlantic is fully characterised by analyses of marine particles that were collected on the same cruise as the present water samples.

Acknowledgements

Chapter 6

CONCLUSIONS

6.1. Major findings

The present thesis underlines the important role that isotope analyses can play in deciphering marine biogeochemical cycles of trace elements. Our new high quality results enabled us to achieve the overall aim of this study, which was to better constrain the geochemical cycles of the trace elements cadmium and neodymium and their isotopes in the marine environment (see Chapter 1). We will outline below in more details how the several specific objectives of this thesis have been fulfilled.

Cadmium isotope measurements were performed on samples from the Siberian Arctic shelf seas (Chapter 2) and show that Siberian rivers have an isotopic composition that is similar to, or only slightly heavier than, average continental crust, thus suggesting that weathering processes generate no significant or only relatively minor Cd isotope fractionations. Besides, our Cd concentration and isotope results show that Cd is released from suspended riverine particles during mixing with seawater, and that this released Cd is identical to or intermediate between the composition of continental crust and marine deep waters. Finally, our results concerning the boreal Kalix river, which features higher Cd concentration and light Cd isotopic composition compared to the Arctic rivers, indicates that the Cd isotope composition of rivers may display significant regional variability, such that more river samples from distinct areas will need to be analysed before the global average Cd isotope composition of the riverine flux to the ocean can be determined with certainty. Overall, our new Cd isotope results provide important constraints, which are not available from concentration data alone, on the cycling of Cd in shelf and riverine environments.

In Chapter 3 we introduced the time and labour effective method developed at the MAGIC laboratories to isolate and analyse the Nd isotopic composition and Nd concentrations of low abundance seawater and/or rock sample. Results illustrate that reliable results are obtained on GEOTRACES intercalibration samples and that storage of seawater in pre-cleaned containers for up to five years does not affect the concentration nor the isotopic composition of Nd. Finally, our methodology allows for precise and accurate results on 5 L seawater samples, enabling an increase in spatial sample resolution on future GEOTRACES cruises.

Our extensive Nd study (Chapters 4 and 5) on 137 samples from the Dutch GEOTRACES cruise GA02 demonstrates at unprecedented resolution that Nd isotopes do behave conservatively in the Northwest Atlantic deep waters away from ocean margins, providing more confidence in applications of Nd isotopes as a palaeo water mass tracer. The data furthermore highlight different behaviour of Nd in regions close to the formation area of deep water masses compared to export areas, thus suggesting that different processes govern its geochemical cycle. Indeed, in the subpolar North Atlantic, boundary exchange processes between seawater and the nearby margin are required to account for the observed Nd signature. In the subtropical western North Atlantic however, the concentration and isotope profiles are decoupled, and Nd concentrations shows an increase with depth, whereas the Nd isotopes feature a quasi conservative behaviour, tracing water masses encountered in this area. We showed that this increase in Nd concentrations with depth is most likely explained by reversible scavenging, which is outcompeted in the middle of the water column by strong lateral advection. Riverine inputs play an important role as Nd source to the surface ocean in the Irminger Sea and in the south of the subtropical gyre, while dissolution of volcanic ash seems to not leave a clear Nd imprint on the surface ocean as demonstrated on a small study of the recent Icelandic volcanic eruption. These observations about Nd inputs in the North Atlantic Ocean highlight the importance of combining isotope and concentration measurements, as the concentration data alone would not have been sufficient to determine the Nd source in this region. Comparison with previously published Nd profiles makes us suggest that in areas where strong currents lead to sediment remobilisation filtration of seawater samples is absolutely essential, and lack thereof may result in differences in Nd concentration and isotopic composition. Finally, our new data illustrate that North Atlantic Deep Water (NADW) can be separated in upper- and lower-NADW, with distinct Nd isotopic compositions, and that the signature of lower NADW tends to be significantly more radiogenic than the accepted value of $\varepsilon_{Nd} = -13.5$, which should be taken into account for future applications.

Overall, our studies showed that isotopes provide information on the geochemical cycles of Cd and Nd that could not be derived by concentration data alone. Furthermore, it underlines the importance of multi-element and parameter studies, thus stressing the usefulness of multi-disciplinary projects such as the GEOTRACES programme.

6.2. Concluding remarks

Concerning the Cd part of this study, an interesting follow up would be to measure the Cd concentration and isotopic composition of samples coming from different riverine system in the world, including polluted areas and different geological settings. By determining the Cd behaviour in such rivers and mixing areas, the overall Cd biogeochemical cycle as well as Cd isotope composition of the riverine flux to the ocean would be better constrained. Furthermore, the hypothesis that weathering processes generate no significant or only relatively minor Cd isotope fractionations could be confirmed (or denied).

Concerning the Nd geochemical cycle in the marine environment, it will be very interesting to see the results on suspended particulates corresponding to the depth profiles analysed in the present study, a step that is planned for the near future in the MAGIC group. Indeed, Nd isotope and concentration data are very sparse for marine particulate phases, and I think that such analyses are key for substantially improving our understanding of the vertical cycling of Nd in the water column. In order to better constrain Nd sources and sinks, the collection of sediment samples and marine aerosols would complement seawater analysis very well. Furthermore, isotopes and concentrations analyses of dissolved and particulate Nd from small river systems would be very useful to better assess the contribution of these inputs to the Nd cycle. Together with the above mentioned, modelling the present dataset may help us to further understand the Nd paradox. Apart from that, I would be interested in analysing more depth profiles coming from the whole Labrador Sea, since Nd data from this area are still scare. Other specific geographic areas of interest are the Denmark Strait and downstream areas of DSOW, as well as in the Iceland-Scotland gap and downstream areas of ISOW. Another, more methodological point of interest would be to carry out more systematic tests to compare filtered and unfiltered samples. Finally, time-series for Nd isotopes and concentration in key areas (e.g., Labrador Sea, BATS, overflows) would allow to develop a more precise idea concerning the evolution of Nd characteristics of seawater through time.

Nevertheless, I think that the present work brings an important contribution to the scientific community. Indeed, the presentation of the Nd data at a recent conference (AGU Ocean Sciences, Hawaii, 2014) spurred broad interest, and many researchers came to discuss my results with me. Furthermore, being able to exchange ideas with scientists studying other trace metals and their isotopes proved once more to be vital for interpreting results due to the complementary information provided. Indeed future comparison of my new data set with the many other trace metals and isotopes analysed on the Pelagia cruises will most certainly open

up new avenues of thought. Luckily, the GEOTRACES program has just reached its first milestone with the release of an online data product to the international community from its initial four years of expeditions. With about twice this time and many more expeditions to come, the programme will enable scientists to compare their results obtained for different elements more readily, and modellers to access the data more freely, providing a unique opportunity to achieve a step change in our understanding of the cycling of trace elements and their isotopes in the oceans.

BIBLIOGRAPHY

Abouchami, W., S. J. G. Galer, H. J. W. de Baar, A. C. Alderkamp, R. Middag, P. Laan, H. Feldmann and M. O. Andreae, 2011. Modulation of the Southern Ocean cadmium isotope signature by ocean circulation and primary productivity. Earth and Planetary Science Letters 305, 83-91.

Abouchami, W., S. J. G. Galer, H. J. W. de Baar, R. Middag, D. Vance, Y. Zhao, M. Klunder, K. Mezger, H. Feldmann and M. O. Andreae, 2014. Biogeochemical cycling of cadmium isotopes in the Southern Ocean along the Zero Meridian. Geochimica Et Cosmochimica Acta 127, 348-367.

Abouchami, W., S. J. G. Galer, T. H. Horner, M. Rekämper, F. Wombacher, Z. Xue, M. Lambelet, M. Gault-Ringold, C. Stirling, M. Schönbächler, A. E. Shiel, D. Weis and P. F. Holdship, 2012. A common reference material for cadmium isotope studies - NIST SRM 3108 Cd. Geostand. Geoanal. Res. In press.

Abouchami, W., S. J. G. Galer, T. J. Horner, M. Rehkämper, F. Wombacher, Z. Xue, M. Lambelet, M. Gault-Ringold, C. H. Stirling, M. Schönbächler, A. E. Shiel, D. Weis and P. F. Holdship, 2013. A Common Reference Material for Cadmium Isotope Studies – NIST SRM 3108. Geostandards and Geoanalytical Research 37, 5-17.

Achterberg, E. P., C. M. Moore, S. A. Henson, S. Steigenberger, A. Stohl, S. Eckhardt, L. C. Avendano, M. Cassidy, D. Hembury, J. K. Klar, M. I. Lucas, A. I. Macey, C. M. Marsay and T. J. Ryan-Keogh, 2013. Natural iron fertilization by the Eyjafjallajökull volcanic eruption. Geophysical Research Letters 40, 921-926.

Akagi, T., 2013. Rare earth element (REE)–silicic acid complexes in seawater to explain the incorporation of REEs in opal and the "leftover" REEs in surface water: New interpretation of dissolved REE distribution profiles. Geochimica Et Cosmochimica Acta 113, 174-192.

Alibo, D. S. and Y. Nozaki, 1999. Rare earth elements in seawater: particle association, shale-normalization, and Ce oxidation. Geochimica Et Cosmochimica Acta 63, 363-372.

Alley, R. B., J. Marotzke, W. D. Nordhaus, J. T. Overpeck, D. M. Peteet, R. A. Pielke, R. T. Pierrehumbert, P. B. Rhines, T. F. Stocker, L. D. Talley and J. M. Wallace, 2003. Abrupt Climate Change. Science 299, 2005-2010.

Amelin, Y. V., E. Y. Ritsk and L. A. Neymark, 1997. Effects of interaction between ultramafic tectonite and mafic magma on Nd-Pb-Sr isotopic systems in the Neoproterozoic Chaya Massif, Baikal-Muya ophiolite belt. Earth and Planetary Science Letters 148, 299-316.

Andersson, P. S., R. Dahlqvist, J. Ingri and O. Gustafsson, 2001. The isotopic composition of Nd in a boreal river: A reflection of selective weathering and colloidal transport. Geochim. Cosmochim. Acta 65, 521-527.

Andreasen, R. and M. Sharma, 2006. Solar nebula heterogeneity in p-process samarium and neodymium isotopes. Science 314, 806-809.

Andrie, C., Y. Gouriou, B. Bourles, C. Oudot and J. F. Ternon, 1997. Deep Circulation in the Western Tropical Atlantic Inferred from CFCs and L-ADCP Measurements during ETAMBOT cruises. International WOCE Newsletter. Southampton, WOCE International Project Office. 28.

Arsouze, T., J. C. Dutay, F. Lacan and C. Jeandel, 2009. Reconstructing the Nd oceanic cycle using a coupled dynamical - biogeochemical model. Biogeosciences 6, 2829-2846.

Bacon, M. P. and R. F. Anderson, 1982. Distribution of thorium isotopes between dissolved and particulate forms in the deep sea. Journal of Geophysical Research: Oceans 87, 2045-2056.

Bertram, C. J. and H. Elderfield, 1993. The geochemical balance of the rare earth elements and neodymium isotopes in the oceans. Geochimica Et Cosmochimica Acta 57, 1957-1986.

BIO, 1984. BIO Review '84. M. P. Latremouille, Bedford Institute of Oceanography.

Böning, P., H. J. Brumsack, M. E. Böttcher, B. Schnetger, C. Kriete, J. Kallmeyer and S. L. Borchers, 2004. Geochemistry of Peruvian near-surface sediments. Geochim. Cosmochim. Acta 68, 4429-4451.

Bostock, H. C., P. J. Sutton, M. J. M. Williams and B. N. Opdyke, 2013. Reviewing the circulation and mixing of Antarctic Intermediate Water in the South Pacific using evidence from geochemical tracers and Argo float trajectories. Deep Sea Research Part I: Oceanographic Research Papers 73, 84-98.

Boyle, E. A., 1988. Cadmium: chemical tracer of deepwater paleoceanography. Paleoceanogr. 3, 471-489.

Boyle, E. A., S. S. Huested and B. Grant, 1982. The Chemical Mass Balance of the Amazon Plume .2. Copper, Nickel, and Cadmium. Deep Sea Res. 29, 1355-1364.

Boyle, E. A., S. John, W. Abouchami, J. Adkins, Y. Echegoyen-Sanz, K. Fornace, C. Gallon, B. S. Galer, M. Gault-Ringold, F. Lacan, A. Radic, M. Rehkämper, O. Rouxel, Y. Sohrin and C. Stirling, 2012. GEOTRACES IC1 (BATS) Contamination-prone trace element isotopes Cd, Fe, Pb, Zn, Cu and Mo intercalibration. Limnol. Oceanogr. Methods In press.

Boyle, E. A., F. Sclater and J. M. Edmond, 1976. Marine geochemistry of cadmium. Nature 263, 42-44.

Broecker, W. S., 1991. The Great Ocean Conveyor. Oceanography 4, 11.

Broecker, W. S., H. Craig, D. Spencer and al., 1974. GEOSECS - Geochemical Ocean Sections - A U.S. program for the International Decade of Ocean Exploration.

Brown, E., A. Colling, D. Park, J. Phillips, D. Rothery and J. Wright, 2001. Chapter 6 - Global fluxes and the deep circulation. Ocean Circulation (Second Edition). E. Brown, A. Colling, D. Park et al. Oxford, Butterworth-Heinemann: 190-255.

Bruland, K. W., 1980. Oceanographic distributions of cadmium, zinc, nickel, and copper in the North Pacific. Earth Planet. Sci. Lett. 47, 176-198.

Charlier, B. L. A., C. Ginibre, D. Morgan, G. M. Nowell, D. G. Pearson, J. P. Davidson and C. J. Ottley, 2006. Methods for the microsampling and high-precision analysis of strontium and rubidium isotopes at single crystal scale for petrological and geochronological applications. Chemical Geology 232, 114-133.

Chavagnac, V., T. F. Nägler and J. D. Kramers, 1999. Migmatization by metamorphic segregation at subsolidus conditions: implications for Nd–Pb isotope exchange. Lithos 46, 275-298.

Chester, R., 2000. Marine Geochemistry.

Chu, Z. Y., F. K. Chen, Y. H. Yang and J. H. Guo, 2009. Precise determination of Sm, Nd concentrations and Nd isotopic compositions at the nanogram level in geological samples by thermal ionization mass spectrometry. Journal of Analytical Atomic Spectrometry 24, 1534-1544.

Comans, R. N. J. and C. P. J. Vandijk, 1988. Role of complexation processes in cadmium mobilization during estuarine mixing. Nature 336, 151-154.

Copard, K., C. Colin, N. Frank, C. Jeandel, J. C. Montero-Serrano, G. Reverdin and B. Ferron, 2011. Nd isotopic composition of water masses and dilution of the Mediterranean outflow along the southwest European margin. Geochemistry Geophysics Geosystems 12.

Crocket, K. C., M. Lambelet, T. van de Flierdt, M. Rehkämper and L. F. Robinson, 2014. Measurement of fossil deep-sea coral Nd isotopic compositions and concentrations by TIMS as NdO+, with evaluation of cleaning protocols. Chemical Geology 374–375, 128-140.

Cullen, J. T., T. W. Lane, F. M. M. Morel and R. M. Sherrell, 1999. Modulation of cadmium uptake in phytoplankton by seawater CO_2 concentration. Nature 402, 165-167.

Curry, R., B. Dickson and I. Yashayaev, 2003. A change in the freshwater balance of the Atlantic Ocean over the past four decades. Nature 426, 826-829.

Curry, R. G., M. S. McCartney and T. M. Joyce, 1998. Oceanic transport of subpolar climate signals to mid-depth subtropical waters. Nature 391, 575-577.

Dahlqvist, R., K. Andersson, J. Ingri, T. Larsson, B. Stolpe and D. Turner, 2007. Temporal variations of colloidal carrier phases and associated trace elements in a boreal river. Geochim. Cosmochim. Acta 71, 5339-5354.

Dai, M. H. and J. M. Martin, 1995. First data on trace metal level and behavior in 2 major arctic river-estuarine systems (Ob and Yenisey) and in the adjacent Kara Sea, Russia. Earth Planet. Sci. Lett. 131, 127-141.

Davis, X. J., F. Straneo, Y. O. Kwon, K. A. Kelly and J. M. Toole, 2013. Evolution and formation of North Atlantic Eighteen Degree Water in the Sargasso Sea from moored data. Deep-Sea Research Part Ii-Topical Studies in Oceanography 91, 11-24.

de Baar, H. J. W., M. P. Bacon, P. G. Brewer and K. W. Bruland, 1985. Rare-Earth Elements in the Pacific and Atlantic Oceans. Geochimica Et Cosmochimica Acta 49, 1943-1959.

de Baar, H. J. W., P. M. Saager, R. F. Nolting and J. van der Meer, 1994. Cadmium versus phosphate in the world ocean. Mar. Chem. 46, 261-281.

Dickson, B., I. Yashayaev, J. Meincke, B. Turrell, S. Dye and J. Holfort, 2002. Rapid freshening of the deep North Atlantic Ocean over the past four decades. Nature 416, 832-837.

Dickson, R. R. and J. Brown, 1994. The Production of North-Atlantic Deep-Water - Sources, Rates, and Pathways. Journal of Geophysical Research-Oceans 99, 12319-12341.

Draxler, R. R. and G. D. Rolph, 1997. Description of the HYSPLIT 4 modeling system. Technical Memorandum ERL ARL-224, NOAA Air Resources Laboratory, Silver Spring, MD. .

Duce, R. A., P. S. Liss, J. T. Merrill and e. al., 1991. The atmospheric input of trace species to the world ocean. Glob. Biogeochem. Cycles 5, 193-259.

Duinker, J. C. and R. F. Nolting, 1977. Dissolved and particulate trace metals in the Rhine estuary and the Southern Bight. Mar. Pollut. Bull. 8.

Elbaz-Poulichet, F., J. M. Garnier, D. M. Guan, J. M. Martin and A. J. Thomas, 1996. The conservative behaviour of trace metals (Cd, Cu, Ni and Pb) and As in the surface plume of stratified estuaries: Example of the Rhone River (France). Estuar. Coast. Shelf Sci. 42, 289-310.

Elbaz-Poulichet, F., J. M. Martin, W. W. Huang and J. X. Zhu, 1987. Dissolved Cd behavior in some selected french and chinese estuaries - Consequences on Cd supply to the ocean. Mar. Chem. 22, 125-136.

Elderfield, H., 1988. The Oceanic Chemistry of the Rare-Earth Elements. Philosophical Transactions of the Royal Society a-Mathematical Physical and Engineering Sciences 325, 105-126.

Elderfield, H. and M. J. Greaves, 1982. The Rare-Earth Elements in Sea-Water. Nature 296, 214-219.

England, M. H., 1992. On the Formation of Antarctic Intermediate and Bottom Water in Ocean General Circulation Models. Journal of Physical Oceanography 22, 918-926.

Fogelqvist, E., J. Blindheim, T. Tanhua, S. Østerhus, E. Buch and F. Rey, 2003. Greenland–Scotland overflow studied by hydro-chemical multivariate analysis. Deep Sea Research Part I: Oceanographic Research Papers 50, 73-102.

Frank, M., 2002. Radiogenic isotopes: tracers of past ocean circulation and erosional input. Reviews of Geophysics 40, 1-1-1-38.

Ganachaud, A., 2003. Large-scale mass transports, water mass formation, and diffusivities estimated from World Ocean Circulation Experiment (WOCE) hydrographic data. Journal of Geophysical Research-Oceans 108.

Garcia-Solsona, E., C. Jeandel, M. Labatut, F. Lacan, D. Vance, V. Chavagnac and C. Pradoux, 2014. Rare earth elements and Nd isotopes tracing water mass mixing and particle-seawater interactions in the SE Atlantic. Geochimica Et Cosmochimica Acta 125, 351-372.

Gault-Ringold, M., 2011. The marine biogeochemistry of cadmium - Studies of cadmium isotopic variations in the Southern Ocean. Chemistry. Dunedin, Otago, New Zealand, University of Otago. Doctor of Philosophy**:** 125.

Gault-Ringold, M., T. Adu, C. Stirling, R. D. Frew and K. A. Hunter, 2012b. Anomalous biogeochemical behavior of cadmium in subantarctic surface waters: Mechanistic constraints from cadmium isotopes. Earth Planet. Sci. Lett. 341-344, 10.

Gault-Ringold, M., T. Adu, C. H. Stirling, R. D. Frew and K. A. Hunter, 2012b. Anomalous biogeochemical behavior of cadmium in subantarctic surface waters: Mechanistic constraints from cadmium isotopes. Earth and Planetary Science Letters 341–344, 94-103.

GEOTRACES Science Plan, 2006. S.C.O.R.(*). Baltimore**:** 79 pp.

Godfrey, L. V., B. Zimmermann, D. C. Lee, R. L. King, J. D. Vervoort, R. M. Sherrell and A. N. Halliday, 2009. Hafnium and neodymium isotope variations in NE Atlantic seawater. Geochemistry Geophysics Geosystems 10.

Goldstein, S. J. and S. B. Jacobsen, 1987. The Nd and Sr Isotopic Systematics of River-Water Dissolved Material - Implications for the Sources of Nd and Sr in Seawater. Chemical Geology 66, 245-272.

Goldstein, S. J. and S. B. Jacobsen, 1988. Nd and Sr Isotopic Systematics of River Water Suspended Material - Implications for Crustal Evolution. Earth and Planetary Science Letters 87, 249-265.

Goldstein, S. L., N. T. Arndt and R. F. Stallard, 1997. The history of a continent from U☐Pb ages of zircons from Orinoco River sand and Sm☐Nd isotopes in Orinoco basin river sediments. Chemical Geology 139, 271-286.

Goldstein, S. L. and S. Hemming, 2003. Long lived isotopic tracers in oceanography, paleoceanography, and ice sheet dynamics. Treatise on Geochemistry. H. Elderfield. New York, Elsevier: 453-489.

Griselin, M., J. C. van Belle, C. Pomiès, P. Z. Vroon, M. C. van Soest and G. R. Davies, 2001. An improved chromatographic separation technique of Nd with application to NdO+ isotope analysis. Chemical Geology 172, 347-359.

Grousset, F. E., P. E. Biscaye, A. Zindler, J. Prospero and R. Chester, 1988. Neodymium Isotopes as Tracers in Marine-Sediments and Aerosols - North-Atlantic. Earth and Planetary Science Letters 87, 367-378.

Guay, C. K. H., A. V. Zhulidov, R. D. Robarts, D. A. Zhulidov, T. Y. Gurtovaya, R. M. Holmes and J. V. Headley, 2010. Measurements of Cd, Cu, Pb and Zn in the lower reaches of major Eurasian arctic rivers using trace metal clean techniques. Environ. Pollut. 158, 624-630.

Guieu, C., W. W. Huang, J. M. Martin and Y. Y. Yong, 1996. Outflow of trace metals into the Laptev Sea by the Lena River. Mar. Chem. 53, 255-267.

Hanawa, K. and L. D. Talley, 2001. Mode Waters. Ocean circulation and climate. I. f. M. Gerold Siedler, Universitat Kiel, Kiel, Germany, and Instituto Canario de Ciencias Marinas, Telde, Spain, A. C. a. C. M. R. John Church, Hobart, Australia, S. O. C. John Gould, Southampton, U.K. and S. Griffies, Academic Press: 373-386.

Hartin, C. A., R. A. Fine, B. M. Sloyan, L. D. Talley, T. K. Chereskin and J. Happell, 2011. Formation rates of Subantarctic mode water and Antarctic intermediate water within the South Pacific. Deep Sea Research Part I: Oceanographic Research Papers 58, 524-534.

Harvey, J. and E. F. Baxter, 2009. An improved method for TIMS high precision neodymium isotope analysis of very small aliquots (1–10 ng). Chemical Geology 258, 251-257.

Hatje, V., T. E. Payne, D. M. Hill, G. McOrist, G. F. Birch and R. Szymczak, 2003. Kinetics of trace element uptake and release by particles in estuarine waters: effects of pH, salinity, and particle loading. Environ. Internatl. 29, 619-629.

Henderson, G. M., 2002. New oceanic proxies for paleoclimate. Earth and Planetary Science Letters 203, 1-13.

Horner, T. J., M. Schönbächler, M. Rehkämper, S. G. Nielsen, H. Williams, A. N. Halliday, Z. Xue and J. R. Hein, 2010. Ferromanganese crusts as archives of deep water Cd isotope compositions. Geochem. Geophys. Geosyst. 11.

Huang, K.-F., D. W. Oppo and W. B. Curry, 2014. Decreased influence of Antarctic intermediate water in the tropical Atlantic during North Atlantic cold events. Earth and Planetary Science Letters 389, 200-208.

Huh, Y., G. Panteleyev, D. Babich, A. Zaitsev and J. M. Edmond, 1998. The fluvial geochemistry of the rivers of eastern Siberia: II. Tributaries of the Lena, Omoloy, Yana, Indigirka, Kolyma, and Anadyr draining the collisional/accretionary zone of the Verkhoyansk and Cherskiy ranges. Geochim. Cosmochim. Acta 62, 2053-2075.

Huynhngoc, L., N. E. Whitehead and B. Oregioni, 1988. Cadmium in the Rhone River. Water Res. 22, 571-576.

Ingri, J., 1996. Kalixälvens hydrogeokemi. Länsstyrelsens i Norbotten. Luleå, Luleå University of Technology.

Ingri, J., P. Torssander, P. S. Andersson, C. M. Morth and M. Kusakabe, 1997. Hydrogeochemistry of sulfur isotopes in the Kalix River catchment, northern Sweden. Appl. Geochem. 12, 483-496.

Ingri, J., A. Widerlund and M. Land, 2005. Geochemistry of major elements in a pristine boreal river system; Hydrological compartments and flow paths. Aquat. Geochem. 11, 57-88.

Innocent, C., N. Fagel, R. K. Stevenson and C. Hillaire-Marcel, 1997. Sm☐Nd signature of modern and late Quaternary sediments from the northwest North Atlantic: Implications for deep current changes since the Last Glacial Maximum. Earth and Planetary Science Letters 146, 607-625.

Jacobsen, S. B. and G. J. Wasserburg, 1980. Sm-Nd Isotopic Evolution of Chondrites. Earth and Planetary Science Letters 50, 139-155.

Jarrard, D. R., K. A. Dadey and W. H. Busch, 1989. Velocity and density of sediments of Eirik Ridge, Labrador Sea: control by porosity and mineralogy. Proceedings of the Ocean Drilling Program, Scientific Results. S. P. Srivastava, Arthur, M., Clement, B., et al. 105.

Jeandel, C., 1993. Concentration and Isotopic Composition of Nd in the South-Atlantic Ocean. Earth and Planetary Science Letters 117, 581-591.

Jeandel, C., J. K. Bishop and A. Zindler, 1995. Exchange of neodymium and its isotopes between seawater and small and large particles in the Sargasso Sea. Geochimica Et Cosmochimica Acta 59, 535-547.

Jeandel, C., H. Delattre, M. Grenier, C. Pradoux and F. Lacan, 2013. Rare earth element concentrations and Nd isotopes in the Southeast Pacific Ocean. Geochemistry Geophysics Geosystems 14, 328-341.

Jeandel, C., D. Thouron and M. Fieux, 1998. Concentrations and isotopic compositions of neodymium in the eastern Indian Ocean and Indonesian straits. Geochimica Et Cosmochimica Acta 62, 2597-2607.

Johannesson, K. H. and D. J. Burdige, 2007. Balancing the global oceanic neodymium budget: Evaluating the role of groundwater. Earth and Planetary Science Letters 253, 129-142.

Kieke, D., B. Klein, L. Stramma, M. Rhein and K. P. Koltermann, 2009. Variability and propagation of Labrador Sea Water in the southern subpolar North Atlantic. Deep-Sea Research Part I-Oceanographic Research Papers 56, 1656-1674.

Kieke, D., M. Rhein, L. Stramma, W. M. Smethie, D. A. LeBel and W. Zenk, 2006. Changes in the CFC inventories and formation rates of Upper Labrador Sea Water, 1997-2001. Journal of Physical Oceanography 36, 64-86.

Kruk, M. and K. Podbielska, 2005. Trace metal fluxes in a sphagnum peatland - humic lake system as a consequence of drainage. Water Air Soil Pollut. 168, 213-233.

Kumar, A., W. Abouchami, S. J. G. Galer, V. H. Garrison, E. Williams and M. O. Andreae, 2014. A radiogenic isotope tracer study of transatlantic dust transport from Africa to the Caribbean. Atmospheric Environment 82, 130-143.

Lacan, F., R. Francois, Y. Ji and R. M. Sherrell, 2006. Cadmium isotopic composition in the ocean. Geochimica Et Cosmochimica Acta 70, 5104-5118.

Lacan, F., R. Francois, Y. C. Ji and R. M. Sherrell, 2006. Cadmium isotopic composition in the ocean. Geochim. Cosmochim. Acta 70, 5104-5118.

Lacan, F. and C. Jeandel, 2004a. Denmark Strait water circulation traced by heterogeneity in neodymium isotopic compositions. Deep-Sea Research Part I-Oceanographic Research Papers 51, 71-82.

Lacan, F. and C. Jeandel, 2004b. Neodymium isotopic composition and rare earth element concentrations in the deep and intermediate Nordic Seas: Constraints on the Iceland Scotland Overflow Water signature. Geochemistry Geophysics Geosystems 5, -.

Lacan, F. and C. Jeandel, 2004c. Subpolar Mode Water formation traced by neodymium isotopic composition. Geophysical Research Letters 31, -.

Lacan, F. and C. Jeandel, 2005. Acquisition of the neodymium isotopic composition of the North Atlantic Deep Water. Geochemistry Geophysics Geosystems 6, -.

Lacan, F. and C. Jeandel, 2005a. Neodymium isotopes as a new tool for quantifying exchange fluxes at the continent-ocean interface. Earth and Planetary Science Letters 232, 245-257.

Lacan, F. and C. Jeandel, 2005b. Acquisition of the neodymium isotopic composition of the North Atlantic Deep Water. Geochemistry Geophysics Geosystems 6, -.

Lacan, F., K. Tachikawa and C. Jeandel, 2012. Neodymium isotopic composition of the oceans: A compilation of seawater data. Chemical Geology 300, 177-184.

Lane, T. W., M. A. Saito, G. N. George, I. J. Pickering, R. C. Prince and F. M. M. Morel, 2005. A cadmium enzyme from a marine diatom. Nature 435, 42-42.

Lavender, K. L., R. E. Davis and W. B. Owens, 2000. Mid-depth recirculation observed in the interior Labrador and Irminger seas by direct velocity measurements. Nature 407, 66-69.

Li, C.-F., F. Chen and X.-H. Li, 2007. Presice isotopic measurments of sub-nanogram Nd of standard reference material by thermal ioniozation mass spectrometry using the NdO^+ tehcnique. International Journal of Mass Spectrometry 266, 34-41.

Lozier, M. S., V. Roussenov, M. S. C. Reed and R. G. Williams, 2010. Opposing decadal changes for the North Atlantic meridional overturning circulation. Nature Geoscience 3, 728-734.

Mackey, D. J., E. C. V. Butler, P. D. Carpenter, H. W. Higgins, J. E. OSullivan and R. B. Plaschke, 1996. Trace elements and organic matter in a pristine environment: Bathurst Harbour, Southwestern Tasmania. Sci. Tot. Environ. 191, 137-151.

Mariotti, A., A. Landreau and B. Simon, 1988. N-15 isotope biogeochemistry and natural denitrification process in groundwater - Application to the chalk aquifer of northern France. Geochimica Et Cosmochimica Acta 52, 1869-1878.

Marshall, J. and K. Speer, 2012. Closure of the meridional overturning circulation through Southern Ocean upwelling. Nature Geosci 5, 171-180.

Martin, J. M., D. M. Guan, F. Elbaz-Poulichet, A. J. Thomas and V. V. Gordeev, 1993. Preliminary assessment of the distributions of some trace elements (As, Cd, Cu, Fe, Ni, Pb and Zn) in a pristine aquatic environment - the Lena River estuary (Russia). Mar. Chem. 43, 185-199.

McCartney, M. S. and L. D. Talley, 1982. The Subpolar Mode Water of the North Atlantic Ocean. Journal of Physical Oceanography 12, 1169-1188.

McManus, J. F., R. Francois, J. M. Gherardi, L. D. Keigwin and S. Brown-Leger, 2004. Collapse and rapid resumption of Atlantic meridional circulation linked to deglacial climate changes. Nature 428, 834-837.

Measures, C. I., G. M. Henderson, R. F. Anderson, J. Adkins, P. Andersson, E. A. Boyle, G. Cutter, H. de Baar, A. Eisenhauer, M. Frank, R. Francois, K. Orians, T. Gamo, C. German, W. Jenkins, J. Moffett, C. Jeandel, T. Jickells, S. Krishnaswami, D. Mackey, J. K. Moore, A. Oschlies, R. Pollard, M. R. D. van der Loeff, R. Schlitzer, M. Sharma, K. von Damm, J. Zhang, P. Masque and S. W. Grp, 2007. GEOTRACES –

An international study of the global marine biogeochemical cycles of trace elements and their isotopes. Chemie der Erde - Geochemistry 67, 85-131.

Measures, C. I., W. M. Landing, M. T. Brown and C. S. Buck, 2008. High-resolution Al and Fe data from the Atlantic Ocean CLIVAR-CO2 Repeat Hydrography A16N transect: Extensive linkages between atmospheric dust and upper ocean geochemistry. Global Biogeochemical Cycles 22, GB1005.

Measures, C. I. and S. Vink, 2000. On the use of dissolved aluminum in surface waters to estimate dust deposition to the ocean. Global Biogeochemical Cycles 14, 317-327.

Moran, S. B. and W. L. Woods, 1997. Cd, Cr, Cu, Ni and Pb in the water column and sediments of the Ob-Irtysh Rivers, Russia. Mar. Pollut. Bull. 35, 270-279.

Murphy, K., M. Rehkämper and T. van de Flierdt, Comment on "The isotopic composition of cadmium in the water column of the South China Sea". Geochimica Et Cosmochimica Acta.

Nier, A. O., 1950. A Redetermination of the Relative Abundances of the Isotopes of Carbon, Nitrogen, Oxygen, Argon, and Potassium. Physical Review 77, 789-793.

Nozaki, Y., 1997. A fresh look at element distribution in the North Pacific Ocean. Eos, Transactions American Geophysical Union 78, 221-221.

Nozaki, Y. and D. S. Alibo, 2003. Importance of vertical geochemical processes in controlling the oceanic profiles of dissolved rare earth elements in the northeastern Indian Ocean. Earth and Planetary Science Letters 205, 155-172.

Oka, A., H. Hasumi, H. Obata, T. Gamo and Y. Yamanaka, 2009. Study on vertical profiles of rare earth elements by using an ocean general circulation model. Global Biogeochemical Cycles 23, GB4025.

Paalman, M. A. A., C. H. Vanderweijden and J. P. G. Loch, 1994. Sorption of cadmium on suspended matter under estuarine conditions - Competition and complexation with major sea-water ions. Water Air Soil Pollut. 73, 49-60.

Pahnke, K., T. van de Flierdt, K. M. Jones, M. Lambelet, S. R. Hemming and S. L. Goldstein, 2012. GEOTRACES intercalibration of neodymium isotopes and rare earth element concentrations in seawater and suspended particles. Part 2: Systematic tests and baseline profiles. Limnology and Oceanography-Methods 10, 252-269.

Pearce, C. R., M. T. Jones, E. H. Oelkers, C. Pradoux and C. Jeandel, 2013. The effect of particulate dissolution on the neodymium (Nd) isotope and Rare Earth Element (REE) composition of seawater. Earth and Planetary Science Letters 369, 138-147.

Pekka, L., H. Halmeenpaa, F. Ecke, K. M. Vuori, O. Mokrotovarova, B. Ohlander and J. Ingri, 2008. Assessing pollution in the Kola River, northwestern Russia, using metal concentrations in water and bryophytes. Boreal Environ. Res. 13, 15-30.

Piepgras, D. J. and G. J. Wasserburg, 1980. Neodymium Isotopic Variations in Seawater. Earth and Planetary Science Letters 50, 128-138.

Piepgras, D. J. and G. J. Wasserburg, 1983. Influence of the Mediterranean Outflow on the Isotopic Composition of Neodymium in Waters of the North-Atlantic. Journal of Geophysical Research-Oceans and Atmospheres 88, 5997-6006.

Piepgras, D. J. and G. J. Wasserburg, 1987. Rare-Earth Element Transport in the Western North-Atlantic Inferred from Nd Isotopic Observations. Geochimica Et Cosmochimica Acta 51, 1257-1271.

Piepgras, D. J., G. J. Wasserburg and E. J. Dasch, 1979. Isotopic Composition of Nd in Different Ocean Masses. Earth and Planetary Science Letters 45, 223-236.

Piotrowski, A. M., S. L. Goldstein, S. R. Hemming and R. G. Fairbanks, 2004. Intensification and variability of ocean thermohaline circulation through the last deglaciation. Earth and Planetary Science Letters 225, 205-220.

Porcelli, D., P. S. Andersson, G. J. Wasserburg, J. Ingri and M. Baskaran, 1997. The importance of colloids and mires for the transport of uranium isotopes through the Kalix River watershed and Baltic Sea. Geochim. Cosmochim. Acta 61, 4095-4113.

Price, N. M. and F. M. M. Morel, 1990. Cadmium and cobalt substitution for zinc in a marine diatom. Nature 344, 658-660.

Rahmstorf, S., 2002. Ocean circulation and climate during the past 120,000 years. Nature 419, 207-214.

Rehkämper, M., F. Wombacher, T. J. Horner and Z. Xue, 2011. Natural and anthropogenic Cd isotope variations. Berlin Heidelberg, Springer-Verlag.

Reid, J. L., 1994. On the Total Geostrophic Circulation of the North-Atlantic Ocean - Flow Patterns, Tracers, and Transports. Progress in Oceanography 33, 1-92.

Reisberg, L. and A. Zindler, 1986. Extreme isotopic variations in the upper mantle: evidence from Ronda. Earth and Planetary Science Letters 81, 29-45.

Rempfer, J., T. F. Stocker, F. Joos, J.-C. Dutay and M. Siddall, 2011. Modelling Nd-isotopes with a coarse resolution ocean circulation model: Sensitivities to model parameters and source/sink distributions. Geochimica Et Cosmochimica Acta 75, 5927-5950.

Rhein, M., J. Fischer, W. M. Smethie, D. Smythe-Wright, R. F. Weiss, C. Mertens, D. H. Min, U. Fleischmann and A. Putzka, 2002. Labrador Sea Water: Pathways, CFC Inventory, and Formation Rates. Journal of Physical Oceanography 32, 648-665.

Rhein, M., D. Kieke, S. Hüttl-Kabus, A. Roessler, C. Mertens, R. Meissner, B. Klein, C. W. Böning and I. Yashayaev, 2011. Deep water formation, the subpolar gyre, and the meridional overturning circulation in the subpolar North Atlantic. Deep Sea Research Part II: Topical Studies in Oceanography 58, 1819-1832.

Rickli, J., M. Frank, A. R. Baker, S. Aciego, G. de Souza, R. B. Georg and A. N. Halliday, 2010. Hafnium and neodymium isotopes in surface waters of the eastern Atlantic Ocean: Implications for sources and inputs of trace metals to the ocean. Geochimica Et Cosmochimica Acta 74, 540-557.

Rickli, J., M. Frank and A. N. Halliday, 2009. The hafnium-neodymium isotopic composition of Atlantic seawater. Earth and Planetary Science Letters 280, 118-127.

Ripperger, S. and M. Rehkämper, 2007a. Precise determination of cadmium isotope fractionation in seawater by double spike MC-ICPMS. Geochim. Cosmochim. Acta 71, 631-642.

Ripperger, S., M. Rehkämper, D. Porcelli and A. N. Halliday, 2007b. Cadmium isotope fractionation in seawater - A signature of biological activity. Earth Planet. Sci. Lett. 261, 670-684.

Ruttenberg, K. C., 2003. The global phosphorus cycle. In: Schlesinger, H.W. (Ed), Biogeochemistry: in Treatise on Geochemsitry, vol. 8 Elsevier, Oxford: 585-643.

Sarafanov, A., H. Mercier, A. Falina, A. Sokov and P. Lherminier, 2010. Cessation and partial reversal of deep water freshening in the northern North Atlantic: observation-based estimates and attribution. Tellus Series a-Dynamic Meteorology and Oceanography 62, 80-90.

Sarafanov, A., A. Sokov, A. Demidov and A. Falina, 2007. Warming and salinification of intermediate and deep waters in the Irminger Sea and Iceland Basin in 1997-2006. Geophysical Research Letters 34.

Schlitzer, R., 2012. Ocean Data View. http://odv.awi.de.

Schmitt, A. D., S. J. G. Galer and W. Abouchami, 2009. Mass-dependent cadmium isotopic variations in nature with emphasis on the marine environment. Earth Planet. Sci. Lett. 277, 262-272.

Schmitz, W. J., 1996. On the world ocean circulation. Volume 1. Some global features/North Atlantic circulation. Woods Hole Oceanographic Institution Technical Report, WHOI: 149.

Semiletov, I. P., P. Andersson and t. s. party, 2008. International Siberian Shelf Study 2008 (ISSS-08). Cruise Report.

Shabani, M. B., T. Akagi and A. Masuda, 1992. Preconcentration of Trace Rare-Earth Elements in Seawater by Complexation with Bis(2-Ethylhexyl) Hydrogen Phosphate and 2-Ethylhexyl Dihydrogen Phosphate Adsorbed on a C18 Cartridge and Determination by Inductively Coupled Plasma Mass-Spectrometry. Analytical Chemistry 64, 737-743.

Shiller, A. M. and E. A. Boyle, 1991. Trace-Elements in the Mississippi River-Delta Outflow Region - Behavior at High Discharge. Geochim. Cosmochim. Acta 55, 3241-3251.

Sholkovitz, E. R., W. M. Landing and B. L. Lewis, 1994. Ocean particle chemistry: The fractionation of rare earth elements between suspended particles and seawater. Geochimica Et Cosmochimica Acta 58, 1567-1579.

Siddall, M., S. Khatiwala, T. van de Flierdt, K. Jones, S. L. Goldstein, S. Hemming and R. F. Anderson, 2008. Towards explaining the Nd paradox using reversible scavenging in an ocean general circulation model. Earth and Planetary Science Letters 274, 448-461.

Sigmarsson, O., I. Vlastelic, R. Andreasen, I. Bindeman, J. L. Devidal, S. Moune, J. K. Keiding, G. Larsen, A. Hoskuldsson and T. Thordarson, 2011. Remobilization of silicic intrusion by mafic magmas during the 2010 Eyjafjallajokull eruption. Solid Earth 2, 271-281.

Sloyan, B. M. and S. R. Rintoul, 2001. Circulation, Renewal, and Modification of Antarctic Mode and Intermediate Water*. Journal of Physical Oceanography 31, 1005-1030.

Smethie, W. M., R. A. Fine, A. Putzka and E. P. Jones, 2000. Tracing the flow of North Atlantic Deep Water using chlorofluorocarbons. Journal of Geophysical Research-Oceans 105, 14297-14323.

Spivack, A. J. and G. J. Wasserburg, 1988. Neodymium Isotopic Composition of the Mediterranean Outflow and the Eastern North-Atlantic. Geochimica Et Cosmochimica Acta 52, 2767-2773.

Steinfeldt, R. and M. Rhein, 2004. Spreading velocities and dilution of North Atlantic Deep Water in the tropical Atlantic based on CFC time series. Journal of Geophysical Research-Oceans 109.

Stichel, T., M. Frank, J. Rickli and B. A. Haley, 2012. The hafnium and neodymium isotope composition of seawater in the Atlantic sector of the Southern Ocean. Earth and Planetary Science Letters 317–318, 282-294.

Stordal, M. C. and G. J. Wasserburg, 1986. Neodymium isotopic study of Baffin Bay water: sources of REE from very old terranes. Earth and Planetary Science Letters 77, 259-272.

Stramma, L., D. Kieke, M. Rhein, F. Schott, I. Yashayaev and K. P. Koltermann, 2004. Deep water changes at the western boundary of the subpolar North Atlantic during 1996 to 2001. Deep-Sea Research Part I-Oceanographic Research Papers 51, 1033-1056.

Swift, J. H., 1984. The Circulation of the Denmark Strait and Iceland Scotland Overflow Waters in the North-Atlantic. Deep-Sea Research Part a-Oceanographic Research Papers 31, 1339-1355.

Sy, A., M. Rhein, J. R. N. Lazier, K. P. Koltermann, J. Meincke, A. Putzka and M. Bersch, 1997. Surprisingly rapid spreading of newly formed intermediate waters across the North Atlantic ocean. Nature 386, 675-679.

Tachikawa, K., V. Athias and C. Jeandel, 2003. Neodymium budget in the modern ocean and paleo-oceanographic implications. Journal of Geophysical Research-Oceans 108.

Tachikawa, K., C. Jeandel and M. Roy-Barman, 1999. A new approach to the Nd residence time in the ocean: the role of atmospheric inputs. Earth and Planetary Science Letters 170, 433-446.

Talley, L. D. and M. S. McCartney, 1982. Distribution and Circulation of Labrador Sea-Water. Journal of Physical Oceanography 12, 1189-1205.

Tanaka, T., S. Togashi, H. Kamioka, H. Amakawa, H. Kagami, T. Hamamoto, M. Yuhara, Y. Orihashi, S. Yoneda, H. Shimizu, T. Kunimaru, K. Takahashi, T. Yanagi, T. Nakano, H. Fujimaki, R. Shinjo, Y. Asahara, M. Tanimizu and C. Dragusanu, 2000. JNdi-1: a neodymium isotopic reference in consistency with LaJolla neodymium. Chemical Geology 168, 279-281.

Tanhua, T., K. A. Olsson and E. Jeansson, 2005. Formation of Denmark Strait overflow water and its hydro-chemical composition. Journal of Marine Systems 57, 264-288.

Thirlwall, M. F., 1991. High-Precision Multicollector Isotopic Analysis of Low-Levels of Nd as Oxide. Chemical Geology 94, 13-22.

van Aken, H. M., 2010. Hydrography GEOTRACES, NW-Atlantic, 2010, cruises PE 319 & PE 321, a first hydrographic description. Netherlands, NIOZ Physical Oceanography Department.

van de Flierdt, T. and M. Frank, 2010. Neodymium isotopes in paleoceanography. Quaternary Science Reviews 29, 2439-2441.

van de Flierdt, T., K. Pahnke, H. Amakawa, P. Andersson, C. Basak, B. Coles, C. Colin, K. Crocket, M. Frank, N. Frank, S. L. Goldstein, V. Goswami, B. A. Haley, E. C. Hathorne, S. R. Hemming, G. M. Henderson, C. Jeandel, K. Jones, K. Kreissig, F. Lacan, M. Lambelet, E. E. Martin, D. R. Newkirk, H. Obata, L. Pena, A. M. Piotrowski, C. Pradoux, H. D. Scher, H. Schoberg, S. K. Singh, T. Stichel, H. Tazoe, D. Vance, J. J. Yang and G. I. Partici, 2012. GEOTRACES intercalibration of neodymium isotopes and rare earth element concentrations in seawater and suspended particles. Part 1: reproducibility of results for the international intercomparison. Limnology and Oceanography-Methods 10, 234-251.

van Geen, A., D. C. McCorkle and G. P. Klinkhammer, 1995. Sensitivity of the phosphate-cadmium-carbon isotope relation in the ocean to cadmium removal by suboxic sediments. Paleoceanogr. 10, 159-169.

van Hulten, M. M. P., A. Sterl, A. Tagliabue, J. C. Dutay, M. Gehlen, H. J. W. de Baar and R. Middag, 2013. Aluminium in an ocean general circulation model compared with the West Atlantic Geotraces cruises. Journal of Marine Systems 126, 3-23.

von Blanckenburg, F., 1999. Tracing Past Ocean Circulation? Science 286, 1862-1863.

Waeles, M., R. D. Riso, J. Y. Cabon, J. F. Maguer and S. L'Helguen, 2009. Speciation of dissolved copper and cadmium in the Loire estuary and over the North Biscay continental shelf in spring. Estuar. Coast. Shelf Sci. 84, 139-146.

Waeles, M., R. D. Riso and P. Le Corre, 2005. Seasonal variations of cadmium speciation in the Penze estuary, NW France. Estuar. Coast. Shelf Sci. 65, 143-152.

Waeles, M., R. D. Riso, J. F. Maguer and P. Le Corre, 2004. Distribution and chemical speciation of dissolved cadmium and copper in the Loire estuary and North Biscay continental shelf, France. Estuar. Coast. Shelf Sci. 59, 49-57.

Wasserburg, G. J., S. B. Jacobsen, D. J. Depaolo, M. T. Mcculloch and T. Wen, 1981. Precise Determination of Sm/Nd Ratios, Sm and Nd Isotopic Abundances in Standard Solutions. Geochimica Et Cosmochimica Acta 45, 2311-2323.

Weigold, F. and M. Baborowski, 2009. Consequences of delayed mixing for quality assessment of river water: Example Mulde-Saale-Elbe. J. Hydrol. 369, 296-304.

Weis, D., B. Kieffer, C. Maerschalk, J. Barling, J. de Jong, G. A. Williams, D. Hanano, W. Pretorius, N. Mattielli, J. S. Scoates, A. Goolaerts, R. M. Friedman and J. B. Mahoney, 2006. High-precision isotopic characterization of USGS reference materials by TIMS and MC-ICP-MS. Geochemistry Geophysics Geosystems 7.

Wombacher, F., M. Rehkämper, K. Mezger and C. Munker, 2003. Stable isotope compositions of cadmium in geological materials and meteorites determined by multiple-collector ICPMS. Geochim. Cosmochim. Acta 67, 4639-4654.

Worthington, L. V., 1958. The 18° water in the Sargasso Sea. Deep Sea Research (1953) 5, 297-305.

Xu, Y., L. Feng, P. D. Jeffrey, Y. G. Shi and F. M. M. Morel, 2008. Structure and metal exchange in the cadmium carbonic anhydrase of marine diatoms. Nature 452, 56-U53.

Xue, Z., M. Rehkämper, T. J. Horner, W. Abouchami, R. Middag, T. van de Flierd and H. J. W. de Baar, 2013. Cadmium isotope variations in the Southern Ocean. Earth and Planetary Science Letters 382, 161-172.

Xue, Z., M. Rehkämper, M. Schönbächler, P. J. Statham and B. J. Coles, 2012. A new methodology for precise cadmium isotope analyses of seawater. Anal. Bioanal. Chem.

Yang, S.-C., D.-C. Lee and T.-Y. Ho, 2012. The isotopic composition of Cadmium in the water column of the South China Sea. Geochimica Et Cosmochimica Acta 98, 66-77.

Yashayaev, I., M. Bersch and H. M. van Aken, 2007. Spreading of the Labrador Sea Water to the Irminger and Iceland basins. Geophysical Research Letters 34, L10602.

Yashayaev, I. and A. Clarke, 2006. Recent warming of the Labrador Sea. AZMP Bulletin PMZA 5, 12-21.

Yashayaev, I. and J. W. Loder, 2009. Enhanced production of Labrador Sea Water in 2008. Geophysical Research Letters 36.

(*) The GEOTRACES planning group is composed of: Henderson, G. M.; Anderson, R. F.; Adkins, J.; Andersson, P.; Boyle, E. A.; Cutter, G.; de Baar, H.; Eisenhauer, A.; Frank, M.; Francois, R.; Orians, K.; Gamo, T.; German, C.; Jenkins, W.; Moffett, J.; Jeandel, C.; Jickells, T.; Krishnaswami, S.; Mackey, D.; Measures, C. I.; Moore, J. K.; Oschlies, A.; Pollard, R.; van der Loeff, M. R. D.; Schlitzer, R.; Sharma, M.; von Damm, K.; Zhang, J.; Masque, P.; SCOR Working Grp.